

---

# Volcanic tuffs as natural building stones:

## Mineralogy, technical properties, deterioration and conservation strategies

---

Dissertation

zur Erlangung des mathematisch-naturwissenschaftlichen Doktorgrades

„Doctor rerum naturalium“

der Georg-August-Universität Göttingen

im Promotionsprogramm Geowissenschaften

der Georg-August University School of Science (GAUSS)

vorgelegt von

Christopher Pötzl

aus Tiftlingerode

Göttingen 2020

Betreuungsausschuss

**Prof. Dr. Siegfried Siegesmund**

Abteilung Strukturgeologie und Geodynamik  
Geowissenschaftliches Zentrum der Georg-August-Universität Göttingen

**Dr. Rubén López-Doncel**

Geologisches Institut der Autonomen Universität San Luis Potosi, Mexiko

Mitglieder der Prüfungskommission

Referent: **Prof. Dr. Siegfried Siegesmund**

Abteilung Strukturgeologie und Geodynamik  
Geowissenschaftliches Zentrum der Georg-August-Universität Göttingen

Korreferent: **Prof. Dr. Rolf Sneathlage**

Naturstein, Bauchemie und Bauphysik in der Denkmalpflege, Bamberg

Weitere Mitglieder der Prüfungskommission:

**Dr. Reiner Dohrmann**

Abteilung Technische Mineralogie, Sedimentologie  
Bundesanstalt für Geowissenschaften und Rohstoffe, LBEG Hannover

**Prof. Dr. Jonas Kley**

Abteilung Strukturgeologie und Geodynamik  
Geowissenschaftliches Zentrum der Georg-August-Universität Göttingen

**Prof. Dr. Robert Sobott**

Fachlabor für Baudenkmalpflege, Naumburg

**Dr. Graciela M. Sosa**

Abteilung Angewandte Geologie  
Geowissenschaftliches Zentrum der Georg-August-Universität Göttingen

Tag der mündlichen Prüfung: 23.11.2020

## Abstract

The present thesis deals with the deterioration and durability of volcanic tuff rocks used as building stones in historical architecture and presents a combined approach on identifying the main parameters responsible for the severe damages that can be observed.

A comprehensive study on a dataset of over 500 tuffs from the literature regarding the technical parameters of tuff, in combination with an in-depth study of their petrographical properties, allows for the correlation of individual parameters and to identify key parameters, that influence the weathering behavior of tuff stones. A better evaluation of the weathering behavior of tuff stones can consequently allow for a more precise estimation of their durability. The results demonstrate that pore radii distributions are a good estimator for durability, since micropores ( $< 0.1 \mu\text{m}$ ) have a particularly strong influence on the weathering behavior of tuffs. Therefore, the important influence of the micropores on salt weathering in tuff rocks is stressed. In addition, the effective porosity and bulk density are identified as reliable estimators to predict the strength (UCS, TS) and durability of tuff rocks (UCS reduction).

The hydric expansion of tuff rocks can exceed values multiple times higher than other rock types and is considered to be an important factor for the deterioration of tuffs. It is typically associated with the presence of swellable clay minerals and two types of swelling mechanisms are generally discussed: stepwise intracrystalline swelling and continuous osmotic swelling. A mechanism that can cause expansion in the absence of swellable clay minerals, which is characterized by interaction of surface forces, is the disjoining pressure. The identification of the primary mode of swelling is important for understanding and finally preventing the swelling damage in tuff stones. The swelling experiments show, that intracrystalline swelling is the predominant mechanism for clay swelling in the investigated tuffs. The osmotic swelling on the other hand has only a minor influence on the clay swelling. Therefore, with a clay mineral analyses at hand, the swelling experiments proved to be a useful tool to differentiate between both clay swelling mechanisms in tuff rocks. Also, the importance of the location of the clay minerals in the tuff rock needs to be stressed. We could confirm that even small amounts of swellable clay minerals can cause significant expansion of the material if they are located in critical spots in the rock fabric. The role of the disjoining pressure is still unclear. New analytical techniques have to be developed to quantify its role in moisture expansion of tuff rocks.

In addition, the effects of two consolidation agents, tetraethoxysilane (TEOS) and tetramethoxysilane (TMOS), on a larger set of tuffs was evaluated by comparative analyses of petrophysical properties and weathering behavior before and after the treatments. The goal of this approach was to identify a general suitability of the consolidation treatments for different types of tuff. The application of tetramethoxysilane (TMOS) was also conducted with the aim of identifying if this consolidant can be absorbed more efficiently by tuffs with a high share of micropores, due to its smaller molecule size compared to TEOS. The investigation provided a variety of data that indicate, that TMOS may be a suitable candidate to overcome the bottlenecks in the pore space of tuffs, which limit the consolidation success of current products.

## Table of Contents

Betreuungsausschuss .....	I
Abstract .....	II
1 Introduction .....	1
1.1 Motivation .....	1
1.2 Objectives and thesis structure .....	3
2 Methodology.....	7
2.1 Sample preparation and orientation .....	7
2.2 Petrographical properties.....	7
2.3 Petrophysical properties.....	8
2.3.1 Pore space properties .....	8
2.3.2 Water transport and retention properties.....	9
2.3.3 Strength properties .....	10
2.3.4 Weathering behavior .....	12
2.4 Statistical analyses.....	13
3 Tuffs under investigation .....	15
3.1 Definition and classification .....	15
3.2 Selected tuffs .....	16
3.2.1 Petrographic summary .....	16
3.2.2 Short profiles .....	19
4 Deterioration of volcanic tuff rocks from Armenia .....	28
4.1 Introduction.....	28
4.1.1 Geological background.....	32
4.1.2 Utilization and deterioration.....	32
4.2 Petrography and mineralogy .....	36
4.2.1 Type, location and structure of clay minerals.....	47
4.3 Petrophysical properties.....	47
4.3.1 Density.....	49
4.3.2 Porosity, microporosity, pore radii distribution and specific surface area.....	49
4.3.3 Capillary water absorption and water vapor diffusion .....	51
4.3.4 Hygroscopic water sorption and saturation degree .....	51
4.3.5 Moisture expansion.....	52
4.3.6 Salt weathering resistance .....	53
4.4 Discussion .....	55
4.4.1 Correlation of results and limiting parameters.....	55
4.4.2 Water transport and retention as a function of the pore space properties.....	57
4.4.3 Moisture expansion related to the pore space properties and water absorb ..	61
4.4.4 Influence of clay minerals on pore space properties and moisture expansion .	64
4.4.5 Salt weathering.....	66
4.5 Conclusions.....	69
5 Key parameters of volcanic tuffs: a statistical approach .....	72
5.1 Introduction.....	72
5.2 Materials and methods.....	75
5.2.1 Statistical methodology.....	75
5.2.2 Difficulties in data comparability .....	75

## Table of contents

5.3	Results and discussion .....	77
5.3.1	Petrography and mineralogy.....	77
5.3.2	Petrophysical properties and weathering behavior: univariate analysis.....	80
5.3.3	Petrophysical properties and weathering behavior: bivariate analysis.....	88
5.3.4	Material behavior of crystal, vitric, lithic tuffs and influence of the pore radii.	92
5.4	Summary and Conclusions.....	96
6	Clay swelling mechanism in tuff stones – case study Hilbersdorf .....	99
6.1	Introduction .....	99
6.1.1	Geological setting .....	101
6.1.2	Utilization and deterioration.....	102
6.2	Materials and methods.....	103
6.3	Petrography and mineralogy .....	104
6.4	Petrophysical properties.....	109
6.4.1	Density.....	110
6.4.2	Porosity, microporosity, pore radii distribution and specific surface area.....	111
6.4.3	Capillary water absorption and water vapor diffusion .....	112
6.4.4	Hygroscopic water sorption and saturation degree .....	112
6.4.5	Tensile strength.....	112
6.4.6	Moisture expansion.....	113
6.4.7	Thermal expansion .....	114
6.4.8	Salt weathering resistance .....	114
6.5	Swelling experiments.....	115
6.6	Type, location and structure of clay minerals .....	116
6.7	Discussion .....	118
6.7.1	Location of clay material .....	120
6.7.2	Primary mode of swelling.....	120
6.7.3	Softening properties and weathering resistance.....	120
6.8	Conclusions.....	121
7	Consolidation of volcanic tuffs.....	123
7.1	Introduction .....	123
7.2	Materials and methods.....	125
7.2.1	Selected tuffs.....	125
7.2.2	Conservation materials and application .....	126
7.3	Results.....	128
7.3.1	Petrography.....	128
7.3.2	Quantitative absorption of TEOS and TMOS.....	132
7.3.3	Aesthetic changes.....	133
7.3.4	Modification of petrophysical properties .....	135
7.3.4.1	Modification of pore space properties .....	135
7.3.4.2	Modification of the water transport and retention properties.....	139
7.3.4.3	Modification of the expansional behavior.....	144
7.3.4.4	Modification of the ultrasonic velocity and dyn modulus of elasticity ....	148
7.4	Discussion .....	149
7.5	Conclusions.....	153
8	General conclusions .....	155
9	References .....	160
	Acknowledgments.....	180
	Lebenslauf .....	181

Table of contents

Appendix..... I  
Appendix I – Tables..... I  
Appendix II – Figures ..... XI

## 1 Introduction

# 1 Introduction

## 1.1 Motivation

Throughout cultures and epochs volcanic tuffs have been used as building material for the creation of important architectural heritage, artworks and sculptures. Famous examples of their utilization can be found all over the world, from the pre-Columbian pyramids of Mexico or the antique Armenian monasteries to the mysterious Moai statues of the Easter Islands, the Hercules monument in Germany or the rock-cut architecture of Cappadocia.

Tuffs are relatively soft rocks and easy to quarry, even with primitive tools. They exhibit good insulation properties and a high aesthetic variability and are therefore an appreciated building material until today (Fig. 1.1.).



Figure 1.1: Intensive utilization of volcanic tuff rocks in the historic city centers of Central and Western Mexico. **a** Teatro Juárez in Guanajuato (Loseros tuff). **b** Marketplace and Parroquia San Miguel Arcángel in San Miguel el Alto (San Miguel el Alto tuff). **c** El Reloj Monumental de Pachuca in Pachuca de Soto (Blanca de Pachuca). **d** Caja de Agua in San Luis Potosi (Cantera Rosa).

However, the softness of the tuffs is also one of their main disadvantages in construction. It is typically connected to high porosity and water absorption as well as an abundance of clay minerals. These and other factors cause a low strength and high susceptibility to weathering. As a result, tuffs suffer from extensive deterioration, leading to massive damage in our monumental heritage. In addition, the replacement of deteriorated tuff with newly quarried material is becoming more complicated, because many quarries are decayed or backfilled. Stone replacement is generally a cost-intensive and resource depleting endeavor that considerably impacts the environment (Fig. 1.2). We are therefore in need to obtain better knowledge about the mechanisms that are responsible for tuff weathering and develop conservation measures for the protection against further deterioration of cultural heritage.

## 1 Introduction



Figure 1.2: **a** Active tuff quarry at Mt. Aragats (Armenia). **b** The proportion of unusable raw blocks is very high and usually remains as large heaps at the quarry

This thesis presents investigations on three basic issues that are frequently encountered when dealing with deterioration of tuff stones:

- (1) What are the main problems? (forms of deterioration)
- (2) What are the influencing factors? (responsible mechanisms)
- (3) What can we do about it? (developing protective measures)

Studies on volcanic tuff rocks as dimensional stones are significantly underrepresented in the literature, when compared to other magmatic building stones, sandstones or limestones for example. The comparability of tuff rocks often turns out to be a challenging task, because of their great heterogeneity, even when looking at small scale comparison of material from the same outcrop. Many authors were able to identify interrelationships between different rock properties and the particular influence on their weathering behavior. Although, these studies led to a better understanding and prediction of material behavior, the findings are often limited to certain types of rock and only applicable for individual cases, because they are generally conducted on small datasets and do not include the investigation of the mineralogy, fabric and anisotropic behavior of the material.

(1) A comprehensive study on a large compilation of data from the literature regarding the technical parameters of tuff, in combination with an in-depth study of their petrographical properties, could allow for the correlation of the individual parameters and identify key parameters, that influence the weathering behavior of tuff stones. A better evaluation of the weathering behavior of tuff stones will consequently allow for a more precise estimation of their durability. It will also allow to focus the research on the main influencing factors.

(2) Hydric expansion is considered to be an important factor for the weathering behavior and deterioration of tuffs, which are utilized as building stones. It is typically associated with the presence of swellable clay minerals. Two types of swelling mechanisms are discussed when swellable clay minerals are present: stepwise intracrystalline swelling and continuous osmotic swelling. A mechanism that can cause expansion in the absence of swellable clay minerals, which is characterized by interaction of surface forces, is the disjoining pressure. The identification of the primary mode of swelling is important for understanding and finally preventing the swelling damage in tuff stones.



## 1 Introduction

(3) Tuff is considered a problematic stone when it comes to conservation measures and a satisfactory consolidation of volcanic tuff rocks has shown to be a challenging task. Due to their high porosities and unfavorable pore size distributions, as well as their partly high content of swellable clay minerals, volcanic tuff rocks demand a lot of requirements for a successful treatment. Standardized techniques applied on tuff stones do often not lead to satisfying results. Instead, special procedures with formulations adjusted to the individual case have to be developed, which is a time consuming and costly endeavor. Especially the insufficient absorption of the consolidant is a frequent problem with tuff stones.

In this work, the effects of two consolidation agents, tetraethoxysilane (TEOS) and tetramethoxysilane (TMOS), on a larger set of tuffs was evaluated by comparative analyses of petrophysical properties and weathering behavior before and after the treatments. The goal of this approach was to identify a general suitability of the consolidation treatments for different types of tuff. In addition, the application of tetramethoxysilane (TMOS) was conducted with the aim of identifying if this consolidant, that was withdrawn from the market decades ago can be absorbed more efficiently by tuffs with a high share of micropores, due to its smaller molecule size compared to TEOS.

### 1.2 Objectives and thesis structure

Three main issues are addressed in this thesis:

- (1) How do tuffs deteriorate, what are the main influencing parameters on the weathering of tuff stones and can we identify certain types of tuffs to be particularly resistant/susceptible to weathering (Chapter 4 and 5):

The work starts with an exemplary investigation of the influencing factors on the individual weathering behavior of Armenian tuff stones, that were used as building stones in the historical architecture of Armenia (Chapter 4). This case study includes on-site investigations of a variety of historical monuments in central and northern Armenia, with the aim of identifying the main forms of deterioration of the individual material and their potential causes, also with respect to the specific environmental conditions, like climate or exposition. Laboratory investigations characterize the petrographic and technical properties of the tuffs, as well as their weathering behavior under accelerated conditions. The combinatory discussion of the results of both laboratory and on-site investigation allows for the correlation of the technical parameters with certain forms of weathering and the identification of specifically resistant or susceptible types of tuff.

To investigate if the findings from the Armenian case study can be globally transferred and if general statements concerning relevant parameters for the durability prediction of different types of tuff stone can be made, a statistical study is conducted on base of a comprehensive dataset of different types of tuff stones from the literature, including own data (Chapter 5). The study regards petrographical, petrophysical and weathering properties and incorporates a set of 15 representatively selected tuffs, to evaluate if the findings of the statistical study apply to them.

## 1 Introduction

- (2) Identifying the primary swelling mechanisms responsible for moisture expansion in tuff rocks (Chapter 6):

Hydric expansion is considered an important factor for the weathering behavior and deterioration of tuffs and typically associated with the presence of swellable clay minerals. Although the concept of clay swelling is an intensely researched topic in other research fields, until now it is unclear, which process is primarily driving the clay swelling in tuff stones and if other processes than clay swelling also play a role. The identification of the primary mode of swelling is important for understanding and finally preventing the swelling damage in tuff stones.

Therefore, Chapter 6 exemplarily investigates the swelling mechanism on a set of tuffs from Germany. The Hilbersdorf tuff was chosen for this study, because its hydric expansion can exceed the values of typical volcanoclastic material by multiples, but partly shows the absence of swellable clay minerals. In this case study, extensive mineralogical and petrophysical investigations on five varieties of the Hilbersdorf Tuff are performed, with a focus on the structure and location of the clay minerals in the rock fabric. Swelling experiments should identify if a certain swelling mechanism plays a major role in moisture expansion of tuff rocks.

- (3) Investigating the suitability and influence of two consolidants on the petrophysical properties and material behavior of different types of tuff stones (Chapter 7):

Since decades the consolidation of volcanic tuff stones is a challenging topic. Many products that proved to produce satisfying results for other types of porous stones may fail in the application on tuff. The reasons are diverse and under constant discussion.

In Chapter 7 a selection of nine tuff stones with highly varying mineralogy and technical properties have been treated with two different consolidation agents and in combination with a pretreatment of a coupling agent and/or a swelling reducer. The goal was: (a) to investigate a general suitability and influence of the consolidants on the petrophysical properties and material behavior of different types of tuff stones, (b) to determine the effects of a primer component and anti-swelling agent on consolidation treatments of different volcanic tuff stone and (3) to investigate if a commercially withdrawn product with smaller molecule sizes is being absorbed more effectively by tuffs with a high share of nanopores than common products on the market.

Following this short overview of the thesis structure, Chapter 2 will now present the applied techniques, that were used to obtain the relevant petrographic, petrophysical and durability parameters for this work. The subsequent Chapter 3 will give a brief petrographic presentation of the representative tuffs that were selected for the studies in Chapters 5 and 7.

## 1 Introduction

### This thesis incorporates the following publications:

- Chapter 4: Pötzl, C., Siegesmund, S., Dohrmann, R., Koning, JM, Wedekind, W. (2018) Deterioration of volcanic tuff rocks from Armenia: constraints on salt crystallization and hydric expansion. *Environ Earth Sci* 77: 660
- Chapter 5: Pötzl, C., Siegesmund, S., López-Doncel, R., Dohrmann, R. (2021) Key parameters of volcanic tuffs used as building stone: a statistical approach. *Environ Earth Sci* (in press)
- Pötzl, C., Siegesmund, S., Dohrmann, R., Koning, JM, Wedekind, W. (2018) Deterioration of volcanic tuff rocks from Armenia: constraints on salt crystallization and hydric expansion. *Environ Earth Sci* 77: 660.
- Pötzl, C., Dohrmann, R., Siegesmund, S. (2018) Clay swelling mechanism in tuff stones: an example of the Hilbersdorf Tuff from Chemnitz, Germany. *Environ Earth Sci* 77: 188.
- Rucker, S., Pötzl, C., Wendler, E., Dohrmann, R., López-Doncel, R., Siegesmund, S. (2020) Improved consolidation of volcanic tuff rocks with TEOS. In: Siegesmund, S. & Middendorf, B. (Eds.). *Monument future: Decay and conservation of stone. Proceedings of the 14th international congress on the deterioration and conservation of stone.* Mitteldeutscher Verlag, pp. 597-602.
- Kück, A., Pötzl, C., López-Doncel, R., Dohrmann, R., Siegesmund, S. (2020) Tuffs in Pre-Colombian and colonial architecture of Oaxaca, Mexico. In: Siegesmund, S. & Middendorf, B. (Eds.). *Monument future: Decay and conservation of stone. Proceedings of the 14th international congress on the deterioration and conservation of stone.* Mitteldeutscher Verlag, pp. 53-58.
- Kück, A., Pötzl, C., López-Doncel, R., Dohrmann, R., Siegesmund, S. (2020) Effects of zeolites and swellable clay minerals on water-related properties and thermal dilatation in volcanic tuff rocks. In: Siegesmund, S. & Middendorf, B. (Eds.). *Monument future: Decay and conservation of stone. Proceedings of the 14th international congress on the deterioration and conservation of stone.* Mitteldeutscher Verlag, pp. 119-124.
- Teipel, M., Pötzl, C., Wedekind, W., Middendorf, B., Siegesmund, S. (2020) Approach on developing stone replacement mortars for the cultural heritage of Armenia. In: Siegesmund, S. & Middendorf, B. (Eds.). *Monument future: Decay and conservation of stone. Proceedings of the 14th international congress on the deterioration and conservation of stone.* Mitteldeutscher Verlag, pp. 603-608.
- Török, A., Germinario, L., López-Doncel, R., Pötzl, C., Siegesmund, S. (2020) Comparative analysis of volcanic tuffs from Europe, Asia and North-America. In: Siegesmund, S. & Middendorf, B. (Eds.). *Monument future: Decay and conservation of stone. Proceedings of the 14th international congress on the deterioration and conservation of stone..* Mitteldeutscher Verlag, pp. 131-136.
- Pötzl, C., López-Doncel, R., Wedekind, W., Siegesmund, S. (2016) Las Casas Tapadas de Plazuelas - Structural damage, weathering characteristics and technical properties of volcanic rocks in Guanajuato, Mexico. In: Hughes, J., & Howind, T. (Eds.). *Science and Art: A Future for Stone: Proceedings of the 13th International Congress on the*

## 1 Introduction

Deterioration and Conservation of Stone, Volume 2. Paisley: University of the West of Scotland, pp. 1237-1245.

Chapter 6: Pötzl, C., Dohrmann, R., Siegesmund, S. (2018) Clay swelling mechanism in tuff stones: an example of the Hilbersdorf Tuff from Chemnitz, Germany. *Environ Earth Sci* 77: 188

Chapter 7: Pötzl, C., Rucker, S., Wendler, E., Siegesmund, S. (2021) Consolidation of volcanic tuffs with TEOS and TMOS: a systematic study. *Environ Earth Sci* (in press)

Rucker, S., Pötzl, C., Wendler, E., Dohrmann, R., López-Doncel, R., Siegesmund, S. (2020) Improved consolidation of volcanic tuff rocks with TEOS. In: Siegesmund, S. & Middendorf, B. (Eds.). *Monument future: Decay and conservation of stone. Proceedings of the 14th international congress on the deterioration and conservation of stone – Mitteldeutscher Verlag*, pp. 597-602

## 2 Methodology

The data presented in this work originates from 32 volcanic tuff rocks that were analyzed in greater detail by laboratory analyses of the petrography, petrophysical properties and weathering behavior. The following chapter presents a short overview of the applied techniques that were used to determine the relevant parameters.

### 2.1 Sample preparation and orientation

Tuff rocks often show a pronounced anisotropy, expressed by a directional dependence in their technical properties. Therefore, prior to the preparation of the test specimens, the tuff blocks were oriented with regard to a Cartesian X-Y-Z coordinate system. The orientations were set to visible fabric elements, like bedding and elongated clasts. The XY plane represents the bedding plane, with the X direction set parallel to the lineation. The Z direction is oriented perpendicular to the bedding plane.

### 2.2 Petrographical properties

The petrographical analyses of each sample were performed on oriented thin sections under a polarization microscope, as well as on a scanning electron microscope (SEM) with adjacent energy dispersive X-ray spectroscopy (EDX) for mineral identification. The orientation of the thin section was set horizontal and perpendicular to the bedding plane. For the analyses on the SEM, carbon coated sample fragments of 10 mm were used. The SEM was especially helpful for locating and characterizing clay minerals, zeolites, volcanic glass and the amorphous silica gel formed due to the consolidation experiments.

Further mineralogical analyses were done using X-ray diffraction (XRD) of whole rock samples and oriented slides of the clay fraction  $< 2 \mu\text{m}$ , that was separated by the Atterberg method following Stoke's Law. The analyses, especially regarding the clay minerals, were supported by X-ray fluorescence (XRF) analysis and cation-exchange capacity (CEC), determined after the copper (II) triethylenetetramine method of Dohrmann and Kaufhold (2009) modified from Meier and Kahr (1999).

The XRF, XRD, CEC and SEM analyses were mainly performed at the department of technical mineralogy of the Federal Institute for Geosciences and Natural Resources (BGR) in Hannover. Several XRF, XRD and SEM analyses were performed at the Geoscience Center Göttingen (GZG), as well as several SEM analyses at the geological department of the Freiberg University of Mining and Technology (TU Freiberg).

## 2 Methodology

### 2.3 Petrophysical properties

The petrophysical properties determined for this work can be divided into pore space properties, water transport and retention properties, mechanical and elastic properties, as well as weathering behavior. All properties were determined at the GZG in Göttingen.

#### 2.3.1 Pore space properties

The pore space properties determined in this work include the determination of the effective porosity, bulk and matrix density, pore radii distribution and specific surface area (SSA). A majority of the technical parameters of stone are directly or indirectly influenced by the pore space, as they are controlled by the type and shape of pores, their size and distribution, as well as their cross-linking.

##### Effective porosity, bulk and matrix density

The effective porosity (accessible to fluids and gases), the bulk and matrix densities were determined by hydrostatic weighing on sample cubes of 65 mm edge length after DIN 772-4.

The sample cubes were dried at 40°C until mass consistency (dry weight  $m_d$ ) and fully saturated with demineralized water for 24 h, after 24 h of vacuum in a desiccator. Subsequent measurements of the wet ( $m_w$ ) and buoyancy weight  $m_b$  (by weighing with an under-floor balance while submerging the sample in demineralized water) allow the calculation of the effective porosity ( $\phi$ ), bulk ( $\rho_{bulk}$ ) and matrix density ( $\rho_{mat}$ ) according to the following equations:

$$\begin{aligned} \text{Effective porosity:} \quad \phi &= \frac{m_w - m_d}{m_w - m_b} * 100 && [\text{vol.\%}] \\ \text{Bulk density:} \quad \rho_{bulk} &= \frac{m_d}{m_w - m_b} && [\text{g/cm}^3] \\ \text{Matrix density:} \quad \rho_{mat} &= \frac{m_d}{m_d - m_b} && [\text{g/cm}^3] \end{aligned}$$

##### Pore radii distribution, specific surface area (SSA)

The pore radii distribution of the samples was determined on sample fragments after DIN 66133 by mercury intrusion porosimetry (MIP) using low (PASCAL 140) and high pressure (PASCAL 440) units from Thermo Fisher Scientific. Sample fragments were placed in a glass dilatometer, which was then evacuated and subsequently filled with mercury. Progressively increasing pressure is then forcing the mercury into the sample. Every capillary pore radius is thereby characterized by a certain pressure needed to push the mercury into the pore (Doveton 1987). This, however, only applies to non-wetting fluids with a contact angle of  $\theta > 90^\circ$  (like mercury). With a maximum pressure of 400 MPa, the detection of the smallest possible pore radius is limited to 1 nm. The determination of the pore throat radii distribution is based on the Washburn equation, with  $r_p$  = pore throat radius,  $\gamma$  = surface tension at fluid interface,  $\Theta$  = liquid-solid contact angle,  $P$  = pressure:

$$\text{Washburn equation:} \quad r_p = \frac{-2 \cdot \gamma \cdot \cos \theta}{P}$$

## 2 Methodology

The software (SOLID) of the MIP unit also allows for the calculation of the specific surface area (SSA) on base of the particle size distribution (Rotare and Prenzlöw 1967). The conical model used by the software is accurate for most rock material, although at the same time tuffs are characterized by a considerable amount of bottleneck pores, that may be better described by a spherical model. In the case of the consolidation study (Chapter 7), the calculated values at least allowed for a comparison of relative changes due to the treatment. The SSA was determined more accurately by means of N<sub>2</sub> gas adsorption based on the Brunauer–Emmett–Teller theory (BET) at the BGR Hanover.

### 2.3.2 Water transport and retention properties

Water is recognized as the main driving factor for inducing deterioration processes in natural stones (Mirwald 1997; Siegesmund and Dürrast 2011; Snethlage 1984; Weiss 1992), for example by inducing clay swelling mechanism or distributing harmful salts into the pore space. Tuff stones are especially affected by these processes due to their typically high porosity and abundance of swellable clay minerals. Water can be absorbed, transported and retained within the pore network of the rock in liquid or gas form. Different water transport and retention properties were determined in this work. They characterize the overall capability and intensity of water absorption and retention and the connectivity of the pore network.

Klopfer (1985) differentiated between three different pore size categories, associated to their preferred mechanisms of water transport. He defined micropores as pores < 0.1 µm and capillary pores between 0.1 µm and 1 mm. In micropores the water vapor diffusion is the main moisture transport mechanism, whereas for capillary pores, the capillary suction of liquid water becomes relevant. The equilibration of higher and lower water vapor concentration is the main driving force of the water vapor transport mechanism. In macropores > 1 mm the transport of water in liquid form (fluid flow) emerges.

#### Capillary water absorption coefficient (w value)

The capillary water absorption coefficient (w) describes how much water the material can absorb due to capillary forces over a certain area (m<sub>w</sub>) and time (t):

$$w \text{ value:} \quad w = \frac{m_w}{\sqrt{t}} \quad [\text{kg/m}^2 \cdot \sqrt{\text{h}}]$$

The w value (capillary water uptake) was determined according to DIN EN ISO 15148 in a closed cabinet while weighing over time. The dry sample cube (65 mm edge length) attached to an under-floor balance and in minimal surface contact (≤5 mm) with a bath of demineralized water, was subsequently weighed over time. The increasing weight was registered every five seconds with the software WinWedge. The w value was mostly determined for the X and Z directions.

#### Water absorption by total immersion (vac./atm.), saturation coefficient S

The determination of the maximum capacity of water absorption W<sub>vac</sub> was determined by the weight difference of the dry and fully water saturated sample cube (65 mm edge length) under forced (vacuum) conditions (for 24 h). The voluntary water absorption W<sub>atm</sub> was determined under atmospheric conditions. The quotient of both values is described by the dimensionless

## 2 Methodology

saturation coefficient  $S$  and allows for the estimation of the frost resistance of the stone after Hirschwald (1912):

$$S \text{ value:} \quad S = \frac{W_{atm}}{W_{vac}} \quad [-]$$

The saturation coefficient describes the amount of pore space that is accessible to water absorption and ranges between 0 – 1. After Hirschwald (1912), values < 0.75 point to a weathering and frost resistant rock, while the frost resistance is uncertain until further investigations with values between 0.75 and 0.9. Rocks with  $S$  values > 0.9 are classified as not weathering and frost resistant.

### Hygroscopic water sorption

The hygroscopic water sorption (sometimes only labeled as sorption) describes the amount of water that the specific surface area of the pores adsorb from the air. It was determined on dried (40°C for 7 days) cylindrical samples of 15 mm diameter and 50 mm length in a climate chamber (Feutron KPK 400) at 23°C temperature and stepwise increase of the relative humidity (RH) from 25 to 95 % according to DIN EN ISO 12571. Due to time constraints (constant mass due to high ratios of micropores can sometimes only be reached after weeks), the humidity was increased 10 % every 48 h while determining the weight difference before every humidity increase. The hygroscopic water sorption gives information about which relative humidities are already relevant for the water adsorption behavior of the material and subsequent desorption curves give an insight about the drying behavior (Siegesmund and Dürrast 2011).

### Water vapor diffusion resistance ( $\mu$ value)

An important property for the characterization of the drying behavior of stones is their gas permeability. The dimensionless coefficient of water vapor diffusion resistance ( $\mu$ ) characterizes the diffusion resistance of the material towards the moisture of the adjacent air (Siegesmund and Dürrast 2011) and was determined according to DIN EN ISO 12572 with the wet cup method. Sample discs of 40 mm diameter and 10 mm length were placed in a Teflon cup, filled with demineralized water and the amount of water diffusing through the sample at 23°C and 50 % was determined every 24 h. The dimensionless  $\mu$  value can be calculated by the following equation:

$$\mu \text{ value:} \quad \mu = \delta L \cdot p_s \cdot \Delta a \cdot A \cdot \frac{t}{s} \cdot \Delta m \quad [-]$$

with  $\mu$  = coefficient of water vapor diffusion resistance [-],  $\delta L$  = water vapor diffusion coefficient of air [kg/Pa·m·s],  $p_s$  = partial pressure of saturated air [ $2.49 \times 10^3$  Pa],  $\Delta a$  = difference of relative humidity,  $A$  = effective sample area [m<sup>2</sup>],  $t$  = diffusion time [s],  $s$  = sample thickness [m] and  $\Delta m$  = weight change [kg].

### 2.3.3 Strength properties

The mechanical properties define how long a material can withstand stress before it yields and therefore characterize its strength. Many rocks show a reduction in strength upon wetting. Therefore, the strength properties were determined on dry and fully saturated specimens.



## 2 Methodology

### Tensile strength

By means of the Brazil test (or indirect tensile strength test) according to DIN 22024, the tensile strength (TS) was measured on disc-shaped specimens of 20°mm length and 40°mm diameter under dry and water saturated conditions. A universal press from Walter & Bai applied a progressive compressional load (increasing 30 N/s) on the uniaxial test setup, on which the sample discs are attached, which results in a tensile stress perpendicular to the direction of the applied pressure. The tensile strength can be calculated by the following equation, with  $\sigma_T$  = tensile strength at failure [MPa],  $F$  = loading force [N],  $l$  = length of the specimen [mm],  $\pi$  = diameter of the specimen [mm]:

$$\text{Tensile strength:} \quad \sigma_T = \frac{2 \cdot F}{d \cdot l \cdot \pi} \quad [\text{MPa}]$$

### Compressive strength

The uniaxial compressive strength (UCS) under dry and water saturated conditions was determined according to DIN EN 1926 on cylindrical samples of 50 mm length and diameter on a universal press with a strain rate of 1000 N/s until failure. The UCS expresses the value of where the material experiences a total loss of cohesion (Siegesmund and Dürrast 2011). The compressive strength can be calculated by the following equation, with  $F_{max}$  = breaking load [kN],  $A_0$  = initial cross-sectional area [mm<sup>2</sup>):

$$\text{Compressive strength:} \quad \beta_{UCS} = \frac{F_{max}}{A_0} \quad [\text{MPa}]$$

In order to identify anisotropic behavior of the tuffs, both TS and UCS were determined parallel (X direction) and perpendicular (Z direction) to the bedding plane, on a minimum of six specimens per direction.

### Ultrasonic velocity (P-wave velocity)

Ultrasonic P-wave velocity was determined via direct transmission of the ultrasonic travel time through a respective travel distance according to DIN 14579 (with a frequency of 350 kHz). In this work it was mainly used as a non-destructive tool to obtain the dynamic Young's modulus ( $E_{dyn}$ ), which is proportional to the rock strength (Siegesmund and Dürrast 2011). It was determined on sample cubes of 65 mm edge length and cylindric samples of 50 mm length.

### Static/dynamic modulus of elasticity $E_{stat}/E_{dyn}$ (Young's modulus)

The static Young's modulus  $E_{stat}$  is based on the relation between stress and strain and measures the stiffness of the material (resistance against deformation). It can be derived from the linear portion of the stress strain curve of the uniaxial compressive strength by the following equation, with  $E_{stat}$  = static modulus of elasticity [GPa],  $\sigma$  = applied strength [MPa],  $\varepsilon$  = strain [%]:

$$\text{stat. Young's modulus:} \quad E_{stat} = \frac{d\sigma}{d\varepsilon} \quad [\text{GPa}]$$

## 2 Methodology

The dynamic Young's modulus  $E_{dyn}$  can be derived from the P-wave velocity by the following equation:

$$\text{dyn. Young's modulus: } E_{dyn} = v_p^2 \frac{(1+\mu)(1-2\cdot\mu)}{1-\mu} \cdot \rho \quad [\text{GPa}]$$

with  $v_p$  = P-wave velocity,  $\rho$  = bulk density and  $\mu$  = Poisson's ratio. The Poisson's ratio is characteristic for every mineral and can be determined with the help of the P-wave velocity and the transversal wave velocity ( $V_s$ ) (Siegesmund and Dürrast 2011).

$E_{dyn}$  is typically expected to be higher than  $E_{stat}$  (Schön 2015).

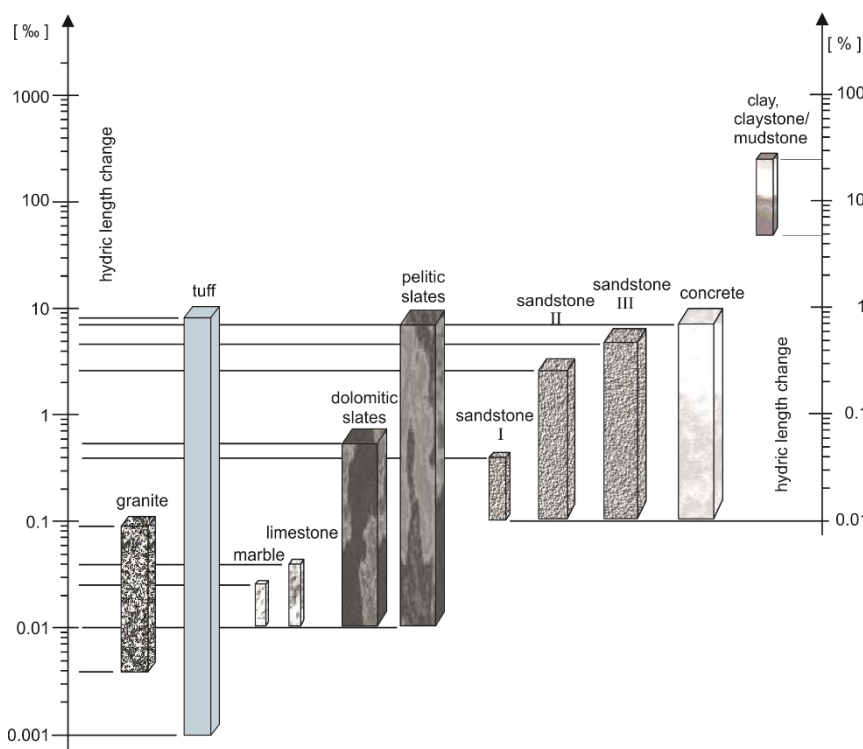
### 2.3.4 Weathering behavior

In order to constrain the behavior of tuffs related to environmental changes, different weathering experiments were conducted under accelerated laboratory conditions.

The expansional behavior of tuff rocks is mainly induced by temperature and moisture changes and one of the main processes that leads to their deterioration. The determination of the expansional behavior is therefore a critical parameter for the estimation of the quality or durability of tuff. The expansional behavior often shows a strong directional dependence and thus determined parallel (X) and perpendicular (Z) to the bedding.

#### Hydric expansion

The hygric/hydric expansion of tuff rocks can exceed the values of other rock types by multiples (Fig. 2.1) and is often connected to the abundance of swellable clay minerals or the presence of a high share of micropores (Pötzl et al. 2018a; Wedekind et al. 2013; Wendler et al. 1996). Hygric expansion refers to expansion due to moisture changes up to 99 % RH, while hydric expansion refers to expansion under complete immersion.



expansion was measured on cylindrical samples of 50 mm length and 15 mm diameter under conditions of complete immersion in demineralized water following DIN 13009. A displacement transducer with a resolution of 0.1  $\mu\text{m}$  measured the linear expansion as a function of time.

Figure 2.1: Hydric expansion from different types of rock. Modified with own data (for tuffs) after Siegesmund and Dürrast (2011) from Kocher (2005) and references within

## 2 Methodology

### Thermal expansion

Thermal expansion behavior was determined in a climate chamber via pushrod dilatometer and displacement transducer with a resolution of 0.1  $\mu\text{m}$  following DIN EN 14581. The cylindrical samples of 15 mm diameter and 50 mm length were exposed to two heating and cooling cycles under dry and wet conditions, respectively. In each cycle the dry samples (40°C for 7 days) were heated from 20°C to 90°C and subsequently cooled down to 20°C, with a heating/cooling rate of 1°C/min. Both minimum (20°C) and maximum (90°C) temperatures were hold for 6 hours.

The coefficient of expansion  $\alpha$  usually represents the thermal expansion. It is calculated from the slope of the strain curve by the following equation, with  $\alpha$  = expansion coefficient [ $\text{K}^{-1}$ ],  $\Delta l$  = length change [mm],  $\Delta T$  = temperature change [ $\text{K}^{-1}$ ],  $l$  = sample length [mm]:

$$\text{Expansion coefficient } \alpha: \quad \alpha = \frac{\Delta l}{l \cdot \Delta T} \quad [10^{-6}\text{K}^{-1}]$$

Absolute length changes are characterized by the resulting residual strain  $\varepsilon$ , which is determined by:

$$\text{Residual strain } \varepsilon: \quad \varepsilon = \frac{\Delta l}{l} \quad [\text{mm/m}]$$

### Salt bursting test

The salt weathering resistance of the investigated tuffs was determined by a cyclic salt weathering test, inspired by the standard DIN EN 12370 on cubes of 65 mm edge length. For one cycle of the test, the dry cubes were put in a 10 % solution of sodium sulfate ( $\text{Na}_2\text{SO}_4$ ) for 4 hours. The samples were afterwards dried in an oven (60°C) for 24 h and subsequently weighed. This process was repeated until a minimum weight loss of at least 30 % was achieved.

## 2.4 Statistical analyses

The statistical analyses in Chapter 5 were conducted on a large set of data, collected from the literature, including the own analyses, with the goal of identifying key parameters for the estimation of material and weathering behavior of characteristic types of tuff.

Univariate and bivariate statistical analyses were applied on up to 528 tuffs from the database with the open software 'RStudio'. Box-and-whisker plots (boxplots) were used to display the distribution of single rock properties (univariate method). They essentially consist of two parts: a box and a set of whiskers. The box displays the interquartile range (IQR) in which 50 % of the values are present, limited by the median of the lower (25 % quartile) and upper (75 % quartile) half of the dataset. A horizontal line inside the box represents the median of the whole dataset and its position allows for an estimation of the skewness of the data distribution. The whiskers are drawn until the minimum and maximum values. Their length is limited to 1.5 times of the IQR (Tukey 1977) and any lower or higher values are plotted as outliers. The data of the 15 representative tuffs of this study is included into the big dataset. To visualize, however, the representativity of the selected tuffs, the range of their single rock properties is presented as a red line next to the boxplots.

## 2 Methodology

Regression analyses investigate the relationship of two properties and reveal if the parameters are comparable (bivariate method). The data is presented in point diagrams with the correlation coefficient  $r$  expressing the relation between two parameters (Spearman rank correlation coefficient). The correlation coefficient  $r$  varies between +1 and -1, whereby values close to +1 or -1 describe a significant correlation between the parameters and values close to 0 describe a lack of relationship. Under the assumption that the rock properties show normal distribution, confidence regions with 80 % probability range are displayed as ellipses within the regression analyses.

### 3 Tuffs under investigation

## 3 Tuffs under investigation

### 3.1 Definition and classification

The International Union of Geological Sciences (IUGS) defines tuff rocks as volcanoclastic rocks, that consist of at least 75 % volcanic ash <2 mm (Le Maitre et al. 2002). However, commonly accepted the term tuff is used as a collective term, to describe any volcanoclastic rock with > 75 % pyroclasts of any size. The term pyroclast refers to any fragment generated directly as a result of volcanic activity and includes individual crystals, glass and rock fragments. Tuff rocks can be further classified according to the size of their pyroclastic fragments (Fisher 1966) or to the type of pyroclastic fragments (Schmid 1981) (see Fig. 3.1). The total alkali versus silica (TAS) classification system after Le Bas et al. (1986) is used for the geochemical classification of pyroclastic rocks (Fig. 3.2), since the modal content of tuff cannot always be determined accurately with the QAPF diagram (Le Maitre et al. 1989; Streckeisen 1978), due to the often cryptocrystalline and glassy texture of the groundmass.

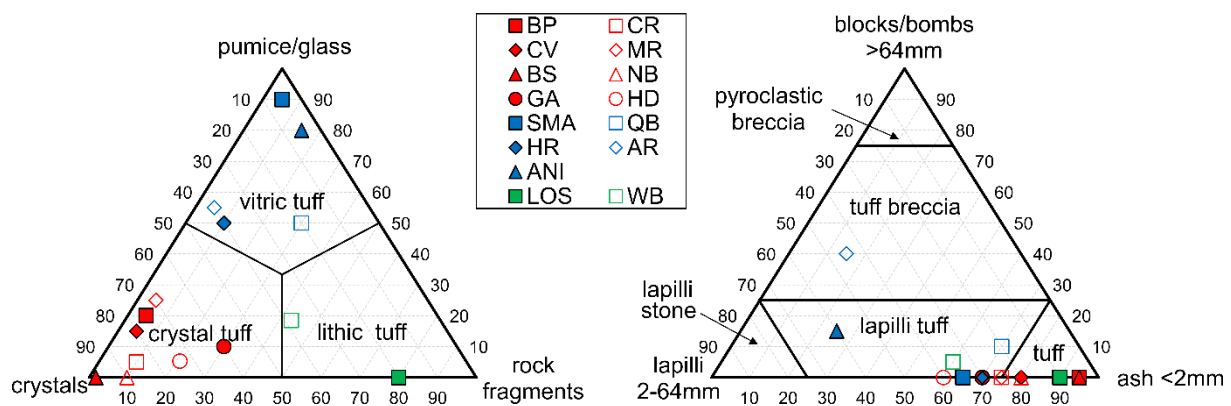


Figure 3.1: Classification of the selected tuffs for Chapter 5 and 7, based on the type of their components (Schmid 1981) (left) and based on the size of components (Fisher 1966) (right). The tuffs are colored after their main pyroclastic content: crystal tuff in red, vitric tuff in blue and lithic tuff in green. In Chapters 5 and 7 it will be referred to this figure

The main components of tuff are usually rock fragments, ash particles and scoria, that were ejected and deposited by violent volcanic eruptions and subsequently compacted and welded together to different degrees. The initial composition and cooling rate of the magma, the ratio of the dragged along and incorporated components, degassing processes, different depositional and reworking environments, subsequent diagenesis and alteration processes that may form new minerals with high impact on the strength and durability, and many more contributing factors open the possibility to almost limitless heterogeneity in tuff rocks.

The mineralogical and fabric heterogeneity of tuff rocks make it very difficult to determine reliable durability parameters and predict material behavior, which in turn is crucial for their quality assessment. Additionally, the weathering resistance of tuffs is typically reduced, due to characteristic high porosity, strong affinity for water absorption and a frequent abundance in swellable clay minerals (discussion in Chapter 4 + 6).

### 3 Tuffs under investigation

#### 3.2 Selected tuffs

In the course of this work 72 different tuff rocks that are used as building stones in Armenia, Germany and Mexico were investigated regarding their petrography, petrophysical properties and weathering behavior, of which 32 tuffs were investigated more comprehensively to be presented in this thesis (Chapters 4 – 7). Nineteen Armenian tuffs and five German tuffs were utilized for the respective case studies in Chapter 4 and 6.

Finally, fifteen representative tuffs were selected (Tab. 3.1) to be presented in the statistical study (Chapter 5), of which nine tuffs were then again selected for the consolidation experiments in Chapter 7. As these 15 tuffs will reappear several times in this work, their general petrographic characteristics will be briefly displayed here. Their petrophysical properties and specific weathering behavior, as well as the characterization and influence of clay minerals and zeolites or other mineralogical particularities will be discussed in the according Chapters 4 – 7.

Table 3.1: Overview of the investigated tuffs. Classifications according to Figures 3.1 and 3.2

Sample	ID	Origin	Age	Classification LeBas et al. (1986)	Classification Schmidt (1981)	Classification Fisher (1966)
Blanca Pachuca	BP	Mexico	Pliocene	Rhyolite	crystal	ash tuff
Cantera Rosa	CR	Mexico	Oligocene	Rhyolite	crystal	ash-lapilli tuff
Cantera Verde	CV	Mexico	Miocene	Rhyolite	crystal	ash tuff
Mitla Rosa	MR	Mexico	Miocene	Rhyolite	crystal	ash-lapilli tuff
Blue Sevan	BS	Armenia	Cretaceous	Rhyolite	crystal	ash tuff
Noyemberyan	NB	Armenia	Cretaceous	Rhyolite	crystal	ash tuff
Golden Armenia	GA	Armenia	Cretaceous	Rhyolite	crystal	lapilli tuff
Hilbersdorf	HD	Germany	Permian	Rhyolite	crystal	lapilli tuff
San Miguel el Alto	SMA	Mexico	Paleogene	Rhyolite	vitric	lapilli tuff
Queretaro Blanco	QB	Mexico	Pliocene	Rhyolite	vitric	lapilli tuff
Hoktemberyan Red	HR	Armenia	Pleistocene	Trachyte	vitric	lapilli tuff
Artik Rosa	AR	Armenia	Pleistocene	Trachyte	vitric	tuff breccia
Ani Peach	ANI	Armenia	Quaternary	Rhyolite	vitric	lapilli tuff
Loseros	LOS	Mexico	Oligocene	Rhyolite	lithic	ash tuff
Weibern	WB	Germany	Pleistocene	Trachyt-Phonolite	lithic	lapilli tuff

##### 3.2.1 Petrographic summary

Geochemically most of the investigated tuffs are of rhyolitic and trachytic composition (Tab. 3.1, Fig. 3.2). Only the Weibern tuff (WB) shows an intermediate trachytic to phonolitic composition, with low SiO<sub>2</sub> (59.1 wt.%) and high Na<sub>2</sub>O and K<sub>2</sub>O content (>10 wt.%). Note that all crystal tuffs are clearly acid, with SiO<sub>2</sub> content >70 % (compare Fig. 3.2 and Tab. 3.2). The Na<sub>2</sub>O + K<sub>2</sub>O content of the vitric tuffs is relatively consistent around 8 wt.%. In the dataset, vitric tuffs are generally young rocks of Cenozoic age, while crystal tuffs may be multiple times older (up to Permian) (Tab. 3.1). It reflects the fact that, over the course of time, the glassy material in the older tuffs, due to its' thermodynamic instability, is often altered to fine clay and zeolite crystals (Fisher and Schmincke 2012).

### 3 Tuffs under investigation

After the classification scheme of Schmid (1981), BP, CR, CV, MR, BS, NB, GA and HD can be defined as crystal tuffs. SMA, QB, HR, AR and ANI can be classified as vitric tuffs and LOS and WB are lithic tuffs (Fig. 3.1). Regarding the size of pyroclastic fragments (Fisher 1966), the investigated tuffs are mainly defined as ash tuffs and lapilli tuffs. AR is the only representative of tuff breccia. Notice that the crystal rich tuffs are mostly ash tuffs and lapilli tuffs with high ash content. Only the vitric tuffs show higher amounts of lapilli and bombs, which are often present in the form of pumice clasts.

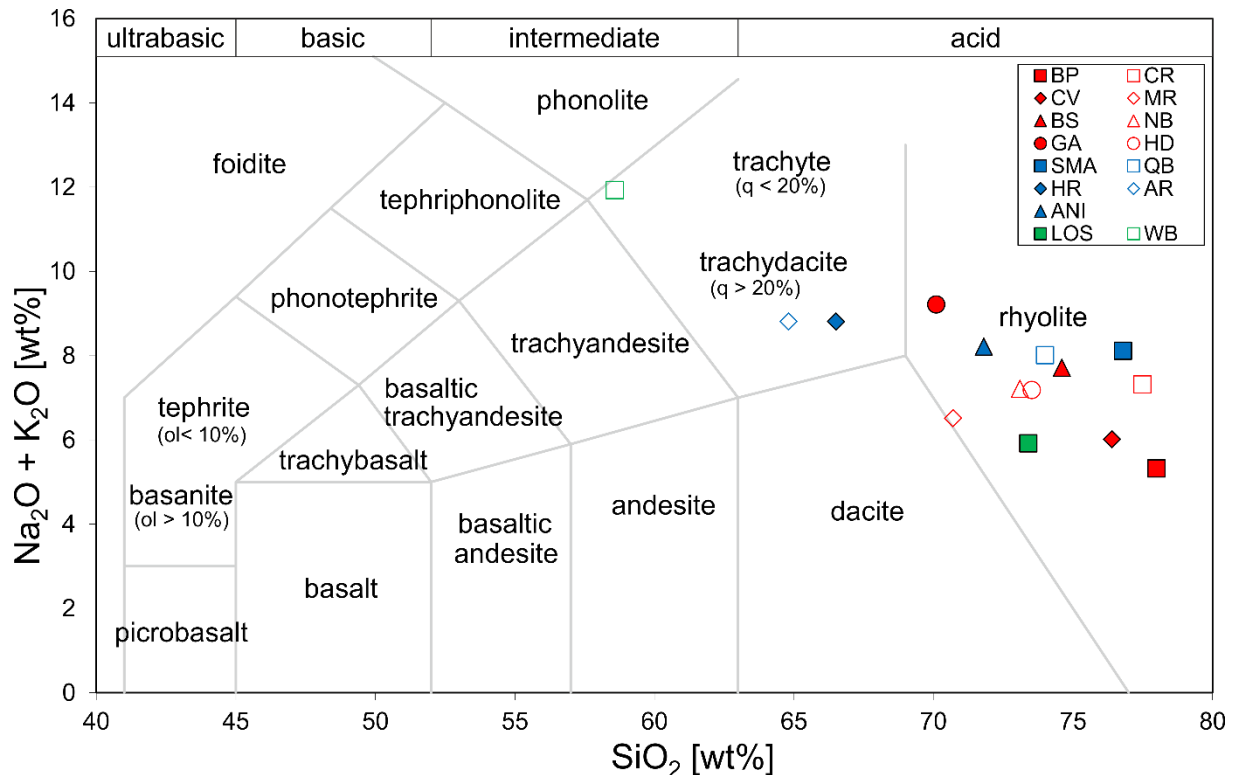


Figure 3.2: Geochemical classification of the volcanic igneous rocks according to the total alkali-silica diagram after Le Bas et al. (1986). The tuffs are colored after their main pyroclastic content: crystal tuff in red, vitric tuff in blue and lithic tuff in green.

Table 3.2: XRF data in [wt. %] as source data for Figure 3.2

Sample	SiO <sub>2</sub>	Al <sub>2</sub> O <sub>3</sub>	Fe <sub>2</sub> O <sub>3</sub>	CaO	MgO	K <sub>2</sub> O	Na <sub>2</sub> O	MnO	TiO <sub>2</sub>	P <sub>2</sub> O <sub>5</sub>
BP	78.0	13.2	1.1	1.9	0.3	4.0	1.3	0.01	0.1	0.01
CR	77.5	12.7	1.4	0.4	0.2	5.5	1.8	0.02	0.1	0.02
CV	76.4	13.0	1.5	2.0	0.7	5.1	0.9	0.03	0.1	0.03
MR	70.7	15.8	2.3	3.3	0.7	2.8	3.7	0.03	0.4	0.11
BS	74.6	13.5	1.5	1.3	0.8	4.8	2.9	0.03	0.3	0.05
NB	73.1	14.0	1.8	2.8	0.5	4.9	2.3	0.04	0.2	0.04
GA	70.1	14.7	3.4	1.0	1.0	6.0	3.2	0.10	0.4	0.08
HD	73.5	12.3	2.4	1.1	0.4	7.0	0.1	0.05	0.1	0.02
SMA	76.8	12.7	1.7	0.2	0.1	5.0	3.1	0.04	0.1	0.01
QB	74.0	13.5	2.5	0.9	0.5	4.1	3.9	0.04	0.3	0.06
HR	66.5	15.9	3.6	2.5	1.1	3.9	4.9	0.08	0.9	0.23
AR	64.8	16.1	4.2	3.1	1.3	4.0	4.8	0.09	1.0	0.29
ANI	71.8	15.1	2.0	1.7	0.5	4.2	4.0	0.06	0.4	0.07
LOS	73.4	13.2	2.4	3.4	0.9	4.1	1.8	0.10	0.2	0.07
WB	59.1	20.1	4.1	2.7	0.9	6.1	5.7	0.17	0.51	0.15





### 3 Tuffs under investigation

#### 3.2.2 Short profiles

##### **Blanca Pachuca (BP)** – (Pachuca de Soto, Mexico)

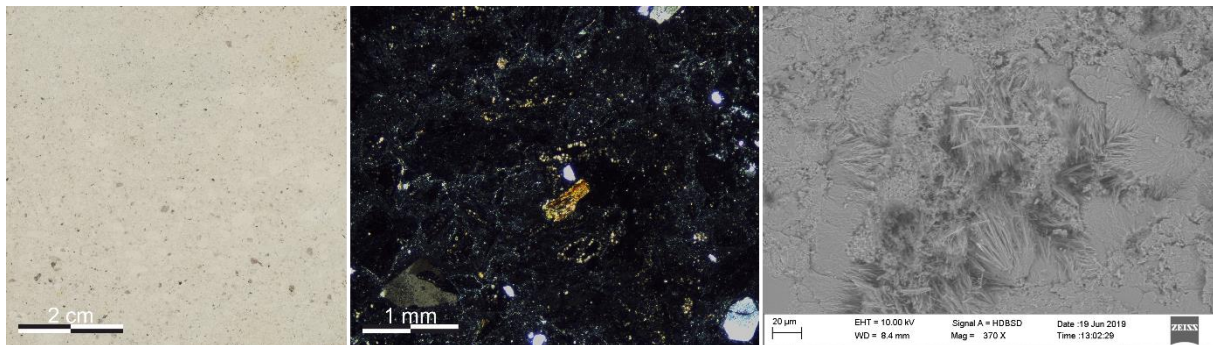


Figure 3.3: Macroscopic scan (left), thin section photomicrograph (center) and SEM photomicrograph (right)

The Blanca Pachuca (BP) is a fine-grained ash tuff of rhyolitic composition, with a whitish groundmass and plenty of greyish-brownish, rarely reddish and black, phenocrysts that give a slightly speckled appearance (Fig. 3.3), but cannot be identified macroscopically. In thin section, quartz, potassium feldspar, plagioclase, biotite and clay minerals can be observed in a cryptocrystalline matrix. XRD identified swellable clay minerals (smectite) and a range of zeolites (mordenite, heulandite, clinoptilolite). SEM photomicrographs show mordenite needles reaching into the pore space. Overall, the glassy matrix is mainly altered to zeolite and clay (Fig. 3.3). BP has a notably high cation exchange capacity (CEC) of 12 meq/100 g and a specific surface area (BET) of 17 m<sup>2</sup>/g. The former glass rich BP is, due to alteration processes, now characterized as highly rich in clay and zeolite crystals. After the classification system of Schmid (1981) and Fisher (1966), BP categorizes as crystal-rich ash tuff (Fig. 3.1).

##### **Cantera Rosa (CR)** – (San Luis Potosi, Mexico)

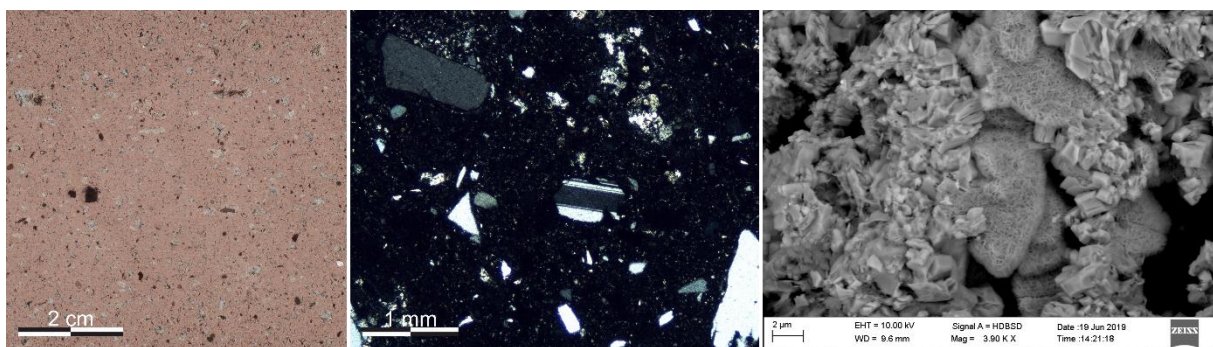


Figure 3.4: Macroscopic scan (left), thin section photomicrograph (center) and SEM photomicrograph (right)

Cantera Rosa (CR) is a massive, crystal rich rhyolite of characteristic pinkish color. It macroscopically and microscopically shows a porphyritic texture, with large amounts of quartz and feldspar phenocrysts as well as pumice clasts up to 20 mm in size, embedded in a fine cryptocrystalline groundmass (Fig. 3.4). In thin section, quartz and sanidine crystals are especially abundant. In SEM photomicrographs the groundmass shows to be altered and devitrified and now consists of a mix of clay, quartz and feldspar crystals. XRD identified the clay minerals as swellable smectite, as well as muscovite/illite and kaolinite. The CEC is

### 3 Tuffs under investigation

accordingly increased (6 meq/100 g). CR is classified as crystal tuff according to Schmid (1981) and as lapilli rich ash tuff to Fisher (1966).

#### Cantera Verde (CV) – (Etna, Mexico)

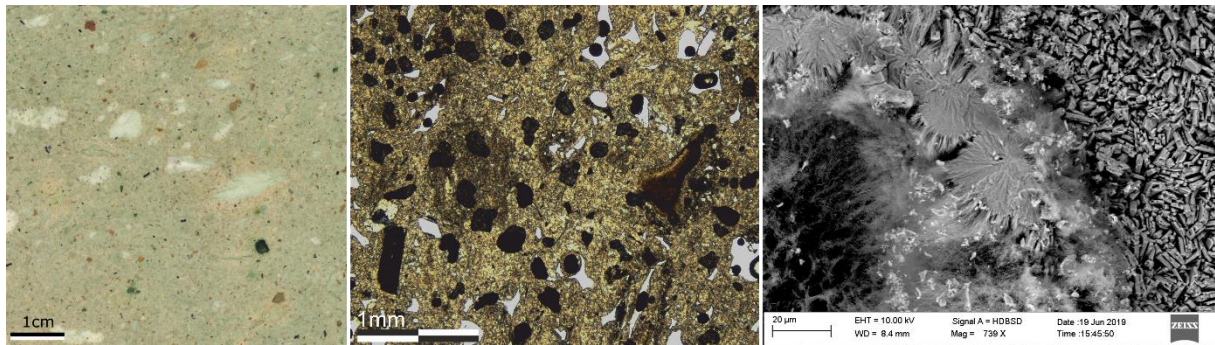


Figure 3.5: Macroscopic scan (left), thin section photomicrograph (center) and SEM photomicrograph (right)

Cantera Verde (CV) is a relatively homogenous, light-pistaccio green crystal-rich ash tuff (according to Fisher (1966) and Schmid (1981)) of rhyolitic composition. Macroscopically noticeable are white clay lenses (Fig. 3.5), which dissolve when in contact with water. The crystals are often strongly weathered. CV has a hypocrystalline to cryptocrystalline matrix with vitrophyric texture. The vitreous matrix, however, is strongly altered to zeolite (clinoptilolite and mordenite) and clay minerals (smectite, illite, chlorite and potentially kaolinite). The crystals are often strongly weathered. SiO<sub>2</sub> is present in the form of cristobalite. Pablo-Galán (1986) describes the formation of zeolites in CV by alkaline diagenesis of rhyolitic glass. SEM photomicrographs reveal very fine-grained zeolites in CV, causing its high specific surface area. They are mainly euhedral mordenite needles and clinoptilolite laths, which were also reported by Mumpton (1973) and Llanes-Monter et al. (2007).

#### Mitla Rosa (MR) – (Mitla, Mexico)

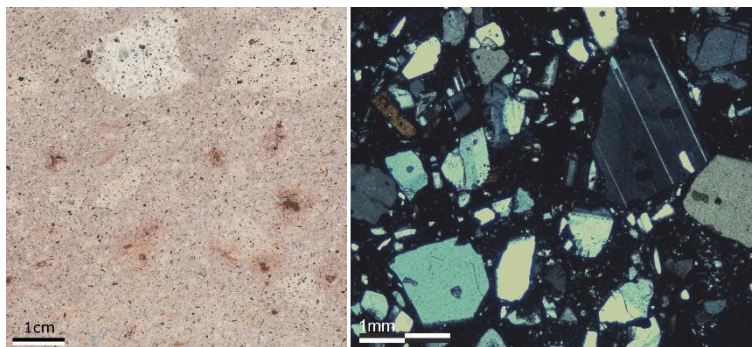


Figure 3.6: Macroscopic scan (left), thin section photomicrograph (right)

Mitla Rosa (MR) is a dense, rhyolitic crystal tuff with small pores and crystals of up to 3 mm size. It has a pink matrix, which is in some parts discolored (leached) to white (Fig. 3.6). The macroscopically white areas of the matrix show a higher amount of fine ash than the pink areas, while both are very similar in texture. The thin section shows an overall small proportion (10 %) of cryptocrystalline to microcrystalline matrix with seriate texture. The crystals are hypidiomorphic and poorly altered. Plagioclase, quartz, potassium feldspar, biotite, hornblende and clay minerals were identified. XRD identified high amounts of smectite and

### 3 Tuffs under investigation

moderate amounts of muscovite/illite. The coloration of Mitla Rosa may be induced by chemical alteration, rather than petrological variation, as it migrates through the specimen. According to Schmid (1981) MR can be classified as crystal tuff and after Fisher (1966) as lapilli-rich ash tuff.

#### **Blue Sevan (BS)** – (Noyemberyan, Armenia)

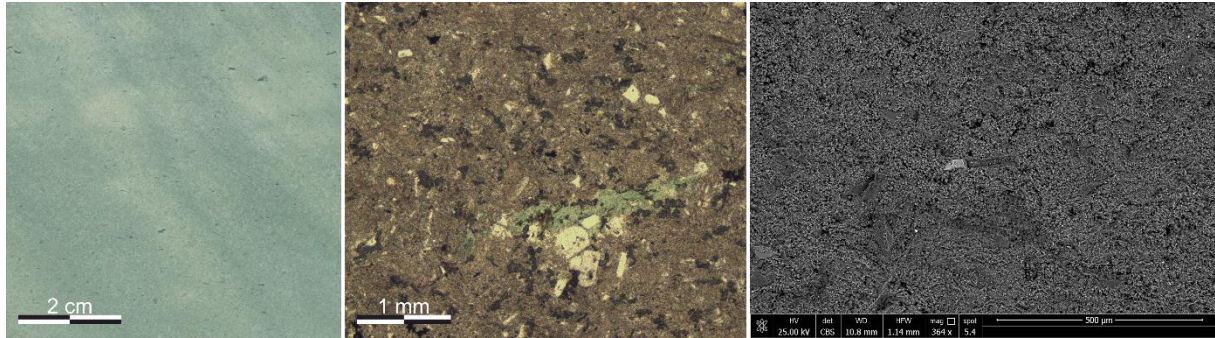


Figure 3.7: Macroscopic scan (left), thin section photomicrograph (center) and SEM photomicrograph (right)

The Blue Sevan (BS) (which is named Haghartsin Green (HG) in Chapter 4) has a characteristic green color and is of rhyolitic composition. It is very fine-grained and bottle-green elongated fragments, in the micrometer to millimeter scale, indicate a lamination (Fig. 3.7). In thin section, this tuff shows about 80 % cryptocrystalline matrix, with few mono- and polycrystalline quartz crystals as well as feldspar phenocrysts embedded. The bottle-green fragments often show chloritization processes. In SEM photomicrographs, huge amounts of frayed edge clay minerals are oriented parallel to the bedding. They are located both at grain contacts and mixed into the fine-grained matrix consisting of quartz and feldspar. XRD of separated clay fractions identified them as intracrystalline swellable smectites (Tab. 3.3). Illite/muscovite, kaolinite and analcime, a mineral of the zeolite group, could also be identified. Huge apatites and feldspar relics as well as muscovites can occasionally be observed. The CEC is very high (9 meq/100 g). BS is classified as crystal-rich ash tuff according to Schmid (1981) and Fisher (1966).

#### **Noyemberyan (NB)** – (Noyemberyan, Armenia)

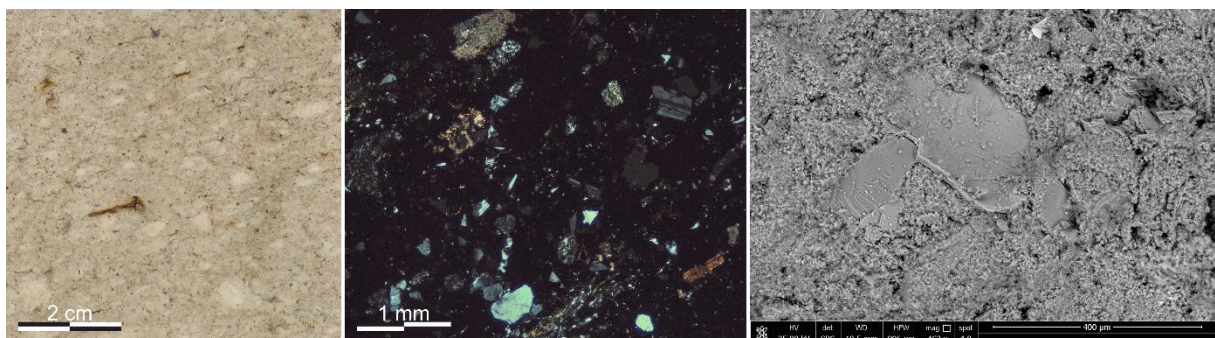


Figure 3.8: Macroscopic scan (left), thin section photomicrograph (center) and SEM photomicrograph (right)

The Noyemberyan tuff (NB) is a white to slightly greenish tuff of rhyolitic composition, which shows a weak lamination in form of white and grey elongated lithic fragments (Fig. 3.8). Many of the grey lithic fragments are framed by slightly orange to reddish margins. Macroscopic NB

### 3 Tuffs under investigation

appears to be a fine-grained tuff. Only in exceptional cases the lithic fragments reach sizes up to one centimeter. Thin section images confirm the large amounts of fine matrix groundmass (70 %). The remaining 30 % of the rock consist of partly large angular and zoned plagioclase crystals as well as small, rounded quartz fragments. SEM photomicrographs identify huge amounts of fibrous mordenite clusters and frayed edge clay minerals (see Chapter 4). Calcites and muscovites can reach dimensions up to 300  $\mu\text{m}$ . Rarely apatite can be observed. Huge amounts of mordenite, a mineral of the zeolite group, and intracrystalline swellable smectitic layers in an illite–smectite mixed layer mineral were identified by XRD on separated clay fractions and confirm a moderate CEC of 3.1 meq/100 g. The classification system after Schmid (1981) and Fisher (1966) categorize NB as crystal-rich ash tuff.

#### **Golden Armenia (GA)** – (Noyemberyan, Armenia)

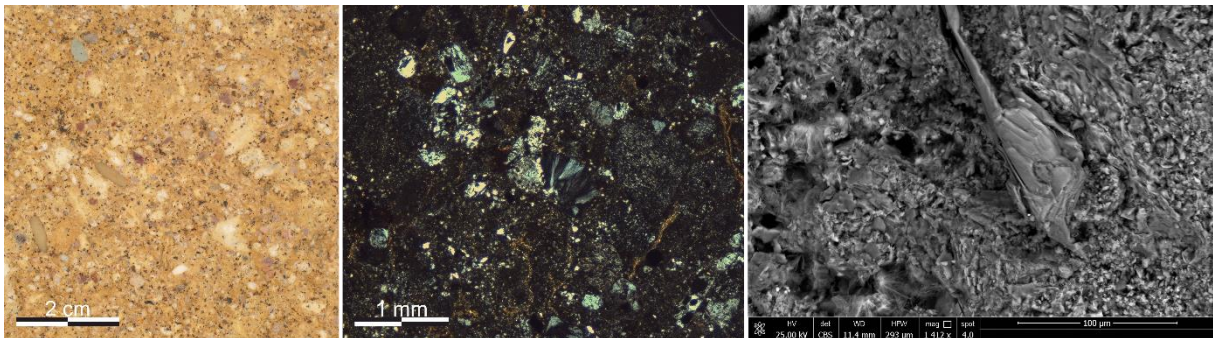


Figure 3.9: Macroscopic scan (left), thin section photomicrograph (center) and SEM photomicrograph (right)

The Golden Armenia (GA) tuff is of rhyolitic composition. It shows a yellowish-golden ground mass with beige, grey and slightly reddish clasts embedded (Fig. 3.9). GA appears rather massive, with high amounts of dense, volcanic fragments as well as feldspar and quartz phenocrysts. In thin section Golden Armenia (GA) shows high amounts of volcanic lithoclasts and relics of feldspar in a glass- and crystal-rich matrix (~25 %), as well as a considerable amount of vitric fragments (5 %). SEM images confirm the presence of clay minerals especially at grain boundaries and in the open pore space. The clay minerals show a cornflake microstructure and frayed edges. XRD on separated clay fractions identified them as illite/muscovite and corrensite (Tab. 3.3), a mixed layer clay mineral with intracrystalline swellable vermiculite layers. Devitrification processes and prismatic apatites as well as biotite and augite were observed in SEM photomicrographs. The CEC of 3 meq/100 g is moderate. According to the classification systems of Schmid (1981) and Fisher (1966), GA can be classified as crystal-rich lapilli tuff.

### 3 Tuffs under investigation

#### Hilbersdorf (HD) – (Chemnitz, Germany)

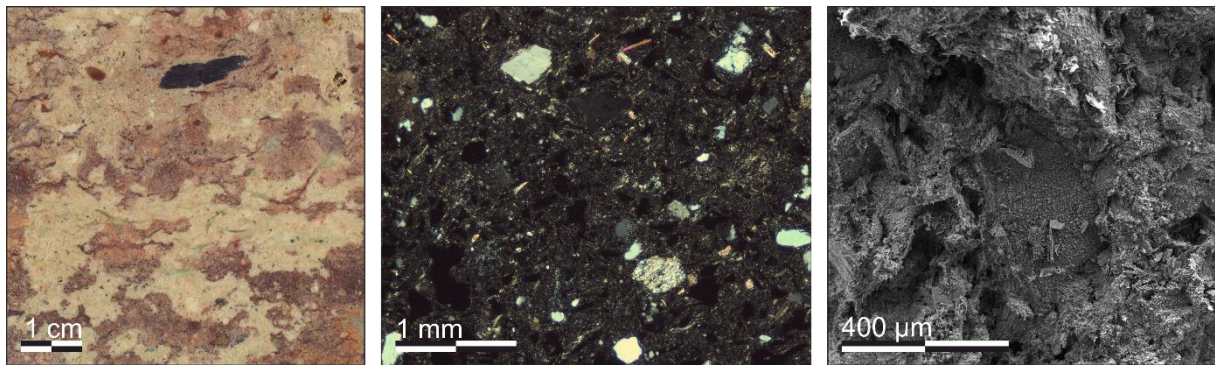


Figure 3.10: Macroscopic scan (left), thin section photomicrograph (center) and SEM photomicrograph (right)

The Hilbersdorf tuff (HD) occurs in different varieties with regard to its macroscopic appearance and application as a building material. The varieties differ in grain size and color. They can appear versatile and transitions are likely. Based on the macroscopic appearance and its local occurrence, the Hilbersdorf tuffs were subdivided into seven varieties that are used as natural building stones, of which five varieties were analyzed in greater detail in Chapter 6. According to the subdivision, the variety presented here is labeled Hilbersdorf Regular (HR) in Chapter 6.

The Hilbersdorf tuff (HD) represents a frequently used material in construction in Chemnitz and its surroundings. It appears irregularly speckled and partly marbled in colors of pale pink to dark purple and bright beige to greenish with fluent transitions. Various types of elongated lapilli inclusions at the millimeter to centimeter scale are embedded and can indicate a lamination (Fig. 3.10). This variety can contain several millimeters to centimeter large cavities, partly filled with loose clayey material, which disintegrate when in contact with water. The microscopic difference between the reddish and bright parts of the rock is highly visible. In thin section, mono- and polycrystalline quartz, relics of feldspar and lithic clasts (rich in sericite) are found, as well as small and columnar muscovites. They are embedded in a glassy matrix (~ 70 %) mostly altered to clay and give a hypocrystalline texture. Rarely, calcite can be found. Especially in the bright areas, the eutaxitic texture is striking. The clasts and crystals in the bright area are of much smaller size. Devitrified glass shards can also be observed in the bright parts of this variety. Iron oxides, probably hematite (confirmed by XRD), are well distributed throughout the red colored parts of the stone. SEM images show high amounts of clay material (illite/muscovite) as well as pseudo-hexagonal booklets of kaolinite. In SEM, traces of calcite and fluorite were detected. The clay material shows varying appearance in the different areas of the rock. Illite/muscovite and kaolinite were identified in separated clay fractions by XRD (Tab. 3.3). Intracrystalline swellable layers (smectitic layers) were  $\pm$  absent. The CEC is very small (< 1 meq/100 g). HR can be classified as crystal-rich lapilli tuff according to Schmid (1981) and Fisher (1966).

### 3 Tuffs under investigation

#### San Miguel el Alto (SMA) – (San Miguel el Alto, Mexico)

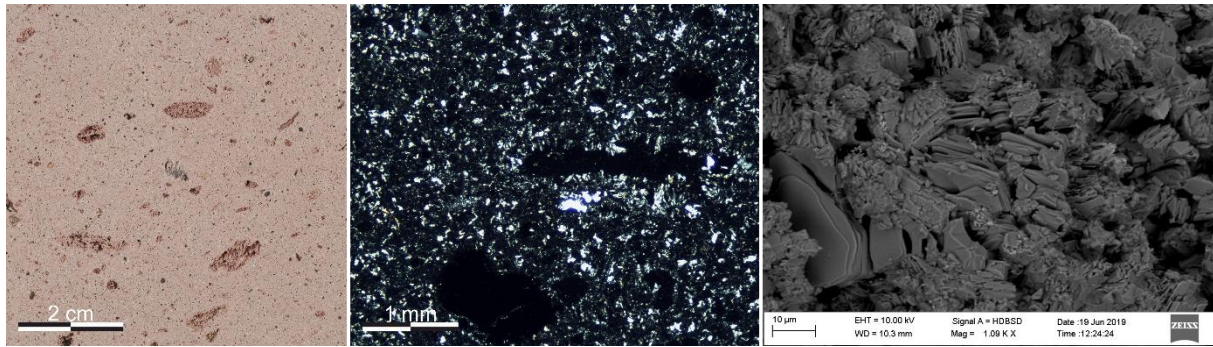


Figure 3.11: Macroscopic scan (left), thin section photomicrograph (center) and SEM photomicrograph (right)

The rhyolitic San Miguel el Alto (SMA) consist of a fine and homogenous vitric groundmass of characteristic pinkish color, in which plenty of elongated pumice clasts are embedded. The pumice clasts are typically in the millimeter to centimeter range and indicate direction. In thin section, SMA shows an abundance of small quartz and feldspar crystals, embedded in a glass rich matrix. XRD identified rare kaolinite-smectite mixed-layer minerals, which are abundant in SEM photomicrographs (Fig. 3.11). Glass shards and biotite are rarely seen. With 4 meq/100 g, the CEC is moderately high. According to Schmid (1981) and Fisher (1966), SMA can be classified as vitric lapilli tuff.

#### Queretaro Blanco (QB) – (Queretaro, Mexico)

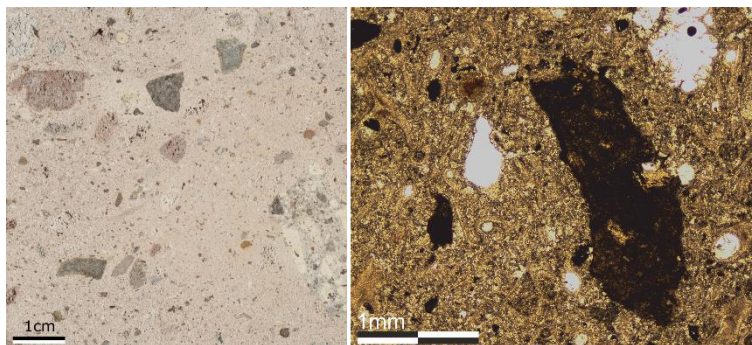


Figure 3.12: Macroscopic scan (left), thin section photomicrograph (right)

Querétaro Blanco (QB) is a white to gray rhyolitic lapilli tuff with a high amount of pumice and glass within the matrix. It has a very porous appearance and lithic fragments of more than 1 cm size are macroscopically visible (Fig. 3.12). The lithic fragments have a wide range of colors and are often angular. The thin section of QB shows a vitrophyric texture with very few crystals and lithoclasts embedded in a glassy matrix. The crystals are identified as plagioclase, quartz and hornblende and are often strongly altered. XRD identified high temperature modifications of  $\text{SiO}_2$  (tridymite and cristobalite) and swellable clay minerals (smectite). With 2 meq/100 g, the CEC is considerably low. QB is classified as vitric lapilli tuff (Fisher 1966; Schmid 1981).

### 3 Tuffs under investigation

#### Hoktemberyan Red (HR) – (Armawir, Armenia)

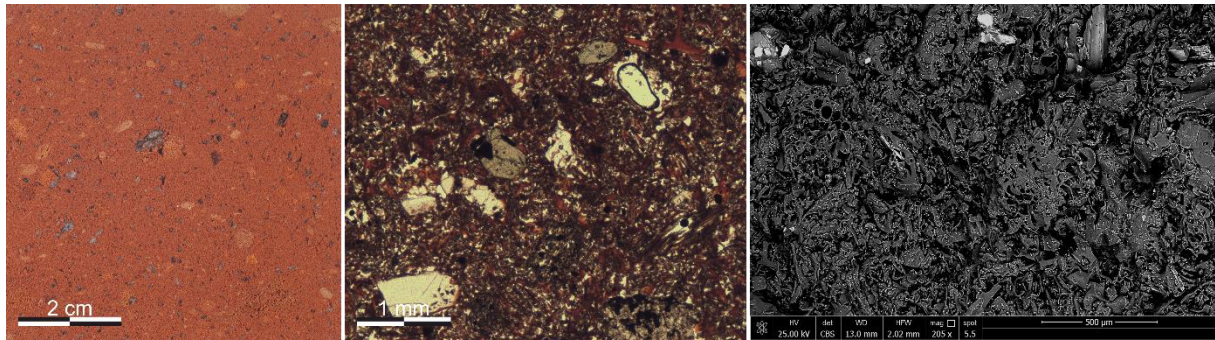


Figure 3.13: Macroscopic scan (left), thin section photomicrograph (center) and SEM photomicrograph (right)

The Hoktemberyan Red (HR) has a striking brick-red color and chemically classifies as trachyte (Fig. 3.13). In its glass rich ground mass, huge amounts of elongated white feldspar phenocrysts and glass particles are embedded and give a slightly speckled appearance. Black and red elongated pumice at the millimeter to centimeter scale, are embedded in the groundmass and indicate an orientation. In thin section, HR shows feldspar and amphibole phenocrysts embedded in a high amount of glassy matrix (~ 75 %), with high amounts of iron oxides. Volcanic lithoclasts and opaque minerals each make about 5 % of the sample. In SEM micrographs, the difference in porosity between matrix and clasts is striking. Huge parts of these consist of amorphous glass and especially in the matrix area, tiny pores are present. Rarely clay minerals with characteristic frayed edges in the pores of the glassy matrix are observed. HR shows a low CEC (1.2 meq/100 g). HR is classified as vitric lapilli tuff (Fisher 1966; Schmid 1981).

#### Artik Rosa (AR) – (Artik, Armenia)

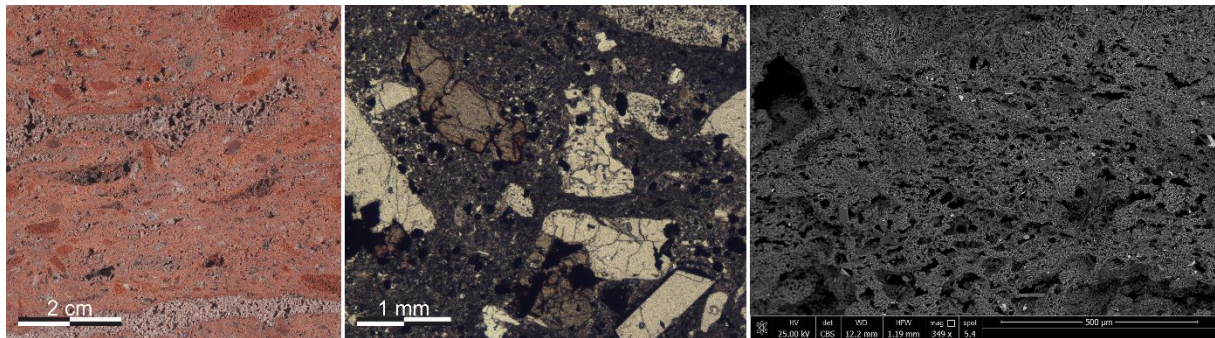


Figure 3.14: Macroscopic scan (left), thin section photomicrograph (center) and SEM photomicrograph (right)

The Artik Rosa (AR) is a highly porous tuff of pink to reddish color, which classifies as vitric tuff breccia according to Schmid (1981) and Fisher (1966). Various types of elongated lapilli, mostly clasts of pumice at the centimeter to decimeter scale, are embedded (Fig. 3.14). The pumice clasts that range in size from few millimeters up to 30 centimeter are of red, brown and grey color, while larger pumice up to the decimeter scale are of grey tones, with transition to brown on their edges. The pumice clasts often show open pores in the centimeter range. Another distinct characteristic of the AR is the huge amount of partly elongated white phenocrysts and glass particles at the millimeter scale. Rarely basaltic clasts at the millimeter to centimeter scale are observable. In thin section, the Artik tuffs show a porphyritic texture with varying,

### 3 Tuffs under investigation

but always high, amounts of large feldspar crystals (up to 40 %), relicts of amphiboles and muscovites as well as lithic clasts of intermediate composition in a cryptocrystalline, glassy matrix of up to 60 % (Fig. 3.14). The matrix and pumice clasts are typically covered by considerable amounts of iron oxides. SEM micrographs point out the apparent differences of huge pores in the pumice clasts and smaller pores in the matrix area. Apatites and longprismatic amphiboles are often observed in the big open pores of the pumice clasts. They reach as single crystals into the open pore space. Seldom small pyroxenes and ilmenites can be identified in the matrix. The barely observed muscovites are usually located as thin plates reaching into the open pore space of the pumice clasts. XRD on whole rock identified cristobalite, a high temperature modification of  $\text{SiO}_2$ . Illite/muscovite was identified by XRD of separated clay fractions. The CEC is low (1.2 meq/100 g).

#### Ani Peach (ANI) – (Armarwir, Armenia)

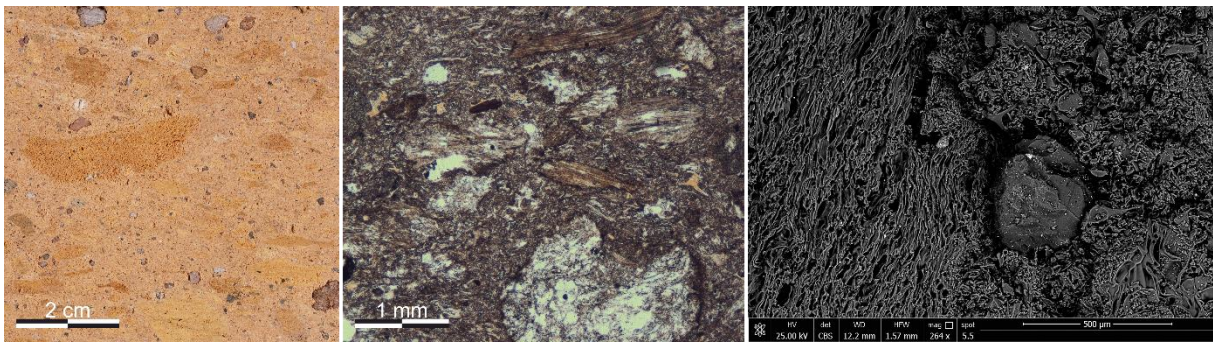


Figure 3.15: Macroscopic scan (left), thin section photomicrograph (center) and SEM photomicrograph (right)

The Ani Peach tuff (ANI) is of rhyolitic composition (Fig. 3.2) and consists of a huge amount of large, elongated, yellow to brownish clasts of pumice, embedded in a violet to peach-colored matrix. Reddish to black rock fragments in the millimeter to centimeter scale show a rather round shape. The pumice clasts are oriented, as shown in thin section and SEM (Fig. 3.15), and make up to 55 % of the rock. The fine-grained matrix makes up to 40 % of the rock and contains huge amounts of curved shape glass shards. Around 5 % of plagioclase crystals and small amounts of biotite can be observed. XRD confirms glass (large amorphous hump) and plagioclase. Traces of biotite and magnetite could be present as well, however, this is not clear by XRD (Chapter 4). ANI is classified as vitric lapilli tuff (Fisher, 1966; Schmid, 1981).

#### Loseros (LOS) – (Guanajuato, Mexico)

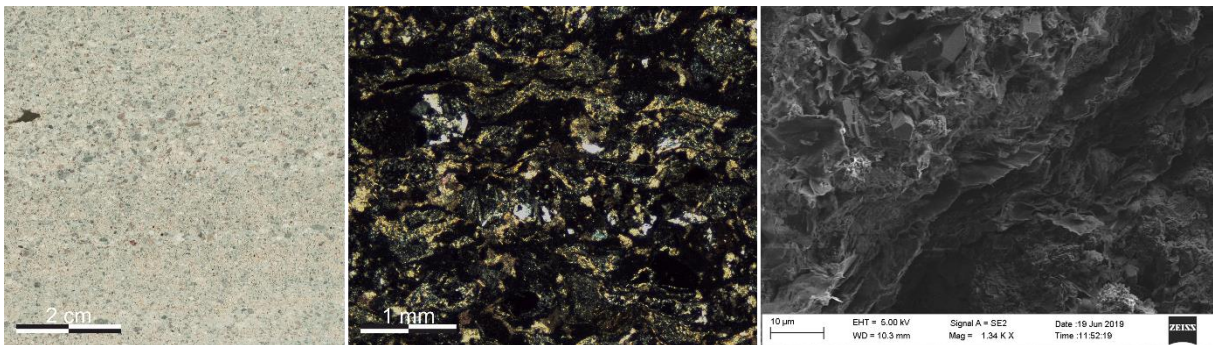


Figure 3.16: Macroscopic scan (left), thin section photomicrograph (center) and SEM photomicrograph (right)



### 3 Tuffs under investigation

The Loseros tuff (LOS) is characterized by a greenish laminated appearance (sometimes with a slightly purple or reddish tint), which is mainly caused by sand-sized crystals and rock fragments embedded in a fine, ash-rich matrix (Fig. 3.16). LOS is of rhyolitic composition and classifies as lithic ash tuff (Fisher 1966; Schmid 1981). In thin section, the main components are identified as lithic fragments, quartz, feldspar and plagioclase phenocrysts, whereby the lithic components dominate. LOS contains around 10 % of opaques and shows chloritization phenomena. The individual grains are cemented with a calcereous and argillaceous matrix. XRD identified smectitic mixed-layer minerals and kaolinite. SEM analyses located the clay minerals preferably at grain contacts. LOS shows a moderate CEC of 5 meq/100 g

#### **Weibern (WB)** – (Weibern, Germany)

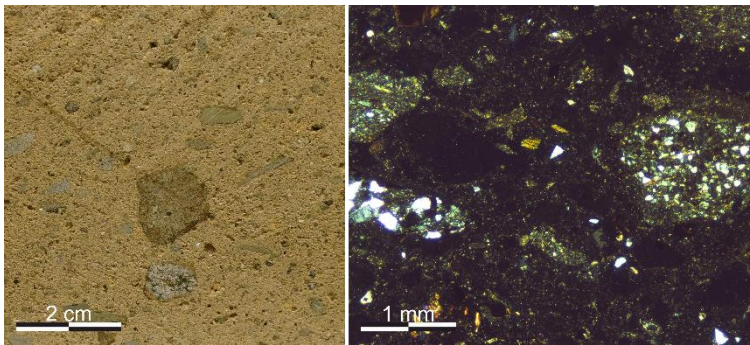


Figure 3.17: Macroscopic scan (left), thin section photomicrograph (right)

The Weibern tuff (WB) is of trachytic to phonolitic composition. In the literature, the reported composition of WB is usually phonolitic (Egloffstein 1998; Poschlod 1990; Stück et al. 2008). It has a characteristic fine-grained, yellowish to brownish groundmass, in which plenty of partly elongated volcanic and sedimentary clasts are embedded. Beside basalt, chert and sandstone clasts in the centimeter scale, yellowish pumice clasts of few millimeter size are abundant. Quartz, feldspar, leucite, calcite, hornblende and biotite could be identified in thin section. Some opaque minerals could not be identified. In thin section, also the high amount of lithics (~40 %) is striking (Fig. 3.17). Other authors report far less lithic components and higher amounts of vitric groundmass (Egloffstein 1998; Stück et al. 2008; Wedekind et al. 2013). These authors did also report significantly smaller sizes for the embedded rock fragments. SEM analyses were not conducted on WB. However, XRD analyses identified an abundance of zeolite material (analcime) and potential smectitic mixed-layer minerals, which points to the fact that the vitric groundmass of the tuff is already altered, like reported from van Hees et al. (2003). The CEC is moderately high (5meq/100 g). WB can be classified as lithic lapilli tuff according to Schmid (1981) and Fisher (1966). The boundary, however, is fluent. Since we did not determine the cryptocrystalline groundmass any further by SEM, it as well may not be altered to zeolite yet and therefore classify as vitric tuff.

## 4 Deterioration of volcanic tuff rocks from Armenia

In this chapter, the focus is on the investigation of the weathering behavior of volcanic tuff stones, that were applied in architectural monuments. The aim was to identify the main deterioration processes and their relation to the mineralogy (with special focus on the role of clay minerals) and rock physical properties of the tuff stones, in order to: (1) identify which types of tuff are especially resistant/susceptible to weathering and (2) to identify which parameters are mainly responsible for it. For that reason, a set of 19 tuffs (as well as two basaltic/trachyandesitic lavas) with a wide range of properties were investigated.

### 4.1 Introduction

For centuries, volcanic tuffs have been used as building material in many countries worldwide. Amongst others, prominent monuments made of tuff can be found in Columbia, Germany, Hungary, Italy, Mexico, Turkey as well as Armenia. The application of natural building stones, especially tuffs, in the unique Armenian architecture, which unites European with Persian and Indian style, has a long tradition. As the first country in the world, Armenia proclaimed Christianity as its state religion in 301 AD. Many sacred structures emerged in the early Christian period and endured natural and manmade hazards, such as earthquakes and armed conflicts. The UNESCO lists several constructions and artworks made of volcanic tuff stone in Armenia as World Heritage Sites and Intangible Cultural Heritage. Monasteries and medieval academies litter the country and demonstrate the great importance of education and tradition in Armenia, which are considered outstanding to this day. Along with basalt and limestone, volcanic tuff is the most popular natural stone used in the application (Gasparyan and Safaryan 2014). Due to the vast distribution of tuff deposits within the country, the material was and is still quarried and used for countless buildings nationwide (Fig. 4.1). Almost every facade is clad with varieties of the volcanic rocks in most diverse colors (Fig. 4.2). In the last decades, great efforts have been made to restore the monumental heritage of the country. Numerous ruinous monasteries and churches were reconstructed, but the original building stones were never conservationally treated and are subjected to a progressive weathering. Therefore, the building materials show various forms of deterioration and severe damages due to natural or anthropogenic causes. Architectural details disappear due to loss of surface phenomena such as sanding, flaking or scaling. Of particular importance is the loss of material, if thereby the stability of the building is endangered.

Main factors that influence the weathering behavior of tuff rocks are their specific petrophysical properties. Tuffs show considerable variation within each type. Their matrix grain sizes range from fine clay minerals up to silt size, in which crystals, glass and lithic rock fragments up to the gravel and block-size, can be embedded. Considerable amounts of clay mineral and zeolites are common and the arrangement of all tuff components together can create a very wide spectrum of porosities and fabrics (Fisher 1961; Le Maitre et al. 2002). Especially, if they are exposed to moisture and humidity, these characteristics cause tuff rocks to be less resistant towards deterioration (Ruedrich et al. 2011; Siedel 2010; Steindlberger 2004). Deterioration on buildings is often concentrated in areas where moisture is permanent or temporary available and leads to distinct damage phenomena. As a result of the regionally

#### 4 Deterioration of volcanic tuff rocks from Armenia

different geological conditions of origin, considerable differences result in the specific rock properties and the weathering behavior. The two factors that are recognized as major factors contributing to the weathering and deterioration of natural building stones are moisture expansion (Ruedrich et al. 2011; Weiss et al. 2004) and salt crystallization (Flatt 2002; Rodriguez-Navarro and Doehne 1999; Steiger et al. 2011). Moisture expansion is mostly associated with the swelling and shrinking behavior of clay minerals (De la Calle and Suquet 1988; Dixon and Weed 1989; Gonzalez and Scherer 2004; Graf v. Reichenbach and Beyer 1995; Schuh 1987; Snethlage et al. 1995; Stück et al. 2008). Recent studies also discuss the contribution of pores  $< 0.1 \mu\text{m}$  to a clay free swelling process referred to as disjoining pressure (Pötzl et al. 2018a; Ruedrich et al. 2011; Wedekind et al. 2013). For a detailed overview of the different swelling modes, see Kocher (2005) and Ruedrich et al. (2011). The intensity of moisture expansion varies markedly depending on the type of stone. Especially, tuff rocks have a wide range of moisture expansion (see Wedekind et al. (2013)). Furthermore, salt crystallization is considered one of the most aggressive forms of decay (Correns and Steinborn 1939; Doehne 2002; Hosono et al. 2006; López-Arce et al. 2011; Siegesmund and Dürrast 2011; Steiger et al. 2011). Salt crystallization within the pores of natural building stones generates stress that can lead to crack development and the disintegration of the rock (Flatt 2002; Rodriguez-Navarro and Doehne 1999).

#### 4 Deterioration of volcanic tuff rocks from Armenia



Figure 4.1: Historic buildings and artwork erected with local tuff stones all over Armenia. **a** Hayravank monastery at the western shores of Lake Sevan. **b** Hovhannavank monastery at the edge of the Kasagh River canyon. **c** Characteristic tessellated tuff facade at the Republic Square in Yerevan. **d** Colorful tuff facade at the Christian Education Center of the Apostolic Church in Etchmiadzin. **e** Open Air Altar at the residence of the Catholicos in Etchmiadzin. **f** Khachkars along the gavit of the Sevanavank monastery

#### 4 Deterioration of volcanic tuff rocks from Armenia

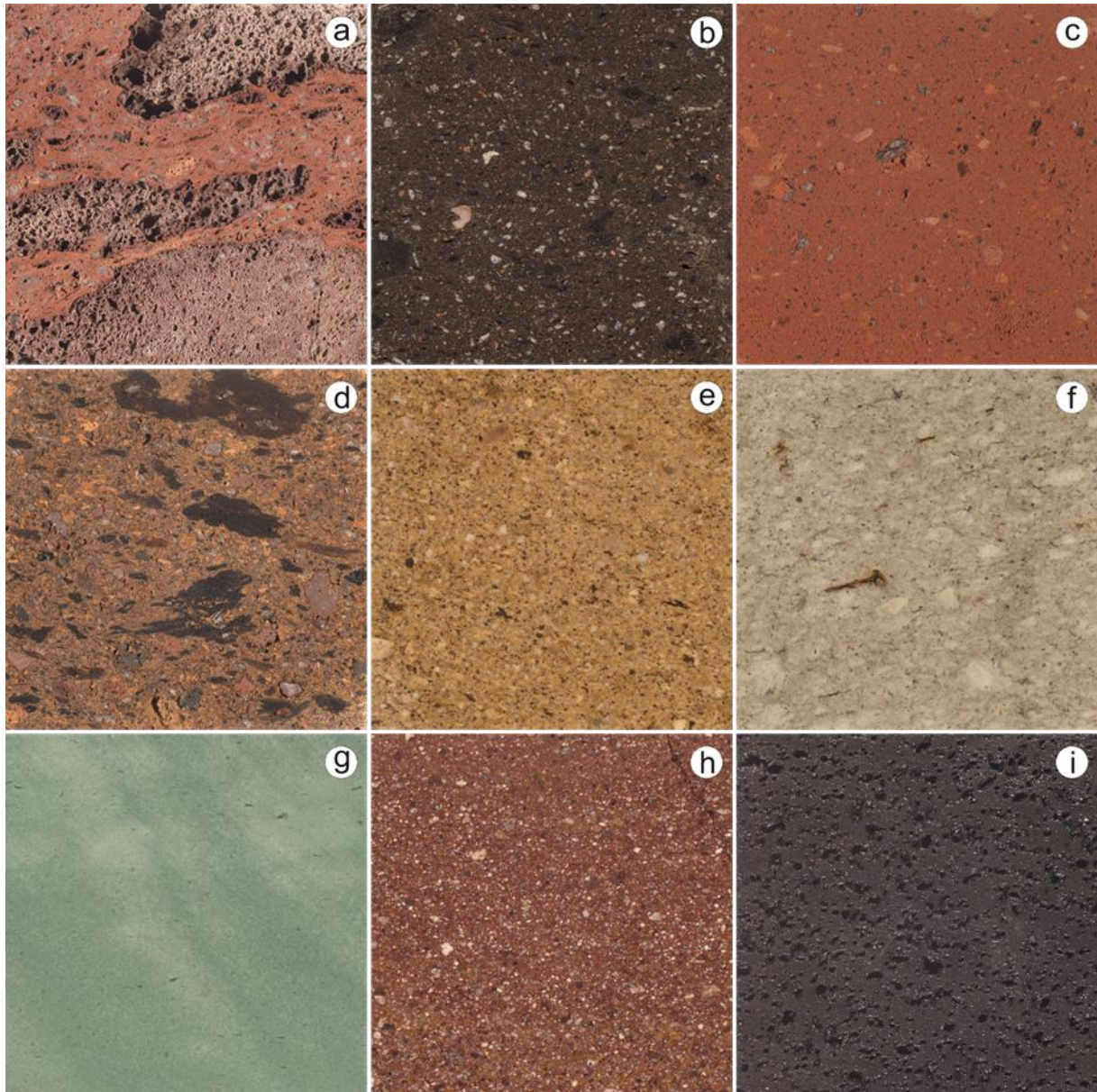


Figure 4.2: The chromatic and structural variation at mesoscopic scale of selected volcanites from Armenia (wet polished sections): **a** Artik 4 (ART4), **b** Hoktemberyan Brown (HB), **c** Hoktemberyan Red (HR), **d** Ujan Yellow (UY), **e** Golden Armenia Fine (GAF), **f** Noyemberyan (NB), **g** Haghartsin Green (HG), **h** Voskepar Red (VR), **i** Armenia Black (AB) (size of the photos: 6 cm × 6 cm).

The salt crystallization mechanisms are mostly influenced by the properties of the rock, the properties of the salt solution and the growing salt, as well as the environmental conditions. According to the capillary pressure model of Wellman and Wilson (1965), stones with mainly capillary pores are more susceptible to salt crystallization processes. Sousa et al. (2018) discuss the different features of salt crystallization and give an overview on controlling factors of salt crystallization in granitoids. For a more detailed overview on salt crystallization in volcanic tuff rocks, see López-Doncel et al. (2016). To understand the effect of crystal growth of salts in the porous structures of the tuffs from Armenia, the damage phenomena during accelerated aging due to salt bursting tests were observed. This study aims to evaluate the behavior of Armenian volcanic tuff rocks during wetting and accelerated aging due to salt bursting tests and understand how their mineralogy, their porous network as well as their water transport and retention properties affect the hydric expansion and salt weathering behavior. A deeper

## 4 Deterioration of volcanic tuff rocks from Armenia

understanding of the significant factors on hydric expansion and salt weathering of tuff rocks could finally lead to future prevention. To date there are no studies that systematically characterize the specific properties and the weathering behavior of Armenian tuff rocks that are used as building stone. As a result, the main reasons for the deterioration of these rocks remain unknown. In this study, for the first time ever, the petrographical and petrophysical properties as well as the weathering behavior of 21 Armenian volcanites, mainly tuffs, were systematically investigated. On the basis of this investigation, the causes and processes for specific weathering forms can be identified.

### 4.1.1 Geological background

Throughout its entire geological history, the country of Armenia was subjected to volcanic activity. Nevertheless, at the late-collision stage of the formation of the Armenian highland, the volcanic activity was most intense (Karapetian et al. 2001). Armenia is located in the northeastern part of the Anatolian–Armenian–Iranian plateau, which represents an intensely deformed segment of the Alpine–Himalayan belt (Meliksetian et al. 2014). A complex mosaic of tectonic blocks consisting of fragments of volcanic arcs, continental crust and exhumed oceanic crust represents the geological structure of this region (Meliksetian et al. 2014). At the northern part of the plateau, the Armenian Highlands are defined by the Lesser Caucasus, which represent the former active margin of Eurasia (Neill et al. 2013; Sheth et al. 2015). The southern part of Armenia is underlain by the South Armenian Block, a microcontinental fragment of Gondwana origin (Neill et al. 2013). The ophiolitic Sevan–Akeru suture zone forms a 300 km long boundary between the South Armenian Block, which consists of Proterozoic metamorphic rocks, Devonian to Jurassic sediments, Jurassic and younger ophiolites and Paleocene to Early Oligocene subduction-related volcanic rocks (Rolland et al. 2009), and the Mesozoic arc of the Lesser Caucasus (Neill et al. 2013). The Anatolian–Armenian–Iranian plateau is the product of the Cenozoic collision of the Arabian and Eurasian plates during the closure of the Neotethys between 35 and 20 Ma (Allen and Armstrong 2008; Keskin 2007). The collision resulted in an orogenic uplift and intense post-collisional volcanism from the late Miocene to the present day (Karapetian et al. 2001; Neill et al. 2013; Rolland 2017; Sheth et al. 2015). In the Lesser Caucasus, it is particularly attributed to the Miocene subduction, roll-back and potentially delayed detachment of the northern Neotethys slab (Neill et al. 2013). The erupted products are mostly basalts, ash fall deposits and ignimbrites. They can exceed up to a kilometer in thickness and cover a wide range from mafic to felsic composition (e.g., (Adamia et al. 2011; Allen et al. 2013; Azizi and Moinevaziri 2009; Karapetian et al. 2001).

### 4.1.2 Utilization and deterioration

The tuffs that are investigated in this study are widely used in the Armenian architecture and represent building stones of the country's most precious cultural heritage sites (Fig. 4.1). The Artik tuffs (Fig. 4.2a) are from the Shirak and Aragatsotn provinces, around the Aragats volcano. The Artik region is a centrum of the natural stone industry where at numerous outcrops tuffs are quarried. One of the most famous and best preserved monasteries in this region and all over Armenia, made of Artik tuff, is the Harichavank monastery near the town of Artik (Fig. 4.3).

#### 4 Deterioration of volcanic tuff rocks from Armenia



Figure 4.3: Schematic map of Armenia and the localization of the monuments where samples were taken during the field campaign

The oldest part of the monastery is the seventh century church of Saint Gregory the Illuminator, the patron saint and first official head of the Armenian Apostolic Church, who is credited with converting Armenia from paganism to Christianity in 301 AD. The building stones show many permanently moist areas and heavy salt contamination (Fig. 4.4a, b), which result in partly intensive alveolar weathering (Fig. 4.5a, b). West of the capital Yerevan, in the Armavir province, more sacral architectures are erected with the present Yerevan-type tuff rocks (Figs. 4.1b, d, e, 4.2b–d). The holy city and the country's spiritual capital Etchmiadzin (now Vagharshapat) is the domicile of the Catholicos of the Armenian Apostolic Church and its cathedral and churches are UNESCO World Heritage Site since 2000. The Cathedral of Etchmiadzin, respectively its original predecessor, is considered by several authors the oldest cathedral in the world, erected between 301 and 303 AD (Dhilawala 1997; Utudjian 1968). Especially at salt contaminated areas in the base area of the buildings, extensive crumbling and back weathering can be observed (Fig. 4.4). The typical back weathering of the matrix leads to a distinct protruding of the pyroclastic material. One of the popular Yerevan-type tuff varieties is the Oshakan tuff. It is quarried in the Aragatsotn province and amongst others was used to build the monastery of Hovhannavank in the beginning of the fourth century, at the edge of the Kasagh river canyon near the village Ohanavan (Fig. 4.1b). In salt contaminated and moist areas, the building stones show extensive back weathering in the form of intensive scaling (Fig. 4.4b).

#### 4 Deterioration of volcanic tuff rocks from Armenia

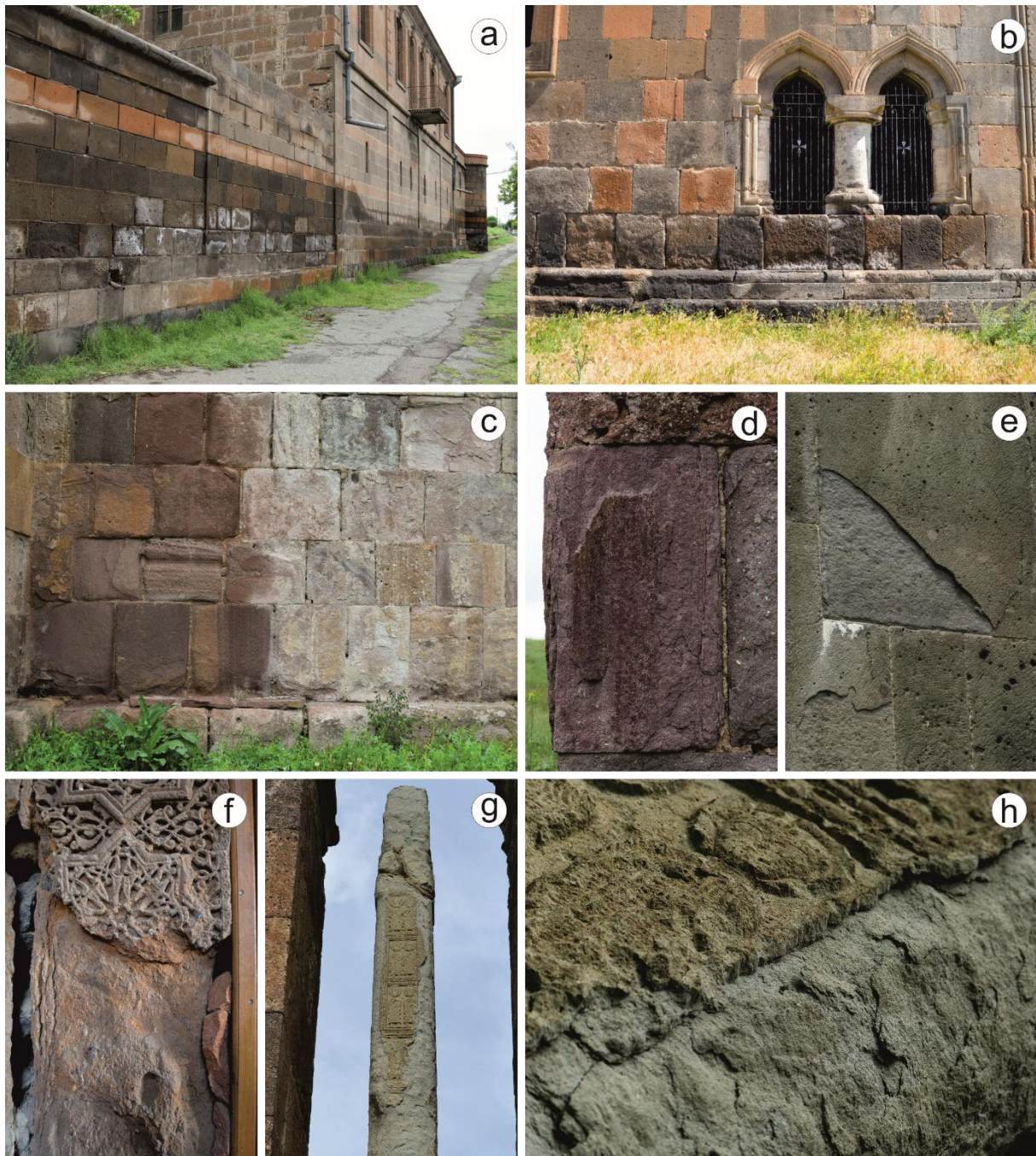


Figure 4.4: Different moisture and salt-related weathering forms: **a** Salt efflorescence at permanent moist areas of a compound wall in Etchmiadzin. **b** Crumbling and loss of material at the base area of the Hovhannavank monastery. **c** Extensive back weathering in moist areas and **d** scaling at the facade of the fifth century Voskepar monastery. **e** Scaling of a grey basalt at the Haghpat monastery. **f** Crumbling and scaling at the doorframe ornaments from the main church of the Hovhannavank monastery. **g**, **h** Scaling of the Haghartsin Green tuff (HG) at a stele from a funerary monument near the Odzun Church in the Lori province

The nowadays very popular, yellow tuffs with the trade name Golden Armenia (GAF, GAC) (Fig. 4.2e) were only used sporadic in historic architecture. Individual cross stones, the so-called khachkars (Fig. 4.1f), of this material can be found for instance at the Makaravank monastery or at the Sanahin monastery in the Tavush and Lori provinces, in the northeastern part of the country. Even though the rocks are located in protected recess areas, they show intensive weathering and deterioration forms. A breakup at the rock edges accompanied with intensive scaling and extensive loss of material is typical for this tuff variety. In addition, in the Tavush



#### 4 Deterioration of volcanic tuff rocks from Armenia

province, at the Haghartsin monastery, a green colored tuff (Fig. 4.2g) was used for several khachkars and stelae. Other prominent examples can be found near the Sevanavank monasteries at Lake Sevan (Fig. 4.1a, f) as well as the Odzun Church of the Lori province (Fig. 4.4g, h). The deterioration of the Haghartsin Green (HG) tuff is characterized by an intensive surface parallel flaking (Fig. 4.4g, h). At the seventh century Holy Mother of God Church in Voskepar, located at the Azerbaijanian border, a red and white speckled tuff (VR) was utilized for construction (Fig. 4.2h). The entire surface of the building is affected by intensive weathering. Dry areas show intensive scaling parallel to the rock surface, while in run-off areas of rainwater the rock material is evenly back weathered (Fig. 4.4c, d).

In the Lake Sevan area, basaltic and andesitic rocks were the preferred material for the construction of historical architecture (Fig. 4.2i). Famous examples are the Sevanavank and Hayravank monasteries, which are located at the northwestern Sevan peninsula and the southwest shores of Lake Sevan, respectively (Fig. 4.3). The facade areas that are protected from direct precipitation show intensive alveolar weathering (Fig. 4.5c). Overall, the field observations point out a widespread influence of salt crystallization and moisture expansion to the observed forms of weathering in Armenian tuff stones. Additionally, anthropogenic influence and natural hazards can cause diverse deterioration forms in the tuffs (Fig. 4.6). Severe structural damages such as deformation and crack formation can often be related to earthquakes (Fig. 4.6d, e), whereas inadequately executed mortar repairs are not only esthetically unsatisfactory, they are often themselves an additional source for damaging salts (Fig. 4.6b, c).

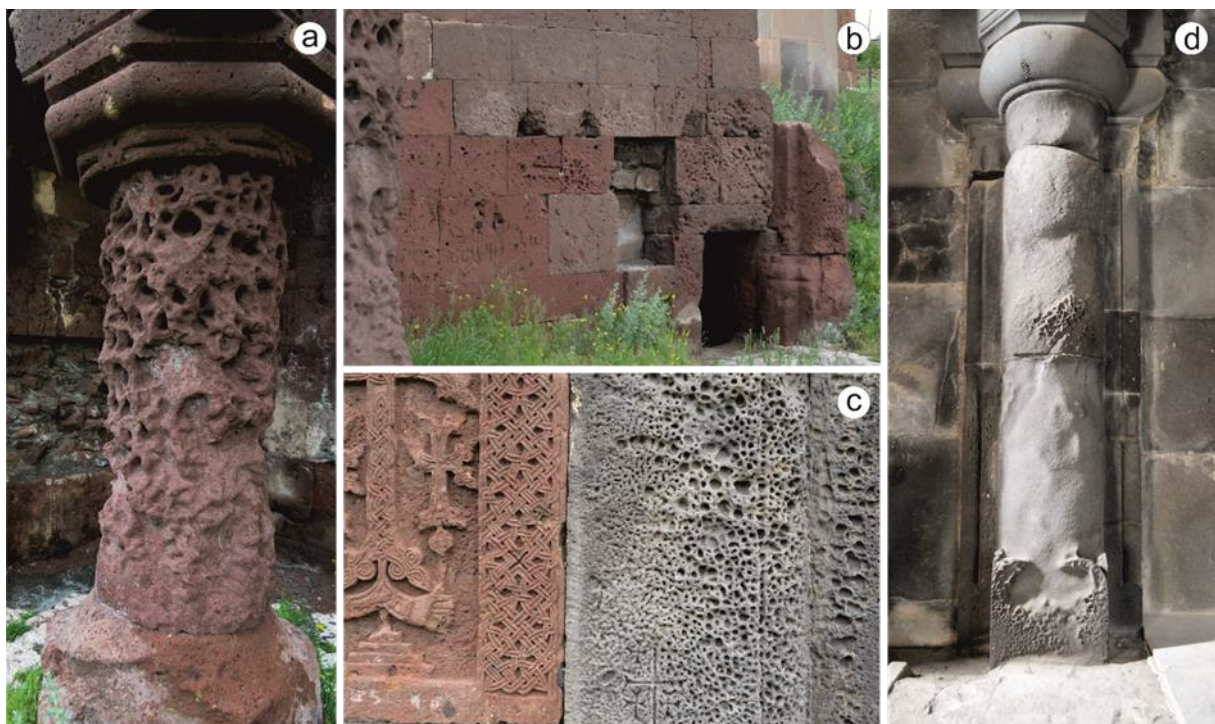


Figure 4.5: Different forms of alveolar weathering in Armenian tuffs and basalt: **a** Hand-sized alveoli at columns of the Harichavank monastery. **b** Alveolar weathering in moist areas of the tuff facade at the Harichavank monastery. **c** Alveolar honeycomb weathering of the Armenia Grey basalt (AG) at the Hayravank monastery. **d** Back weathering and alveolar weathering of a basalt column at the Makaravank monastery

#### 4 Deterioration of volcanic tuff rocks from Armenia



Figure 4.6: Different forms of deterioration due to anthropogenic and natural hazard causes: **a** Man-made carvings at the facade of the Khor Virap monastery. **b, c** Inadequately executed mortar repairs at the Sevanavank monastery. **d, e** Earthquake-related crack formation and deformation of tuff facades

#### 4.2 Petrography and mineralogy

In this study, a total of 21 volcanic stones from Armenia (Table 4.1), mainly tuff rocks, were investigated in terms of their petrographical and petrophysical properties, as well as their weathering characteristics. They correspond to 14 commercial varieties. The naming of the samples is linked to their quarry location or their trade names, respectively: Artik 1–7 (ART), Ani Peach (ANI), Hoktemberyan Brown (HB), Hoktemberyan Red (HR), Oshakan Black (OB), Oshakan Red (OR), Ujan Brown (UB), Ujan Yellow (UY), Golden Armenia Fine and Coarse (GAF,

#### 4 Deterioration of volcanic tuff rocks from Armenia

GAC), Noyemberyan (NB), Haghartsin Green (HG) (also called Blue Sevan), Voskepar Red (VR) Armenia Black (AB) and Armenia Grey (AG). Please note, that different commercial varieties can originate from the same volcanic event.

Table 4.1: List of the studied volcanic rocks. Sample name, abbreviation, total alkali-silica, classification after Le Bas et al. (1986)

Sample ID	Abbreviation	Total alkali-silica [wt.%]			Classification after Le Bas et al. (1986)
		SiO <sub>2</sub>	Na <sub>2</sub> O	K <sub>2</sub> O	
Artik 1	ART1	63.0	4.7	3.4	trachyte
Artik 2	ART2	64.3	5.0	4.0	trachyte
Artik 3	ART3	64.8	4.8	4.0	trachyte
Artik 4	ART4	64.5	5.0	3.8	trachyte
Artik 5	ART5	65.2	5.0	4.0	trachyte
Artik 6	ART6	60.7	4.5	3.6	trachyandesite
Artik 7	ART7	64.3	4.8	3.7	trachyte
ANI Peach	ANI	71.8	4.0	4.1	rhyolite
Hoktemberyan Brown	HB	64.5	4.7	3.8	trachyte
Hoktemberyan Red	HR	66.5	4.9	3.9	trachyte
Oshakan Black	OB	64.6	4.7	3.7	trachyte
Oshakan Red	OR	63.6	4.9	3.6	trachyte
Ujan Brown	UB	63.4	4.5	3.5	trachyte
Ujan Yellow	UY	63.0	4.5	3.3	trachyte
Golden Armenia Fine	GAF	69.2	3.8	5.2	rhyolite
Golden Armenia Coarse	GAC	70.1	3.2	6.0	rhyolite
Noyemberyan	NB	73.1	2.3	4.9	rhyolite
Haghartsin Green	HG	74.6	2.9	4.8	rhyolite
Voskepar Red	VR	69.0	0.1	0.5	dacite
Armenia Black	AB	58.5	4.1	2.6	trachyandesite
Armenia Grey	AG	48.0	3.8	1.1	basalt

The studied volcaniclastic rocks show a broad variety of color, grain size and clast content (Fig. 4.2). Their classification into the total alkali-silica diagram after Le Bas et al. (1986) is illustrated in Figure 4.7. For a better overview they were subdivided into several groups according to the condition of their formation, their structure and texture. The division partly took place according to the classification of Armenian tuffs by Shirinyan (1962), which is mainly based on regional distribution than generic similarities. (1) The Artik type tuffs are mainly found in the Shirak and Aragotsotn provinces and (2) pyroclastic tuffs of the Yerevan type originate from the western and northwestern parts of the capital. A third group (3) consists of the nowadays very popular Golden Armenia types and the Noyemberyan tuff, which are quarried in the northeast of Armenia, nearby the Georgian and Azerbaijanian border, respectively. A last group (4) consists of different tuffs quarried and used north of Lake Sevan, as well as two lavas from the Sevan area. The mineralogical composition of the investigated tuffs, including clay minerals, is listed in Table 4.2. Please note that due to the partly high amounts of glass and iron oxides within the cryptocrystalline matrix of the samples, the thin section micrographs will not be very informative in a printed version of the report, as for the major part they appear in very dark tones.

#### 4 Deterioration of volcanic tuff rocks from Armenia

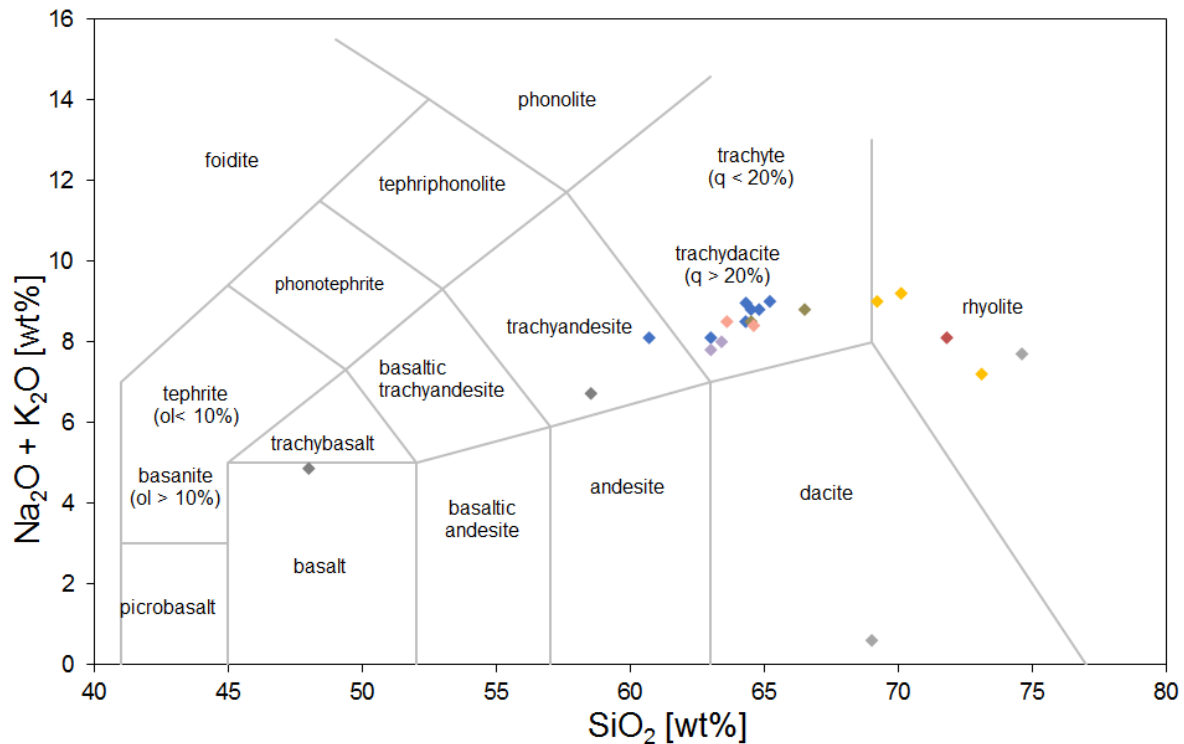


Figure 4.7: Chemical composition of the investigated volcanic rocks displayed in the total alkali–silica diagram after Le Bas et al. (1986)

Table 4.2: Mineralogical composition (XRD) and CEC (meq/100 g) of the studied samples. If the presence of a mineral is not absolutely verified by XRD, it is marked by a question mark (?)

Sample ID	Major	Minor/traces	CEC
ART1	Feldspar	Quartz Muscovite-illite Hematite	0.4
ART2	Feldspar	Quartz Muscovite-illite	-
ART3	Feldspar	Cristobalite/tridymite Muscovite-illite Hematite	1.2
ART4	Feldspar	Cristobalite/tridymite Muscovite-illite	0.6
ART5	Feldspar	Quartz Muscovite-illite	0.6
ART6	Feldspar	Quartz Muscovite-illite	0.7
ART7	Feldspar	Cristobalite/tridymite	1.1
ANI	Glass	Feldspar Biotite? Magnetite?	-
HB	Feldspar	Quartz	1.5
HR	Feldspar	Quartz Hematite	1.2
OB	Feldspar	Quartz	0.6
OR	Feldspar	Quartz	0.6
UB	Feldspar	Quartz	0.6
UY	Feldspar	Quartz	1.9
GAF	Quartz	Feldspar Muscovite-illite Corrensite Augite	7.6
GAC	Quartz	Feldspar Muscovite-illite Corrensite Augite	3.0
NB	Quartz	Feldspar Muscovite-illite I-S Mordenite Calcite	3.1
HG	Quartz	Feldspar Muscovite-illite I-S Kaolinite Analcime Augite	8.0
VR	Quartz	I-S Kaolinite Calcite	1.2

(1) The Artik tuffs (ART1-7) are characterized by an acidic composition and can be defined as trachytes using the total alkali–silica diagram after Le Bas et al. (1986) (Fig. 4.7). However, ART6 shows a trachyandesitic composition with a distinct lower SiO<sub>2</sub> content. The Artik tuffs are highly porous rocks of pink (ART1-6) to reddish brown (ART7) color (Fig. 4.2a). Various types of elongated lapilli, mostly clasts of pumice at the centimeter to decimeter scale, are embedded. The pumice clasts that range in size from few millimeter up to 30 centimeter are

#### 4 Deterioration of volcanic tuff rocks from Armenia

of red, brown and grey color, while larger pumice up to the decimeter scale are of grey tones, with transition to brown on their edges. The pumice clasts of ART1-5 often show macropores at the centimeter range. Another distinct characteristic of the Artik tuffs is the huge amount of partly elongated white glass particles and feldspar phenocrysts at the millimeter scale (Fig. 4.2a). Rarely greyish clasts of high density at the millimeter to centimeter scale are observable. Under the polarization microscope, these clasts show intermediate composition. Due to the high amount and size of the lapilli clasts, ART1-5 can be classified as lapilli tuffs with transition to tuff breccia, after Fisher (1966). ART6 and ART7 show smaller clasts overall and can be classified as lapilli tuff after Fisher (1966). In thin section, the Artik tuffs show a porphyritic texture with varying, but always high, amounts of large feldspar crystals (up to 40 %), relicts of amphiboles and muscovites as well as lithic clasts of intermediate composition in a cryptocrystalline, glassy matrix of up to 60 % (Fig. 4.8a). The matrix and pumice clasts, especially in ART2, ART3, ART4 and ART6, are typically covered by huge amounts of iron oxides. SEM micrographs point out the apparent differences of huge pores in the pumice clasts and smaller pores in the matrix area (Fig. 4.9a). Apatites and longprismatic amphiboles are often observed in the big open pores of the pumice clasts. They reach as single crystals into the open pore space. Seldom small pyroxenes and ilmenites can be identified in the matrix. The barely observed muscovites are usually located as thin plates reaching into the open pore space of the pumice clasts. XRD on whole rock identified cristobalite/tridymite, high temperature modifications of SiO<sub>2</sub>, in ART3, ART4 and ART7 (Table 4.2). Illite/muscovite was identified by XRD of separated clay fractions for nearly all types of Artik tuff. The CEC for the Artik tuffs is always small and ranges between 0.4 meq/100 g for ART1 up to 1.2 meq/100 g for ART3 (Table 4.2).

(2) Depending on their origin, the Yerevan-type tuffs were subdivided into tuffs from Ani, Hoktemberyan, Oshakan and Ujan. The Ani Peach tuff (ANI) is of rhyolitic composition (Table 4.1; Fig. 4.7) and consists of a huge amount of large, elongated, yellow to brownish clasts of pumice, embedded in a violet to peach-colored matrix. Reddish to black rock fragments in the millimeter to centimeter scale show a rather round shape. The pumice clasts are oriented, as shown in thin section (Fig. 4.8b) and SEM (Fig. 4.9b), and make up to 55 % of the rock. The fine-grained matrix makes up to 40 % of the rock and contains huge amounts of curved shape glass shards. Around 5 % of plagioclase crystals and small amounts of biotite can be observed. XRD confirms glass (large amorphous hump) and plagioclase. Traces of biotite and magnetite could be present as well, however, this is not clear by XRD (Table 4.2).

The Hoktemberyan Brown tuff (HB) shows an acidic composition and is classified as trachyte (Table 4.1; Fig. 4.7). In its dark brown ground mass, small red and grey clasts in the millimeter range, as well as black elongated pumice at the millimeter to centimeter scale, are embedded (Fig. 4.2b). Like in all Yerevan- and Artik-type tuffs, a huge amount of elongated white and grey feldspars and glass particles are characteristic. In thin section, huge amounts of feldspar phenocrysts as well as volcanic lithoclasts are observable in a cryptocrystalline matrix. A considerable amount of minerals of opaque nature (~ 10 %) was identified in thin section. In SEM micrographs, the difference in porosity between matrix and clasts is striking (Fig. 4.9c). Huge parts of these consist of amorphous glass and especially in the matrix area, tiny pores are present. Large olivine crystals and a slight coating of iron oxides are observable. Clay

#### 4 Deterioration of volcanic tuff rocks from Armenia

minerals were neither identified in thin section nor in SEM. The CEC is low (1.5 meq/100 g). The Hoktemberyan Red (HR) has a striking brick-red color (Fig. 4.2c) and chemically classifies as trachyte (Table 4.1; Fig. 4.7). In its glass rich ground mass, huge amounts of elongated white feldspar phenocrysts and glass particles are embedded and give a slightly speckled appearance. Also black elongated pumice at the millimeter to centimeter scale, are embedded in the groundmass and indicate an orientation. In thin section, HR shows less feldspar and amphibole phenocrysts than the brown variety embedded in a high amount of glassy matrix (~ 75 %), with high amounts of iron oxides. Volcanic lithoclasts and opaque minerals each make about 5 % of the sample. In SEM micrographs, the difference in porosity between matrix and clasts is striking. Huge parts of these consist of amorphous glass and especially in the matrix area, tiny pores are present. Rarely clay minerals with characteristic frayed edges in the pores of the glassy matrix are observed. HR shows a low CEC (1.2 meq/100 g).

#### 4 Deterioration of volcanic tuff rocks from Armenia

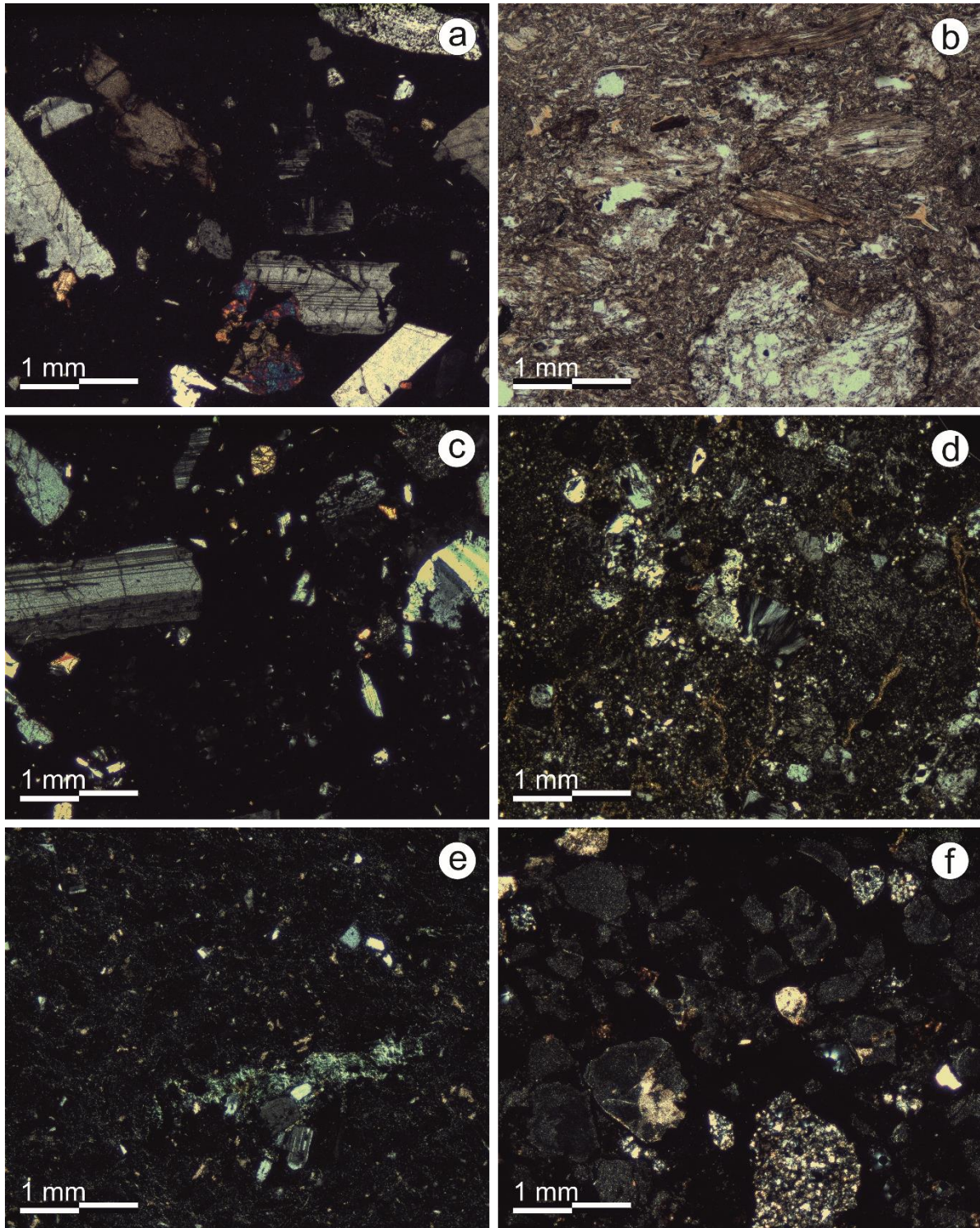


Figure 4.8: Representative thin section photomicrographs of **a** Artik 1 (ART1), **b** Ani Peach (ANI), **c** Oshakan Black (OB), **d** Golden Armenia Fine (GAF), **e** Haghartsin Green (HG) and **f** Voskepar Red (VR)

#### 4 Deterioration of volcanic tuff rocks from Armenia

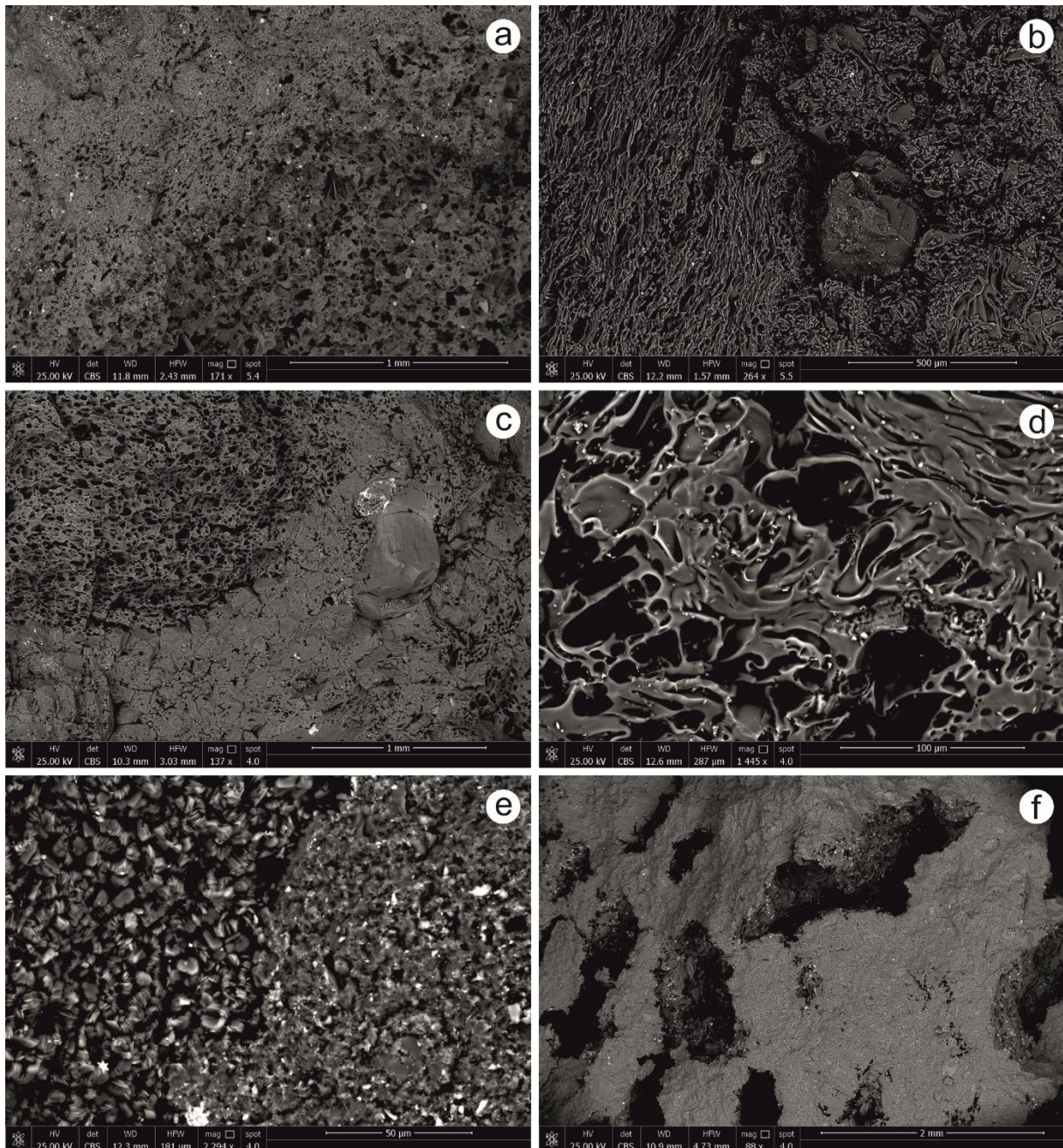


Figure 4.9: Different textural features of the investigated tuffs. **a** Boundary of groundmass (top left) and pumice clast (bottom right) in Artik 1 (ART1). **b** Elongated and orientated pumice clast (left) next to a huge feldspar crystal and the glass-rich matrix of Ani Peach (ANI). **c** Huge differences in porosity of pumice clast (top left) and glass-rich matrix of Hoktemberyan Brown (HB). On the right side a large olivine crystal is visible. **d** Thin pore throats caused by matrix glass of Ujan Brown (UB). **e** Pure booklets of pseudo-hexagonal kaolinite (left) adjacent to I-S rich groundmass in Voskepar Red (VR). **f** Huge but not interconnected pores in Armenia Black (AB)

The Oshakan Black (OB) and Oshakan Red (OR) tuffs possess the same trachytic composition similar to the Artik and Hoktemberyan tuffs (Table 4.1; Fig. 4.7). With their striking black and red ground mass, respectively, and their red and black pumice fiammes, as well as small red and grey clasts, the appearance of OB and OR is similar to the Hoktemberyan tuffs. The peculiarity of OB and OR is the much higher content of white-elongated feldspar phenocrysts and glass particles, which give them a speckled aspect. Additionally, the red and black clasts of pumice can reach sizes at the decimeter scale. In thin section, Oshakan Black (OB) shows a dark, glassy matrix (30 %) and a huge amount of feldspar phenocrysts, seldom amphiboles as



#### 4 Deterioration of volcanic tuff rocks from Armenia

well as a moderate amount of volcanic lithoclasts (Fig. 4.8c). Oshakan Red (OR) consists of a peculiar reddish, glassy matrix with a considerably higher content of iron oxides. The amount of volcanic lithoclasts seems much higher compared to OB and the amount of opaque minerals is slightly lower (5 %). Fissures in the rock fabric are partly filled with calcite. The CEC of the Oshakan tuffs is very low (0.6 meq/100 g) (Table 4.2).

The Ujan Brown (UB) and Ujan Yellow (UY) tuffs are classified as trachytes and show peculiar ground masses of olive brown and ochre, respectively. Like the tuffs from Oshakan, they embed large elongated pumice clasts up to the decimeter scale, as well as other lithic clasts of red and grey color (Fig. 4.2d). The content of glass fragments and feldspar phenocrysts in UB and UY is slightly less though. UY additionally contains large clasts of yellow to ochre pumice. In thin section, the Ujan tuffs appear to be similar to the Oshakan tuffs, containing a high amount of feldspar phenocrysts and volcanic lithoclasts in a glassy matrix (30 %). Seldom small biotites can be observed. In Ujan Yellow (UY), the amount of volcanic lithoclasts is higher though. In SEM images, huge amounts of amorphous glass with often elongated pore throats are observable (Fig. 4.9d). In general, the matrix shows a high porosity and weathering processes on huge feldspars are observable. The CEC of Ujan Brown is very low (0.6 meq/100 g). With 1.9 meq/100 g, the CEC of Ujan Yellow (UY) is three times higher, but still low (Table 4.2).

(3) The Golden Armenia Fine (GAF) and Golden Armenia Coarse (GAC) tuff rocks are of rhyolitic composition, with less sodium but the highest potassium contents of the investigated volcanites (Table 4.1; Fig. 4.7). Both varieties show a yellowish-golden ground mass with beige, grey and slightly reddish clasts embedded (Fig. 4.2e). The clasts of the coarse variety (GAC) appear to be larger and less orientated. Additionally, GAC contains a higher amount of dense, greyish clasts with andesitic composition. In thin section, Golden Armenia Fine (GAF) shows high amounts of volcanic lithoclasts and relics of feldspar in a glass-rich matrix (40 %), as well as a considerable amount of vitric fragments (5 %) (Fig. 4.8d). Rarely opaque minerals and biotites can be observed. The edges of the feldspar crystals often show sericitization processes. SEM images confirm the presence of huge amounts of clay minerals especially at grain boundaries and in the open pore space (Fig. 4.10a). The clay minerals show a cornflake microstructure and frayed edges. XRD on separated clay fractions identified them as illite/muscovite and corrensite (Fig. 4.11), a mixed layer clay mineral with intracrystalline swellable vermiculite layers. The huge amount of clay material observable in SEM micrographs (Fig. 4.10a), corresponds to the very high CEC of 7.6 meq/100 g (Fig. 4.11). Furthermore, devitrification processes and prismatic apatites were observed in SEM micrographs of both GAF and GAC. In contrast to GAF, the coarse variety GAC shows considerably larger volcanic fragments and feldspar as well as quartz phenocrysts. The amount of matrix is accordingly smaller (~ 25 %). XRD of separated clay fractions show similar types of clay minerals, such as illite/muscovite and intracrystalline swellable corrensite, in Golden Armenia Coarse (GAC). However, SEM images illustrate a considerable lower clay mineral content in the matrix (Fig. 4.10b), which is also displayed by a lower CEC of 3 meq/100 g. The clay minerals, such as in GAF, have also frayed edges. Additionally, SEM images of GAC seldom show the presence of apatite, biotite and augite.

#### 4 Deterioration of volcanic tuff rocks from Armenia

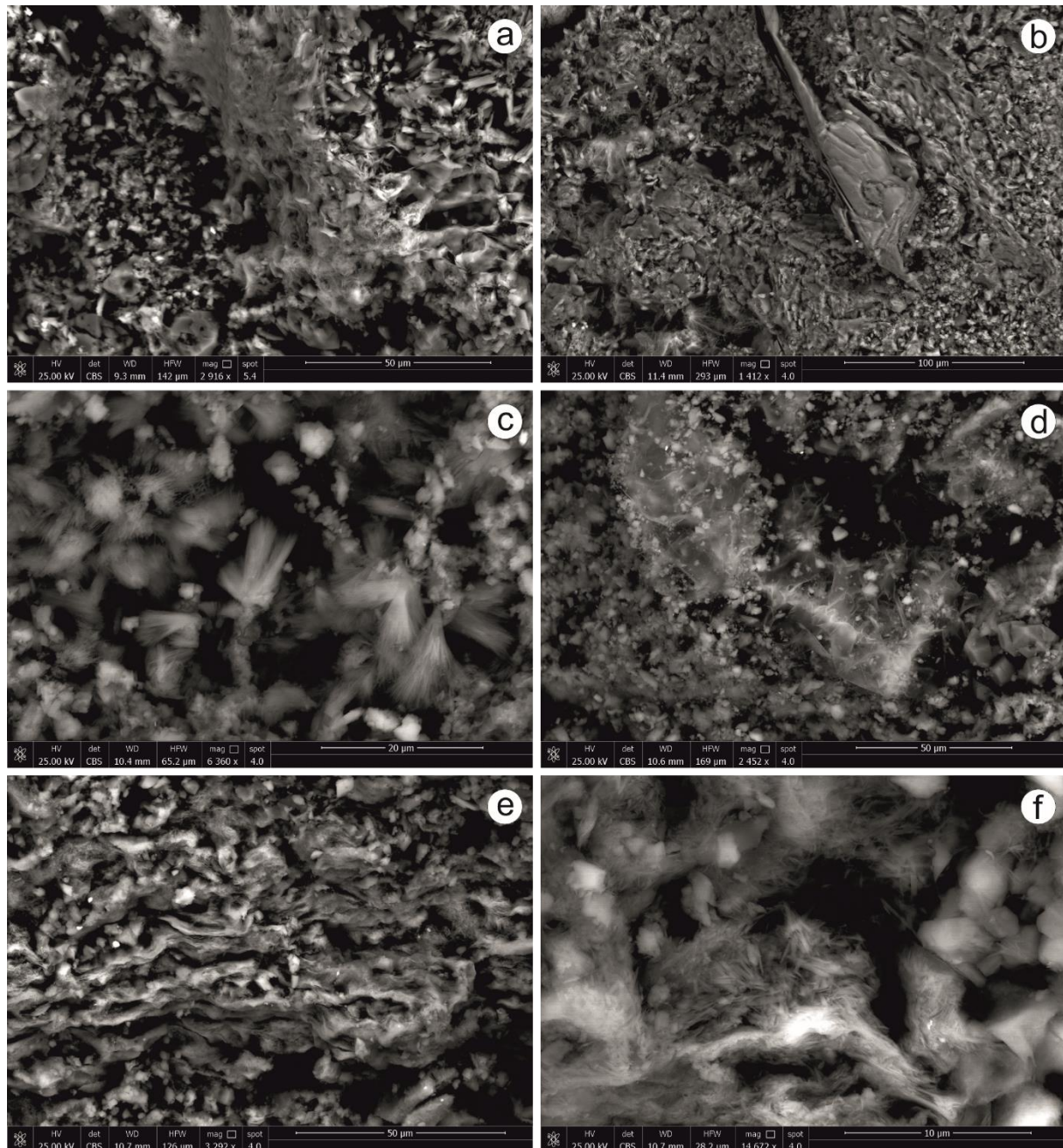


Figure 4.10: Different appearance and location of clay minerals in SEM micrographs. **a** Coating of the groundmass, especially at detachment areas of frayed edge illite minerals in Golden Armenia Fine (GAF). **b** Large flaking muscovite in the center and many fibrous and frayed edge-like clay minerals in the left part of the picture of Golden Armenia Coarse (GAC). **c** Typical fibrous clusters of mordenite in Noyemberyan (NB). **d** Cornflake microstructure of illite in the center (NB). **e** Frayed edge-like illite–smectite oriented parallel to the bedding in Haghartsin Green (HG). **f** Fibrous clusters of illite–smectite as filling in the pore space (HG)

The Noyemberyan tuff (NB) is a rather white to slightly greenish rhyolitic tuff, which shows a weak lamination in form of white and grey elongated lithic fragments (Fig. 4.2f). Many of the grey lithic fragments are framed by slightly orange to reddish margins. Macroscopic NB appears to be a fine-grained tuff. Only in exceptional cases the lithic fragments reach sizes up to one centimeter. Thin section images confirm the large amounts of fine matrix groundmass (70 %). The remaining 30 % of the rock consist of partly large angular and zoned plagioclase crystals as well as small, rounded quartz fragments. SEM micrographs show huge amounts of fibrous mordenite clusters and frayed edge clay minerals (Fig. 4.10c, d). Calcites and

#### 4 Deterioration of volcanic tuff rocks from Armenia

muscovites can reach dimensions up to 300  $\mu\text{m}$ . Rarely apatite can be observed. Huge amounts of mordenite, a mineral of the zeolite group, and intracrystalline swellable smectitic layers in an illite–smectite mixed layer mineral were identified by XRD on separated clay fractions and confirm a moderate CEC of 3.1 meq/100 g (Fig. 4.11). Note that zeolites may have large CEC values. However, with the CEC method used, zeolite CEC cannot be measured (Meier and Kahr 1999). XRD on separated clay fractions also identified illite/muscovite.

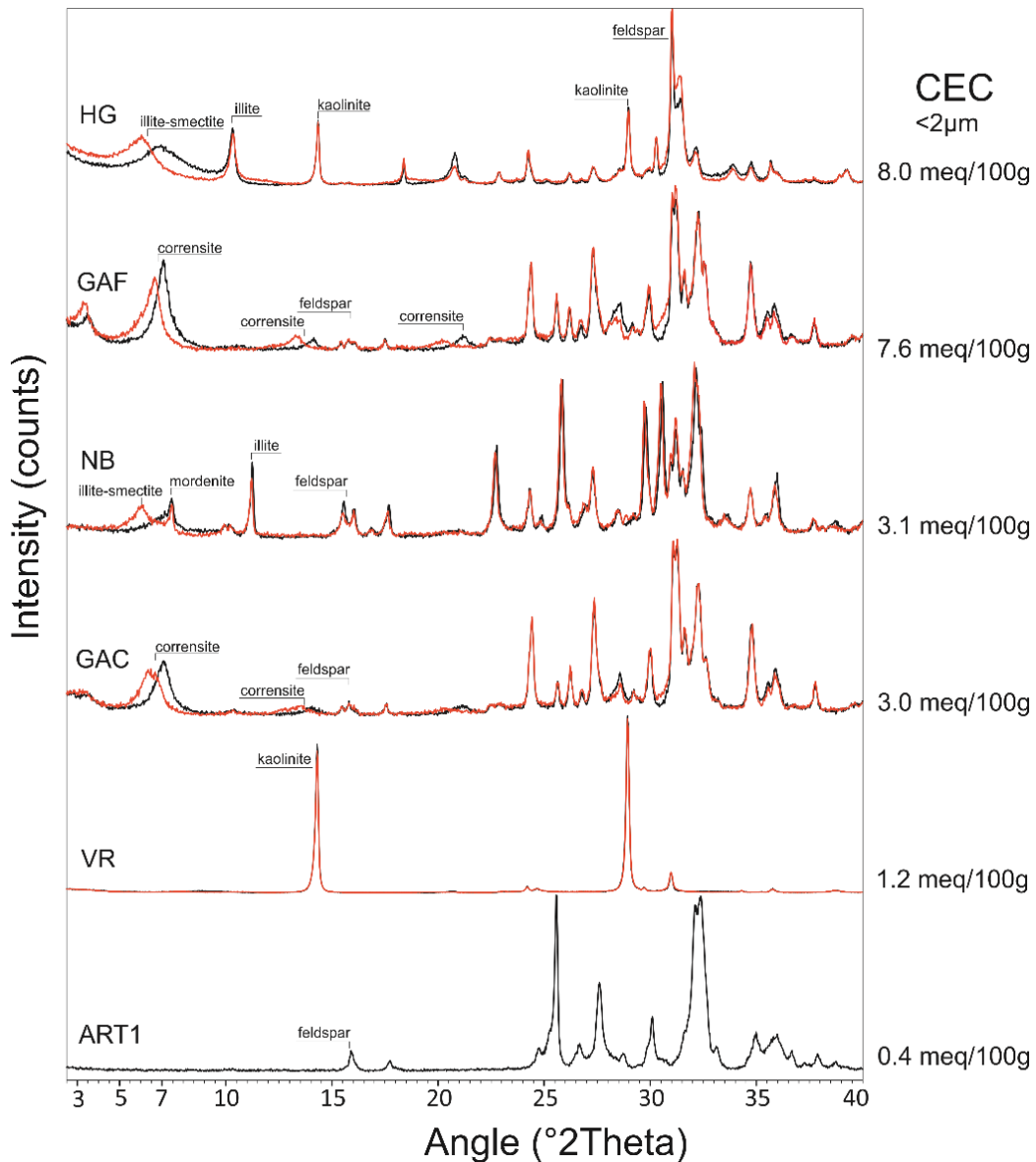


Figure 4.11: XRD analyses of clay fractions (oriented mounts). black: air-dry, red: ethylene glycol solvated

(4) The Haghartsin Green tuff (HG) has a characteristic green color and is of rhyolitic composition. It is very fine-grained and bottle-green-elongated fragments, in the micrometer to millimeter scale, indicate a lamination (Fig. 4.2g). In thin section, this tuff shows about 80 % cryptocrystalline matrix, with few mono- and polycrystalline quartz crystals as well as feldspar phenocrysts embedded (Fig. 4.8e). The bottle-green fragments often show chloritization processes. In SEM micrographs, huge amounts of frayed edge clay minerals are oriented parallel to the bedding (Fig. 4.10e). They are located both at grain contacts and mixed into the fine-grained matrix consisting of quartz and feldspar. XRD of separated clay fractions

#### 4 Deterioration of volcanic tuff rocks from Armenia

identified them as intracrystalline swellable smectites (Fig. 4.11). Illite/muscovite, kaolinite and analcime, a mineral of the zeolite group, could also be identified. Huge apatites and feldspar relics as well as muscovites can occasionally be observed. The CEC is very high (8 meq/100 g).

The Voskepar Red tuff (VR) is of dacitic composition (Table 4.1; Fig. 4.7). Countless fragments of white, grey, red and black color are homogeneously distributed in a characteristic red groundmass (Fig. 4.2h). The lithic fragments are in the millimeter scale and give the rock a speckled appearance. In thin section, it becomes apparent that VR consists mainly of volcanic lithoclasts (95 %) that cause a brecciated fabric, which is cemented by a cryptocrystalline matrix (Fig. 4.8f). The matrix is heavily coated by iron oxides, which presumably cause the characteristic red coloration. SEM images show the nature of the lithic fragments with an average radius of about 500  $\mu\text{m}$ . Many lithic fragments were transformed, but still bear their former hexagonal shape. Apatite, calcite and iron oxides appear frequently. Most fragments consist of pure booklets of pseudohexagonal kaolinite, which cause a higher porosity than the fine, with cornflake structure and frayed edge-type clay minerals coated adjacent matrix (Fig. 4.9e). The frayed edge minerals were identified with the Rietveld method using the models described in Ufer et al. (2012a, 2012b) on basis of XRD analyses on separated clay fractions. They classify as illite with traces of intracrystalline swellable smectite, the so-called interstratified illite–smectite (I–S) (Table 4.2; Fig. 4.11). The CEC is low (1.2 meq/100 g).

The Armenia Black (AB) is of trachyandesitic composition and of characteristic black color (Fig. 4.2i). The macroscopic pores are in the millimeter to centimeter range. In addition, in thin section, the porosity is noticeable. The trachytic texture of the rock shows large amounts of oriented plagioclase crystals, which form the groundmass of the rock and indicate flow directions. In thin section as well as in SEM micrographs, about 5 % of olivine crystals and relictic pyroxenes are observable in the plagioclase-rich groundmass. Especially, in SEM images, the absent pore connection is striking (Fig. 4.9f). The pores are filled with phyllosilicates and few iron oxides. The Armenia Grey (AG) is a volcanite of basaltic composition (Fig. 4.7). It is of typical grey color and occasionally contains air inclusions in the centimeter scale. In thin section, the rock shows large strip-like plagioclase crystals which are partly subophitic included by pyroxenes. Olivine crystals and few apatite prisms are identified by SEM. The SEM images also display the absence of a pore connection between the individual pores.

All investigated samples differ with respect to their amount of smectitic layers. Smectitic layers are characterized by expandable interlayers and the smectitic layer regions possess a high specific surface area as well as a high CEC of up to 130 meq/100 g as pure minerals (Christidis 2013). Exchangeable cations can be replaced in the interlayer regions of smectites by any competing cations present in the pore water. The ion exchange causes expansion or shrinkage, respectively. Except for vermiculite the CEC of other clay minerals is very small. The CEC can be used as indicator for the smectite content or the content of smectitic layers in interstratified clay minerals present in natural building stones (compare discussion in Ruedrich et al. 2011).

## 4 Deterioration of volcanic tuff rocks from Armenia

### 4.2.1 Type, location and structure of clay minerals

A broad spectrum of different clay minerals with diverse structures can be observed in the Armenian tuff rocks (Table 4.2; Figs. 4.10, 4.11). The Artik tuffs, the Golden Armenia tuffs as well as the Noyemberyan (NB) and Haghartsin Green (HG) tuff are characterized by partly large amounts of muscovite/illite (Table 4.2; Fig. 4.10). Golden Armenia fine and coarse (GAF, GAC), Noyemberyan (NB), Haghartsin Green (HG) and Voskepar Red (VR) contain intracrystalline swellable smectitic layers in form of irregular illite–smectite mixed layers (NB, HG, VR) or corrensite, a regular inter-stratified chlorite–smectite (GAF, GAC) (Table 4.2; Fig. 4.11). The illite often covers the groundmass along with quartz and feldspar crystals and coats the open pores. Frayed edges, fibrous clusters and cornflake-like microstructures of the clay minerals can indicate the presence of smectitic layers (Fig. 4.10a, d, e, f). In Golden Armenia Fine and Coarse (GAF, GAC), Noyemberyan (NB) and Haghartsin Green (HG) the frayed edge minerals are mainly located at the grain contacts parallel to the bedding plane (Fig. 4.10a, e). Especially in HG, the SEM micrographs prove that the detachment areas are typically associated with frayed edge-like clay minerals (Fig. 4.10e). Another peculiarity of the Noyemberyan (NB) tuff is the countless fibrous clusters of mordenite that pervade the rock (Fig. 4.10c). Mordenite, a zeolite mineral, can be found in every open pore space of NB. Voskepar Red (VR) is showing vast amounts of kaolinite minerals. Former mineral grains now transformed and filled with huge amounts of pseudo-hexagonal kaolinite booklets, show a much higher porosity than the adjacent groundmass and grain fragments (Fig. 4.9e).

### 4.3 Petrophysical properties

To determine the anisotropic behavior of the tuffs, petrophysical and weathering analyses were performed in all three directions of the rocks. The bedding and lamination plane is defined as XY plane, while the Z direction is defined as the direction perpendicular to the bedding (see Chapter 2.1). The directions were set arbitrary, if no preferred orientation was visible. The anisotropy was determined using the relation of the highest and lowest value, respectively. The petrophysical properties of all samples are displayed in Table 4.3.

## 4 Deterioration of volcanic tuff rocks from Armenia

Table 4.3: Summary of petrophysical properties and weathering behavior of the investigated rocks. CEC = cation exchange capacity, SSA = specific surface area by N<sub>2</sub> adsorption

Sample ID	ART1	ART2	ART3	ART4	ART5	ART6	ART7	ANI	HB	HR	OB	OR	UB	UY	GAF	GAC	NB	HG	VR	AG	AB
Porosity [vol.%]	38.9	42.2	53.2	43.9	41.5	44.2	44.6	43.5	35.0	35.6	22.9	26.0	33.0	27.1	20.8	21.5	26.2	11.3	14.6	14.1	15.9
Matrix density [g/cm <sup>3</sup> ]	2.65	2.63	2.65	2.57	2.62	2.66	2.67	2.26	2.49	2.46	2.50	2.49	2.46	2.54	2.60	2.60	2.39	2.43	2.68	2.93	2.67
Bulk density [g/cm <sup>3</sup> ]	1.62	1.52	1.24	1.45	1.53	1.48	1.48	1.28	1.62	1.59	1.93	1.85	1.65	1.85	2.06	2.04	1.76	2.16	2.29	2.52	2.25
Mean pore radius [μm]	1.29	0.71	2.24	1.04	1.40	2.71	3.34	0.94	1.24	1.98	0.30	0.59	0.74	0.38	0.13	0.11	0.07	0.03	0.06	0.45	0.09
Micropores [%]	13	15	5	17	12	8	6	9	15	9	40	23	18	22	42	47	57	93	58	50	66
CEC [meq/100g]	0.4	-	1.2	0.6	0.6	0.7	1.1	-	1.5	1.2	0.6	0.6	0.6	1.9	7.6	3.0	3.1	8.0	1.2	-	-
SSA by N <sub>2</sub> [m <sup>2</sup> /g]	2.1	-	2.1	1.3	1.4	1.5	2.0	-	1.0	1.0	0.6	1.8	1.7	1.2	6.1	5.7	9.2	8.9	8.0	-	-
Saturation degree S	0.61	0.47	0.52	0.50	0.71	0.64	0.66	0.65	0.69	0.71	0.34	0.37	0.65	0.61	0.62	0.64	0.68	0.78	0.54	0.31	0.17
w value [kg/m <sup>2</sup> vh]																					
X	14.6	7.8	30.8	5.6	12.6	24.4	41.0	25.9	30.0	37.4	4.3	4.5	28.0	14.3	1.9	2.6	4.6	0.6	0.9	0.9	0.5
Y	18.0	7.9	32.6	5.0	10.2	28.9	42.5	26.2	31.2	36.4	5.1	7.1	28.4	13.5	1.4	2.7	4.4	0.7	0.8	0.9	0.3
Z	7.3	5.8	15.2	3.2	13.1	26.1	47.4	20.3	32.0	36.4	2.8	4.2	23.7	10.6	1.3	2.0	3.5	0.6	0.7	0.6	0.3
Anisotropy [%]	59	27	53	43	22	16	13	22	6	3	45	41	16	26	31	24	22	13	16	36	39
μ value																					
X	7.3	10.5	6.6	5.7	10.3	7.6	8.5	-	-	11.0	14.6	25.3	-	13.6	19.7	18.0	13.5	14.9	-	28.9	-
Y	8.8	8.7	6.8	7.4	12.2	5.9	7.8	-	-	9.9	20.5	22.8	-	12.8	19.2	17.0	12.6	-	-	23.6	-
Z	9.9	11.4	8.0	8.2	12.5	8.4	8.8	-	-	12.7	22.1	27.1	-	22.6	21.6	18.1	15.9	17.9	25.3	35.4	-
Anisotropy [%]	29	24	18	31	17	30	11	-	-	22	34	16	-	43	11	6	20	17	-	33	-
Sorption 95 % rh [wt.%]	0.32	0.13	0.11	0.26	0.09	0.81	0.07	-	-	0.06	0.07	0.19	-	0.25	1.51	1.28	2.69	2.66	1.00	0.22	-
Hydric expansion [mm/m]																					
X	0.032	0.004	0.036	0.268	0.022	0.022	0.001	-	0.022	0.013	-0.014	0.012	-0.009	0.011	0.896	0.579	0.641	0.714	0.159	0.026	-
Y	0.063	0.001	0.027	0.219	0.017	0.021	-0.001	-	0.034	0.013	-0.018	0.004	-0.012	-	0.858	0.514	0.669	0.585	0.173	0.025	-
Z	0.187	0.036	0.031	0.255	0.033	-0.132	-0.079	-	0.030	0.009	-0.011	0.011	-0.068	0.023	1.021	0.728	0.681	2.200	0.304	0.040	-
Max	0.187	0.036	0.036	0.268	0.033	0.022	0.001	-	0.034	0.013	-0.011	0.012	-0.009	0.023	1.021	0.728	0.681	2.200	0.304	0.040	-
Anisotropie [%]	83	97	23	18	48	-	-	-	35	32	39	67	86	55	16	29	6	73	48	38	-
Salt cycles	30	>150	65	16	67	144	>150	>75	>150	>150	>150	>150	106	64	34	78	109	20	75	>150	>150

## 4 Deterioration of volcanic tuff rocks from Armenia

### 4.3.1 Density

The Armenian Grey basalt (AG) shows both the highest bulk and matrix densities, with  $2.52 \text{ g/cm}^3$  and  $2.93 \text{ g/cm}^3$ , respectively, and has to be considered an exceptional case, since petrophysical properties of basalts can differ greatly from the tuffs. The bulk and matrix densities from the tuffs range from  $1.24 \text{ g/cm}^3$  for ART3 up to  $2.29 \text{ g/cm}^3$  for VR and from  $2.26 \text{ g/cm}^3$  for ANI up to  $2.68 \text{ g/cm}^3$  for VR, respectively (Table 4.3). Overall, the Artik tuffs (ART1-7) and ANI show low bulk densities up to  $1.62 \text{ g/cm}^3$ . The Yerevan-type tuffs (HB, HY, OB, OR, UB, UY) and NB show intermediate bulk densities up to  $1.98 \text{ g/cm}^3$ . GAF, GAC, HG, VR and AB possess high bulk densities of up to  $2.29 \text{ g/cm}^3$ . Regarding the matrix densities ANI, NB and HG show the lowest values between  $2.26 \text{ g/cm}^3$  and  $2.43 \text{ g/cm}^3$ . The Yerevan-type tuffs (HB, HR, OB, OR, UB, UY) as well as the Golden Armenia tuffs show intermediate particle densities of up to  $2.60 \text{ g/cm}^3$ . The highest density values are shown by the Artik-type tuffs (ART1-7) as well as VR and AB of up to  $2.68 \text{ g/cm}^3$  (Table 4.3).

### 4.3.2 Porosity, microporosity, pore radii distribution and specific surface area

Regarding the effective porosity, three groups can be distinguished. Group 1 consists of HG, VR, AB and AG and shows low porosities between 10 and 20 vol.%. Group 2 consists of HB, HR, OB, OR, UB, UY, GAF, GAC and NB with intermediate porosities ranging between 20 and 35 vol.%. Group 3 shows very high porosities greater 35 vol% and consists of the Artik tuffs (ART1-7) and ANI. The lowest porosity is displayed by HG with 11.3 vol.%. With 53.2 vol.%, ART3 shows by far the highest porosity value (Table 4.3). Klopfer (1985) defined micropores as pores smaller than  $0.1 \mu\text{m}$  and capillary pores as pores between  $0.1$  and  $1000 \mu\text{m}$ . Pores  $>1 \text{ mm}$  are defined as macropores. The percentage of micropores is of special interest and ranges wide in the investigated tuffs (Fig. 4.12). Low percentages of micropores under 25 % are displayed by the Artik tuffs (ART1-7), HB, HR, OR, UB and UY. OB, GAF, GAC as well as AG possess intermediate amounts of micropores up to 50 %. NB, VR and AB show high percentage of micropores of up to 66 %. HG, with 93 % micropores, is located far beyond that (Fig. 4.12).

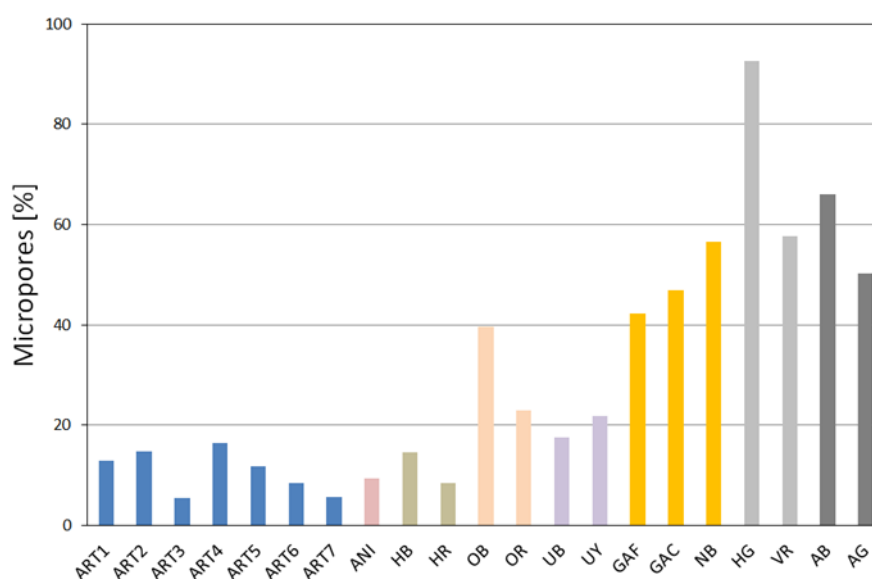


Figure 4.12: Percentage of micropores of the investigated tuffs Artik 1–7 (ART1-7), Ani Peach (ANI), Hoktemberyan Brown and Red (HB, HR), Oshakan Black and Red (OB, OR), Ujan Brown and Yellow (UB, UY), Golden Armenia Fine and Coarse (GAF, GAC), Noyemberyan (NB), Haghartsin Green (HG), Voskepar Red (VR), Armenia Black and Grey (AB, AG)

#### 4 Deterioration of volcanic tuff rocks from Armenia

After Siegesmund and Dürrast (2011), the pore radii distributions of the investigated rocks can be described as either unimodal unequal or bimodal unequal. The Artik tuffs show either unimodal unequal pore size distribution with a distinct maximum in the range between 1 and 10  $\mu\text{m}$  (ART1, ART5, ART6, ART7) or bimodal unequal pore size distributions with a second maximum around 0.25  $\mu\text{m}$  (ART2, ART3, ART4) (Fig. 4.13). All Artik tuffs show a minor amount of micropores around 0.01  $\mu\text{m}$ . The mean pore radius ranges from 0.71  $\mu\text{m}$  for ART2 up to 3.34  $\mu\text{m}$  for ART7 (Table 4.3). The Yerevan tuffs ANI, HB, HR, OR, UB and UY are mainly characterized by a unimodal unequal pore radii distribution with a maximum in the range between 1 and 5  $\mu\text{m}$  (Fig. 4.13). Only Oshakan Black (OB) shows a bimodal unequal distribution with a second maximum around 0.01  $\mu\text{m}$ . Especially, the Oshakan and Ujan tuffs possess small mean pore radii between 0.30 up and 0.74  $\mu\text{m}$ . The remaining tuffs from the Golden Armenia type (GAF, GAC), Noyemberyan (NB), Haghartsin Green (HG) and Voskepar Red (VR) are characterized by distinct smaller mean pore radii, ranging between 0.03  $\mu\text{m}$  for Haghartsin Green (HG) and 0.13  $\mu\text{m}$  for Golden Armenia Fine (GAF). The Golden Armenia types show a bimodal unequal distribution of their pores with maxima around 0.4 and 0.06  $\mu\text{m}$ , while Noyemberyan (NB) and Voskepar Red (VR) possess unimodal unequal distributions with maxima around 0.1  $\mu\text{m}$  (Fig. 4.13). At the Armenia Grey basalt (AG) and the dacitic Armenia Black (AB), no pores in the range between 0.1 and 1  $\mu\text{m}$  can be observed. Both rocks show distinct amounts of pores smaller 0.01  $\mu\text{m}$  as well as around 10  $\mu\text{m}$ .

The specific surface area of the Artik, Hoktemberyan, Oshakan and Ujan tuffs is consistently low and ranges between 0.6 and 2.1  $\text{m}^2/\text{g}$  (Table 4.3). Intermediate values of up to 6.1  $\text{m}^2/\text{g}$  are displayed by the Golden Armenia tuffs, whereas the Noyemberyan (NB), Haghartsin (HG) and Voskepar (VR) tuffs show higher values up to 9.2  $\text{m}^2/\text{g}$  (NB).

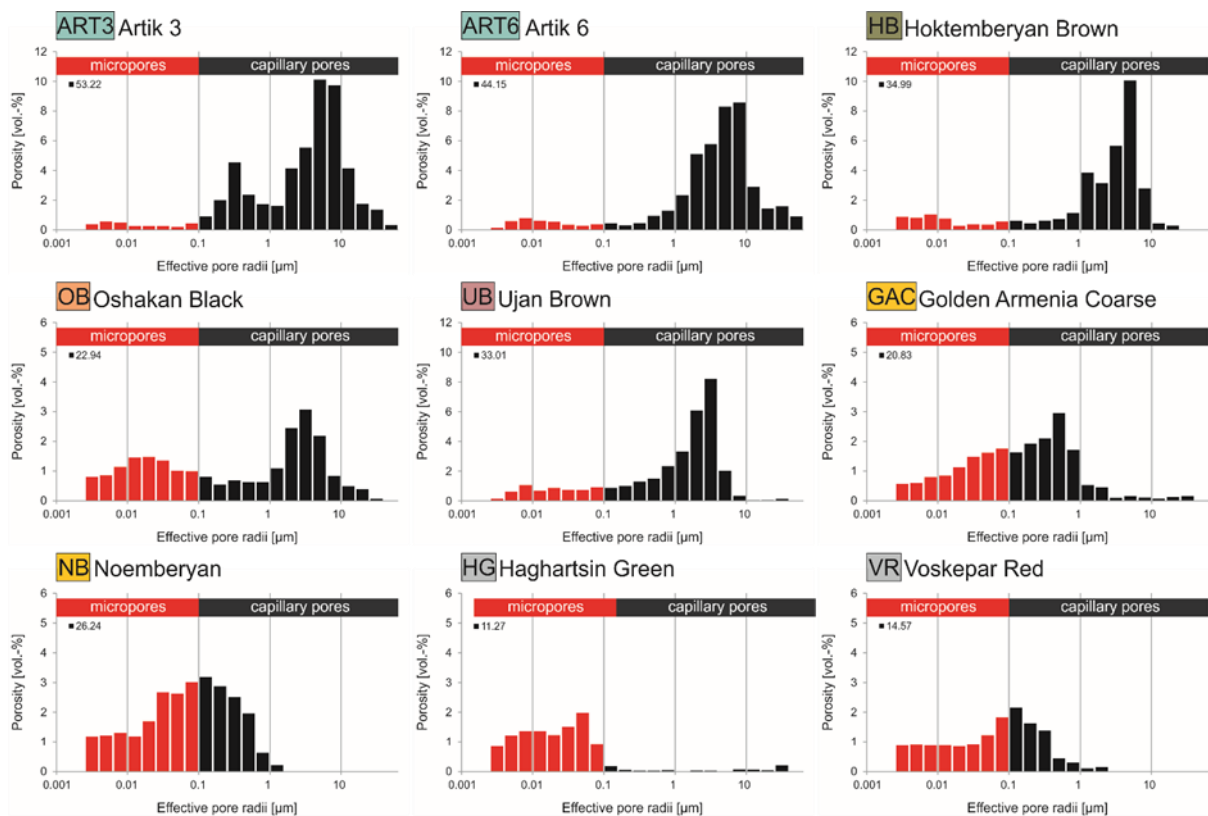


Figure 4.13: Representative pore radii distributions of the investigated tuffs measured by mercury intrusion porosimetry



## 4 Deterioration of volcanic tuff rocks from Armenia

### 4.3.3 Capillary water absorption and water vapor diffusion

The capillary water absorption coefficient ( $w$ ) for all directions is given in Table 4.3 and ranges between 0.28 kg/m<sup>2</sup>·h for Armenian Black (AB) and 47.39 kg/m<sup>2</sup>·h for ART7. Generally, the samples show lower values in Z direction. Especially some Artik and Oshakan tuffs show huge anisotropic behavior. Low values < 5 kg/m<sup>2</sup>·h are displayed by ART4, OB, OR, GAF, GAC, NB, HG, VR, AB and AG. Moderate values between 5 and 20 kg/m<sup>2</sup>·h are shown by ART1, ART2, ART5 and UY. The remaining tuffs (ART3, ART6, ART7, ANI, HB, HR and UB) possess high absorption coefficient values, ranging from 20 to nearly 50 kg/m<sup>2</sup>·h.

Regarding the water vapor diffusion resistance ( $\mu$ ), the Artik tuffs show the lowest resistance values, with ART6 showing the lowest value of 5.88 (Table 4.3). With exception of ART2 and ART5, the values are lower than 10. HR, GAC, NB and HG show intermediate resistance with values between 10 and 20. High resistance against water vapor diffusion, with values > 20, is shown by OB, OR, UY, GAF, UN21 and AG, with the maximum value of 35 for AG. In general, the tuffs show a higher resistance in Z direction. Especially, the Artik tuffs, OB, UY and AG show a very strong anisotropic behavior (Table 4.3).

### 4.3.4 Hygroscopic water sorption and saturation degree

The hygroscopic water sorption was measured by weighing and its values are given in percentage (wt.%) of the bulk sample. The Artik tuffs, HR, OB, OR, UY and AG all show very low values < 1 wt.% (Fig. 4.14). ART7, HR and OB show barely any sorption effect. GAF, GAC and VR show intermediate values ranging between 1 and 2 wt.%, while Noyemberyan (NB) and Haghartsin Green (HG) show high hygroscopic sorption of 2.66 and 2.69 wt.%, respectively. The total amount of pore space that is accessible to water adsorption is described by the saturation coefficient ( $S$ ). Higher amounts of water in the rock can result in a higher risk of taking damage due to salt and ice crystallization. Thus, the saturation coefficient ( $S$ ) provides a value for the evaluation of the frost resistance (Siegesmund and Dürrast 2011). With the exception of Haghartsin Green (HG), all samples show lower values than 0.75 (Table 4.3) and are therefore rated frost resistant after Hirschwald (1912). Thus, with a saturation coefficient of 0.78, the frost resistance for HG is uncertain.

## 4 Deterioration of volcanic tuff rocks from Armenia

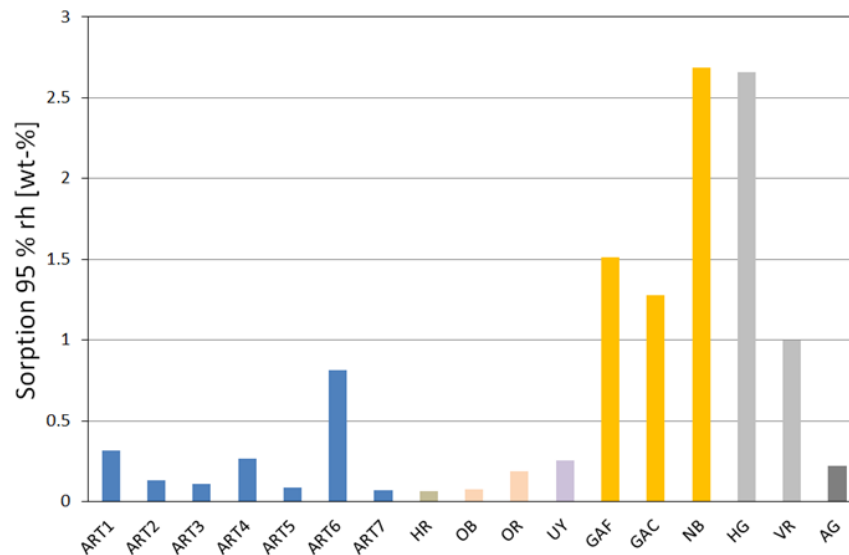


Figure 4.14: Maximum moisture content of the rocks by hygroscopic water sorption at 95% relative humidity

### 4.3.5 Moisture expansion

The investigated tuffs show hydric expansion values ranging from slight contraction of the Oshakan and Ujan tuffs up to an expansion of 2.20 mm/m for Haghartsin Green (HG) (Table 4.3). With values < 0.10 mm/m, ART2, ART3, ART5, ART6, ART7, HB, HR, OB, OR, UB, UY and AG show barely any expansion. ART1, ART4, GAC, NB and VR show low to intermediate expansion ranging between 0.10 and 1.00 mm/m. High expansion values are displayed by Golden Armenia Fine (GAF) and Haghartsin Green (HG) with 1.02 and 2.20 mm/m, respectively. With the exception of Noyemberyan (NB) all samples show moderate to high anisotropic behavior (Table 4.3), with higher expansion perpendicular to the bedding (Z direction). Especially, ART1, ART2, UB and HG show very high anisotropy of up to 97 %. Please note that a high anisotropy at low expansion values can be misleading due to the higher impact of even small expansion changes. Therefore, the anisotropic behavior of some samples showing very low hydric expansion values has to be regarded with caution. Figure 4.15 shows representative hydric expansion values for the different groups of tuffs.

## 4 Deterioration of volcanic tuff rocks from Armenia

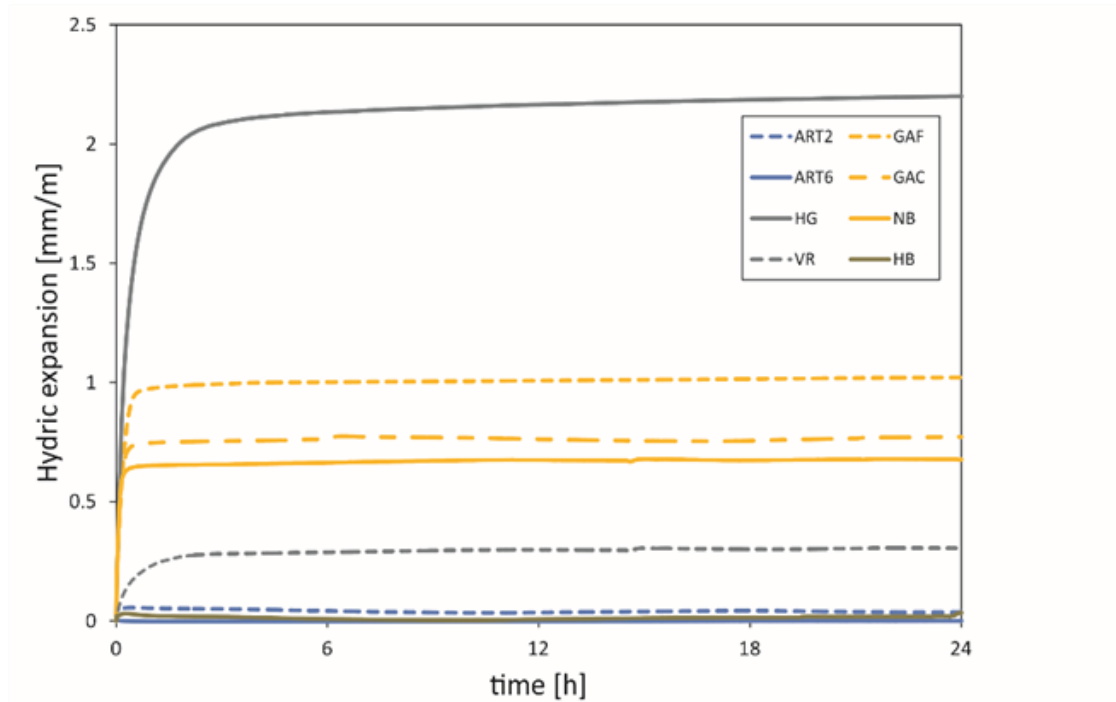


Figure 4.15: Maximum hydric expansion under water-saturated conditions of representative samples Artik 2 and 6 (ART2, ART6), Hoktemberyan Brown (HB), Golden Armenia Fine and Coarse (GAF, GAC), Noyemberyan (NB), Haghartsin Green (HG) and Voskepar Red (VR)

### 4.3.6 Salt weathering resistance

The rocks show a broad spectrum of weathering resistance under laboratory conditions. Starting from 16 salt cycles until a weight loss of more than 30 %, many Armenian tuffs reach over 150 salt cycles, and potentially more (Fig. 4.16). Due to the high resistance of numerous samples, the time consuming salt weathering test was concluded at 150 salt cycles. According to their diverse trend of resistance against salt crystallization, four groups could be distinguished. Group 1 consists of ART4, Haghartsin Green (HG), ART1 and Golden Armenia Fine (GAF) with 16, 20, 30 and 34 salt cycles, respectively, until 30 % of weight loss. The second group is defined by moderate resistance and consists of ART3, ART5, Ujan Yellow (UY), Voskepar Red (VR) and Golden Armenia Coarse (GAC) with salt cycles until destruction between 64 and 78. With more than 100 cycles until destruction, high resistance against salt crystallization is displayed by Ujan Brown (UB), Noyemberyan (NB) and ART6 of Group 3. Group 4 comprises ART2, ART7, Armenia Black (AB), Armenian Grey (AG) as well as the Hoktemberyan (HB, HR) and Oshakan (OB, OR) tuffs. These samples show very high resistance against salt crystallization and are still intact after 150 salt cycles. Especially, the Hoktemberyan and Oshakan tuffs show barely any reaction (Fig. 4.17). Together with ART2 they still bear over 100 % of their initial weight mass. Please note that the weight increase of individual samples, especially the Artik tuffs, is accompanied by a simultaneous loss of material (Fig. 4.17). Therefore, not all samples in Figure 4.16 reflect their degree of weathering by their relative change in weight.

#### 4 Deterioration of volcanic tuff rocks from Armenia

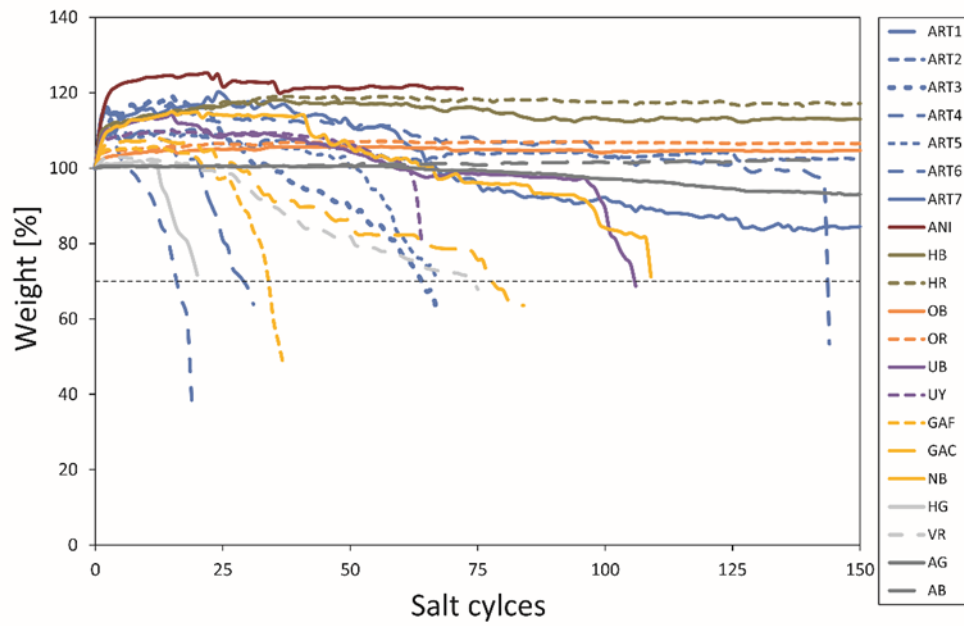


Figure 4.16: Mass weight of the samples as a function of the salt weathering cycles. 1 cycle  $\cong$  4 h salt solution + 24 h drying at 60°C

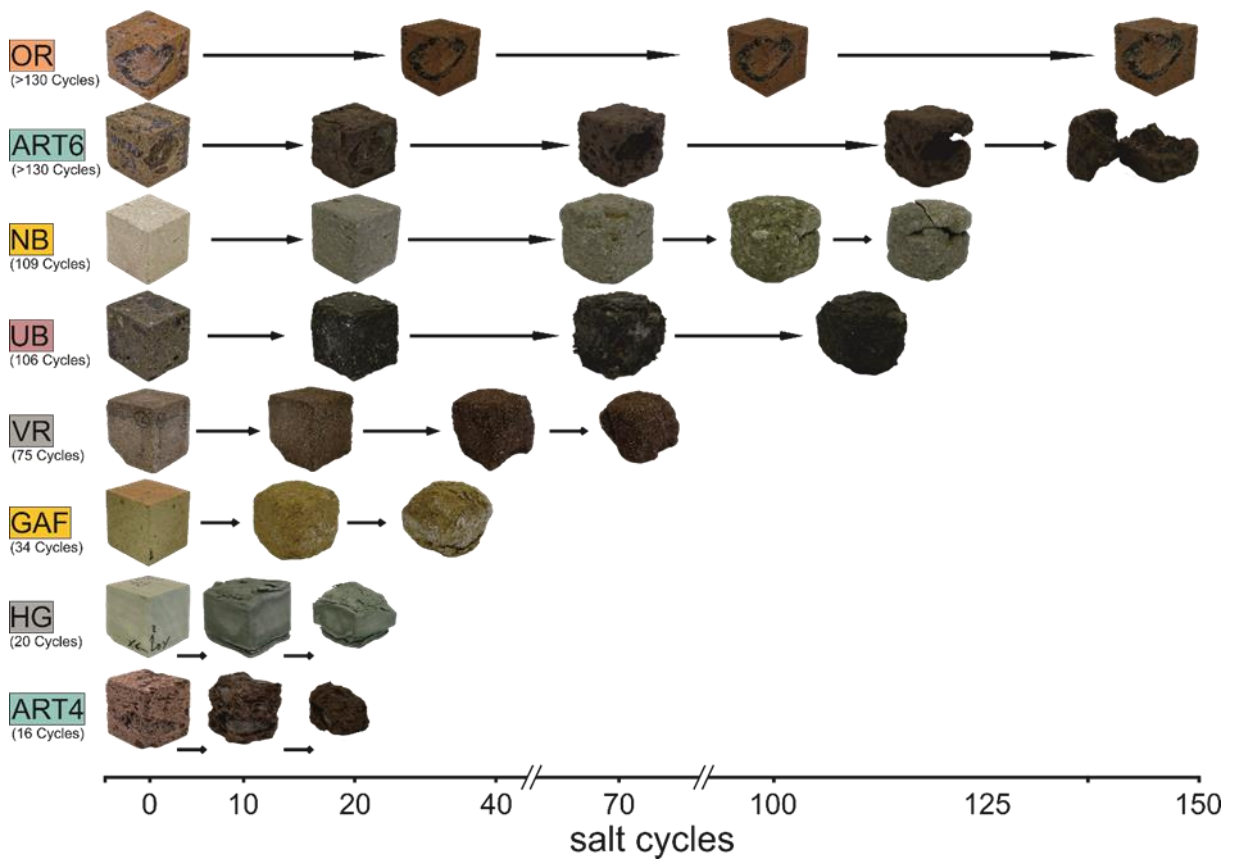


Figure 4.17: Weathering behavior of the most resistant and least resistant tuffs throughout the salt bursting test

## 4 Deterioration of volcanic tuff rocks from Armenia

A general observation during the salt weathering test is that during the first cycles of the test all samples experience a characteristic increase of weight (Fig. 4.16). This first weight increase ranges from minor amounts of < 2 % of the initial weight mass for HG, VR, AB, AG up to 25 % for the ANI tuff, some Artik and the Hoktemberyan tuffs. In addition, a partly very similar weathering behavior among certain groups of tuffs is peculiar. The Hoktemberyan (HB, HR) and Oshakan tuffs (OB, OR), for instance, show absolute equivalent behavior in their relative mass weight changes throughout the whole test. The Ujan tuffs (UB, UY) as well as the Armenian Black and Grey (AB, AG) show the same behavior until the 60th salt cycle. The Artik tuffs, the Golden Armenia (GAF, GAC, NB) tuffs as well as Haghartsin Green (HG) and Voskepar Red (VR) show a wide range of resistance against salt weathering within their group.

The tuffs show various forms of weathering due to the salt crystallization. The ANI and Artik tuffs show a characteristic back weathering of pumice clasts and partly extensive back weathering of their groundmass with consequently protruding clasts of higher resistance (Fig. 4.17). However, the ANI tuff additionally experienced a break off of entire edge regions of the sample cube. The Hoktemberyan and Oshakan tuffs are characterized by a very high resistance against salt their margins and rarely clasts are back weathered. The Ujan tuffs show characteristic forms of flaking and scaling. While the back weathering of the Ujan Yellow (UY) proceeds parallel to the bedding, the Ujan Brown (UB) shows distinct surface parallel scaling (Fig. 4.17). The Golden Armenia fine (GAF) and Haghartsin Green (HG) as well show distinct forms of scaling. While the scaling in GAF proceeds parallel to the surface, the phenomenon in the Haghartsin Green (HG) is strictly limited to the bedding (Fig. 4.17). Surface parallel flaking is the main weathering form observed in the Noyemberyan (NB) tuff, the Voskepar Red (VR) and the Armenia Grey (AG) basalt. It comes along with a constant loss of material (Fig. 4.16). At the Armenia Black (AB), a slight discoloration due to the pore filling salt load can be observed. A loss of material in any form after 150 salt cycles could not be documented.

### 4.4 Discussion

#### 4.4.1 Correlation of results and limiting parameters

The Armenian volcanoclastic rocks that are investigated in this study do not only differ fundamentally in their chroma (Fig. 4.2). They also show a broad variety regarding their chemical composition, mineralogy and petrophysical properties (Tables 4.1, 4.2, 4.3; Fig. 4.7). Their colors range from white and green to yellow, orange, red up to brownish and black, with equally colorful clasts. The investigated rocks cover a wide range of chemical composition, ranging from mafic basalts (Armenian Grey (AG)) to acidic rhyolites (e.g., Golden Armenia Fine and Coarse (GAF, GAC)). However, most of the investigated rocks are chemically classified as intermediate trachytes or acidic rhyolites (Table 4.1; Fig. 4.7). Additionally, the type, amount and structure of clay minerals and zeolites present, varies widely. While many Armenian tuff rocks contain muscovite–illite material, only the Golden Armenia tuffs (GAF, GAC), Noyemberyan (NB), Haghartsin Green (HG) and Voskepar Red (VR) show the presence of swellable clay minerals and/or zeolites (Table 4.2; Fig. 4.11). At the same time, these tuffs show the highest hydric expansion and a high susceptibility towards salt crystallization (Table 4.3), respectively. Therefore, it can be stated that in the case of the Armenian tuff rocks, the accessory minerals, especially swellable clay minerals and zeolites, rather than the main

#### 4 Deterioration of volcanic tuff rocks from Armenia

components determine their weathering behavior. When subjected to salt loads or due to immersion in water, the Armenian volcanoclastic rocks show diverse weathering behavior. The weathering behavior is strongly connected to the rock properties, which will be discussed in this section.

Regarding the pore space properties, the investigated tuffs show a general tendency of higher porosity correlated to a higher mean pore radius (Fig. 4.18). Up to a porosity of approximately 30 %, the mean pore radius stays low. However, tuffs with porosities > 30 % show a successive increase of the mean pore radii connected to an increasing porosity. When correlating the mean pore radius with the amount of micropores, the tuffs show the exact opposite trend (Fig. 4.19). Tuffs with > 25% of micropores show low mean pore radii and with < 25 % micropores, the mean pore radii successively increase with a decreasing amount of micropores. These correlations actually allow estimations about the tendency of the mean pore radii and the amount of micropores in tuff rocks, when only the porosity value is known. Please note that the described tendencies were best observed at porosities > 30 %.

The specific surface area (SSA) represent the surface of porous media that is in constant interaction with the moisture from the surrounding atmosphere (Siegesmund and Dürrast 2011). Thus, higher values imply a greater surface area of the material which can be decayed. The specific surface area plays an important role for condensation processes in porous media, meaning that materials with high specific surface area tend to higher capacity and susceptibility to water condensation and retention (Benavente et al. 2007). Since it is directly related to the porosity and inversely related to the pore size (Gregg et al. 1982), it has therefore a direct relation to the salt crystallization (Benavente et al. 2007). A higher susceptibility towards salt crystallization due to a higher specific surface area could not be observed in this investigation. For many samples the salt bursting test was not finished, because they are still intact after 150 salt cycles. However, amongst others, the distinct relation of the specific surface area with the water transport and retention properties, as well as the type and amount of clay minerals and zeolites, will be presented in the following sections.

#### 4 Deterioration of volcanic tuff rocks from Armenia

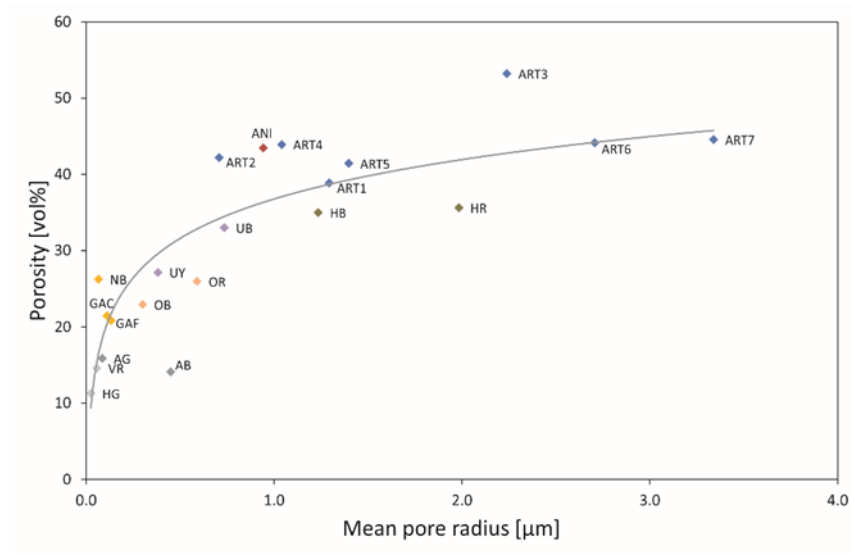


Figure 4.18: Mean pore radius as a function of the porosity of the investigated volcanoclastic rocks

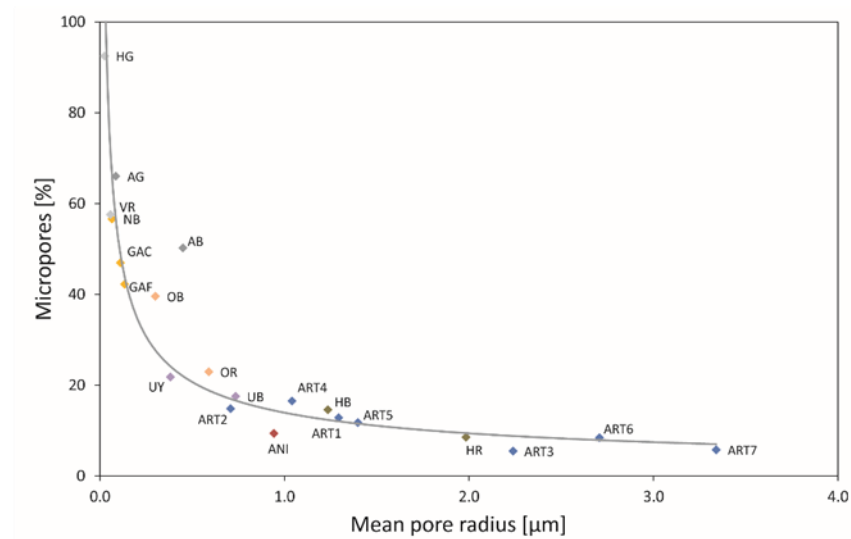


Figure 4.19: Mean pore radius as a function of the ratio of micropores

#### 4.4.2 Water transport and retention as a function of the pore space properties

Most of the weathering processes that occur in natural building stones, such as frost- and salt-related weathering, hygric/hydric and thermo-hygric/hydric expansion are controlled by the presence of water (Siegesmund and Dürrast 2011; Snethlage 1984; Weiss et al. 2004). Many authors have stressed out the important influence of the pore space properties on water transport and retention (compare discussion in Siegesmund and Dürrast (2011) and Steiger et al. (2011)). Since the pore space properties of the investigated Armenian tuff rocks vary significantly, the influence of particular configurations on the water transport and retention properties can be elucidated by plotting them graphically. Regarding the capillary water absorption coefficient ( $w$ ), the water vapor diffusion resistance ( $\mu$ ) and hygroscopic water sorption, the Armenian tuffs show distinct correlations with their porosity and amount of micropores (Figs. 4.20 – 4.25). Looking at Figures 4.20 and 4.21, respectively, the capillary

#### 4 Deterioration of volcanic tuff rocks from Armenia

water adsorption coefficient ( $w$ ), typifying the amount of water that can potentially being absorbed by the rock, shows low values at porosities < 25 %. At porosities > 25 %, the capillary water adsorption coefficient ( $w$ ) is increasing with increasing porosity (Fig. 4.20). The opposite trend is observed when correlating the capillary water absorption coefficient ( $w$ ) with the amount of micropores (Fig. 4.21).

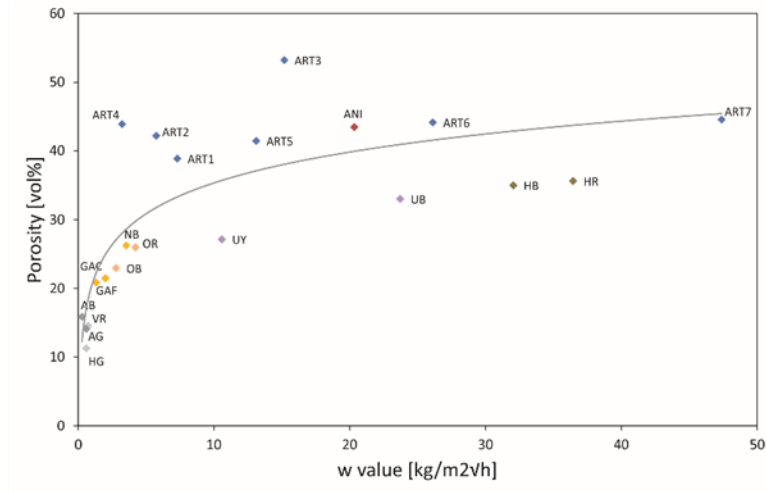


Figure 4.20: Water absorption coefficient ( $w$ ) in Z direction as a function of the porosity

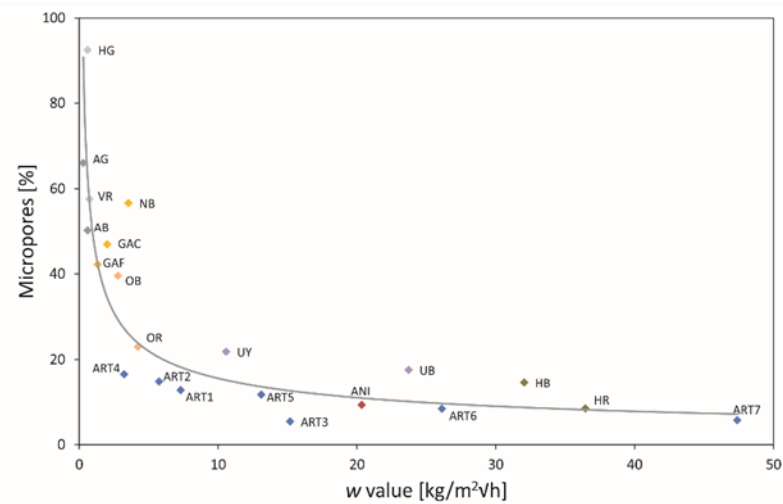


Figure 4.21: Water absorption coefficient ( $w$ ) in Z direction as a function of the percentage of micropores

Tuffs with > 25 % of micropores show low  $w$  values. Under 25 % of micropores, the capillary water adsorption coefficient ( $w$ ) is increasing with decreasing amount of micropores. As the Armenian tuffs with proportions of micropores < 25 % can show a broad spectrum of  $w$  values, it is worth to take a look at their pore radii distribution (Fig. 4.13). As expected, the tuffs showing higher amounts of capillary pores in the 1–10  $\mu\text{m}$  range, also show higher  $w$  values, underlining the important role of capillary pores to the water absorption of natural building stones. Concerning the influence of the porosity on the capillary water adsorption coefficient ( $w$ ), porosities < 25 % and fractions of micropores > 25 % do not seem to have a large impact on the water absorption of tuff rocks (Figs. 4.20, 4.21). However, porosities > 25 % and



#### 4 Deterioration of volcanic tuff rocks from Armenia

fractions of micropores < 25 % can lead to huge differences in the water absorption behavior of tuffs, depending on the aforementioned distribution of capillary active pores. The determination of the rocks' porosity, combined with the identification of the amount and distribution of micropores and capillary active pores, can thus give a fast estimation of the water absorption potential of tuff rocks.

Similar inversions of the relation of porosity and amount of micropores, respectively, are observed for the water vapor diffusion resistance ( $\mu$ ) and the hygroscopic water sorption (Figs. 4.22 – 4.25). Tuff rocks with porosities > 30% show a rather low resistance against water vapor diffusion ( $\mu$  value) and a low hygroscopic water sorption. At porosities < 30 %, the  $\mu$  value and sorption value decrease with lower porosity (Figs. 4.22, 4.24). At < 25 % of micropores,  $\mu$  values and sorption values are observably low. At > 25 % micropores, they tend to increase with higher amounts of micropores (Figs. 4.23, 4.25). As can be seen in Figures 4.20 – 4.25, the tuffs can always be grouped in two groups, which are divided at 25 and 30 % porosities or micropores, respectively. Given these findings, it can be concluded that the pore space properties have a serious and partly inverse impact on the water transport and retention behavior of the Armenian tuff rocks.

Since the investigated tuff rocks show partly high anisotropic behavior, with significantly lower capillary water adsorption as well as higher water vapor diffusion resistance in Z direction (Table 4.3), it is evident that the pore network of the investigated Armenian tuffs is, for the greater part, better interconnected parallel to the bedding plane. With respect to the directional dependent weathering behavior of many tuffs, this fact should be considered when installing boulders of tuff stone in a construction.

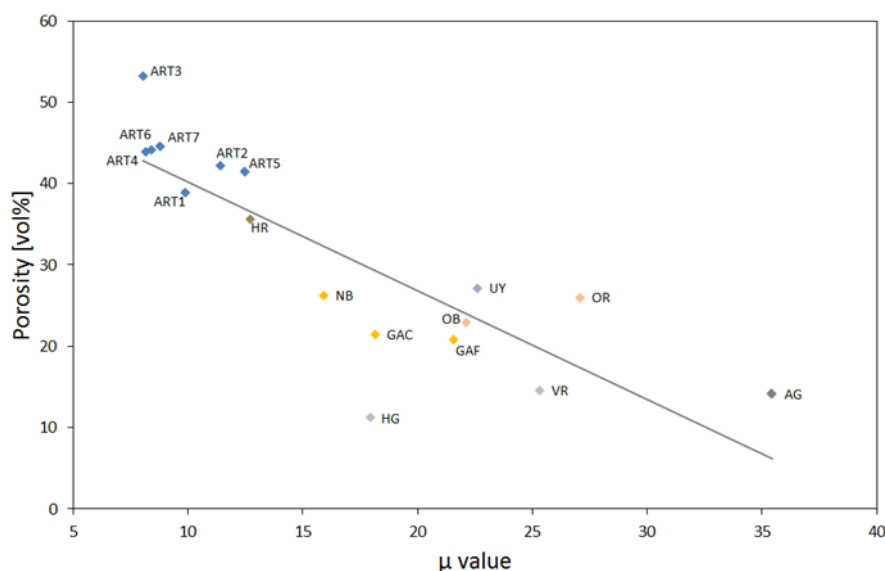


Figure 4.22: Water vapor diffusion resistance ( $\mu$ ) as a function of the porosity

#### 4 Deterioration of volcanic tuff rocks from Armenia

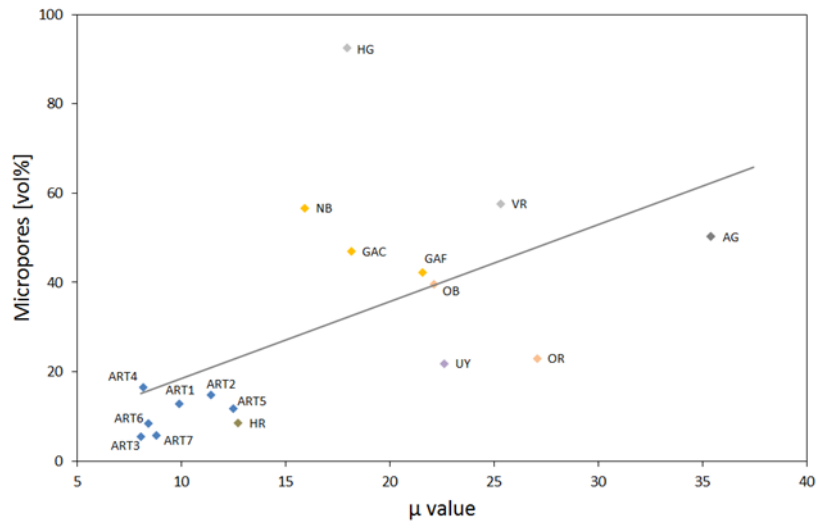


Figure 4.23: Water vapor diffusion resistance ( $\mu$ ) as a function of the percentage of micropores

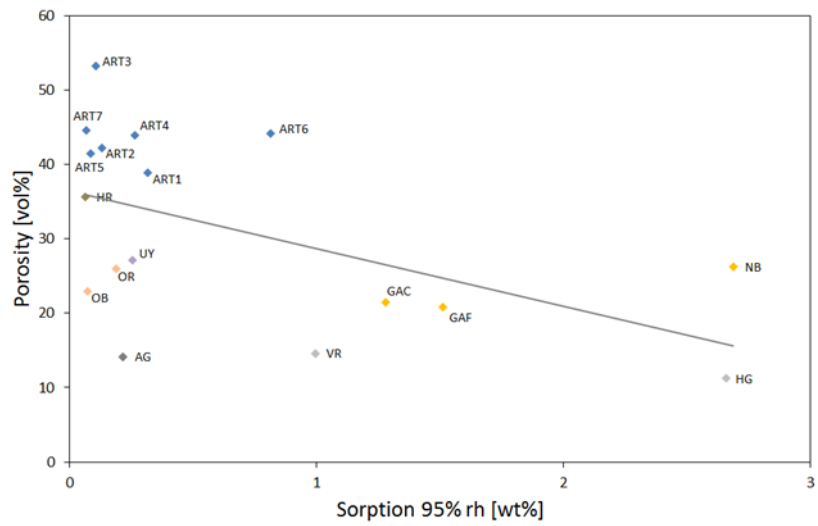


Figure 4.24: Hygroscopic water sorption at 95 % relative humidity as a function of the porosity

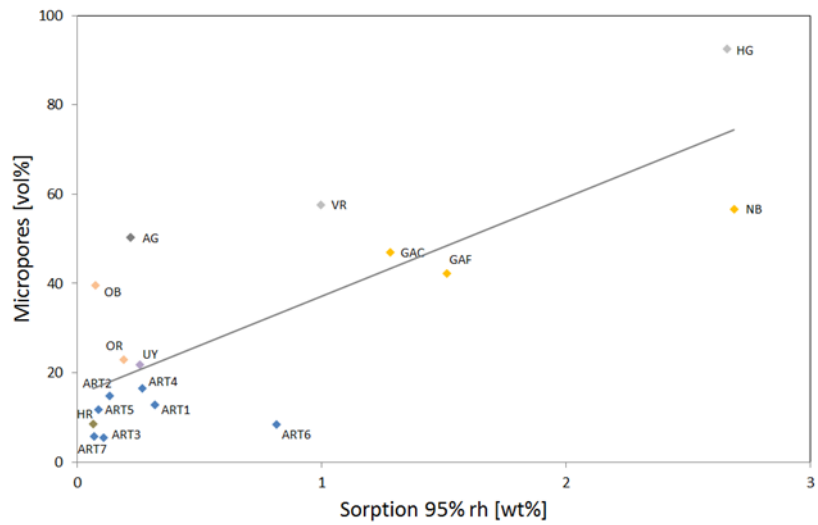


Figure 4.25: Hygroscopic water sorption at 95 % relative humidity as a function of the percentage of micropores

## 4 Deterioration of volcanic tuff rocks from Armenia

### 4.4.3 Moisture expansion related to the pore space properties and water absorption

The hydric expansion values of the investigated tuff rocks show a relation with the mean pore size and the fraction of micropores (Figs. 4.26, 4.27). According to these, the tuffs tend to show a linear increasing hydric expansion with a higher amount of micropores (Fig. 4.27) and a decrease with higher mean pore radii (Fig. 4.26), respectively. The hydric expansion values are low for tuffs with mean pore radii  $< 0.025 \mu\text{m}$  and micropores  $< 25\%$ . Mean pore radii  $> 0.025 \mu\text{m}$  and  $> 25\%$  micropores lead to a wide range of hydric expansion values. The important influence of the pore space properties on the weathering behavior due to hydric expansion processes is well known (Pötzl et al. 2018a; Ruedrich et al. 2011; Wedekind et al. 2013). The Armenian tuff rocks confirm these findings with a striking clarity. Therefore, similar to the conclusion of the previous section, the pore space properties can also be used to estimate the hydric expansion potential of the tuff rocks.

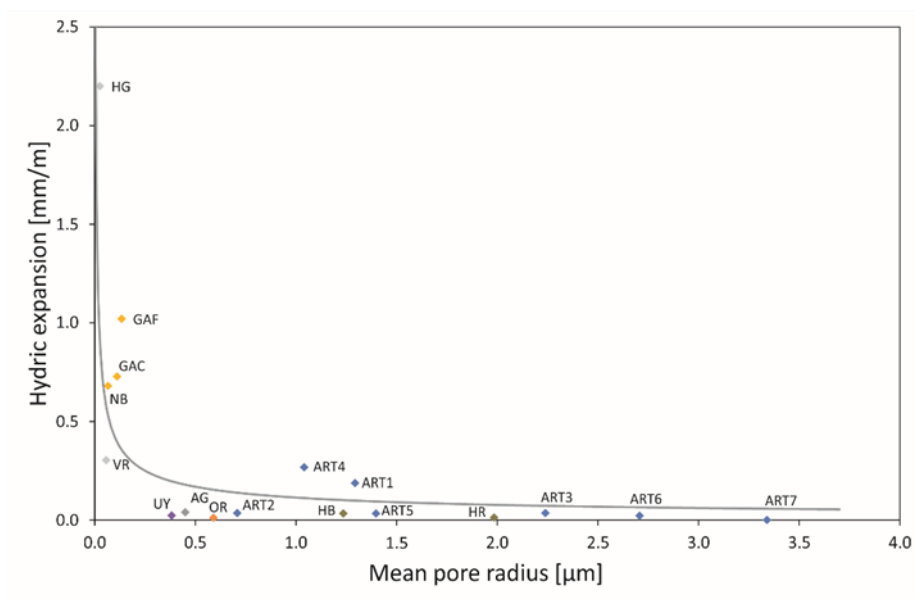


Figure 4.26: Maximum hydric expansion as a function of the mean pore radius

#### 4 Deterioration of volcanic tuff rocks from Armenia

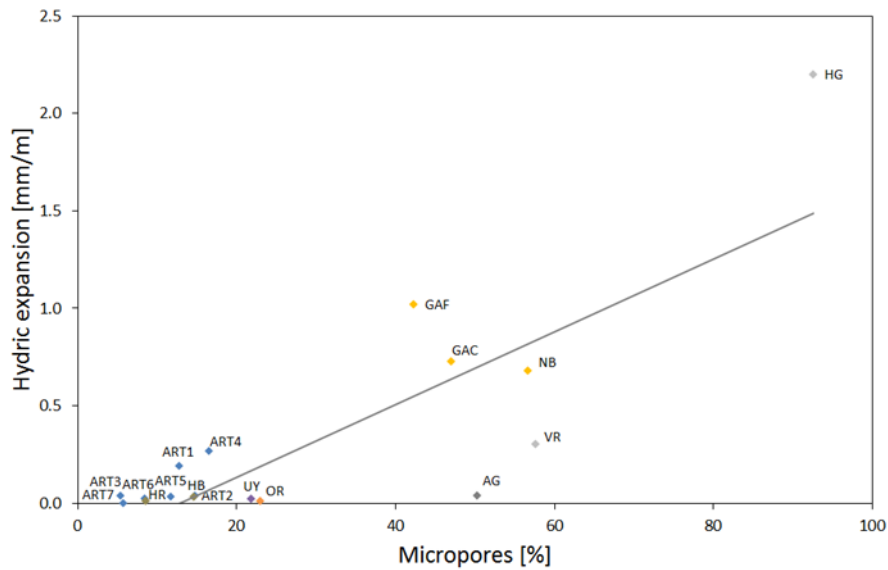


Figure 4.27: Maximum hydric expansion as a function of the percentage of micropores

In Figures 4.28 and 4.29 distinct correlations of the capillary water adsorption coefficient ( $w$  value) as well as the hygroscopic sorption value, which can provide information about the swelling potential of a rock (Kocher 2005), with the hydric expansion of the rocks are observable. These correlations illustrate that a fast or high water uptake not necessarily means that the rock will expand more due to moisture expansion. In fact, in these particular cases, the tuffs show less hydric expansion with increasing water uptake (Fig. 4.28). On the other hand, the maximum sorption values at 95 % relative humidity can be used for an indication whether the rock will show high or low hydric expansion behavior. In this study, with increasing hygroscopic sorption values, the rocks show a tendency to an increasing hydric expansion (Fig. 4.29). The deviations of the Haghartsin Green (HG) and Noyemberyan (NB) tuffs are related to their zeolite content, which can result in an extraordinary high sorption value.

A similar relation of the hydric expansion regarding the cation exchange capacity (CEC) (Fig. 4.30), the amount of micropores and the hygroscopic sorption, respectively, are striking. Low CEC values ( $< 2$  meq/100 g), low amounts of micropores ( $< 25\%$ ) and low sorption values ( $< 1$  wt%) are exclusively shown by tuff rocks with low hydric expansion ( $< 0.3$  mm/m). An increase of the CEC, amount of micropores and/or sorption is always accompanied by a successive increase of the hydric expansion. Therefore, either of these properties can be used for an estimation of the others.

#### 4 Deterioration of volcanic tuff rocks from Armenia

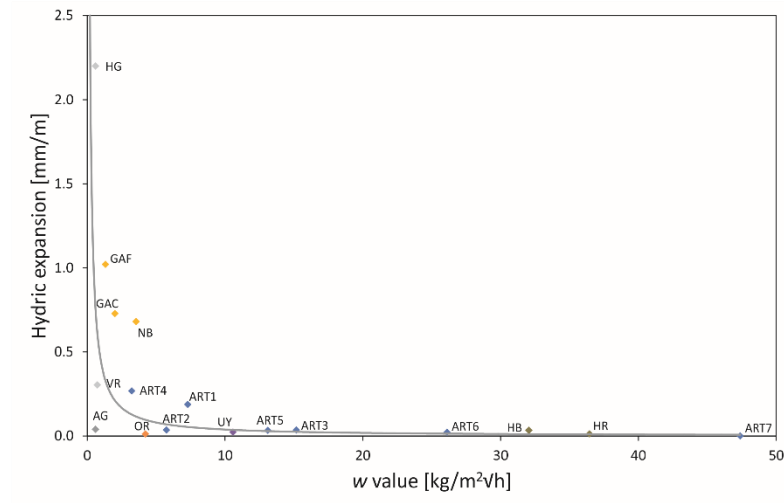


Figure 4.28: Maximum hydric expansion as a function of the capillary water absorption coefficient ( $w$ ) in Z direction

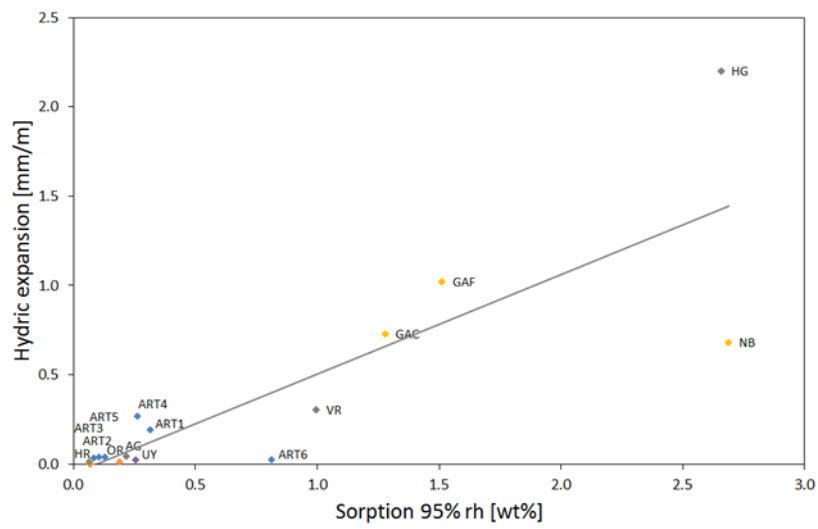


Figure 4.29: Maximum hydric expansion as a function of the hygroscopic sorption at 95 % relative humidity

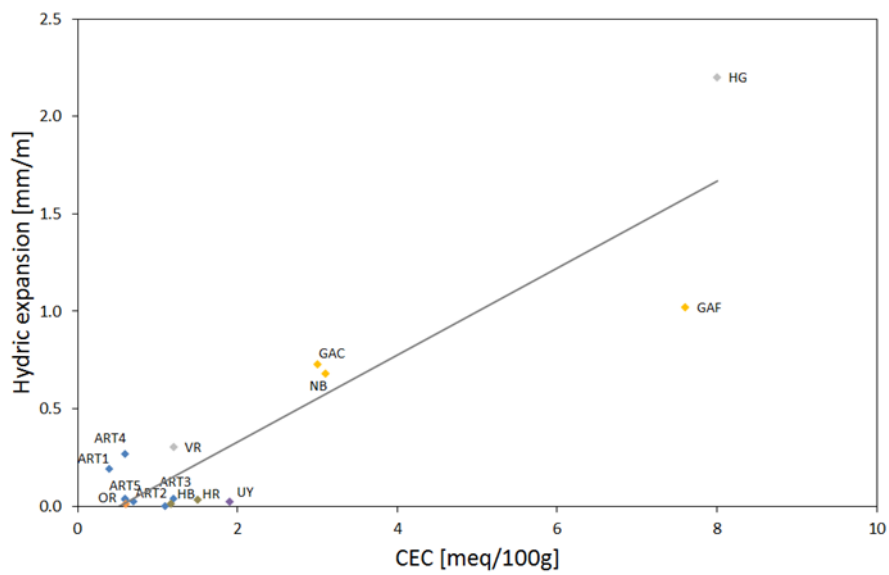


Figure 4.30: Maximum hydric expansion as a function of the cation exchange capacity (CEC)

## 4 Deterioration of volcanic tuff rocks from Armenia

### 4.4.4 Influence of clay minerals on pore space properties and moisture expansion

Clay minerals showed to have a potential impact on the pore space properties of the rocks and therefore on the weathering behavior of tuff building stones. The aforementioned present kaolinite booklets in Voskepar Red (VR), for instance, could cause a difference in porosity compared to adjacent grains (Fig. 4.9e). Significantly larger pores in the predominantly kaolinite-rich areas facilitate capillary water flow and thus provide a faster water uptake and distribution of fluids into the micropores of the groundmass and neighboring grains and fragments. The groundmass of VR, which is verifiably coated with interstratified swellable illite–smectite (I–S) (Fig. 4.11), is thereby provided more swelling fluid and salt load is brought significantly faster into the micropores. In the SEM micrographs in Figure 4.9 the influence of pumice clasts and amorphous glass on the porosity of the tuff rocks is observable. Pumice clasts tend to show considerably larger pores (Fig. 4.9a–c), resulting in a possible faster water uptake and distribution. Occasionally, the pumice clasts show significant elongation and a one-directional pore connection (Fig. 4.9b). This one-directional pore connection may lead to a preferred direction of water distribution, resulting in anisotropic behavior regarding the water transport and weathering behavior. Although it is not clear if the pores in the pumice clasts are connected, this anisotropic behavior is particularly pronounced in the Artik (ART1-7) and Oshakan (OB, OR) tuffs (Table 4.3), which both contain elongated clasts of pumice. As aforementioned and displayed in Table 4.3, the anisotropic behavior of the tuffs regarding the water transport and weathering behavior give a clear indication of the significance of the clastic material, for instance in the Artik tuffs. The same applies for the presence of clay minerals. Clay minerals are typically characterized by thin layers of considerable length and width and a negligible thickness. A parallel embedding of the clay minerals can lead to a densification in Z direction (perpendicular to the bedding) and results in an anisotropic behavior of the rock, as shown by the water transport and retention behavior. Thin pore throats can be formed by amorphous glass and generate high amounts of micropores (Fig. 4.9d). An increase of micropores can cause a higher surface area (Fig. 4.31) which can be potentially exposed to weathering processes. In addition, clay minerals possess a large surface area and are likely to be displayed by higher BET values (Kaufhold et al. 2010). Figure 4.32 shows the impact of the clay minerals and zeolite material, displayed by the CEC value, on the specific surface area (BET value) of the tuff rocks. Two groups can be distinguished. The first group of low CEC ( $< 2$  meq/100 g) shows a low surface area. The second group consists of tuffs with high CEC values, indicating high amounts of swellable clay minerals or zeolites, respectively, showing a simultaneous increase of the specific surface area.

#### 4 Deterioration of volcanic tuff rocks from Armenia

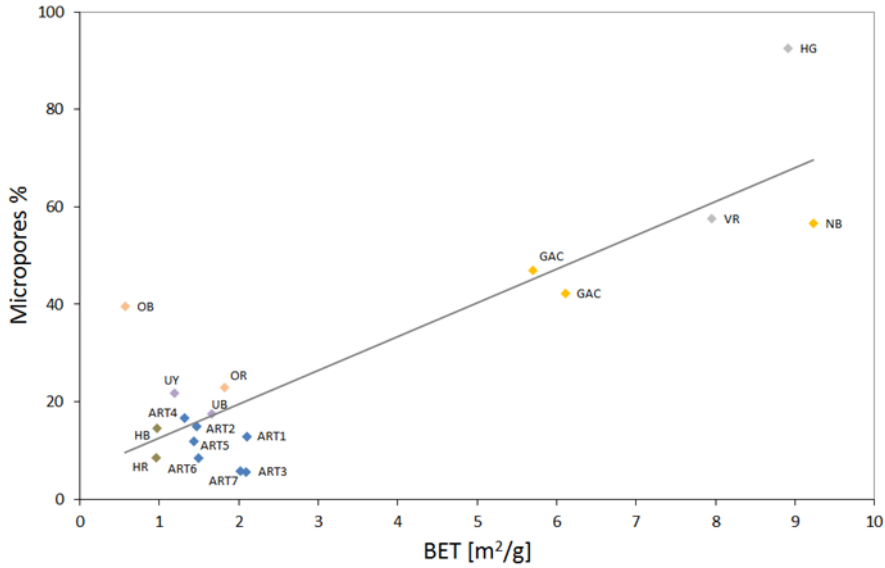


Figure 4.31: Specific surface area determined by BET (m<sup>2</sup>/g) as a function of the percentage of micropores

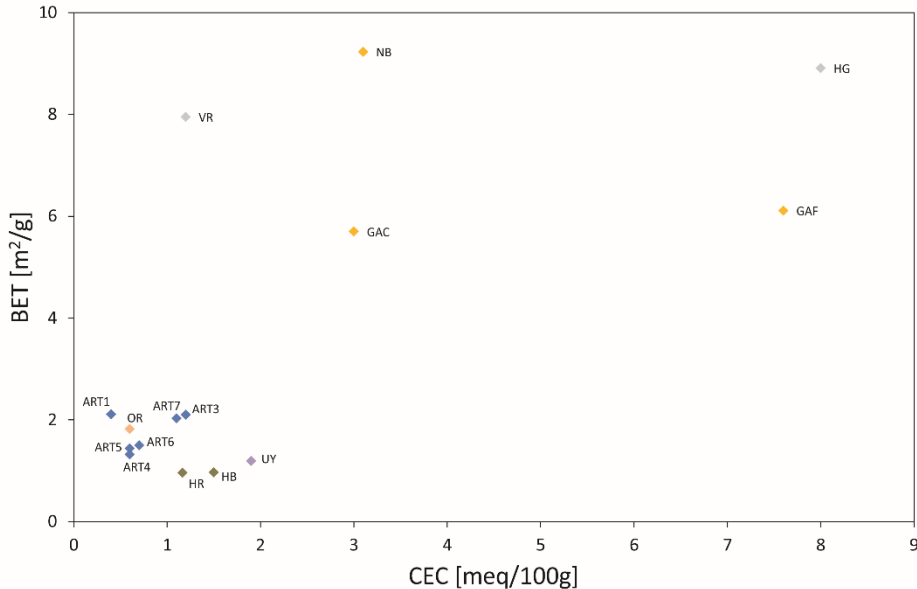


Figure 4.32: Specific surface area determined by BET (m<sup>2</sup>/g) as a function of the cation exchange capacity (CEC)

In Figure 4.30 a correlation of the hydric expansion with the cation exchange capacity (CEC) of the Armenian tuffs can be observed. A higher CEC, which is related to a higher amount of swellable clay minerals (Pötzl et al. 2018a; Ruedrich et al. 2011), comes along with an increasing value of hydric expansion. This confirms the important role of swellable clay minerals on the hydric expansion behavior of the investigated tuffs. The tuffs with higher content of swellable clay minerals such as illite–smectite and corrensite, consequently, show the highest CEC and hydric expansion (Fig. 4.11). However, in other studied tuff rocks, this was not the case (Wedekind et al. 2013). Nevertheless, as discussed above, the pore space properties showed to have a significant relation with the hydric expansion as well. Thus, a potential influence of disjoining pressure cannot be excluded. The mechanism called disjoining pressure is characterized by the interaction of surface forces in rocks with high amounts of micropores smaller than 0.1 μm and can induce swelling in the absence of swellable clay

#### 4 Deterioration of volcanic tuff rocks from Armenia

minerals (Ruedrich et al. 2011; Weimann 2001). A testing for the verification of the influence of disjoining pressure on the moisture expansion process in tuff stones, however, is not yet developed (Pötzl et al. 2018a), and therefore, will not be further discussed in this study. The ability of clay minerals to transfer stresses within the rocks fabric is well known (compare discussion in Pötzl et al. 2018a, Ruedrich et al. 2011, Wangler and Scherer 2008). Especially when located in critical spots such as grain contacts (Fig. 4.10e), even small amounts of swellable clay minerals can lead to a large swelling strain. Haghartsin Green (HG) represents a tuff where both, high amounts of clay minerals and their location in critical spots, are present. Consequently, HG shows the highest hydric expansion values and low resistance against salt crystallization.

Additionally to the high amounts of clay minerals, Noyemberyan (NB) and Haghartsin Green (HG) show considerable amounts of mordenite and analcime, respectively (Table 4.2; Fig. 4.10c). Mordenite and analcime are zeolite minerals and known for their good water retention capacity (Koizumi 1953). Amongst others, their non-swelling behavior, high sorption rates, chemical stability, thermostability and possibility of regeneration make them very attractive for the usage in environmental protection chemistry and industry (Korkuna et al. 2006). One of the main factors controlling the characteristic features of zeolites is their distinctive amount of micropores. Micropores of zeolites are typically  $< 2$  nm and can be further subdivided into supermicropores (0.7 – 2 nm) and ultramicropores ( $< 0.7$  nm) (Korkuna et al. 2006). On the one hand, this explains the high sorption values of NB and HG (Fig. 4.14). On the other hand, it is possible that the extreme small micropores of the zeolites contribute to the creation of environmental conditions in the tuffs fabric, where the mechanism of disjoining pressure can potentially take place. Further investigations on the microporosity of NB and HG, potentially with gas adsorption analyses rather than mercury intrusion porosimetry for a higher resolution in the nanometer scale, could elucidate the contribution of the zeolite micropores. Another feature of zeolites is their dehydration behavior due to thermal stress (Koizumi 1953). Upon heating, zeolitic water is split off from the mineral and can subsequently become available for the initiation of weathering processes in the rock. Thermal and thermohydric expansion analyses as conducted in Siegesmund et al. (2018) could determine if this is actually the case.

##### 4.4.5 Salt weathering

Usually the weight loss of the sample during the salt weathering test functions as the main criterion for the susceptibility to salt crystallization. In some cases (e.g., ART6), the sample already lost one fourth of its mass, but still shows  $> 100$  % of its initial weight after 120 salt cycles (Figs. 4.16, 4.17). The weight of the specimens depends both on the loss of material and the amount of absorbed salt (Lubelli et al. 2014). Therefore, for these samples, the sole evaluation of the salt crystallization susceptibility due to weight changes is inappropriate and precise observations of the rock surface during the salt bursting test are of crucial importance. Lubelli et al. (2018b) point out that so far no criteria exist for the classification of the durability of the tested material in the existing standards. Conclusions are exclusively drawn by comparison between the tested materials, and therefore, supplementary classification criteria could add additional values and modify the whole test procedure (Lubelli et al. 2018b).



#### 4 Deterioration of volcanic tuff rocks from Armenia

The aforementioned characteristic weight increase of the samples at the beginning of the salt bursting test appears to be related to the porosity. With increasing porosity, the samples show an increase in initial weight during the first test cycles of the salt bursting test (Fig. 4.33). The extraordinary high initial weight increase of ANI can be explained by its significantly lower density (Table 4.3). Under the same test conditions, weight changes on sample cubes with significant lower density are expected to have a larger impact.

A very noticeable observation is the difference of the salt crystallization susceptibility of the Armenian tuffs compared to other tuff stones such as those from Mexico and Germany tested in studies of López-Doncel et al. (2016), Padilla-Ceniceros et al. (2017) and Pötzl et al. (2018a), respectively. The majority of German and Mexican tuffs, undergoing the exact same salt weathering test according to the standard DIN EN 12370 was already destroyed after 30 salt cycles at most. Only three Armenian tuffs were destroyed after 30 salt cycles and half of the Armenian tuffs are still intact after 150 salt cycles (Fig. 4.16). According to this, the majority of Armenian tuffs shows to be less susceptible to salt crystallization than German and Mexican tuff varieties applied to the same salt bursting test procedure.

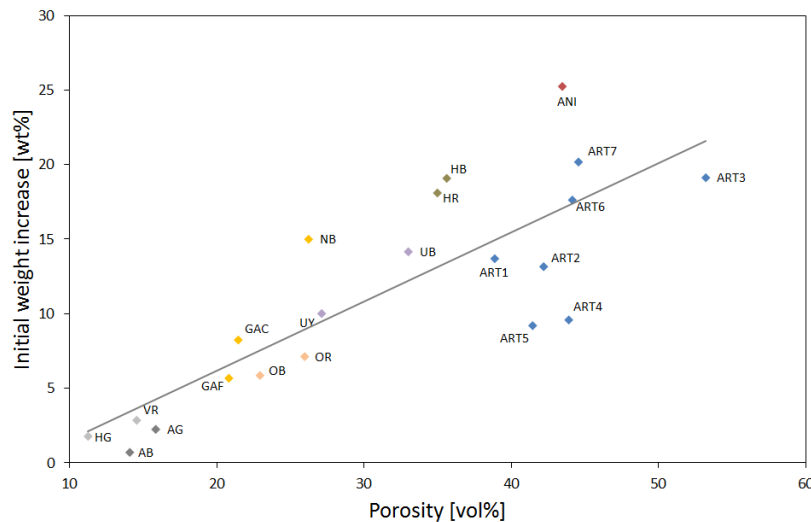


Figure 4.33: Initial weight increase during the first cycles of the salt bursting test as a function of the porosity

Similar to the studies from Mexico and Germany, Armenian tuffs of this study with a well-developed bimodal pore radii distribution and considerable amounts of micropores tend to be more susceptible to salt crystallization than tuffs with unimodal distributions with their maxima  $> 1 \mu\text{m}$ . Snethlage (1984), Scherer (1999), Benavente et al. (2007), Ruedrich and Siegesmund (2007) and others pointed out the particular susceptibility to salt crystallization of rocks with unimodal pore radii distribution containing primarily micropores. The Haghartsin Green tuff (HG) with 97 % micropores and the Golden Armenia Fine (GAF) with at least 42 % micropores display two of the most susceptible tuffs of this investigation. However, the Artik tuffs, ART1 and ART4, are likewise susceptible, while showing the majority of pores in the capillary and macropore size range. While their clearly higher porosity certainly influences their susceptibility due to higher capacity for water retention and storage of salt, both samples represent the only samples in the group of Artik tuffs that show any hydric expansion (Table 4.3). Since the other Artik tuffs show similar petrographic and petrophysical properties, their expansion behavior due to moisture changes is the only characteristic that differentiates them

#### 4 Deterioration of volcanic tuff rocks from Armenia

from each other (Table 4.3). Consequently, the susceptibility towards hydric expansion can potentially be a factor contributing to the salt weathering in this case. As shown in Figure 4.34, the resistance of the tuffs against salt weathering coincides with their hydric expansion behavior. An increasing salt weathering resistance of the samples in combination with a decreasing value of hydric expansion indicates that tuffs with higher hydric expansion values tend to be more susceptible to salt crystallization. Zeolite minerals do not seem to play a significant role for the salt weathering of the tuffs, as the Noyemberyan (NB) tuff does not disintegrate as fast as the Haghartsin Green (HG). Nevertheless, the type and amount of swellable clay minerals (represented by the CEC) show a relation with the salt crystallization resistance of Armenian tuff rocks (Fig. 4.35). An increasing CEC of the tuffs consequently results in a higher susceptibility. Therefore, the swelling behavior during the full immersion in the salt solution, as well as the thermal stress during the drying process of the test procedure (60°C) can be potentially additional factors, contributing to the decay of the tuff rocks. A huge factor contributing to the susceptibility of the Artik tuffs, in general, is perhaps the back weathering of the large pumice clasts. The primary loss of the relatively softer pumice clasts leaves the rock with a higher surface area exposed to the weathering process.

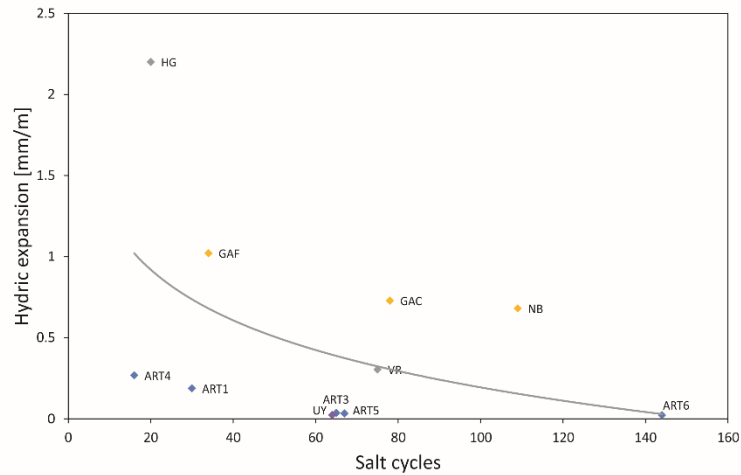


Figure 4.34: Salt weathering resistance as a function of the hydric expansion

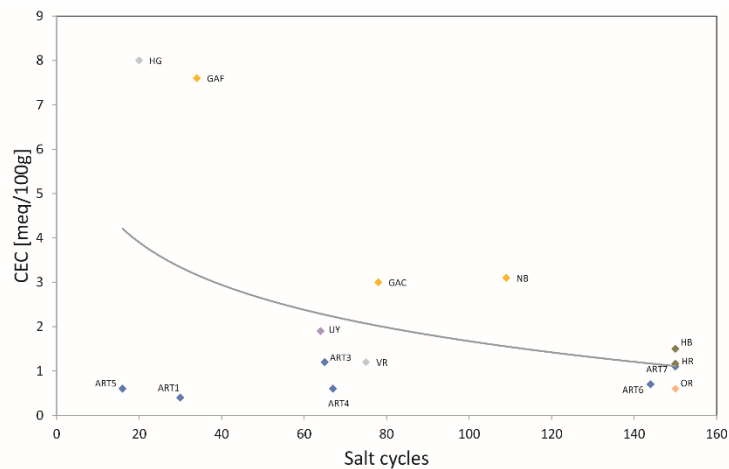


Figure 4.35: Salt weathering resistance as a function of the cation exchange capacity (CEC)

#### 4 Deterioration of volcanic tuff rocks from Armenia

The distinct higher resistance against salt crystallization of Armenian tuffs in the salt bursting test compared to the tuffs in the studies of López-Doncel et al. (2016), Padilla-Ceniceros et al. (2017) and Pötzl et al. (2018a), can be traced back to their mineralogical and fabric differences. While the investigated Mexican and German tuffs represent crystal-rich ash tuffs of rhyolitic composition, many of the Armenian tuffs are classified as glass tuffs (Fig. 4.9) of trachytic composition (Table 4.1). At equal petrophysical conditions, the rigid glass material of the Armenian tuffs is less likely to yield. The effective porosity, the capacity of water uptake and the resistance against water vapor diffusion do not show clear correlation with the resistance against salt crystallization and contradict the behavior of the tuffs in the studies from Mexico and Germany. However, the important influence of the micropores on the salt crystallization is clearly demonstrated (Fig. 4.36). It remains unclear to which degree the welding of the tuff rocks contributes to the cohesion of material and their internal resistance. Future investigations on the mechanical properties of the tuff rocks, such as tensile and compressive strength, could identify possible correlations and enhance the incomplete picture. In addition, the monitoring of the evolution of the pore space properties and crack propagation during the salt bursting test could for example identify if and how a shift of the pore radii distribution is taking place due to salt crystallization (Sousa et al. 2018).

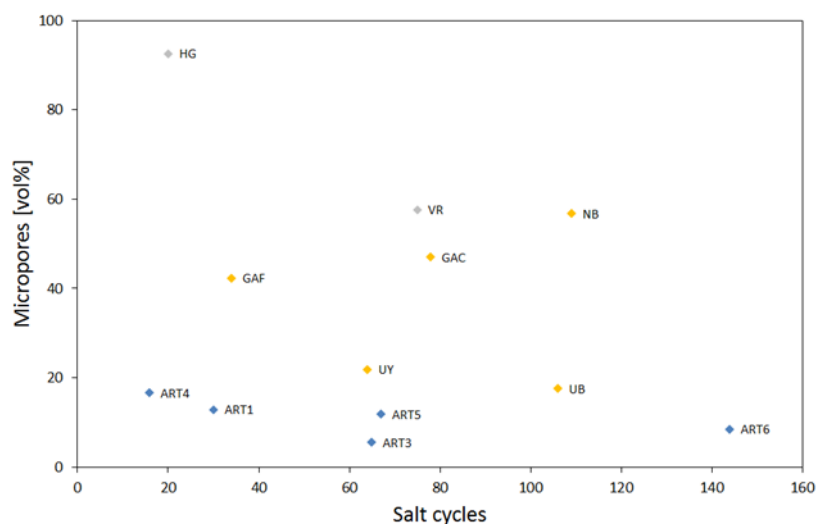


Figure 4.36: Salt weathering resistance as a function of the percentage of micropores

#### 4.5 Conclusions

In this study, a large number of volcanoclastic rocks, mainly tuffs, used as building stone in the historical architecture of Armenia, was investigated regarding their petrographical and petrophysical properties as well as their weathering behavior. The volcanic tuff rocks show a broad spectrum of different chemical and mineralogical composition as well as petrophysical properties and show characteristic weathering behavior towards hydric expansion and salt crystallization. The net result of this work is the identification of the correlation between the individual properties and their influence on the salt crystallization resistance as well as the moisture expansion behavior.

The porosity as well as the amount and distribution of micropores showed to be directly related to the water transport and retention properties of the tuff rock. Interestingly, the limit

#### 4 Deterioration of volcanic tuff rocks from Armenia

for a changing behavior regarding the water transport and retention is located at 30 % porosity and 25 % micropores, respectively. Under 30 % porosity and over 25 % micropores, the tuff rocks show low water uptake and the water vapor diffusion resistance as well as the sorption values show a broad range, but tend to higher values (Figs. 4.20 – 4.25). Tuff rocks with porosities > 30 % and < 25 % micropores show a contrary behavior.

The study revealed a direct relation of the CEC, amount of micropores and sorption value with the hydric expansion. An increase of either of these values is always accompanied by a successive increase of the hydric expansion (Figs. 4.27, 4.29, 4.30), so that all three values showed to be useful for the estimation of the hydric expansion potential of Armenian tuff rocks. Distinct correlations with the hydric expansion illustrate the significant impact of the mean pore radius and amount of micropores on the moisture expansion of tuff rocks (Figs. 4.26, 4.27) and shows that not only clay minerals are responsible for swelling processes. Especially, tuff rocks with high amounts of micropores (< 0.1  $\mu\text{m}$ ) show the highest expansion values, indicating a potential contribution of disjoining pressure to the swelling process. Nevertheless, the important impact of swellable clay minerals for the moisture expansion of tuff rocks could be highlighted. Tuffs with high cation exchange capacity (CEC) show a linear correlation with the hydric expansion (Fig. 4.30), indicating the importance of swellable clay minerals to the swelling process, especially when they are located in critical spots in the rock fabric. Additionally, zeolites showed to cause high specific surface areas and significantly contribute to the sorption rate and potentially to the hydric expansion, by creating conditions for disjoining pressure to take place, due to their distinct amount of micropores < 0.7 nm. The exact pore character and the influence of the zeolites to the hydric expansion should be analyzed in further investigations. Dehydration of zeolites due to thermal stress can result in the release of zeolitic water, which subsequently can become available for the initiation of further weathering processes in the rock. This issue should also be investigated in form of thermal and thermo-hydric expansion analyses in further research on zeolite containing tuff rocks. Overall, we could demonstrate that the accessory minerals, especially swellable clay minerals and zeolites, rather than the main components determine the weathering behavior of the tuff rocks.

Tuff rocks showing a bimodal pore radii distribution with considerable amounts of micropores (< 0.1  $\mu\text{m}$ ) and especially unimodal pore radii distributions with almost exclusively micropores have shown to be particularly susceptible to salt crystallization. Therefore, the important influence of the microporosity on salt weathering in tuff rocks could be clearly demonstrated. The significantly different results of the Armenian glass-rich tuffs, undergoing the exact same test procedure than crystal rich tuffs from Mexico and Germany (López-Doncel et al. 2016; Pötzl et al. 2018a), lead to the conclusion that salt bursting tests inspired by a European standard cannot always be transferred. In this particular case, it should be revised and the local genetic conditions as well as the mineralogical and fabric differences of the tuff rocks should be taken into account, especially regarding future studies on tuff rocks.

What remains unclear is the influence of freeze–thaw cycles on the weathering behavior of the Armenian tuff rocks. Climate tables of northern regions of Armenia show average temperature of –5 to –10°C from December to March. During this time, almost every day the temperatures drop below freezing. Further investigations on the tuffs behavior towards

#### 4 Deterioration of volcanic tuff rocks from Armenia

freeze–thaw cycles could elucidate the role of ice crystallization for these tuffs. It is at least expected to play a role at Voskepar Red (VR), since the tuff showed intensive back weathering and scaling in the construction (Fig. 4.4c, d), but revealing moderate resistance against salt crystallization (Figs. 4.16, 4.17) in the salt bursting test at the same time. In addition, the mechanical properties of the Armenian tuffs were not analyzed in this study. In past studies regarding tuff stones, the mechanical properties showed to play an important role for the durability of the rock (Wedekind et al. 2013) and should be investigated for a better understanding of their impact and development upon weathering effects.

## 5 Key parameters of volcanic tuffs: a statistical approach

### 5.1 Introduction

Availability, good workability, excellent aesthetic variability as well as favorable insulation properties were always convincing reasons for the utilization of volcanic tuffs in the architectural and artistic application. Through all cultures and epochs worldwide tuffs have been used as construction material for the creation of buildings, artworks and sculptures (Fig. 5.1). As popular as the material is, however, it is often very sensitive to weathering and the reasons for their fast deterioration are manifold and have been the subject of many studies (e.g., Auras et al. 2000; Çelik and Sert 2020; Egloffstein 1998; Fitzner and Basten 1994; Pötzl et al. 2018b; Ünal 2011; van Hees et al. 2003; Wedekind et al. 2013; Yu and Oguchi 2010). Some of the main culprits are the characteristic high porosity, a strong affinity for water absorption, low strength values and a frequent abundance in swelling clays (see discussions in López-Doncel et al. (2016) and Pötzl et al. (2018b)).



Figure 5.1: Volcanic tuffs in building heritage. Top left: the city center of San Miguel el Alto, Mexico; top right: the 2<sup>nd</sup> century Mitla Pyramids, Mexico; bottom right: the 16<sup>th</sup> century tulip pulpit in the Freiberg Cathedral, Germany; bottom left: macro photographs (6 x 6 cm) of the fifteen tuffs investigated in this study

The group of rocks that are under investigation here, although they are summarized under the term *tuff*, are truly different in every conceivable way. The International Union of Geological Sciences (IUGS) defines tuffs as volcanoclastic rocks, that consist of at least 75 % volcanic ash <2 mm (Le Maitre et al. 2002). However, commonly accepted the term tuff is used as a collective term, to describe any volcanoclastic rock with > 75 % pyroclasts of any size. The term

## 5 Key parameters of volcanic tuffs: a statistical approach

pyroclast refers to any fragment generated directly as a result of volcanic activity and includes individual crystals, glass and rock fragments. Volcanic tuff is an extrusive igneous rock formed by the consolidation and lithification of volcanic products, which have been ejected by an explosive volcanic eruption. Tuff deposits can reach thicknesses of hundreds of meters and total eruptive volumes of many cubic kilometers. They may be formed by a single eruptive explosion or from successive surges from a single eruption or eruptions that were separated by longer periods of time.

Volcanic tuffs can have a wide variety of textures, depending on the type and amount of pyroclastic content or their degree of welding. They frequently show *fragmented* texture: characteristic texture of pyroclastic rocks with a mixture of rock fragments, crystals and glass; *eutaxitic* or *vitroclastic* texture: formed by collapsed pumice and glass fragments called fiammes; *axiolitic* texture: formed by radial fibers emerging through a core formed by devitrification; or *laminar* texture: if formed by the fall of volcanic ash at different intervals or time-lapses. If the ejected volcanic products were hot enough (>600°C) they were welded together upon impact or compaction. The rock formed from this extraordinary hot ejecta is known as a *welded tuff* or *ignimbrite* (in the case of ash flows).

Tuffs can be classified according to the size of their pyroclastic fragments (Fisher 1966) or to the type of pyroclastic fragments (Schmid 1981). Fragment sizes range from ash (< 2 mm) and lapilli (64 – 2 mm) to blocks and bombs (> 64 cm). The main fragment types are of either crystal, vitric or lithic nature. The total alkali versus silica (TAS) classification system after Le Bas et al. (1986) is used for the geochemical classification of pyroclastic rocks, since the modal content of tuffs cannot always be determined accurately with the QAPF diagram (Le Maitre et al. 1989; Streckeisen 1978), due to the often cryptocrystalline and glassy texture of the groundmass. Usually, volcanic tuff is composed of a high percentage of silica (SiO<sub>2</sub>) and a great amount of the matrix consists of volcanic glass. The formation by explosive eruptions means association with acid magmas, hence minerals like quartz, plagioclase, potassium feldspars and mica are often found in tuffs. However, it is not uncommon to find volcanic tuffs of intermediate to basic composition.

The main components of tuffs are usually rock fragments, ash particles and scoria, that were ejected and deposited by violent volcanic eruptions and subsequently compacted and welded together to different degrees. Many contributing factors open the possibility to almost limitless heterogeneity. Significant contributing factors are the initial composition and cooling rate of the magma, the ratio of the dragged-along and incorporated components, degassing processes, different depositional and reworking environments, as well as subsequent alteration processes that may form new minerals with high impact on the strength and durability. The mineralogical and fabric heterogeneity of tuffs make it very difficult to determine reliable durability parameters and predict material behavior, which in turn is crucial for their quality assessment. Therefore, the evaluation for the construction suitability of tuffs is always associated with comprehensive and cost-intensive material characterization and testing.

For any type of geotechnical engineering purpose, like construction and mining, typically the rock strength is used as one of the basic parameters to classify the quality of the material and

## 5 Key parameters of volcanic tuffs: a statistical approach

its suitability for construction purposes (Benavente et al. 2004; Siegesmund and Dürrast 2011). Together with the pore space properties, it can be used to estimate the stone's durability, which is defined as the ability to maintain essential and distinctive characteristics of the stone over the course of its lifespan. The standardized assessment of strength parameters is often linked to a time- and cost-intensive destructive testing, which requires a formidable amount of sample material. Over the past years, in a growing amount of studies the authors were able to estimate the material behavior of dimension stones based on petrophysical data. Many authors were able to identify interrelationships between different rock properties and their particular influence on their weathering behavior (e.g., Benavente et al. 2004; Binal 2009; Bodnár et al. 2011; Davarpanah et al. 2020; Germinario et al. 2017; Gioncada et al. 2011; González et al. 2019; Ince et al. 2019; Jamshidi et al. 2018; López-Doncel et al. 2016; Morales Demarco et al. 2007; Mosch and Siegesmund 2007; Pötzl et al. 2018b; Sengun et al. 2014; Siegesmund et al. 2000; Snethlage and Wendler 1997; Sousa 2014; Stück et al. 2013; Teymen 2018; Török et al. 2007; Wedekind et al. 2013; Xue et al. 2020). Although, these studies led to a better understanding and prediction of the material behavior, the findings are often limited to certain types of rock and only applicable for individual cases.

Another observation is the frequent use of relatively small datasets and neglect of a deep petrographic investigation, which do not allow for general statements about the wide ranges of rock types and their parameters. However, some authors, like Mosch and Siegesmund (2007) or Stück et al. (2013) conducted studies on hundreds of data points from the literature and were able to establish criteria and systems to better qualify plutonic rocks, limestones and sandstones for construction suitability and predict their weathering behavior. Stück et al. (2013) were even able to create a quality catalogue for different types of sandstone, based on their textural and compositional maturity.

Various studies on volcanic tuffs present a considerable amount of thoroughly treated data (e.g., Auras and Steindlberger 2005; Bozdağ and Ince 2018; Çelik and Çobanoğlu 2019; Ince et al. 2019; Korkanç and Solak 2016; López-Doncel et al. 2016; Steindlberger 2004; Teymen 2018; Török et al. 2007; Wedekind et al. 2013). To the authors knowledge, however, no such comprehensive study for tuffs exists, that integrates petrographic, technical and durability parameters with a larger set of data points. Besides the fact that studies on volcanic tuffs as dimensional stones are significantly underrepresented in the literature when compared to other magmatic building stones, sandstones or limestones for example (Wedekind 2016), the comparability of tuffs often turn out to be a challenging task because of their great heterogeneity even when looking at small scale comparison of material from the same outcrop (Germinario and Török 2019; Siedel 2017).

In this chapter, the petrophysical data of up to 513 tuffs from the literature are used to analyze the distribution and limits of single rock properties and to identify interrelationships between them, with the goal of identifying key parameters for the estimation of their weathering behavior. In addition, 15 selected tuffs were investigated in more detail, in order to extrapolate to the very comprehensive, but less detailed dataset from the literature and achieve larger representability.



## 5 Key parameters of volcanic tuffs: a statistical approach

### 5.2 Materials and methods

A total of fifteen volcanic tuffs from Armenia, Germany and Mexico, which are frequently used as building stones (Tab. 5.1), were investigated in terms of their petrographical and petrophysical properties, as well as their weathering characteristics. This study includes a brief summary of their petrography. Please find more detailed descriptions in Chapter 3. The subsequent section will then present the petrophysical data of these tuffs. In order to obtain a more comprehensive dataset, the data of the detailed study was complemented with additional petrophysical data from 123 literature sources representing a total of 513 tuffs from 21 countries. The references are listed in Table A.1 in the appendix.

#### 5.2.1 Statistical methodology

Univariate and bivariate statistical analyses were applied on up to 528 tuffs from the database with the open software 'RStudio'. Box-and-whisker plots (boxplots) were used to display the distribution of single rock properties (univariate method). They essentially consist of two parts: a box and a set of whiskers. The box displays the interquartile range (IQR) in which 50 % of the values are present, limited by the median of the lower (25 % quartile) and upper (75 % quartile) half of the dataset. A horizontal line inside the box represents the median of the whole dataset and its position allows for an estimation of the skewness of the data distribution. The whiskers are drawn until the minimum and maximum values. Their length is limited to 1.5 times of the IQR (Tukey 1977) and any lower or higher values are plotted as outliers. The data of the 15 representative tuffs of this study is included into the big dataset. To visualize, however, the representativity of the selected tuffs, the range of their single rock properties is presented as a red line, next to the boxplots.

Regression analyses investigate the relationship of two properties and reveal if the parameters are comparable (bivariate method). The data is presented in point diagrams with the correlation coefficient  $r$  expressing the relation between two parameters (Spearman rank correlation coefficient). The correlation coefficient  $r$  varies between +1 and -1, whereby values close to +1 or -1 describe a significant correlation between the parameters and values close to 0 describe a lack of relationship. Under the assumption that the rock properties show normal distribution, confidence regions with 80 % probability range are displayed as ellipses within the regression analyses.

#### 5.2.2 Difficulties in data comparability

The compilation of a summarizing global overview bears certain risks that can potentially lead to an increased scattering of data. First of all, a global compilation of a high number of data points can per se lead to a wider scattering as a limited dataset (Büttgenbach 1990). The determination of technical parameters is usually based on country- or society-specific norms and standards, like the American Society for Testing and Materials (ASTM), German Institute for Standardization (DIN), Turkish Standards Institution (TSE) or International Society for Rock Mechanics (ISMR), to just name a few. Although, in the past decades institutions like the European Committee for Standardization (CEN) or the International Organization for Standardization (ISO) promoted an international alignment of norms and standards, the laboratory testing procedures in many countries are still conducted following deviant

## 5 Key parameters of volcanic tuffs: a statistical approach

standards. When comparing results from different international standards Mosch and Siegesmund (2007) point out the striking example of Peschel (1983), who observed a 10 – 20 % decreased uniaxial compressive strength (UCS) of test specimens with a ratio of  $h/d > 2$ , compared to specimens with a ratio of  $h/d = 1$  (following DIN EN 1926).

Further substantial influences on the results can be the different shape of the test specimens (e.g., cylinders react different to stress than cubes), the particular laboratory conditions (e.g., increased relative humidity), experimental procedure (e.g., different strain rates) and in the end human failure during testing, evaluation and documentation. It is also important to mention, that tuffs, due to their depositional conditions and frequent directional fabric, often show strong directional dependence, as demonstrated by several authors (e.g., Colella et al. 2017; López-Doncel et al. 2013; Martin III et al. 1992; Pötzl et al. 2018a; Stück et al. 2008; Weiss et al. 2004), which, however, is not considered in many studies. In order to maintain a large and representative dataset, the most commonly published mean values of the technical parameters were therefore used for the statistical analyses. However, like in the previous mentioned studies, the results of the additional 15 selected tuffs, which were investigated in more detail, illustrate that the mean values are not always representative and many technical parameters can differ by a multiple when determined parallel or perpendicular to the bedding plane. Please note that for most of the 513 tuffs from the literature not all of the technical parameters that were obtained in the present study, were determined in the respective studies. Therefore, the comparability of various parameters is limited.

## 5 Key parameters of volcanic tuffs: a statistical approach

### 5.3 Results and discussion

#### 5.3.1 Petrography and mineralogy

The petrography of the fifteen tuff rocks investigated in this study is presented in Chapter 3 and will be briefly summarized here. Note, that Table 5.1 corresponds to Table 3.1. The subsequent section (5.3.2) will then present the technical data obtained from these tuffs, which will be then complemented with the big dataset from the literature.

Table 5.1: Overview of the fifteen investigated tuffs. Classifications according to Figure 3.1 and 3.2

Sample	ID	Origin	Age	Classification LeBas et al. (1986)	Classification Schmidt (1981)	Classification Fisher (1966)
Blanca Pachuca	BP	Mexico	Pliocene	Rhyolite	crystal	ash tuff
Cantera Rosa	CR	Mexico	Oligocene	Rhyolite	crystal	ash-lapilli tuff
Cantera Verde	CV	Mexico	Miocene	Rhyolite	crystal	ash tuff
Mitla Rosa	MR	Mexico	Miocene	Rhyolite	crystal	ash-lapilli tuff
Blue Sevan	BS	Armenia	Cretaceous	Rhyolite	crystal	ash tuff
Noyemberyan	NB	Armenia	Cretaceous	Rhyolite	crystal	ash tuff
Golden Armenia	GA	Armenia	Cretaceous	Rhyolite	crystal	lapilli tuff
Hilbersdorf	HD	Germany	Permian	Rhyolite	crystal	lapilli tuff
San Miguel el Alto	SMA	Mexico	Paleogene	Rhyolite	vitric	lapilli tuff
Queretaro Blanco	QB	Mexico	Pliocene	Rhyolite	vitric	lapilli tuff
Hoktemberyan Red	HR	Armenia	Pleistocene	Trachyte	vitric	lapilli tuff
Artik Rosa	AR	Armenia	Pleistocene	Trachyte	vitric	tuff breccia
Ani Peach	ANI	Armenia	Quaternary	Rhyolite	vitric	lapilli tuff
Loseros	LOS	Mexico	Oligocene	Rhyolite	lithic	ash tuff
Weibern	WB	Germany	Pleistocene	Trachyte- Phonolite	lithic	lapilli tuff

Geochemically most of the fifteen investigated volcanic tuffs are acid rhyolites or trachytes. Only the Weibern tuff (WB) shows an intermediate trachytic to phonolitic composition, with low SiO<sub>2</sub> (59.1 wt%) and high Na<sub>2</sub>O and K<sub>2</sub>O content (>10 wt%) (Fig. 3.2). After the classification scheme of Schmid (1981), BP, CR, CV, MR, BS, NB, GA and HD can be defined as crystal tuffs. Note that all crystal tuffs are clearly acid, with SiO<sub>2</sub> content >70 %. SMA, QB, HR, AR and ANI can be classified as vitric tuffs and LOS and WB as lithic tuffs (Tab. 5.1, Fig. 3.1). Regarding the size of pyroclastic fragments (Fisher 1966), the investigated tuffs are mainly defined as ash tuffs and lapilli tuffs. Artik Rosa (AR) is the only representative of tuff breccia. The crystal rich tuffs are mostly ash tuffs and lapilli tuffs with high ash content. Only the vitric tuffs show higher amounts of lapilli and bombs, which are often present in the form of pumice clasts. Most of the tuffs show considerable amounts of swelling clays and/or an abundance of zeolites (Tab. 3.3). The vitric tuffs of this study are generally young rocks of Cenozoic age, while crystal tuffs may be multiple times older (up to Permian) (Tab. 5.1). It reflects the fact that, over the course of time, the glassy material in the older tuffs, due to its' thermodynamic instability, is often altered to fine clay and zeolite crystals (Fisher and Schmincke 2012). The

## 5 Key parameters of volcanic tuffs: a statistical approach

petrographic and petrophysical properties of the tuffs are compiled in Tables 5.1, 5.2 and 3.3. Supplementary data (e.g., XRF, XRD, thin section and SEM photomicrographs) can be found in Chapter 3.

The 15 selected tuffs show a high mineralogical heterogeneity, with varying amounts of main components and accessory minerals such as swelling clays or zeolites (Tab. 3.3). Past studies on tuffs highlight the strong impact of swelling clays (in this study: clay minerals of the smectite group or with smectitic layers) and zeolites on the strength and weathering behavior (Heap et al. 2018; Kück et al. 2020a; Lubelli et al. 2018a; Pötzl et al. 2018a; Pötzl et al. 2018b; Steindlberger 2004; Steindlberger 2007; Wedekind et al. 2013; Wendler 2007). Except for HD, HR, AR and ANI, swelling clays were identified in all investigated tuffs. Furthermore, BP, CV, BS, NB and WB show partly high quantities of zeolitic material.

## 5 Key parameters of volcanic tuffs: a statistical approach

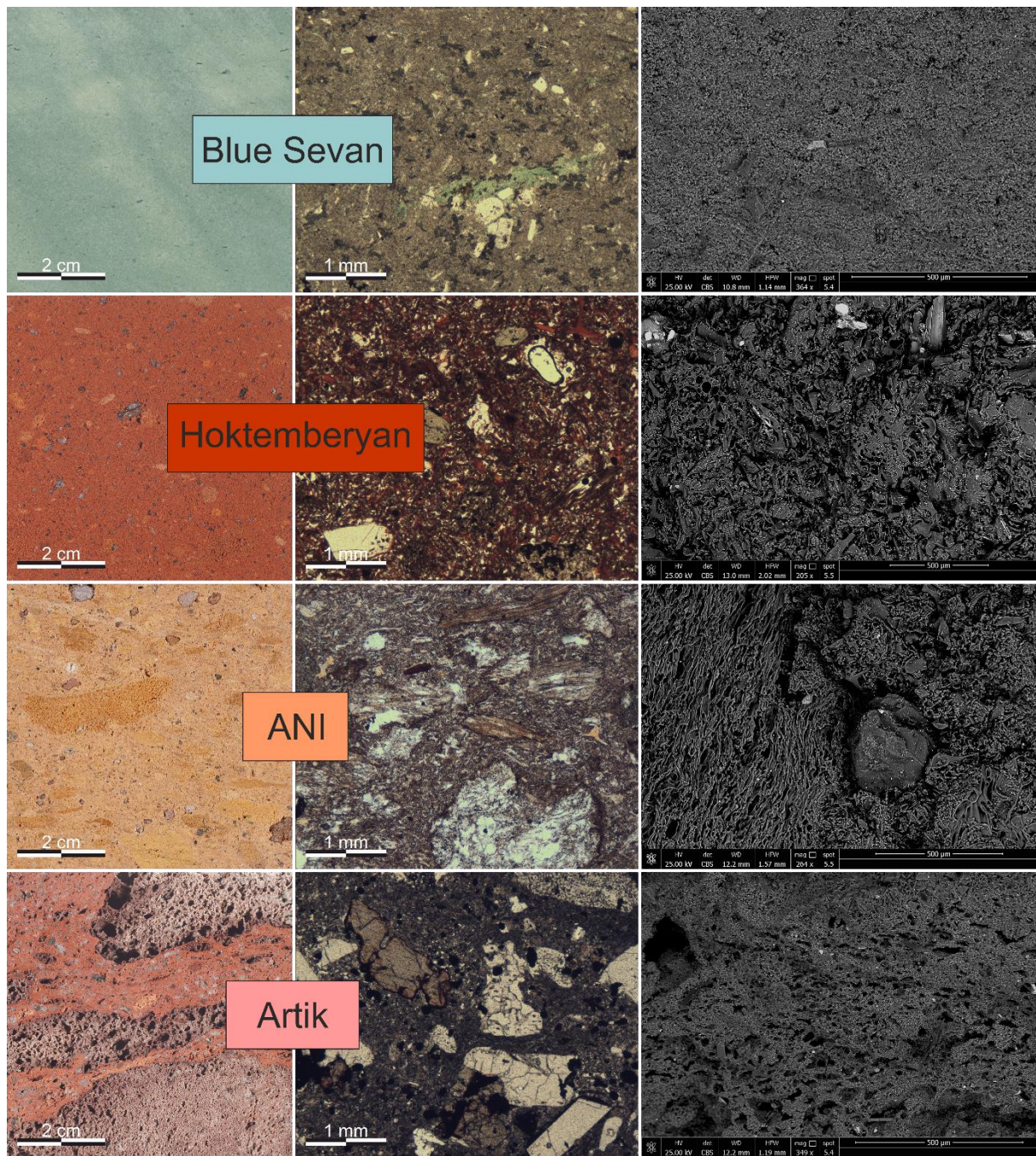


Figure 5.2: Chromatic, structural and compositional variation of a crystal ash tuff (Blue Sevan), vitric ash-rich lapilli tuff (Hoktemberyan Red), vitric lapilli tuff (Ani Peach) and vitric tuff breccia (Artik Rosa), illustrated in polished sections (left column), thin section photomicrographs (central column) and scanning electron photomicrographs (right column)

In general, the vitric tuffs tend to show lower cation exchange capacity (CEC) and specific surface area (SSA) than the crystal and lithic tuffs. Please note that in the literature Blanca Pachuca (BP) and Cantera Verde (CV) are often described as vitric tuffs with high glass content (e.g., Pablo-Galán 1986). In the BP and CV samples of this investigation, the volcanic glass is mostly weathered to clay minerals and zeolites, so that these tuffs now classify as crystal tuffs after Schmid (1981). Also, devitrification in Artik Rosa (AR) is already advanced. Figure 5.2 displays the range of aesthetic, compositional and fabric differences of tuffs by illustrating macro photographs, thin section photomicrographs and SEM micrographs of four examples from the dataset at the same scale.

## 5 Key parameters of volcanic tuffs: a statistical approach

As described above, distinct petrographic differences could be identified between the investigated crystal tuffs and vitric tuffs. Since there are only two representatives of lithic tuffs within the dataset (LOS, WB), it is meaningless to assign them as a separate group. For this study, these rocks will be incorporated into the groups with which they share the most affinity, which is crystal tuffs for Loseros (LOS) and vitric tuffs for Weibern (WB). Only future investigation of a larger group of lithic tuffs can determine if this group shows unique and clearly differential petrophysical properties and weathering behavior.

### 5.3.2 Petrophysical properties and weathering behavior: univariate analysis

In the previous section the classification system after Schmid (1981) turned out to very effectively concur with clear petrographic distinctions of the tuffs, which is also reflected in the distinct petrophysical properties and weathering behavior, as will be characterized below.

In this section two sets of data will be described. First, the large dataset compiled from the literature (in which the data of the 15 additional tuffs is included) will be displayed in the form of boxplots. The according mean and median values as well as standard deviation are listed in Table 5.3. Secondly, the data obtained from the 15 representative tuffs of this study will be visualized as red lines next to the plots. A summary of the parameters of the tuffs investigated in detail is compiled in Table 5.2. The description of the boxplot data will proceed from one parameter to the next, while describing the large dataset first and subsequently the 15 representative tuffs.

A first observation is an asymmetrical distribution and a wide scattering in most of the plotted parameters, which is displayed by the high standard deviation (Tab. 5.3). Properties with high standard deviation are often accompanied by outliers towards higher values (e.g., water vapor diffusion resistance, UCS or hydric expansion) and show a positive skew. The only exceptions with negative skew are the matrix density and saturation coefficient (Fig. 5.3). In the following the median value is considered to be more robust to skewed data and gives a more realistic picture of the data distribution.

Table 5.2: (on the following page) Summary of the technical parameter of the crystal (left row), vitric (central row) and lithic (right row) tuffs, determined in the laboratory. SSA = specific surface area, CEC = cation exchange capacity, w-value = capillary water absorption,  $\mu$ -value = water vapor diffusion resistance, TS = tensile strength, UCS = uniaxial compressive strength, uu = unimodal unequal, bi = bimodal, ue = unimodal equal. <sup>a</sup> from (Wedekind et al. 2013), <sup>b</sup> from (Kück 2019), <sup>c</sup> from (Pötzl et al. 2018a), <sup>d</sup> from (Pötzl et al. 2018b)

## 5 Key parameters of volcanic tuffs: a statistical approach

Sample ID	BP	CR	CV	MR <sup>b</sup>	BS	NB	GA	HD <sup>c</sup>	SMA	QB <sup>b</sup>	HR	AR	ANI	LOS	WB
Porosity [vol%]	14.9	31.1	29.5	15.1	14.9	25.7	21.5	25.9	40.8	46.7	33.1	53.2	35.3	16.8	36.9
Bulk density [g/cm <sup>3</sup> ]	1.85	1.78	1.54	2.22	2.06	1.73	2.04	1.94	1.52	1.28	1.62	1.24	1.38	2.07	1.51
Matrix density [g/cm <sup>3</sup> ]	2.17	2.58	2.18	2.61	2.42	2.34	2.60	2.62	2.57	2.40	2.43	2.24	2.14	2.49	2.40
Water absorption [wt%]	7	14	16	6	6	13	7	9	17	31	15	23	19	7	20
Saturation coefficient S	0.86	0.77	0.85	0.92	0.83	0.87	0.64	0.64	0.65	0.83	0.75	0.52	0.73	0.81	0.84
Micropores [%]	79	18	88	94	90	37	47	45	10	9	4	5	10	85	14
Capillary pores [%]	21	82	12	6	10	63	53	55	90	91	96	95	90	15	86
Mean pore radius [μm]	0.05	0.20	0.04	0.04	0.03	0.14	0.11	0.18	1.50	0.74	3.93	2.24	0.87	0.04	0.51
Pore radii distribution	uu	bi	bi	uu	bi	uu	bi	bi	ue	ue	ue	bi	uu	bi	bi
SSA [m <sup>2</sup> /g]	17	5	26	7	8	3	6	8	7	8	1	2	1	12	14
CEC [meq/100g]	12	6	6	5	9	9	3	<1	4	2	1	1	<1	5	5
w-value [kg/m <sup>2</sup> v <sub>h</sub> ]															
X	0.8	9.4	2.8	1.5	0.8	3.9	2.6	1.2	7.3	43.2	43.2	30.8	22.2	0.8	14.9
Z	0.8	7.1	2.6	1.6	0.5	3.8	2.7	0.9	4.7	41.1	30.9	15.2	16.3	0.7	14.2
μ-value															
X	11.9	7.5	9.2	16.2	14.4	14.4	14.5	11.5	7.4	5.4	8.1	6.6	10.4	27.9	9.1
Z	11.1	8.4	10.1	19.0	14.2	14.5	14.5	11.5	8.1	4.2	9.7	8.0	15.1	13.4	9.1
Sorption 95% RH [wt%]	4.5	2.6	7.9	1.8	2.9	3.5	1.3	1.8	1.2	1.2	0.1	0.1	0.8	2.9	3.2
hydric exp. [mm/m]															
X	0.71	0.10	1.39	0.04	0.35	0.67	0.39	0.70	0.07	0.07	-0.07	0.04	-0.004	0.58	0.56
Z	0.96	0.24	1.68	0.16	1.57	0.76	0.59	2.24	0.23	0.11	-0.13	0.03	-0.01	1.22	0.65
Max	1.14	0.29	2.01	0.16	2.52	0.97	0.64	7.47	0.34	0.11	-0.16	0.04	-0.01	1.78	0.66
P-wave velocity [km/s]															
X	3.3	2.8	2.7	3.8	3.9	3.1	2.7	2.9	2.7	1.6	2.9	2.1	2.9	3.7	2.5
Z	3.2	2.6	2.6	3.7	3.1	3.2	2.7	2.4	2.3	1.3	2.3	1.8	2.3	2.8	2.5
dyn. Youngs's modulus [GPa]															
X	20	14	11	22	31	17	15	16	11	4	14	6	10	28	9
Z	19	12	10	21	20	18	15	11	8	3	9	5	7	16	9
Tensile strength dry βSZ (MPa)															
X	6.9 <sup>a</sup>	-	3.4	5.8	8.7	5.2	4.7	3.6	3.9 <sup>a</sup>	0.8	3.0	3.8	2.5	6.3 <sup>a</sup>	1.9
Z	5.9 <sup>a</sup>	-	3.0	5.3	6.4	5.9	4.8	4.0	4.0 <sup>a</sup>	0.7	2.3	3.3	1.8	8.3 <sup>a</sup>	1.5
Tensile strength sat. βSZ (MPa)															
X	4.0 <sup>a</sup>	-	-	-	4.4	3.6	3.0	2.0	2.6 <sup>a</sup>	0.7	3.3	3.4	2.8	5.8 <sup>a</sup>	1.6
Z	3.1 <sup>a</sup>	-	-	-	3.4	4.1	3.2	2.4	3.0 <sup>a</sup>	0.6	2.5	3.0	2.2	6.7 <sup>a</sup>	1.3
∅ strength reduction	45	-	-	-	49	30	35	41	29	12	-9	9	-19	14	15
UCS dry [MPa]															
X	66.1 <sup>a</sup>	-	-	76.1	107.7	70.2	59.4	43.9	31.9 <sup>a</sup>	5.6	31.4	46.4	22.7	74.3 <sup>a</sup>	16.0
Z	53.7 <sup>a</sup>	-	-	64.6	142.1	67.8	61.6	42.0	32.6 <sup>a</sup>	4.7	31.7	36.9	22.5	58.0 <sup>a</sup>	17.2
UCS sat. [MPa]															
X	-	-	-	-	73.7	49.4	42.3	31.9	21.4	4.2	34.0	43.4	14.6	58.1	11.8
Z	-	-	-	-	66.5	49.4	42.5	22.1	-	4.0	30.2	28.9	14.9	41.7	11.1
∅ strength reduction	-	-	-	-	44	28	30	37	-	21	-2	13	35	25	31
∅ stat. Youngs's modulus [GPa]															
dry	-	-	-	6.3	6.4	5.3	4.9	3.9	-	1.4	4.5	3.9	3.4	-	2.9
wet	-	-	-	-	5.5	4.5	3.9	3.1	2.0	2.1	4.2	3.5	2.5	4.7	2.7
Salt cycles	65	41	15	40	20 <sup>d</sup>	109 <sup>d</sup>	78 <sup>d</sup>	11	>85	39	>150 <sup>d</sup>	65 <sup>d</sup>	>75 <sup>d</sup>	35	-

## 5 Key parameters of volcanic tuffs: a statistical approach

Table 5.3: Mean, median and standard deviations of the data distribution from the literature data compilation (references in Table A.1). n = number of data points, SSA = specific surface area, w-value = capillary water uptake,  $\mu$ -value = water vapor diffusion resistance, TS = tensile strength, UCS = uniaxial compressive strength

	Bulk density [g/cm <sup>3</sup> ]	Matrix density [g/cm <sup>3</sup> ]	Porosity [vol%]	Mean pore radius [ $\mu$ m]	Micropores [%]	SSA [m <sup>2</sup> /g]	
n	511	260	528	156	127	66	
Median	1.66	2.51	28.0	0.30	25	8.6	
Mean	1.68	2.48	28.9	0.87	34	12.6	
Std Dev	0.32	0.17	11.4	1.55	27	15.3	
	TS dry [MPa]	TS sat. [MPa]	UCS dry [Mpa]	UCS sat. [Mpa]	P-wave velocity dry [km/s]	dyn. Young's mod. [GPa]	stat. Young's mod. [GPa]
n	150	50	374	63	262	66	80
Median	3.1	2.0	21.0	12.5	2.37	12.4	4.7
Mean	4.0	2.3	30.2	17.9	2.45	14.6	7.2
Std Dev	4.1	1.7	32.2	18.5	0.66	9.8	8.9
	Water absorption [wt%]	Saturation coeff. S [-]	w-value [kg/m <sup>2</sup> vh]	$\mu$ -value [-]	Sorption 95 RH [wt%]	mean hydric exp. [mm/m]	
n	311	92	161	85	60	131	
Median	16.1	0.75	11.2	12.4	1.8	0.45	
Mean	16.6	0.72	17.4	18.1	2.1	0.78	
Std Dev	8.4	0.16	19.0	16.4	1.9	0.99	

The bulk density of 511 data points is characterized by a wide scattering between 0.91 – 2.48 g/cm<sup>3</sup>, with a median value of 1.66 g/cm<sup>3</sup> (outliers 0.81 and 2.70 g/cm<sup>3</sup>) (Fig. 5.3). The median of the matrix density (n=260) is 2.51 g/cm<sup>3</sup>, with min-max values of 2.05 – 2.87 g/cm<sup>3</sup> and several outliers down to 1.82 g/cm<sup>3</sup>. Note that the crystal tuffs in Table 5.2 are generally characterized by higher bulk densities (1.54 – 2.22 g/cm<sup>3</sup>) than vitric tuffs (1.24 – 1.62 g/cm<sup>3</sup>).

The boxplot displaying the effective porosity of 528 data points, shows that tuffs typically possess a wide range of porosity between 1.5 and 56.5 vol%, with outliers exceeding values up to 64 vol.% (Fig. 5.3). Considering the wide scattering of values, the median of 28.0 vol% and mean of 28.9 vol% are relatively close to each other, indicating a symmetrical distribution. The crystal tuffs of this study tend to show intermediate to high porosities between 14.9 – 31.1 vol%, whereas the vitric tuffs exhibit very high porosities, starting with 33.1 vol% and reaching up to 53.2 vol% (AR) (Tab. 5.2).

With a median of 0.3  $\mu$ m, the values of (n=156) mean pore radii show a distinct positive skew, with 50 % of the data points located in a relatively small IQR between 0.06 and 0.9  $\mu$ m (Fig. 5.3). Including the extreme values, tuffs show mean pore radii ranging from the nanometer range (4 nm) up to 1.98  $\mu$ m. Many outliers exceed mean pore radii up to 10.5  $\mu$ m. A wide scattering of data can also be observed for the fraction of micropores (n=127), which almost covers the whole range from 0 – 100 % (min 2.17 %; max 94 %; median 25 %; outliers up to 97 %). An extreme example is the Hoktemberyan Red (HR) with a mean pore radius of 3.93  $\mu$ m and 96 % of capillary pores (Tab. 5.2). Other extreme examples are the Blanca Pachuca (BP), Loseros (LOS), Cantera Verde (CV) and Blue Sevan (BS) with up to 79 - 90 % micropores. In general, the crystal tuffs show much higher fractions of micropores (37 – 94 %)



## 5 Key parameters of volcanic tuffs: a statistical approach

and accordingly smaller mean pore radii (0.03 – 0.20  $\mu\text{m}$ ) in comparison to the vitric tuffs (micropores 4 – 10 %; mean pore radii 0.74 – 3.93  $\mu\text{m}$ ).

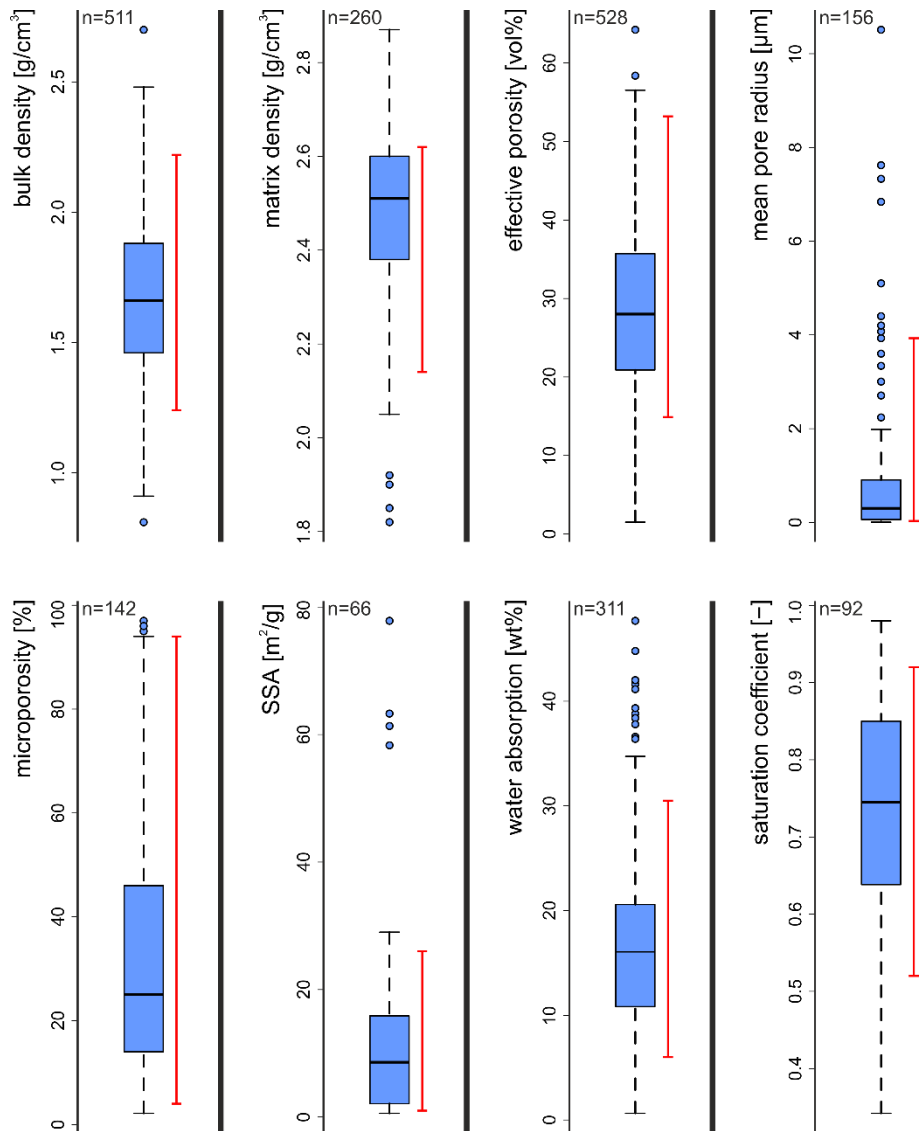


Figure 5.3: Box-whisker plots of the pore space and total water absorption properties from  $n$  = number of tuffs (references in Table A.1). SSA = specific surface area. The blue dots represent outliers; the red line represents the range of properties of the 15 tuffs of this study investigated in more detail

Fifteen samples are certainly not sufficient to derive general laws, but some clear trends can be noted when characterizing the pore size distribution after the classification scheme of Ruedrich and Siegesmund (2006): (1) only vitric tuffs show unimodal equal pore size distributions (although only slightly sometimes); (2) crystal tuffs are exclusively characterized by unimodal unequal or bimodal distributions; (3) lithic tuffs show bimodal distribution. A bimodal distribution is the most volatile of the three, as it can be observed in all three types of tuff (Tab. 5.2, Fig. 5.4).

## 5 Key parameters of volcanic tuffs: a statistical approach

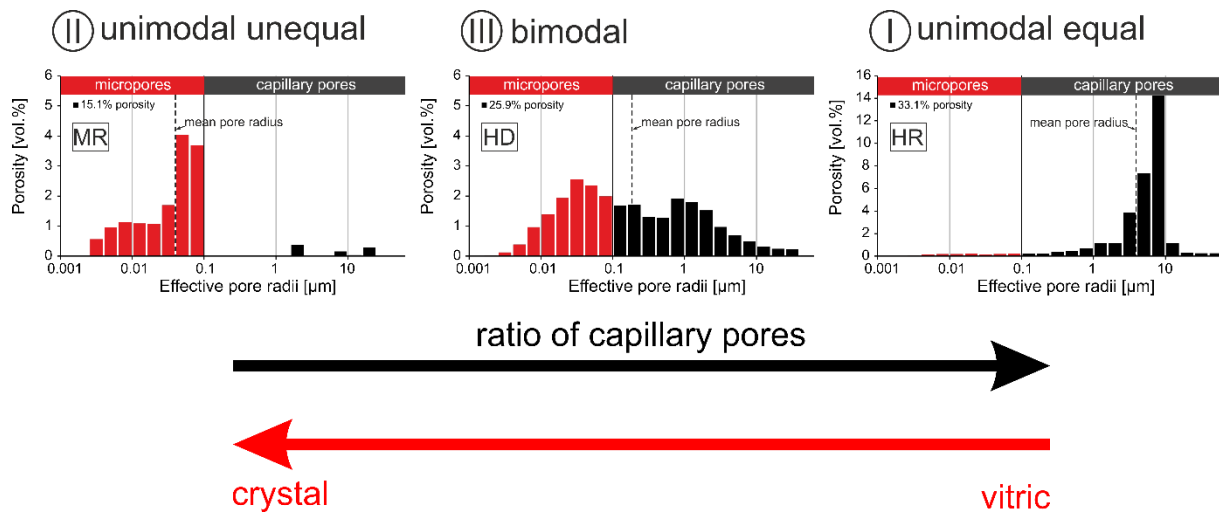


Figure 5.4: Representative pore radii distribution types according to Ruedrich and Siegesmund (2006) observed in three tuffs and schematic relation to the fragmental composition of the rock and ratio of capillary pores as observed in the dataset. The arrows display an increasing ratio of capillary pores and crystal content typical for either of the pore radii types

Under atmospheric conditions tuffs ( $n=311$ ) absorb on average 16.6 wt% water (median 16 wt%). However, the scattering of the data is wide and water absorption values from barely any absorption (0.6 wt%) up to 34.7 wt% are within the range of the whiskers (Fig. 5.3). Outliers display tuffs that even absorb up to 47.7 wt% water under atmospheric conditions. The related saturation coefficients after Hirschwald (1912) show values starting from 0.34 up to 0.98, with an average of 0.72 and a median of 0.75 ( $n=92$ ). Natural stones with  $S$  values  $<0.75$  are considered frost resistant,  $S$  values  $>0.75$  and  $<0.9$  indicate uncertain frost resistance and  $S>0.9$  is not considered to be frost resistant. The average tuff with a saturation coefficient  $<0.75$  is therefore categorized as barely frost resistance after Hirschwald (1912) and looking at the boxplot in Fig. 5.3, many tuffs are classified as not frost resistant building material. The Queretaro Blanco (QB) is an example of extreme water absorption under atmospheric conditions (31 wt%). In contrast, the Mitla Rosa (MR) and Blue Sevan (BS) show the lowest absorption (6 wt%). All of these extreme examples exhibit  $S$  values  $>0.75$  (up to 0.92) and are not considered frost resistant. Regarding water absorption and frost resistance, clear differences can be observed for both crystal and vitric tuffs of this study. While the vitric tuffs tend to a higher water absorption (15 – 31 wt%), crystal tuffs absorb relatively little water (6 – 16 wt%). With the exception of Golden Armenia (GA) and Hilbersdorf (HD), all crystal tuffs show high saturation coefficients ( $S >0.75$ ) meaning frost resistance of the material is uncertain or not existent (Hirschwald 1912). On the other hand, with the exception of Queretaro Blanco (QB), saturation coefficients of vitric tuffs indicate frost resistance of the material.

The specific surface area (SSA) of tuffs ( $n=66$ ), which is of particular importance for adsorption processes and reactions on the materials surface, ranges from 0.6 to 29  $\text{m}^2/\text{g}$  (median 8.6  $\text{m}^2/\text{g}$ ), but also extreme outliers with values up to 77.8  $\text{m}^2/\text{g}$  are recorded (Fig. 5.3). An increased SSA in tuffs is often accompanied by increased clay mineral and/or zeolite content (Kück et al. 2020a). The hygroscopic water sorption, water vapor diffusion resistance and capillary water absorption show similar distributions (Fig. 5.5). With a median of 1.76 wt%, most of the hygroscopic sorption values ( $n=60$ ) are between 0.06 and 4.86 wt%, but also extreme outliers of up to 7.9 wt% (Cantera Verde (CV)) can be observed. Examples of extreme

## 5 Key parameters of volcanic tuffs: a statistical approach

low hygroscopic water sorption are Hoktemberyan Red (HR) and Artik Rosa (AR) (both 0.1 %). The highest values are shown by tuffs that are rich in zeolites and swelling clays (compare Tab. 5.2). As shown in Tables 3.3 and 5.2, crystal tuffs tend to higher SSA (3 – 26 m<sup>2</sup>/g) and CEC values (<1 – 12 meq/100g) than the vitric tuffs (SSA 1 – 8 m<sup>2</sup>/g; CEC <1 – 4 meq/100g). Hygroscopic water sorption of the vitric tuffs is very low (0.1 – 1.2 wt%), while the crystal tuffs of this study show values that are multiple times higher (1.3 – 7.9 wt%).

The values of the water vapor diffusion resistance coefficient  $\mu$  (n=85) show a median of 12.4, with most values located between 4.8 and 29.5 (Fig. 5.5). Extreme outliers of up to three times the maximum value (93) can be observed. The Loseros tuff (LOS) is an example of very high  $\mu$  value, with 27.9 in X direction. The Queretaro Blanco (QB), like most vitric tuffs, shows very low resistance against water vapor diffusion (4.2 in Z direction). The crystal tuffs show moderate resistance towards water vapor diffusion, with  $\mu$  values up to 19. Regarding the capillary water absorption, values (n=161) range between 0.04 and 61.1 kg/m<sup>2</sup>vh, with a median of 11.2 kg/m<sup>2</sup>vh. Outliers reach w-values of up to 94.9 kg/m<sup>2</sup>vh. In this study high capillary water uptake is especially shown by the vitric tuffs, with Queretaro Blanco (QB) and Hoktemberyan Red (HR) on the upper end (both 43.2 kg/m<sup>2</sup>vh in X direction), while low values are shown by crystal tuffs, with extreme low values by Blanca Pachuca (BP), Loseros (LOS), Blue Sevan (BS) and Hilbersdorf (HD) (BS lowest with 0.45 kg/m<sup>2</sup>vh in Z direction). A partly pronounced anisotropic behavior of the tuffs, with usually higher capillary water absorption and lower water vapor diffusion resistance parallel to the bedding plane (X direction) indicates a better connection of the pore network in this direction.

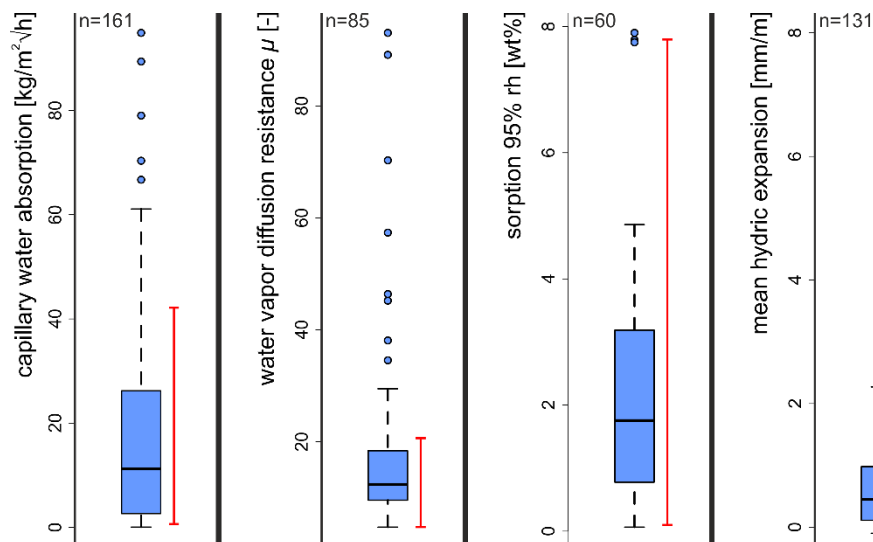


Figure 5.5: Box-whisker plots of the water transport, retention and expansion properties from n = number of tuffs (references in Table A.1). The blue dots represent outliers; the red line represents the range of properties of the 15 tuffs of this study investigated in more detail

The ultrasonic velocity of 262 data points ranges between 0.96 and 4.05 km/s, with a median of 2.37 km/s and outliers of up to 4.38 km/s (Fig. 5.6). Via ultrasonic measurement the dynamic Young's modulus, which is proportional to the rock strength, can be obtained (Siegesmund and Dürrast 2011). Tuffs (n=66) show a median value of 12.4 GPa, with a minimum of 0.9 GPa and maximum of 39 GPa. In this study the lowest ultrasonic velocities and corresponding dynamic Young's moduli are shown by vitric tuffs, especially the Artik Rosa

## 5 Key parameters of volcanic tuffs: a statistical approach

(AR) and Queretaro Blanco (QB) (QB down to 1.3 km/s and 2.8 GPa in Z direction). Particularly high values are shown by Loseros (LOS) and crystal tuffs like Mitla Rosa (MR) and Blue Sevan (BS) with up to 3.9 km/s and 31.5 GPa.

Characterizing mechanical properties like the tensile or compressive strength are of particular importance for the estimation of the rock durability. Compared to other rock types, tuff rocks exhibit relatively low mechanical strength values (Mosch and Siegesmund 2007). Under dry conditions the tensile strength of 150 tuffs is between 0.2 and 8.0 MPa, with a median of 3.1 MPa. Extreme outliers reach values up to 25.7 MPa (Fig. 5.6). Under water saturated conditions the tensile strength values of 50 data points are nearly halved (median 2.0 MPa; min – max 0.1 MPa – 4.7 MPa). Few outliers reach values up to 8.5 MPa.

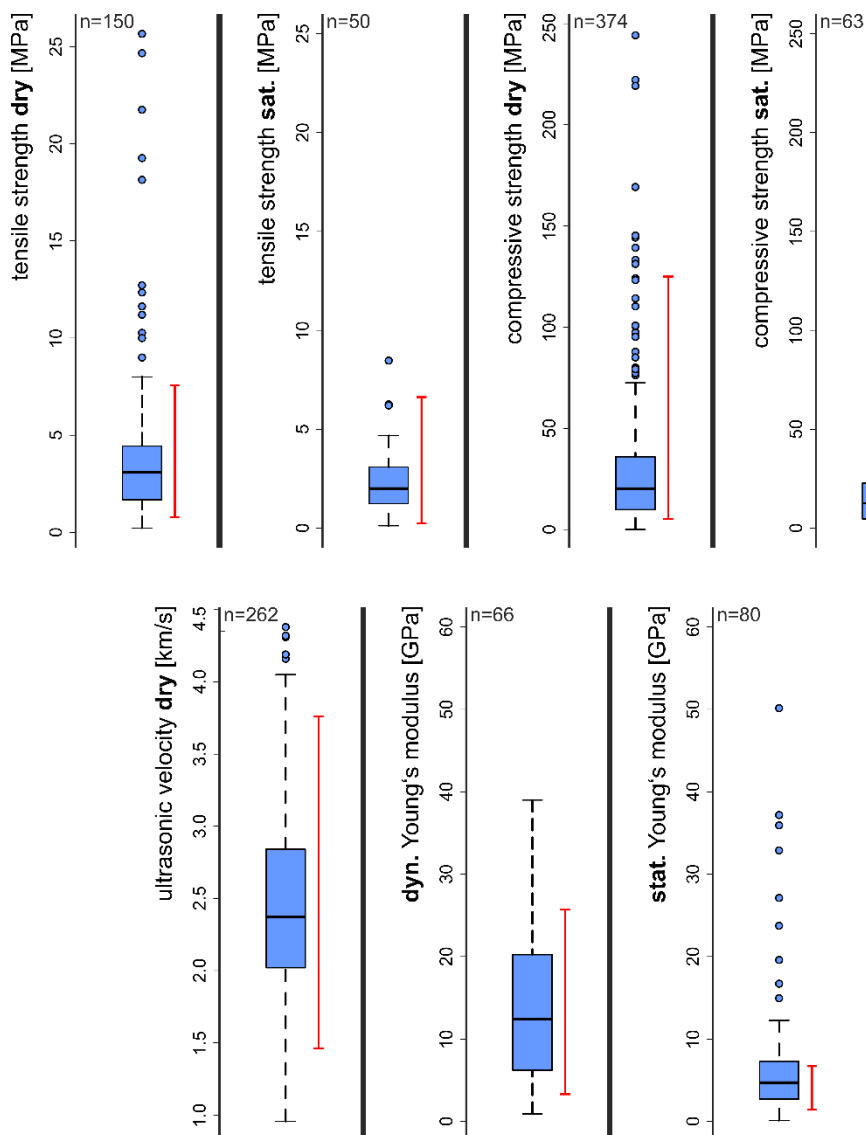


Figure 5.6: Box-whisker plots of the mechanical and elastic properties from  $n$  = number of tuffs (references in Table A.1). The blue dots represent outliers; the red line represents the range of properties of the 15 tuffs of this study investigated in more detail

## 5 Key parameters of volcanic tuffs: a statistical approach

The uniaxial compressive strength (UCS), as one of the most frequently used parameters for the characterization of the rock strength, shows an extraordinary high standard deviation under dry conditions (Tab. 5.3). With a median of 21.0 MPa and a mean of 30.2 MPa, the values of  $n=374$  tuffs range between 0.7 and 73 MPa. A high amount of outliers exceed these values and reach UCS of up to 245 MPa. From the investigated tuffs, Blue Sevan (BS) exceeds the maximum UCS with an average of 124.9 MPa. Under water saturated conditions the mean UCS of  $n=63$  tuffs is significantly lowered (0.2 – 49.4 MPa; median 12.5 MPa; mean 17.9 MPa). Almost half of the additionally investigated tuffs of this study show a strength reduction of more than 1/3 of their original value, both in TS and UCS measurements (Tab. 5.2). Extraordinary high strength reduction is primarily shown by the crystal tuffs, especially Blanca Pachuca (BP), Blue Sevan (BS) and Hilbersdorf (HD), with a loss in strength of almost 50 %. Vitric tuffs show less strength reduction. Special cases are the Hoktemberyan Red (HR) and (in parts) the Ani Peach (ANI) tuff, which show opposite behavior, with slight strength increase due to water saturation. Particularly low strength values in the dataset are presented by the Queretaro Blanco (QB), with an average tensile strength around 0.8 MPa and a UCS of 4.6 MPa. The static Young's modulus, as a parameter for the resistance against deformation of ( $n=80$ ) tuffs was obtained from the UCS measurements and shows a similar trend. Also, here the wide range of values (0.1 – 12.3 GPa; median 4.7 GPa) is exceeded by extreme outliers up to 50.2 GPa. To sum up, the crystal tuffs of this study generally show higher strength values and static Young's moduli than the vitric tuffs, but also higher loss in strength due to water saturation (compare Tab. 5.2).

The characterization of the hydric expansional behavior of the tuffs gives a proper estimation about future response of the material to changing environmental conditions and weathering effects. As the boxplot in Figure 5.5 displays, the response of ( $n=131$ ) tuffs to water immersion is usually an expansional process with mean values around 0.8 mm/m (median 0.5 mm/m) and a maximum of 2.3 mm/m. Outliers expand up to 5.7 mm/m (Hilbersdorf (HD)), but also negative expansion (-0.1 mm/m) is recorded, e.g., Hoktemberyan Red (HR), Ani Peach (ANI) and in parts San Miguel el Alto (SMA) as well as some Artik (AR) types. Some specimens of the Hilbersdorf tuff (HD) expand up to 7.5 mm/m. A general observation on the tuffs of this study is: low hydric expansion (up to contractional behavior) in vitric tuffs; high expansion values in crystal tuffs. An important characteristic that is shared by all tuffs is a partly strong anisotropic behavior of the material, with higher expansion perpendicular to the bedding plane (Z direction) (Tab. 5.2).

Salt bursting tests identify the resistance of the material to crystallization pressure of salts. Sousa et al. (2018) give a detailed overview on controlling factors of salt weathering in granitoids. López-Doncel et al. (2016) investigated the main factors influencing the salt weathering in volcanic tuffs. A critical literature review on salt crystallization tests and new ideas to overcome existing limitations can be found in Lubelli et al. (2018b). In many investigations, especially in timely limited thesis works (e.g., Molina-Maldonado 2016; Teipel 2020; Wittenborn 2015), the salt bursting tests are not continued after a certain amount of cycles and results are extrapolated from the status quo. Individual stones, however, may show significant deterioration only after a high amount of cycles (Pötzl et al. 2018b; Sousa et al. 2018). An extrapolation of the results may be reasonable within individual data sets, but does

## 5 Key parameters of volcanic tuffs: a statistical approach

aggravate the overall comparability with the results of other studies. Some studies extrapolated after 40 cycles, others stopped testing after 150 cycles. The illustration of the range of absolute values in form of a boxplot is therefore misleading and was consequently not done in this study.

Within the dataset of this study, the 15 tuffs show a wide range of different responses and resistance towards salt weathering (Tab. 5.2). An overall trend indicates that on average, crystal tuffs obtain lower resistance (11 – 109 salt cycles; mean 47 cycles) and vitric tuffs higher resistance (39 – >150 salt cycles; mean >83 cycles).

### 5.3.3 Petrophysical properties and weathering behavior: bivariate analysis

In the following, regression analyses of some basic parameters typically investigated for building stones are displayed and discussed. These correlations can be useful for understanding the mutual dependence of the parameters and to estimate certain parameters using others (Liu et al. 2019; Pappalardo et al. 2017; Vernik et al. 1993) In comprehensive statistical studies on other natural building stones like granitoids (Sousa 2014) or sandstones (Stück et al. 2013), the pore space properties showed to have a significant influence on strength values and weathering behavior and are therefore of particular interest.

Both bulk density and porosity are two pore space properties which are fundamental for many investigations on engineering properties of building stones. On 491 data pairs they show a strong negative linear relationship ( $r = -0.81$ ), meaning that high porosity is related to low bulk density and vice versa (Fig. 5.7). The average value of the 80 % confidence ellipsoid amounts to  $1.66 \text{ g/cm}^3$  bulk density and 30 vol.% porosity. Both bulk density and porosity show a strong linear correlation with the water absorption behavior under atmospheric conditions of tuffs ( $r = -0.92$  ( $n=299$ ) and  $0.85$  ( $n=302$ ), respectively). While at higher bulk densities the water absorption decreases, an increasing porosity is accompanied by an increasing water absorption (Fig. 5.7). The mean values of the confidence ellipsoids are at 16.7 % water absorption and a bulk density of  $1.67 \text{ g/cm}^3$  or a porosity of 27.9 vol.%.

Although the ( $n=258$  and  $n=262$ ) data pairs are moderately scattered, both bulk density and porosity show a linear relationship with the ultrasonic velocity ( $r = 0.65$  and  $-0.56$ , respectively) (Fig. 5.7). A positive linear relation with a correlation coefficient of  $r = 0.67$  is displayed by 68 data pairs of the bulk density and the dynamic Young's modulus. While the mean bulk density of  $1.79 \text{ g/cm}^3$  amounts to 13.8 GPa in the 80 % confidence ellipsoid, higher bulk densities correlate with increased dynamic moduli of elasticity (Fig. 5.7).

## 5 Key parameters of volcanic tuffs: a statistical approach

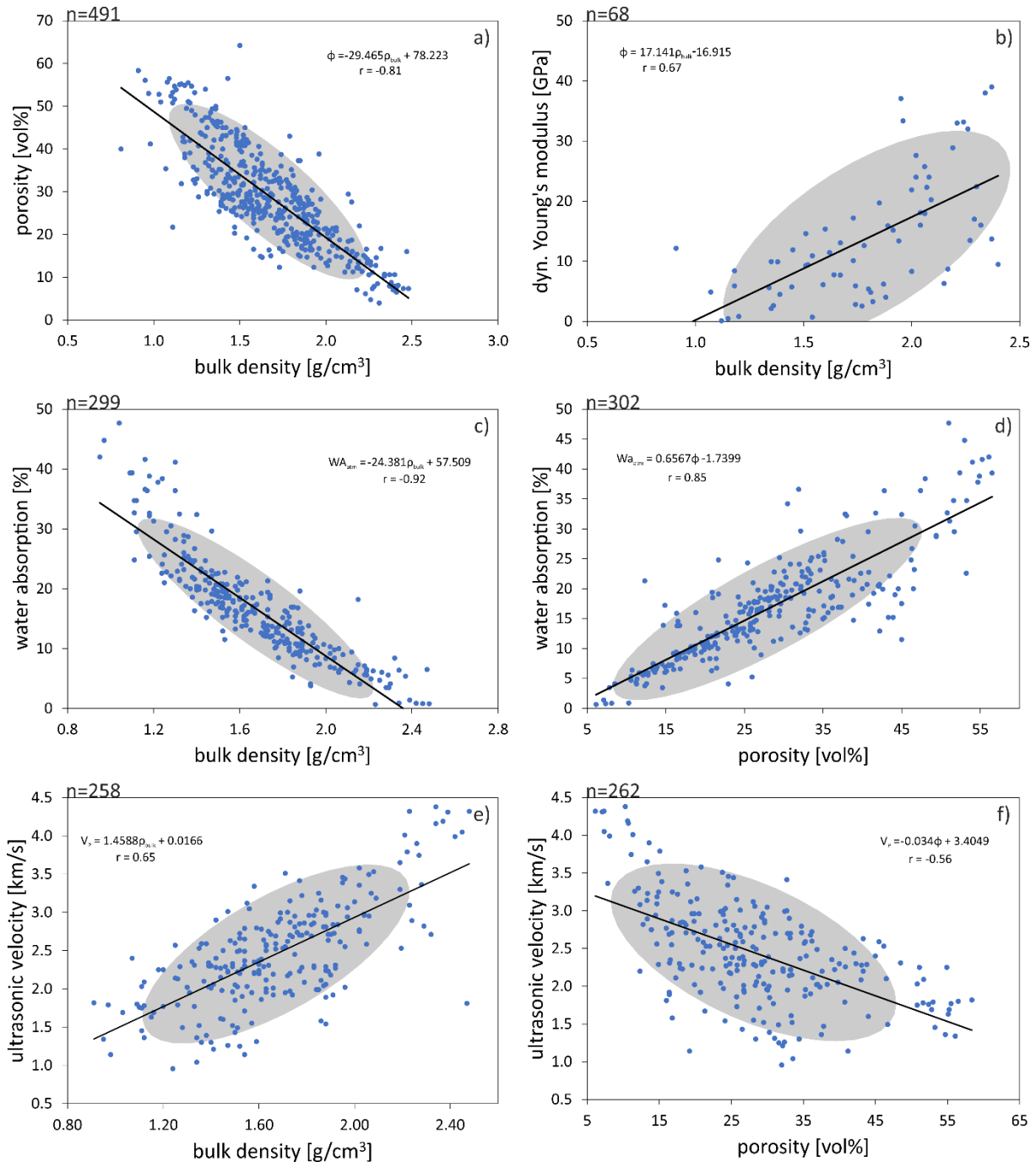


Figure 5.7: Regression analysis of different rock properties with trendlines and r values. The grey ellipses predict an 80 % probability of the data. Data taken from references in Table A.1 (data of this study included). n = number of data pairs

The relationship of the effective porosity and bulk density with strength parameters like compressive and tensile strength is of exponential nature (Fig. 5.8). With increasing bulk density, the compressive and tensile strength are increasing exponentially, whereas increasing porosity is accompanied by an exponential decrease of strength (Fig. 5.8). Correlation coefficients are usually higher for regressions against bulk density and therefore display a stronger relationship (e.g., bulk density vs. UCS:  $r = 0.84$ ; porosity vs. UCS:  $r = 0.75$ ). Both bulk density and porosity show a less pronounced but still moderate to strong exponential correlation with the tensile strength ( $r = 0.68$  and  $-0.65$ , respectively). The ultrasonic velocity strongly correlates with the strength values, showing exponential increase of strength with

## 5 Key parameters of volcanic tuffs: a statistical approach

increasing ultrasonic velocity (Fig. 5.8). Its relation, however, is stronger with the tensile strength ( $r = 0.82$ ) than with the compressive strength ( $r = 0.72$ ). Exponential decrease of compressive strength is related to an increased capacity of water absorption of the material (Fig. 5.9). The coefficient of correlation for  $n = 253$  data pairs is strong ( $r = -0.82$ ).

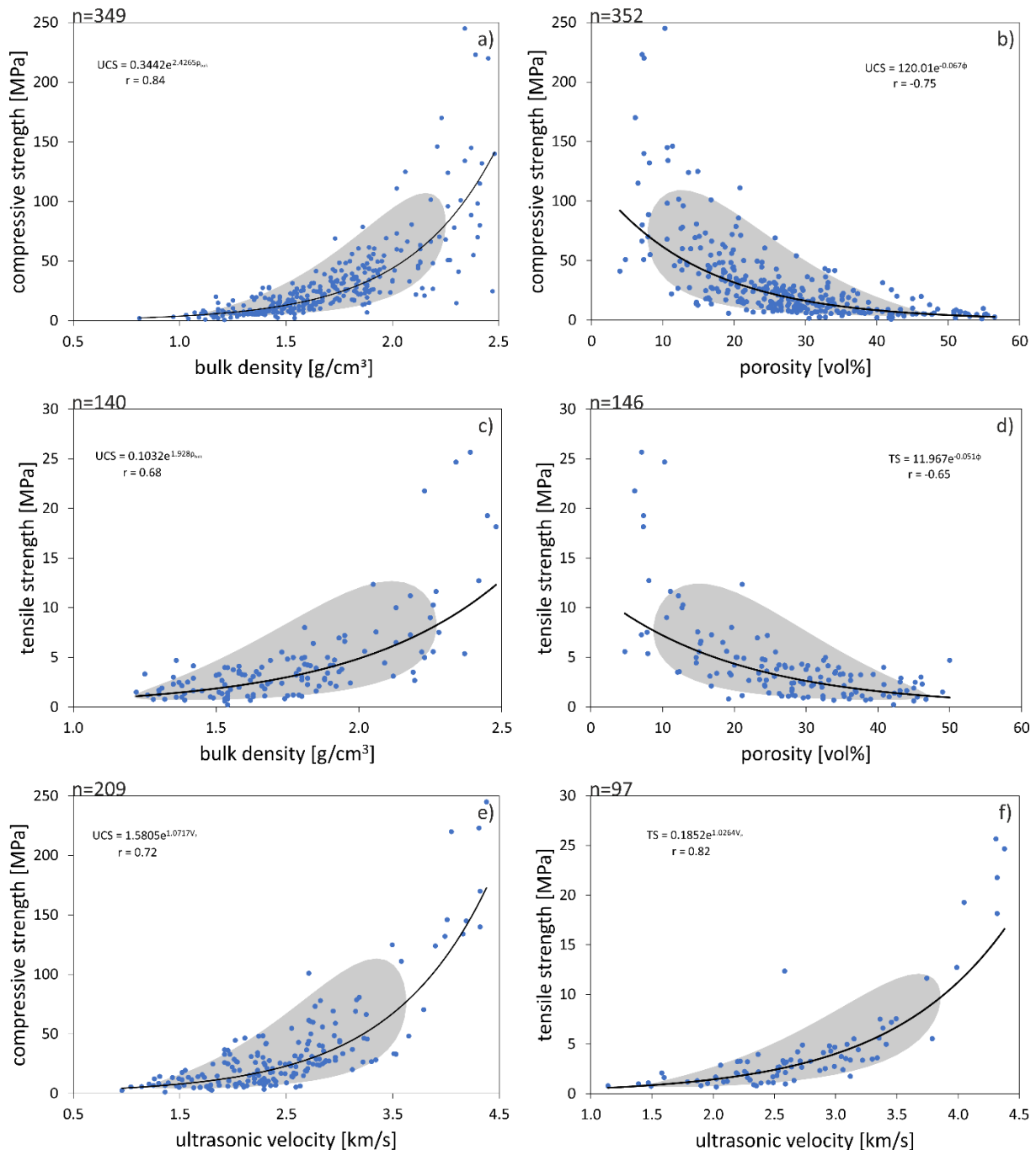


Figure 5.8: Regression analysis of different rock properties with trendlines and  $r$  values. The grey ellipses predict an 80 % probability of the data. Data taken from references in Table A.1 (data of this study included).  $n$  = number of data pairs

Other, weaker and less pronounced correlations can be found for some pore space properties with the water transport properties and expansional behavior of tuff (Fig. 5.9). Regression analysis indicates an exponential relationship between  $n = 98$  data pairs of the capillary water absorption and the fraction of micropores. The correlation coefficient, however, describes only a moderate relationship between these parameters ( $r = -0.56$ ). Between the fraction of



## 5 Key parameters of volcanic tuffs: a statistical approach

micropores and the water vapor diffusion resistance the correlation is even weaker ( $r = 0.49$ ;  $n = 80$ ), while showing a barely linear trend. In contrast, the porosity shows a distinct negative exponential relationship with the water vapor diffusion resistance and a strong correlation coefficient of  $r = -0.79$ . However, regarding capillary water absorption and water vapor diffusion resistance, the data are fairly scattered and confidence ellipses are wide. Consequently, both porosity and fraction of micropores should be used with caution to estimate general trends of the water transport and retention properties of tuffs.

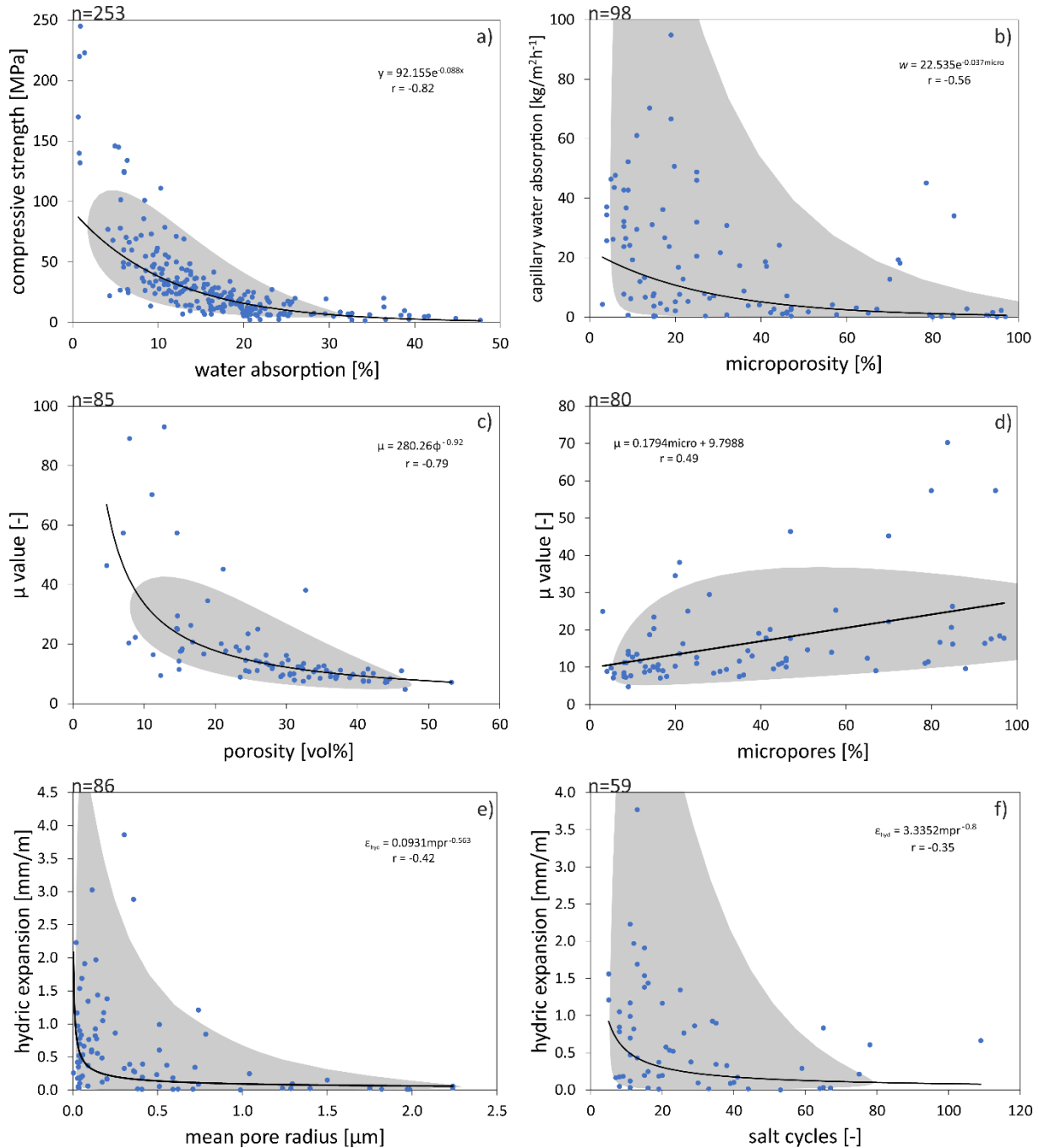


Figure 5.9: Regression analysis of different rock properties with trendlines and  $r$  values. The grey ellipses predict an 80 % probability of the data. Data taken from references in Table A.1 (data of this study included).  $n$  = number of data pairs

## 5 Key parameters of volcanic tuffs: a statistical approach

Regarding their expansional behavior, tuffs with smaller pore radii tend to show higher hydric expansion values (n=86). The relation between hydric expansion and mean pore radius is described by a negative quadratic trend with a weak to moderate correlation of  $r = -0.42$ . An also negative quadratic trend, with weak correlation ( $r = -0.35$ ), can be observed for the hydric expansion and the resistance against salt weathering (n=59). Increasing hydric expansion is consequently related to a lower mean pore radius and lower resistance to salt weathering (Fig. 5.9). The relation between the cation exchange capacity (CEC) and the hydric expansion of 53 data pairs is described by a moderate correlation coefficient ( $r = 0.53$ ), but the data points are widely scattered and no clear trend is observable (Fig. 5.10). The CEC is a proxy for swellable clay minerals (Dohrmann and Kaufhold 2010), accordingly their effect on moisture changes and their role in the tuffs studied is not as clear as expected. On the other hand, 5 of the 15 samples studied contain zeolites that do not show a significant CEC when measured using Cu-trien but may react significantly upon moisture changes, which may explain the poor correlation. It should be noted, however, that many tuffs with very low CEC tend to show hardly any expansion. Some even show contractional behavior.

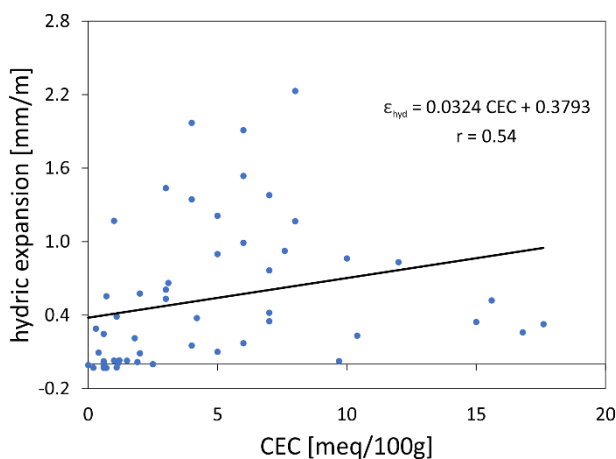


Figure 5.10: Relationship between the cation exchange capacity (CEC) and the hydric expansion of tuffs (n = 53) with trendline and r value. Despite the moderate correlation coefficient, no clear trend is observable

### 5.3.4 Material behavior of crystal, vitric, lithic tuffs and influence of the pore radius

As the classification of tuffs after the recommended system of the IUGS (Schmid 1981) is usually not a part of most investigations, scientific data on this information is scarce, if not absent, in the literature. This, in part, also applies for the characterization of the pore size distributions, since their analysis is associated with increased costs and access to analytical tools. This section, however, should demonstrate the potential that resides in these classification tools. For this purpose, the 15 investigated tuffs of this study plotted in Figures 5.11 and 5.12, were colored according to their classification after the main type of pyroclastic content (Schmid 1981) on the one hand, and on the other after their pore radii distribution type (Ruedrich and Siegesmund 2006).

Several authors found strong relationships between the porosity and water absorption with the UCS for various clay bearing tuffs (e.g., Erguler and Ulusay 2009; Teymen 2018), which can be confirmed by this work (Fig. 5.8, 5.9). Furthermore, significant differences in the strength parameters can be observed when looking at the different types of tuff of this investigation. In Figure 5.11 the relationship of the porosity and hydric expansion with the UCS and the

## 5 Key parameters of volcanic tuffs: a statistical approach

reduction of UCS due to moisture saturation, is displayed. The nature of the relationship between porosity and UCS was already described above as exponential (see Fig. 5.8). However, the onset of the exponential growth is mainly observed for tuffs with porosities <10%. As the 15 selected tuffs of this study do not obtain porosity values <14.9%, the relationship of the parameters in Figure 5.8 would be rather described as linear in the investigated range (compare Fig. 5.11). This demonstrates the critical importance of comprehensive datasets when determining estimators, since the smaller data set produces entirely different predictions.

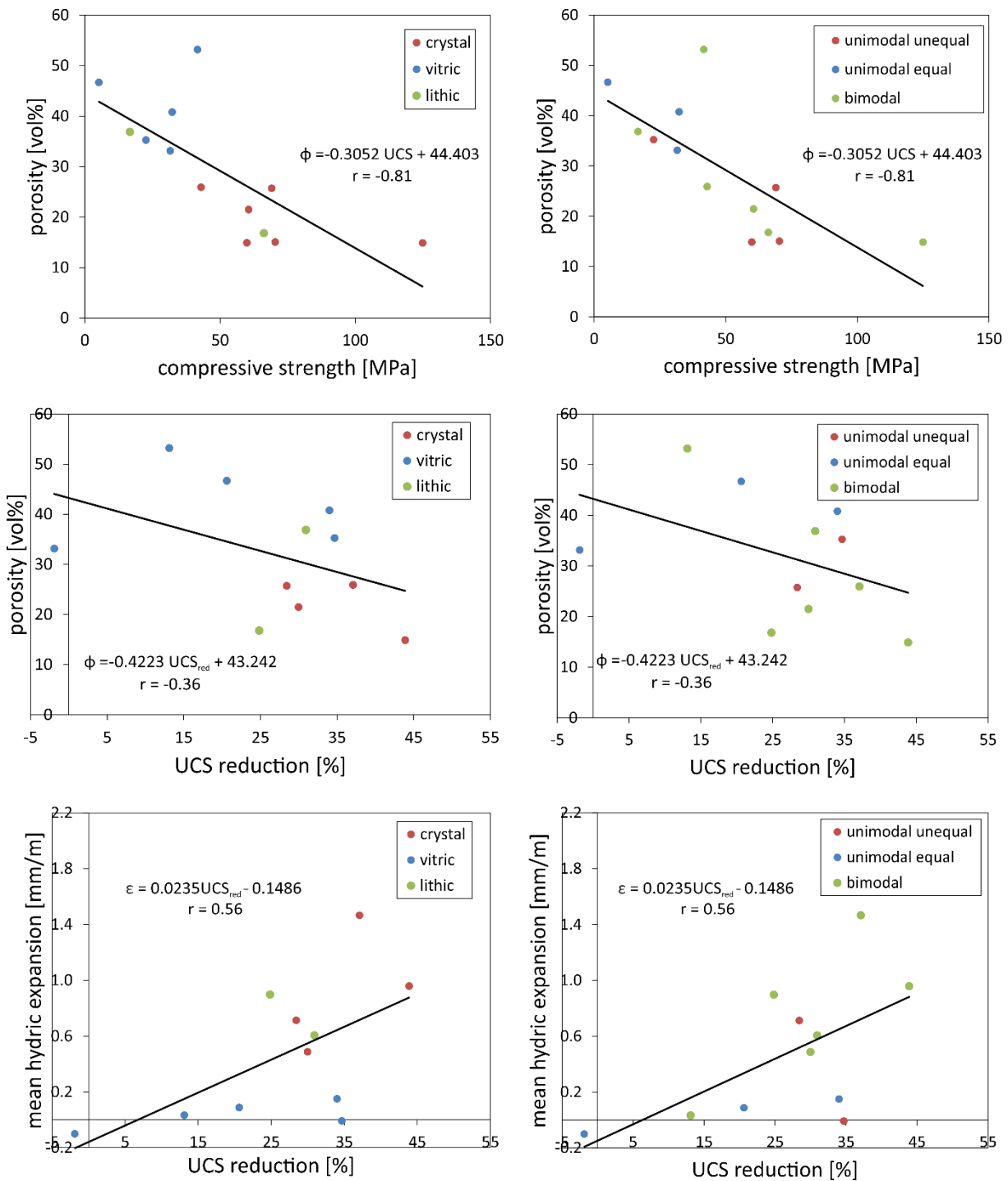


Figure 5.11: Relationship between different rock properties with regard to their pyroclastic content and pore radii distribution type

## 5 Key parameters of volcanic tuffs: a statistical approach

A strength reduction of tuffs due to water saturation is demonstrated by various studies (e.g., Çelik and Ergül 2015; Erguler and Ulusay 2009; Hashiba and Fukui 2015; Kleb and Vásárhelyi 2003; Masuda 2001; Okubo et al. 1992; Török et al. 2004; Vásárhelyi 2002; Wedekind et al. 2013; Yasar 2020). Yasar (2020) reported that already low amounts of moisture content, such as 0.2 wt%, can lead to serious strength reduction. An overall observation in Figure 5.11 is that tuffs with lower porosity usually show higher UCS, but also stronger UCS reduction due to water saturation. A more detailed examination identifies the differential material behavior by certain types of tuff, which was already indicated by the univariate analysis above. A grouping of tuffs above and below 30 vol.% porosity seems possible (supporting the findings of Pötzl et al. 2018b, Chapter 4), since vitric tuffs (>30 vol.% porosity) regularly show lower UCS and strength reduction than crystal tuffs (<30 vol.% porosity). Because unimodal equal pore radii distribution is only represented by vitric tuffs of this study and unimodal unequal distribution mainly by crystal tuffs, a grouping by these two pore radii types seems also possible. Thus, unimodal equal pore distribution types display high porosity tuffs with lower UCS and accordingly lower UCS reduction than the unimodal unequal types, which show lower porosities and increased UCS, as well as higher UCS reduction due to water saturation. Bimodal pore radii types, however, are scattered over the whole range of porosities and strength values and do not seem to be suitable for a further differentiation of tuff characteristics. The classification of tuffs according to the type of pyroclasts (Schmid 1981) and the pore radii distribution type (Ruedrich and Siegesmund 2006) may only be seen as a potential proxy for a fast estimation of rock strength and at this point their utility for this purpose is surely lacking validation from comprehensive data.

Looking at the relationship between hydric expansion and UCS reduction, it becomes apparent that with increasing hydric expansion, the compressive strength decreases (Fig. 5.11). Therefore, vitric tuffs with typical low expansion values experience less strength reduction than crystal and lithic tuffs, which typically show increased hydric expansion (Fig. 5.11). López-Doncel et al. (2018) report similar behavior but with the thermal expansion of tuffs. When classified according to the pore radii distribution type, only the unimodal equal type shows similarities with the behavior of the vitric tuffs. The only clear observation regarding unimodal unequal pore radii types is a typical high strength reduction. Bimodal types again scatter over the whole range of expansion values and UCS reduction, and do not seem suitable for estimating a distinct behavior of the material.

The reduced strength connected to increased expansional behavior of certain tuff groups can also be transferred to their salt crystallization resistance. Low expanding vitric tuffs show higher resistance to salt weathering, unlike the higher expanding crystal tuffs, which show accordingly lower resistance (Fig. 5.12). A grouping after pore radii distribution type is again only suitable to a limited extent. As observed above, unimodal equal types coincide with the behavior of vitric type tuffs. Unimodal unequal types, with typical low to intermediate hydric expansion, show moderate resistance to salt weathering, while bimodal types show wide scattering. The lowest resistance to salt weathering in this study is shown by tuffs of the bimodal type. These results confirm the observations in recent studies, where unimodal unequal and bimodal type tuffs with high fractions of micropores generally show higher susceptibility to salt crystallization (Çelik and Sert 2020; Germinario and Török 2019; López-

## 5 Key parameters of volcanic tuffs: a statistical approach

Doncel et al. 2016; Pötzl et al. 2018b; Yu and Oguchi 2010). It is widely accepted that the generation of high crystallization pressures is facilitated by micropores (e.g., Fitzner and Sneath 1982; Ruedrich et al. 2005; Scherer 1999; Steiger 2005a, 2005b; Wellman and Wilson 1965). However, it should be noted that various authors define different sizes of micropores that facilitate the deterioration due to salt crystallization. Frequent sizes found in the literature range between  $<0.05 \mu\text{m}$  and  $10 \mu\text{m}$  (Benavente 2011; Steiger 2005b). To sum up, the pore size distribution may prove useful as an estimator of the salt weathering resistance of tuffs, as does the distinction between crystal and vitric type tuff, since the crystal type tuff usually shows lower durability (Fig. 5.12).

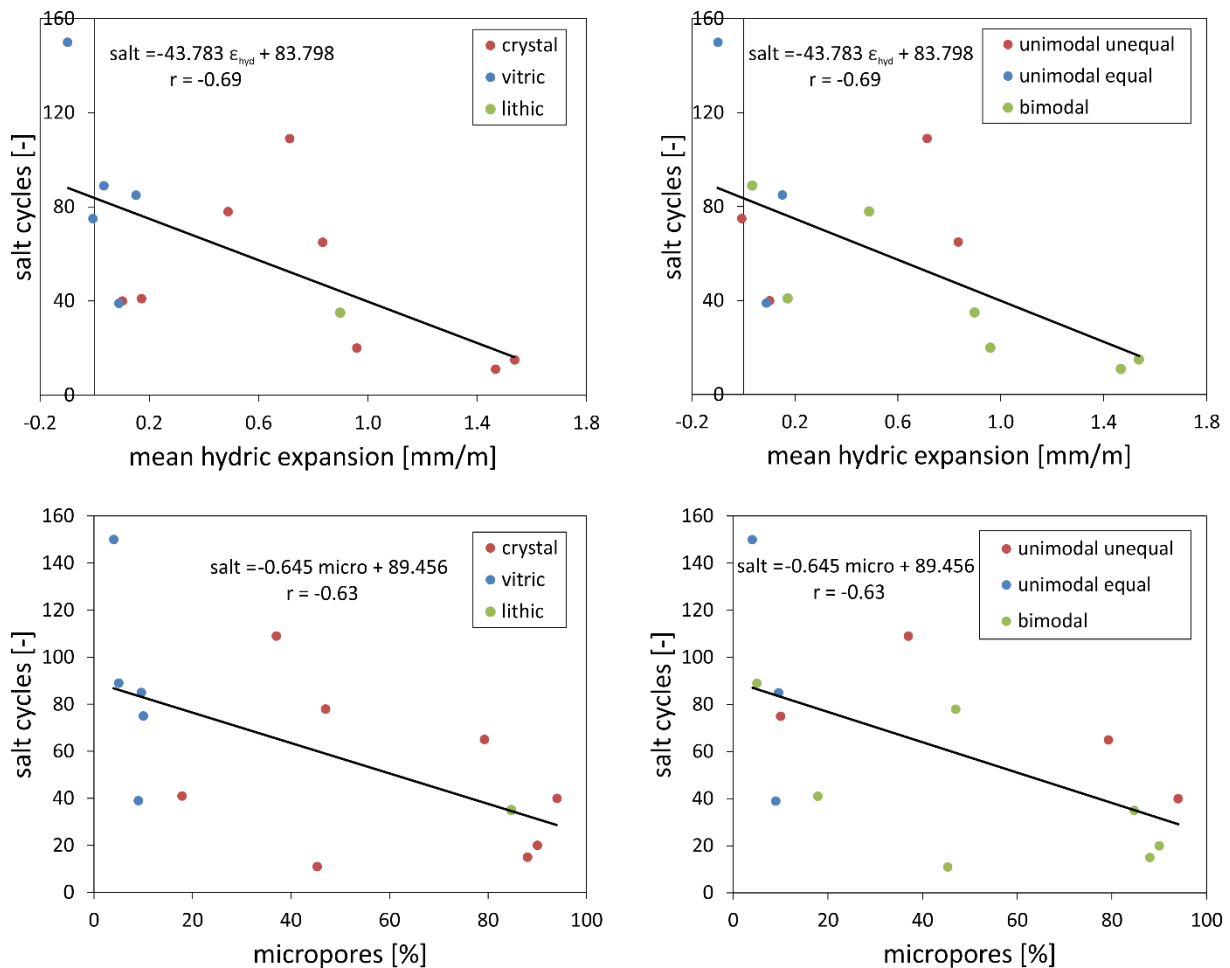


Figure 5.12: Relationship between different rock properties with regard to their pyroclastic content and pore radii distribution type

## 5 Key parameters of volcanic tuffs: a statistical approach

### 5.4 Summary and Conclusions

The goal of this study was to identify key parameters that may be useful in the estimation of the strength and durability of tuffs by analyzing a dataset of more than 500 samples from the literature. Fifteen selected tuffs were investigated in more detail, in order to extrapolate to the very comprehensive, but less detailed dataset from the literature and achieve larger representability. Tuffs demonstrate to bear great mineralogical and fabric heterogeneity, and along with this heterogeneity they show a wide range of technical parameters and responses to weathering. Especially the porosity, water absorption and hydric expansion can exceed values multiple times higher than other rock types (compare Siegesmund and Dürrast 2011). Although the analyses in this study are accompanied by a partly wide scattering of data, some strong correlations can be observed:

- Both porosity and bulk density are strongly related to the uniaxial compressive strength (UCS) and tensile strength (TS) and are therefore reliable estimators to predict the strength and durability of tuffs (UCS reduction).
- Both porosity and bulk density have a strong relation to the ultrasonic velocity, which in turn shows to be a good estimator for the strength of tuffs. This observation is not trivial, since tuffs can incorporate huge amounts of pumice clasts and lithics, that may considerably influence the propagation of the P-wave, e.g., due to increasing the pore space. Therefore, an ultrasonic testing device can help for a fast and non-destructive assessment of the materials quality parameters, like it is reliably done for more homogenous natural stones and concrete (Sharma and Singh 2008).
- The hydric expansion is connected to both strength reduction and salt weathering. The higher the hydric expansion, the lower the tuffs durability. Similar to the observations of Wedekind et al. (2013) and contrary to other studies on clay bearing tuffs (Pötzl et al. 2018b, compare Chapter 4) or sandstones (Ruedrich et al. 2011), the tuffs of this study do not show a clear correlation between the cation exchange capacity (CEC) and the intensity of their moisture expansion. This is possibly because the samples partly contain zeolites that may not increase the CEC, but contribute to the moisture expansion.
- The pore size distribution, categorized in one of the three pore radii types suggested by Ruedrich and Siegesmund (2006) (type I = unimodal equal, type II = unimodal unequal, type III = bimodal), showed to be helpful in estimating general trends of material behavior. In doing so, unimodal unequal pore radii types are associated with crystal tuffs and unimodal equal pore radii types are associated with vitric tuffs. Tuffs with bimodal pore radii distribution turned out to be the most unpredictable in terms of their durability and their pore radii distribution alone may not give meaningful prognosis.
- Crystal and vitric tuffs show strongly differential characteristics in their technical parameters and durability and are potentially useful for their estimation. Some key observations regarding crystal and vitric tuffs are: (1) Vitric tuffs are described by high porosity, with usually large mean pore radii and high water absorption. Their water vapor diffusion resistance, hygroscopic water sorption and hydric expansion is generally low. The

## 5 Key parameters of volcanic tuffs: a statistical approach



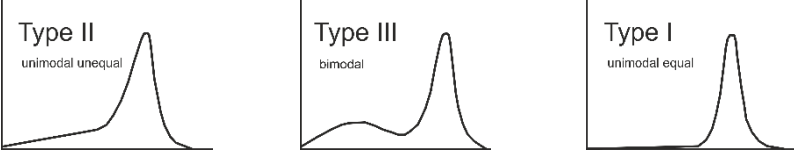
influence of water on their strength properties is considerably low and they show typically high resistance to salt weathering. (2) Crystal tuffs show typically lower porosity, with small mean pore radii and low to moderate water absorption. They often contain high amounts of swelling clays and zeolites that are connected to an increasing hydric expansion and hygroscopic water sorption, as well as a high resistance to water vapor diffusion. Crystal tuffs show the highest strength values, but also the strongest decrease in strength due to water saturation. Their resistance to salt weathering is typically lower. In the practical applicability the initial categorization of crystal and vitric tuffs after the classification system of Schmid (1981) may therefore help to give a broad picture of the expected material parameters (see Tab. 5.4). These observations need validation in future studies, as the literature does not provide sufficient constraints.

The basic relationships between the individual rock parameters found in this study confirm the results of previous studies on other rock types (Siegesmund and Dürrast 2011). They also confirm many findings of case studies on tuffs with relatively small datasets mentioned in the introduction (compare also Chapter 4). The comprehensive dataset of this study, however, does finally allow for more general statements, as this study provides the highest representability of tuffs so far.

Based on the results of this comprehensive dataset, it becomes apparent that the suitability of tuff as building stone also highly depends on the environmental (climate, exposure) conditions. As an example: Tuffs with high potential for water absorption and retention in combination with considerable amounts of swelling clays (in this study often represented by crystal tuffs) should consequently not be applied in climatic zones with increased relative humidity or in areas that experience many wet-dry cycles, as they show a reduced resistance to hydric expansion processes and salt weathering. In dry environments they may, however, be a suitable building material, since they typically possess increased strength values. Tuffs with predominantly large pore radii, low water vapor diffusion resistance and a lack of swelling clays (in this study often represented by vitric tuffs) may absorb more water, but since this water is not retained for long and does not induce expansion processes or a high reduction of strength, they may be a more suitable type of tuff for humid environments. The application of volcanic tuffs in the base area of a building that is in contact with the ground moisture should be reconsidered, since the majority of tuffs show increased potential of capillary water uptake into the rising walls (Fig. 5.5). Many deterioration patterns in Armenian and Mexican tuff facades are associated to this high capillarity (Fig. 5.1). The application of a less porous and capillary active material in the base area, such as basalt, may significantly reduce/inhibit the water uptake and distribution of ground moisture.

## 5 Key parameters of volcanic tuffs: a statistical approach

Table 5.4: Some key differences of crystal and vitric tuffs observed on the set of 15 representative tuffs of this study. UCS = uniaxial compressive strength, w-value = capillary water absorption

	<b>Crystal tuff</b>	<b>Vitric tuff</b>
		
porosity	~15 – 30 %	~30 – 50 %
bulk density	1.5 – 2.2 g/cm <sup>3</sup>	1.2 – 1.6 g/cm <sup>3</sup>
water absorption	~5 – 15 %	~ 15 – 30 %
∅ pore radius	<0.2 μm	>0.7 μm
pore radii distribution type		
w-value	0.5 – 10 kg/m <sup>2</sup> Vh	5 – 44 kg/m <sup>2</sup> Vh
sorption 95% RH	1.3 – 7.9 wt.%	0.1 – 1.2 wt.%
hydic expansion	0.2 – 7.5 mm/m	-0.2 – 0.3 mm/m
P-wave velocity	2.5 – 4 km/s	1.3 – 3 km/s
tensile strength	3 – 9 MPa	0.7 – 4 MPa
UCS	42 – 142 MPa	5 – 46 MPa
∅ strength reduction	~28 – 49 %	-19 – 35 %
dyn.E-modulus	10 – 31 GPa	3 – 14 GPa
stat. E-modulus	3 – 6 GPa	1 – 4 GPa
∅ salt cycles	~47	>83



## 6 Clay swelling mechanism in tuff stones – case study Hilbersdorf

As the previous two chapters highlighted, hydric expansion is to be considered an important factor for the weathering behavior and deterioration of tuffs, which are utilized as building stones. It is typically associated with the presence of swellable clay minerals. Two types of swelling mechanisms are discussed when swellable clay minerals are present: stepwise intracrystalline swelling and continuous osmotic swelling. A mechanism that can cause expansion in the absence of swellable clay minerals, which is characterized by interaction of surface forces, is the disjoining pressure. The identification of the primary mode of swelling is important for understanding and finally preventing the swelling damage in tuff stones. The hydric expansion of the Hilbersdorf Tuff can exceed the values of typical volcanoclastic materials by multiples, but partly shows the absence of swellable clay minerals. In this study, extensive mineralogical and petrophysical investigations on five varieties of the Hilbersdorf Tuff were performed. Swelling experiments demonstrated that intracrystalline swelling plays a major role when swellable clay minerals are present. Furthermore, the importance of the structure and location of the clay minerals in the rock fabric is highlighted. The investigation suggests that the disjoining pressure plays an important role for the hydric expansion of two varieties, which are free of swellable clay minerals but show high microporosity and pores smaller than 2 nm.

### 6.1 Introduction

During the nineteenth and early twentieth centuries, the city of Chemnitz evolved into one of Germany's most important industrial cities in the central part of the republic. After 200 years of industrial history, the city is a technology location with focus on automotive, information and engineering industry. Unlike many industrial cities, the city of Chemnitz today is characterized by its broad variety of utilized natural stone materials in construction. One of the most used materials since the thirteenth century is the Zeisigwald porphyry tuff, subsequently named Hilbersdorf Tuff (Fig. 6.1). This tuff was quarried until the 1960's and gave many districts of the city and its surroundings its characteristic appearance. Its deposits also include the world famous petrified forest of Chemnitz, a preserved Permian ecosystem, which was already observed by Georgius Agricola (1494–1555) and was subject to countless scientific works since the eighteenth century. It is important to note that the Hilbersdorf Tuff includes a wide variety of tuffs that originated during various volcanic eruptions. Due to the lack of existing outcrops and opportunities for direct comparison, the separation of the many varieties is unclear to this day. This study aims to systematically analyze the varieties of the Hilbersdorf Tuff which were used as building materials.

The fact that its hydric expansion can exceed the values of typical volcanoclastic material by multiples makes the Hilbersdorf Tuff a material of special interest. Prior studies already indicated different contents of swellable clay minerals in the Hilbersdorf Tuff. While Siedel (1995) could attribute the swelling for the most part to the presence of considerable amounts of swellable mixed-layer minerals (interstratified minerals with smectitic layers), Wedekind et al. (2013) barely observed swellable clay minerals. Both studies indicated a connection of the hydric expansion with the pore space properties. In fact Wedekind et al. (2013) were able to

## 6 Clay swelling mechanism in tuff stones – case study Hilbersdorf

show that the microporosity can have a significant impact on the degree of the moisture expansion in tuff stones. Thus, the question arises which processes also play a role and which process primarily causes the swelling in tuff stones.



Figure 6.1: Historic buildings erected with different types of Hilbersdorf Tuff in and near the city of Chemnitz. **a** Porphyry house of master stonemason Findewirth, built in 1869. **b** Tulip pulpit in the Freiberg Cathedral made of Sculpture Tuff (1505). **c** Castle church of Chemnitz (fifteenth century). **d** The devil's bridges which served as a trench shoring system for the access road to the Findewirth quarry (1880). **e** Pediment cornice as well as typical window and door jambs from Hilbersdorf Precious Tuff (nineteenth century)

Moisture expansion is recognized as a major factor contributing to the weathering and deterioration of building stones (Ruedrich et al. 2011; Weiss et al. 2004). The expansion is mostly associated with the swelling and shrinking of clay minerals (De la Calle and Suquet 1988; Dixon and Weed 1989; Gonzalez and Scherer 2004; Graf v. Reichenbach and Beyer 1995; Moore and Reynolds 1989; Schuh 1987; Sneath et al. 1995). Clay minerals are phyllosilicates that mainly consist of tetrahedral and octahedral sheets which form thin layers that are characterized by a considerable width and length but a negligible thickness. In general, they can be grouped as minerals with a 1:1 and a 2:1 layer structure. A 1:1 mineral consists of one tetrahedral and one octahedral sheet. A 2:1 mineral consists of two tetrahedral sheets and one octahedral sheet. Among other frequent representatives in tuff stones are kaolinite (1:1, dioctahedral), illite (2:1, dioctahedral), montmorillonite (2:1, dioctahedral, mineral from the smectite group) and mixed-layer minerals. The swellability of clay minerals can play a decisive role in the weathering of building stones.

The different swelling processes, however, that are decisive for the expansion are still under discussion. Two principle modes of swelling are discussed when clays are present in a natural building stone: (1) inner- or intracrystalline swelling which occurs in the interlayer region of

## 6 Clay swelling mechanism in tuff stones – case study Hilbersdorf

expandable clay minerals and (2) inter crystalline or osmotic swelling which acts between clay particles. The intracrystalline swelling is caused by hydration of the interlayer cations and is marked by discrete steps in the interlayer spacing. Each step corresponds to about 2.5 Å, which is approximately one monolayer of water (Wangler and Scherer 2008). During osmotic swelling, the interlayer spacing increases continuously with increasing water activity. This type of swelling is induced by the negative surface charge of the clay minerals. In contact with an electrolyte solution, an electric double-layer forms near the clay mineral surface. The difference in the ionic concentration between the clay mineral surface and the pore solution leads to a balancing reaction of the water. The water, which tends to balance the concentration gradient, is drawn between the clay particles and thus pushes them apart.

If no clay minerals are present, a third mechanism can induce swelling. Schult and Shi (1997) attributed the moisture expansion in clay-poor or clay-free rocks to a swelling effect due to interaction of surface forces like van der Waals attraction, electrical double-layer repulsion and solvation repulsion. The concept of the so-called disjoining pressure was introduced by Derjaguin and Obukov (1936), who defined it the following way: the disjoining pressure  $\Pi$  is equal to the difference between the pressure in the film between two solid surfaces and the pressure in the bulk phase. Its value can be calculated as the derivative of the Gibbs energy of interaction per unit area with respect to distance. Similar to the osmotic swelling, the electrolytic concentration plays an important role in the cause for the disjoining pressure. Weimann (2001) described the decrease in van der Waals forces and resulting electrorepulsion of adjacent particles during moisture changes. The disjoining pressure is especially important for rocks with a high amount of micropores smaller than 0.1  $\mu\text{m}$  (Ruedrich et al. 2011).

Kocher (2005) and Ruedrich et al. (2011) gave a detailed overview of the concepts of the different swelling modes that are addressed here. They also mentioned the importance of the location of the clay minerals in the pore space, since it is crucial if the forces developed by intracrystalline swelling of clay minerals are expanding into the open pores or between the grain boundaries, leading to significant mechanical stress. Given these circumstances comprehensive investigations were carried out to locate the clay minerals in the rock fabric.

### 6.1.1 Geological setting

The city of Chemnitz is located in Saxony in the northeastern part of the Ore Mountain Basin. The sediments of the Rotliegend Group (Permian) of the Ore Mountain Basin are characterized by thick layers of clays, sand- and siltstones as well as conglomerates and limestones. The sediments are interrupted by multiple volcanic eruptions due to the subsequent volcanism of the late phase of Variscan Orogeny (Siedel 2006). The Hilbersdorf Tuff represents the last volcanic activity in the Rotliegend Group of the Ore Mountain Basin, and its distribution is limited to the eastern part of the basin. The Ore Mountain Basin strikes NE-SW and comprises the sedimentary record of the Variscan Orogen. It is limited to the north by the Saxonian Granulite Massif, consisting of Proterozoic to Ordovician granulites, which are surrounded by Cambrian and Devonian schists and to the south by the early Paleozoic schists of the Ore Mountains. The Hilbersdorf Tuff was deposited in the upper part of the lower Rotliegend Group (Leukersdorf Formation) and discordantly overlies the sediments of the Härtensdorf,

## 6 Clay swelling mechanism in tuff stones – case study Hilbersdorf

Planitz and Leukersdorf Formations in an E-W direction. It forms a pyroclastic marker horizon in the Leukersdorf Formation with ages (SHRIMP-U/Pb on zircons) of  $290.6 \pm 1.8$  Ma (Rößler et al. 2009).

The Hilbersdorf Tuff itself is the result of a multi-phase eruption defined by several horizons, in which the final caldera eruption happened at the eastern outskirts of the city of Chemnitz, in the area of the Beutenberg hill, respectively, the Zeisigwald (Eulenberger et al. 1995; Fischer 1990; Rößler et al. 2008; Schneider et al. 2012). The sequence, in ascending order, starts with a basal succession of a reddish-violet to dark violet colored ash tuff to slightly crystalline ash tuff, a pyroclastic flow deposit of violet- red to light red ash tuffs with collapsed lapilli of pumice, a base surge deposit with alternating sequences of unlayered, lapilli-bearing ash tuffs and fine layered ash tuffs, an ignimbritic sequence of at least three flow-units of lapilli-bearing ash tuffs with accretionary lapilli as well as phreatomagmatic air fall tuffs (ash tuffs with low lapilli content). The last sequence consists of a redeposited sequence of tuffites (Fischer 1990; Schneider et al. 2012). Fischer (1990) associated the material of the Zeisigwald quarries to the base surge deposits and the ignimbritic sequence. Here the Hilbersdorf Tuff reaches a thickness of 40–50 m, which decreases in the direction of the city center (Siedel 2006).

### 6.1.2 Utilization and deterioration

The Hilbersdorf Tuff defines the cityscape of Chemnitz like no other building stone. Well-known quarries are located in the Zeisigwald, Schlossberg and the Kapellenberg. Other partly unknown quarries in the urban area of Chemnitz were back-filled during the growth and expansion of the city. The Hilbersdorf Tuff was used as cut stone in masonry (Fig. 6.1a), profiled building elements like window and door jambs, especially in factory and residential buildings of the nineteenth century (Fig. 6.1e), or filler rock of low quality material. The application as sculpture stone especially in the beginning of the sixteenth century gave the Hilbersdorf Tuff a lot of attention. Numerous art works like the tulip pulpit in the cathedral of Freiberg (Fig. 6.1b) reflect the good workability of this natural stone. The overall forms are inspired by the specific taste of the times. Many buildings were erected in art nouveau and neoclassical style of the early twentieth century. Neo-Romanesque and Gothic forms are represented by the castle church of Chemnitz (Fig. 6.1c) and the collegiate church of Ebersdorf, respectively.

Because of its heterogeneity, the varieties of the Hilbersdorf Tuff show quite different deterioration and weathering phenomena. All varieties suffer from a characteristic loss of components (Fig. 6.2a). Significant deterioration is shown by crumbling (Fig. 6.2b), discoloration due to moist areas (Fig. 6.2c), scaling parallel and independent of the bedding (Fig. 6.2d) as well as loss of matrix material (Fig. 6.2e). These destructive phenomena frequently occur in areas of the building where moisture and water are permanently or temporarily available such as base areas, pediment cornices or balconies. The intensity of the deterioration depends on the variety that is used for the construction as well as the exposition to moisture. Especially the Sculpture Tuff (HS) and the Lapilli Tuff (HL) are more affected by weathering than other varieties. The most resistant variety seems to be the Precious Tuff (HP), which was significantly used for pediment cornices as well as door and window jambs of the factory and residential buildings of the nineteenth and early twentieth century (Fig. 6.1e).

## 6 Clay swelling mechanism in tuff stones – case study Hilbersdorf

Since the Hilbersdorf Tuff is the result of various volcanic eruptions and shows a macroscopic heterogeneity in the decimeter range, categorizing the varieties of this material is not easy. For this reason, the study focuses only on the varieties that were used as construction material in the city of Chemnitz. The aim of this study is to provide information about the influence of the pore space properties and chemical composition on the causes and effects of deterioration. The role of the amount and type of different clay minerals present, as well as their location in the pore space of the rock is of special interest for the behavior of moisture expansion.



Figure 6.2: Appearance of different damage and deterioration types observed in the Hilbersdorf Tuff. **a** Loss of components displays the most observed type of deterioration at the Precious Tuff (HP). **b** Back-weathering due to crumbling and scaling of the Regular Tuff (HR) variety in a door jamb. **c** Discoloration in the splash zone of water at the castle church of Chemnitz. **d** Scaling of the Sculpture Tuff (HS) and Regular Tuff (HR) variety at the collegiate church in Chemnitz/Ebersdorf. **e** Loss of matrix that results in protruding lapilli components in the Lapilli Tuff (HL) observed in a door jamb

### 6.2 Materials and methods

Seven varieties of the Hilbersdorf Tuff were investigated in this study, while five varieties were investigated in greater detail. The detailed investigations were carried out on the Hilbersdorf Regular (HR), Hilbersdorf Precious (HP), Hilbersdorf Lapilli (HL), Hilbersdorf Sculpture (HS) and Hilbersdorf Kapellenberg (HK) Tuff. The naming of the Hilbersdorf Tuff varieties was partly transferred from the existing nomenclature in Jentsch (2012). In addition, this study includes results of prior investigations from Siedel (1995) (in this study labeled as HD95) and Wedekind et al. (2013) (HD1).

## 6 Clay swelling mechanism in tuff stones – case study Hilbersdorf

The petrographical analyses of each variety were performed on oriented thin sections under a polarization microscope. The mineralogical and geochemical analyses were done by using X-ray diffraction (XRD) of whole rock samples and oriented slides of the clay fraction < 2 µm along with X-ray fluorescence (XRF) and cation exchange capacity (CEC) analyses as described in Ruedrich et al. (2011). The specific surface area was determined by N<sub>2</sub> gas adsorption based on the Brunauer–Emmett–Teller theory (BET).

Hydrostatic weighing was carried out to acquire the particle and bulk density as well as the porosity and the degree of saturation. The pore radii distribution was measured by mercury intrusion porosimetry. The capillary water adsorption (*w* value) was measured on sample cubes of 65 mm edge length in a closed cabinet while weighing over time. Water vapor diffusion resistance (*μ* value) was measured on samples with a diameter of 40 mm and a thickness of 10 mm, using the wet-cup method. The hygroscopic water sorption can provide information about the swelling potential of the rock (Kocher 2005). It was measured between 25 and 95 % relative humidity (RH) at 20°C in a climate chamber.

The splitting tensile strength (STS) was determined by means of the “Brazilian test,” on cylindrical samples of 40 mm in diameter and 20 mm in thickness under dry and water-saturated conditions. The thermal expansion was determined on samples of 15 mm in diameter and 50 mm in length with a six-rod dilatometer in a climate chamber under dry conditions. To determine the salt weathering resistance of the samples, a cyclic salt weathering test was executed on cubes of 65 mm edge length. For one cycle of the test, the dry samples were put in a 10 % solution of sodium sulfate (Na<sub>2</sub>SO<sub>4</sub>) for four hours. Afterwards the samples were dried in an oven (60°C) for 24 h and subsequently weighed. The procedure was repeated until a minimum loss of mass of at least 30 % was achieved.

The hydric expansion of the samples was measured on cylindrical samples (diameter 15 mm, length 50 mm, respectively, 100 mm) under conditions of complete immersion in distilled water. The linear expansion was measured as a function of time by a displacement transducer with a resolution of 0.1 µm. Additional swelling experiments were performed with salts and solvents obtained from Fisher Scientific. Cationic pre-treatments were performed by soaking the sample in an approximately 3 M solution of chloride salt and subsequent washing in distilled water for several times. In the elimination experiment, the swelling fluid was syringed out and replaced by an approximately 1 M solution of chloride salt.

### 6.3 Petrography and mineralogy

The Hilbersdorf Tuff occurs in different varieties with regard to its macroscopic appearance and application as a building material. The varieties differ in grain size and color. They can be pale pink to brick red, light or dark purple and greenish to yellowish up to white. They often are speckled, spotted, marbled or striped. Only the Hilbersdorf Sculpture Tuff (HS) shows some kind of homogenous coloration. Often lapilli at the centimeter scale are embedded in the fine-grained ash-rich matrix. The varieties can appear versatile and transitions are likely. Based on the macroscopic appearance and its local occurrence, the Hilbersdorf Tuff was subdivided into seven varieties that are used as natural building stones. Five varieties were also analyzed in greater detail in this study.

## 6 Clay swelling mechanism in tuff stones – case study Hilbersdorf

All investigated varieties show a clear acid composition with high SiO<sub>2</sub> contents between 73.5 % (HR) and 75.4 % (HP) and thus can be defined as rhyolitic tuffs after Le Bas et al. (1986). The mineralogical composition, including clay minerals, is listed in Table 6.1.

Table 6.1: Mineralogical composition (XRD) and CEC (meq/100 g)

Sample ID	Major	Minor/Traces					CEC	
HR	Quartz	Feldspar	Muscovite-illite		Kaolinite	Hematite	Calcite	< 1
HP	Quartz	Feldspar	Muscovite-illite	I-S	Kaolinite	Hematite		2
HL	Quartz	Feldspar	Muscovite-illite					3
HS	Quartz	Feldspar	Muscovite-illite	Smectite				4
HK	Quartz	Feldspar	Muscovite-illite	Tosudite				7

The Hilbersdorf Regular Tuff (HR) represents the most used variety in construction in Chemnitz and its surroundings. It appears irregularly speckled and partly marbled in colors of pale pink to dark purple and bright beige to greenish with fluent transitions. Various types of elongated lapilli inclusions at the millimeter to centimeter scale are embedded and can indicate a lamination (Fig. 6.3a). This variety can contain several millimeters to centimeter large cavities, partly filled with loose clayey material. The microscopic difference between the reddish and bright parts of the rock is highly visible. In thin section, mono- and polycrystalline quartz, relics of feldspar and lithic clasts (rich in sericite) are found, as well as small and columnar muscovites. They are embedded in a glassy matrix (~ 70 %) and give a hypocrystalline texture. Rarely, calcite can be found. Especially in the bright areas, the eutaxitic texture is obvious. The clasts and crystals in the bright area are of much smaller size. Devitrified glass shards can also be observed in the bright parts of this variety. Iron oxides, probably hematite, are well distributed throughout the red colored parts of the stone. SEM images show high amounts of clay material (illite/muscovite) as well as pseudo-hexagonal booklets of kaolinite. In SEM, traces of calcite and fluorite were detected. The clay material shows varying appearance in the different areas of the rock. Illite/muscovite and kaolinite were identified in separated clay fractions by XRD (Fig. 6.4). Intracrystalline swellable layers (smectitic layers) were ± absent. The CEC is very small (< 1 meq/100 g). Note that the CEC of a tuff depends on both, type and relative amount of a clay mineral. Differences in CEC may therefore also reflect the clay mineral content, which, however, was not determined in this study.

The Hilbersdorf Precious Tuff (HP) consists of a bright purple to reddish matrix and characteristic beige to yellowish stripes and speckles, which can give a marbled appearance (Fig. 6.3d). It contains embedded concretionary lapilli clasts of red to brown color. Like the lapilli clasts in HL, the lapilli here can show a zonation. It appears to be the most resistant variety. Significant amounts of this material were used for door and window jambs as well as pediment cornices in the constructions of the early twentieth century. Its historical quarries are unknown. In thin section, the well distributed iron oxides in this rock are peculiar. Mono- and polycrystalline quartz, relics of feldspar and muscovites are situated in the glassy matrix of more than 70 %. The lithic clasts show considerable amounts of quartz, feldspar and muscovites. Only the bright areas contain higher amounts of clay. SEM images show that the matrix of HP, contrary to HR, consists of larger quartz and feldspar crystals, mixed with clay

## 6 Clay swelling mechanism in tuff stones – case study Hilbersdorf

material (illite). SEM images also show that a lot of pores are closed by a cover of quartz,

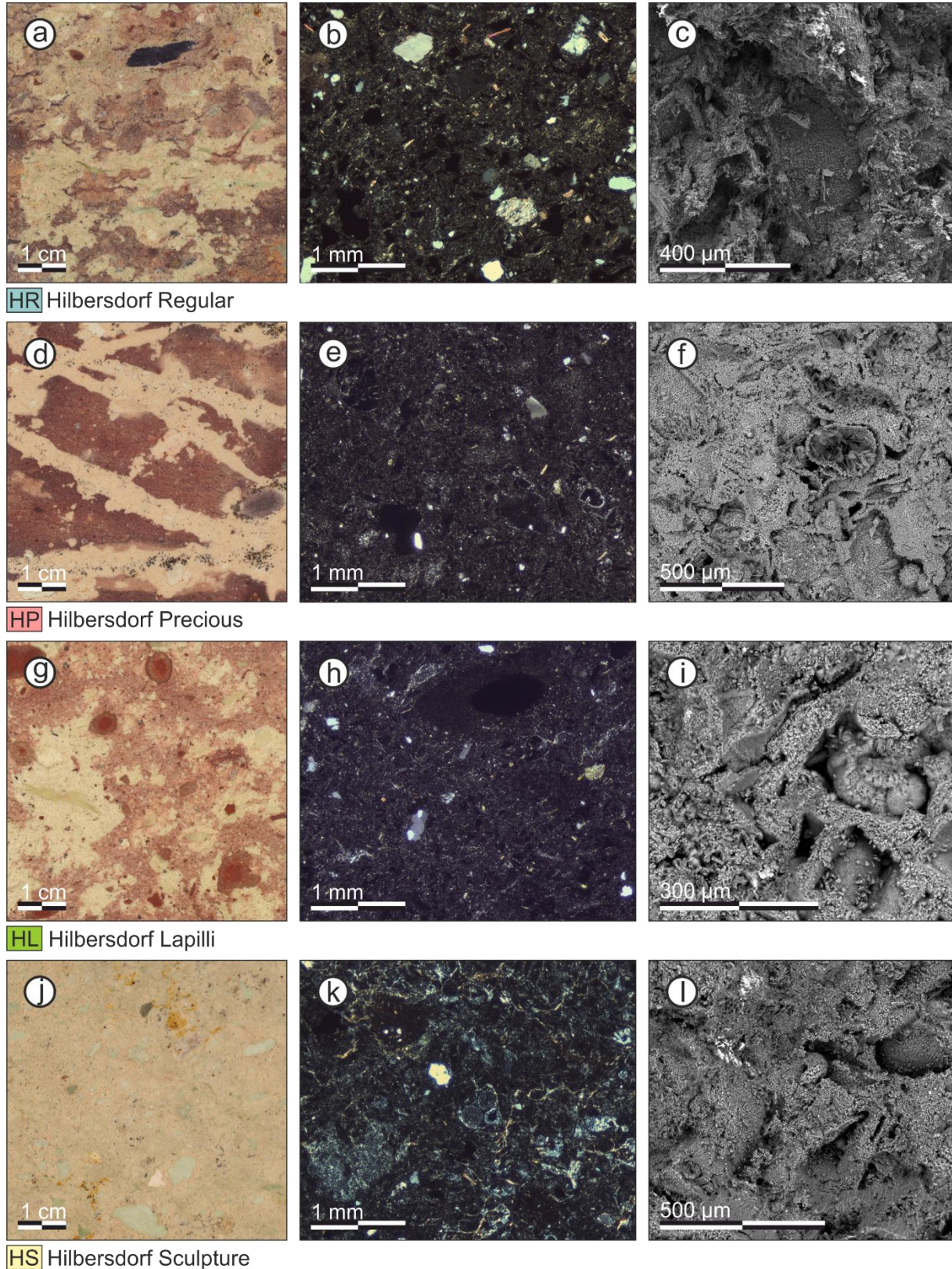


Figure 6.3: Illustration of the investigated varieties of the Hilbersdorf Tuff. **a, d, g, j** Polished section (wet). **b, e, h, k** Thin section under polarized light. **c, f, i, l** SEM photomicrographs

feldspar and clay material (illite), and thus inaccessible for advective water flow (Fig. 6.3f). The open pores are often filled with booklets of kaolinite material. XRD on separated clay fractions



## 6 Clay swelling mechanism in tuff stones – case study Hilbersdorf

identified illite with traces of intracrystalline swellable layers (5–6 % smectitic layers were identified with the Rietveld method using the models described by Ufer et al. (2012a, 2012b). This mineral is called by definition disordered interstratified illite–smectite (I-S)) and kaolinites (Fig. 6.4). The CEC is small (2 meq/100 g).

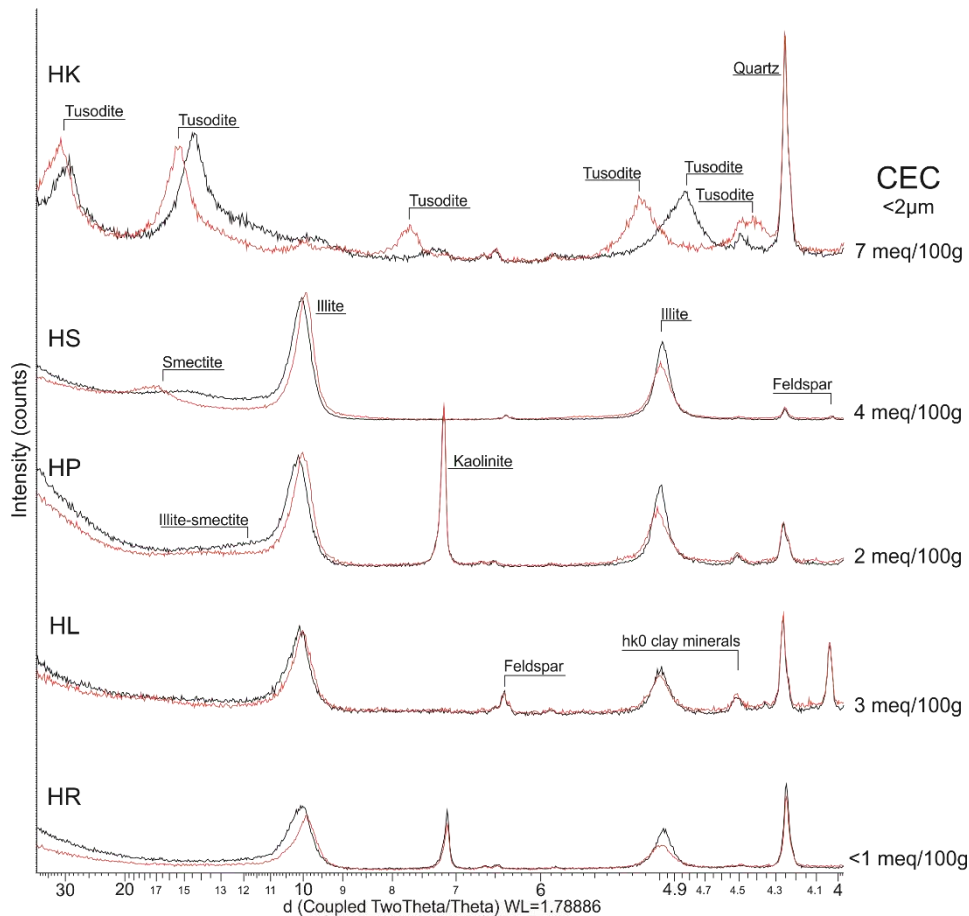


Figure 6.4: XRD analyses of clay fractions (oriented mounts). black: air-dry, red: ethylene glycol solvated

The Hilbersdorf Lapilli Tuff (HL) is characterized by its centimeter scale reddish, concretionary lapilli of pumice that are embedded in the beige and reddish to purple matrix. These lapilli can show zonation. The HL is of lower weathering resistance, which is why it is only used occasionally in construction. Besides quartz, feldspar and muscovite, this variety contains considerable amounts of pumice clasts, as well as clayey cavities. In thin section, the glassy matrix makes up to 60%. Illite/muscovite was identified by XRD of separated clay fractions, while intracrystalline swellable layers (smectitic layers) were  $\pm$  absent (Fig. 6.4). The CEC is small (3 meq/100 g). SEM images demonstrated the presence of fibrous fine-grained illite minerals that line the pore space, while larger muscovites were barely observed. Sticking to the illite material, a huge amount of large, perforated feldspar crystals grow, into the pore space (Fig. 6.3i). The pumice clasts are characterized by much smaller pores and the absence of clay minerals.

The Hilbersdorf Sculpture Tuff (HS) is of light beige to greenish color and appears nearly homogenous in colorization. It contains various clasts of different chroma. Due to its minor resistance against weathering, only in exceptional cases is this variety used in masonry. Its utilization is focused primarily on the application as a sculpture stone. In comparison with the

## 6 Clay swelling mechanism in tuff stones – case study Hilbersdorf

regular variety (HR), HS shows less lithic clasts and only traces of small muscovites. The porosity is visibly higher, and the overall texture is more homogeneous. It contains vesicular, glassy shards that show devitrification on its margins, as well as small amounts of iron oxides. SEM images show huge amounts of clay material that nearly covers the whole sample (Fig. 6.3I). The illite aggregates are characterized by a honeycomb structure, while they appear frayed on their edges. Huge, perforated feldspars reach the open pores. Kaolinites were not observed in this variety. Few clasts are characterized by much smaller pores and the absence of clay material. Illite/muscovite minerals and significant amounts of intracrystalline swellable smectites were identified by XRD on separated clay fractions (Fig. 6.4). The CEC is moderate (4 meq/100 g).

The Hilbersdorf Kapellenberg Tuff (HK) is characteristically mottled in well-defined brick red and beige areas (Fig. 6.5a). It contains clasts of pumice at the centimeter scale, which are often located in the center of beige colored areas, partly showing elongation. This variety is mainly found in Gothic architecture and was quarried at the Kapellenberg. In thin section, mono- and polycrystalline quartz, relics of feldspar and lithoclasts are located in a cryptocrystalline, glassy matrix of about 55 %. The matrix in the beige areas appears greyish. In the beige areas, the pores appear bigger. Additionally, the beige areas contain larger muscovites and glass shards that are absent in the red areas. The lithoclasts in the red areas are larger and mostly framed by reddish minerals, presumably iron oxides. Their composition appears to be analogue to the composition of the beige areas. The SEM images show high amounts of clay material (illite) in the beige areas, especially as pore-filling materials. The illites are typically interwoven with small quartz and feldspar crystals. In the red areas of the rock, large amounts of iron oxides were detected. The quartz crystals in the pores exceed the size of the crystals in the matrix cover by multiples. XRD of separated clay fractions indicated the presence of tosudite, a regular interstratified mineral with 50 % smectitic layers showing intracrystalline swelling (Fig. 6.4). Traces of illite/ muscovite are also present. The CEC is high (7 meq/100 g).

All samples differ with respect to the amounts of smectitic layers. Smectitic layers are characterized by expandable interlayers, these regions have a high specific surface area and a high CEC of up to 130 meq/100 g as pure minerals. In the interlayer regions of smectites, exchangeable cations can be replaced by any competing cations present in the pore water, and ion exchange causes expansion or shrinkage, respectively. The CEC of other clay minerals (except vermiculite which is absent in the building stones studied) is very small, and the CEC can be used as indicator for the smectite content or the content of smectitic layers in interstratified clay minerals present in natural building stones (compare discussion in Ruedrich et al. 2011). In two of the tuffs (HR, HL), smectitic layers were  $\pm$  absent or present in trace amounts. HP contains small amounts of smectitic layers (5–6 %) present as interstratified illite–smectite (I-S). In all three tuffs, the CECs were small (< 1–3 meq/100 g, Table 6.1). The tuff HS contains significant amounts of expandable interlayers (pure smectite), which is reflected by a higher CEC of 4 meq/100 g (Table 6.1) as compared to HR, HL and HP. HK contains even larger amounts of expandable interlayers present as a regular interstratified clay mineral with 50 % smectitic layers (tosudite). This tuff had the largest CEC value of 7 meq/100 g (Table 6.1).

## 6 Clay swelling mechanism in tuff stones – case study Hilbersdorf

Due to a lack of availability and information on its historical quarries, one variety of the Hilbersdorf Tuff rarely used in construction could not be sampled. The Hilbersdorf Stripe Tuff (HST) as described in Jentsch (2012) is a sandy/ beige, partly reddish variety that is pervaded with stripes by brown, undulated deposits of limonite. Its original quarries are unknown, but there are transition areas in some blocks that indicate a close relation to the Hilbersdorf Regular Tuff (HR) of the Zeisigwald area.

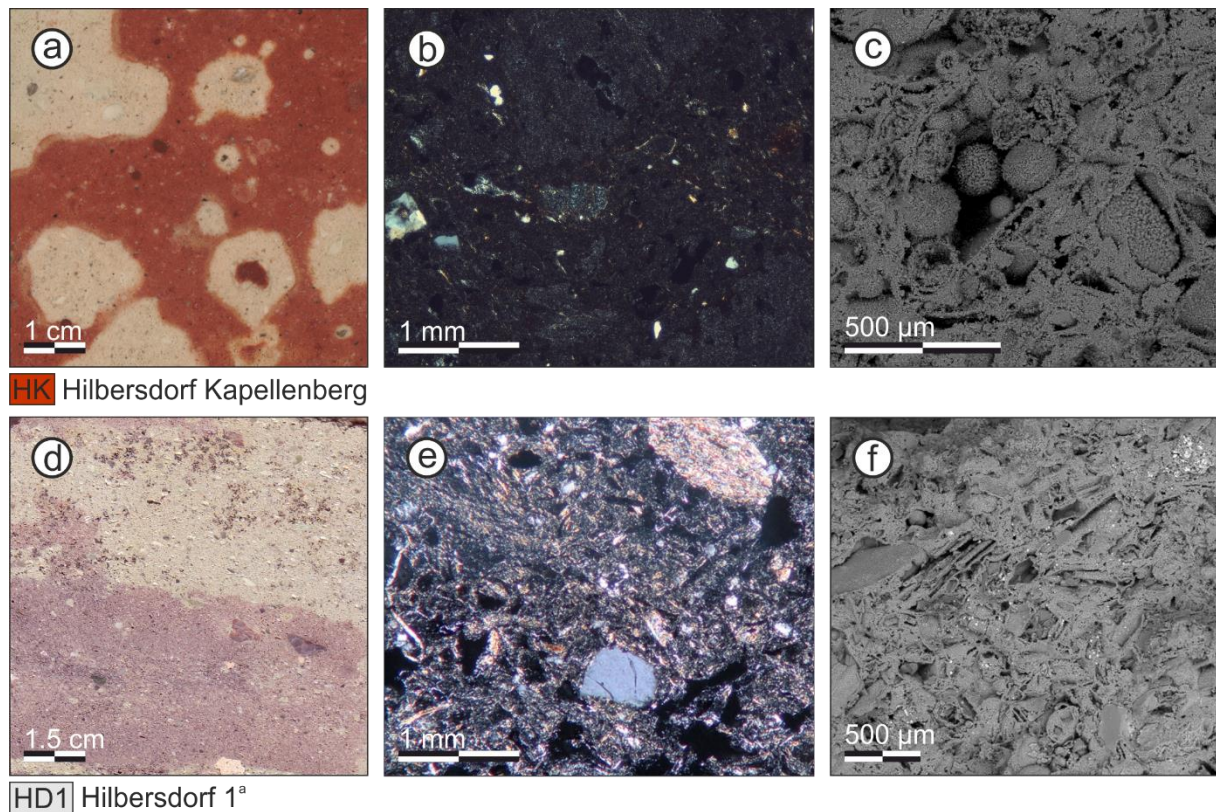


Figure 6.5: Illustration of the investigated varieties of the Hilbersdorf Tuff. **a** Polished section (wet). **d** polished section (dry). **b**, **e** Thin section under polarized light. **c**, **f** SEM photomicrographs <sup>a</sup>(Wedekind et al. 2013)

### 6.4 Petrophysical properties

The petrophysical analyses were performed in all three directions of the rocks. The XY plane is parallel to the bedding and lamination, while the direction perpendicular to the bedding is defined as the Z direction (Fig. 6.6). If no preferred orientation was visible, the directions were set arbitrarily.

## 6 Clay swelling mechanism in tuff stones – case study Hilbersdorf

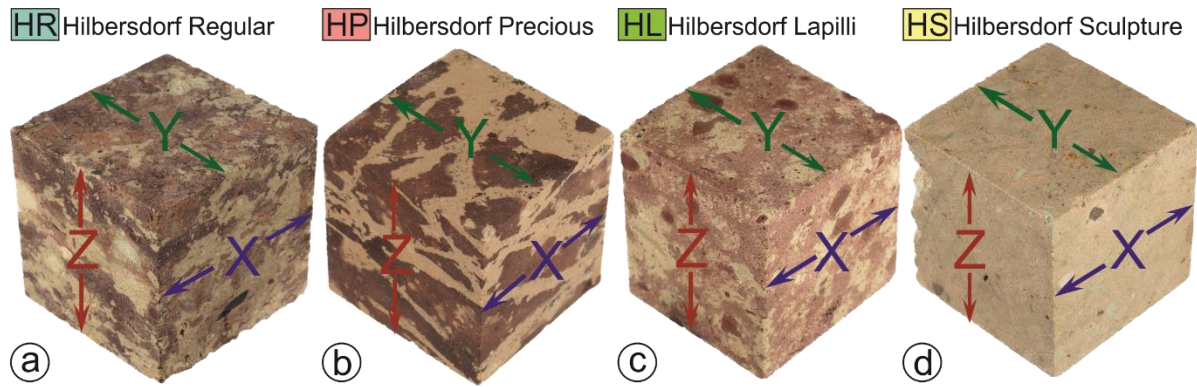


Figure 6.6: Four of the investigated varieties of the Hilbersdorf Tuff illustrating the general texture and their division into the X, Y and Z directions. Elongated clastic material is oriented parallel to possible flow directions and describes the bedding of the tuff (X/Y direction). The direction perpendicular to the bedding is defined as Z direction. **a** Hilbersdorf Regula (HR). **b** Hilbersdorf Precious (HP). **c** Hilbersdorf Lapilli (HL). **d** Hilbersdorf Sculpture (HS)

### 6.4.1 Density

The HR, HP, HL and HD1 show slightly higher matrix densities with  $2.62 \text{ g/cm}^3$  and  $2.63 \text{ g/cm}^3$ , respectively, than HS with  $2.59 \text{ g/cm}^3$  and HK with  $2.57 \text{ g/cm}^3$ . The bulk densities range from  $1.78 \text{ g/cm}^3$  up to  $1.94 \text{ g/cm}^3$  (Table 6.2). HD95 values show both the highest matrix density with  $2.67 \text{ g/cm}^3$  and the lowest bulk density with  $1.78 \text{ g/cm}^3$ .

Table 6.2: Pore space properties, moisture transport and retention properties of the different Hilbersdorf varieties. SSA = specific surface area (via  $\text{N}_2$  adsorption)

Sample	HR	HP	HL	HS	HK	HD 1 <sup>a</sup>	HD 95 <sup>b</sup>
Porosity [vol.%]	25.9	31.6	30.5	30.5	28.0	30.2	32.1
Matrix density [ $\text{g/cm}^3$ ]	2.62	2.62	2.62	2.59	2.57	2.63	2.67
Bulk density [ $\text{g/cm}^3$ ]	1.94	1.79	1.82	1.80	1.85	1.84	1.78
Mean pore radius [ $\mu\text{m}$ ]	0.182	0.110	0.147	0.136	0.202	0.145	0.19 - 0.27
Microporosity [%]	45	65	43	46	46	51	-
SSA [ $\text{m}^2/\text{g}$ ]	8.3	8.9	11.2	13.0	-	-	-
Saturation degree S	0.64	0.55	0.73	0.76	0.64	-	0.65
w value [ $\text{kg/m}^2\text{vh}$ ]							
X	1.15	1.25	2.85	1.66	1.25	1.63	-
Y	1.17	1.32	2.65	1.67	1.50	1.97	-
Z	0.90	1.40	2.62	1.75	1.14	1.75	1.75
Anisotropy [%]	23	10	8	5	24	17	-
$\mu$ value							
X	11.48	10.96	8.51	10.79	10.4	13.83	-
Y	10.42	12.37	9.19	9.63	13.0	12.88	-
Z	11.52	13.90	11.08	9.78	11.9	17.30	12.50
Anisotropy [%]	10	21	23	11	20	26	-
Sorption 95 % RH [wt.%]	1.8	2.4	2.3	2.8	3.7	-	1.8 - 3.0

## 6 Clay swelling mechanism in tuff stones – case study Hilbersdorf

### 6.4.2 Porosity, microporosity, pore radii distribution and specific surface area

The effective porosity of the Hilbersdorf varieties ranges between 25.9 vol.% for HR and 32.1 vol.% for HD95. With 30.2 vol.% and 32.1 vol.%, the values of Wedekind et al. (2013) and Siedel (1995) are close to the effective porosity of 30.5 vol.% for HL and HS (Table 6.2).

The micropores are defined as the pores smaller than 0.1  $\mu\text{m}$ , and the capillary pores range between 0.1 and 1000  $\mu\text{m}$  in size (Klopfer 1985). The amounts of micropores in HR, HS, HL and HK range between 43 and 46 %, while HP shows a much higher amount of 65 % (Table 6.2). HD1 is situated in between these groups with a micropore amount of 51 %. After Ruedrich and Siegesmund (2006), the pore radii distribution of HP can be described as unimodal unequal with an average pore radius of 0.110  $\mu\text{m}$  (Fig. 6.7). HL can also be described with a unimodal unequal pore radii distribution, with a wider peak of pore sizes and an average pore radius of 0.147  $\mu\text{m}$ . HR, HK, HD1 and HS show bimodal unequal distributions, in which HS and HD1 show a dominance of pores around its average pore radius of 0.136 and 0.145  $\mu\text{m}$ , respectively. The average pore radius of 0.182  $\mu\text{m}$  of HR, on the other hand, does not reflect its bimodal distribution with peaks in the micropore and capillary pore range. The same applies to HK, which shows a very similar distribution like HR, while having an average pore radius of 0.202  $\mu\text{m}$ . In general, all varieties show significant amounts of micropores, as well as a second maximum in the capillary range of 1–10  $\mu\text{m}$  (Fig. 6.7). Siedel (1995) observed similar results. HL represents the only variety with a unimodal pore radii distribution around its average radius of 0.147  $\mu\text{m}$ . The specific surface area is low for HR with 8.3 and 8.9  $\text{m}^2/\text{g}$  for HP, while HL and HS show higher values of 11.2 and 13.0  $\text{m}^2/\text{g}$ , respectively.

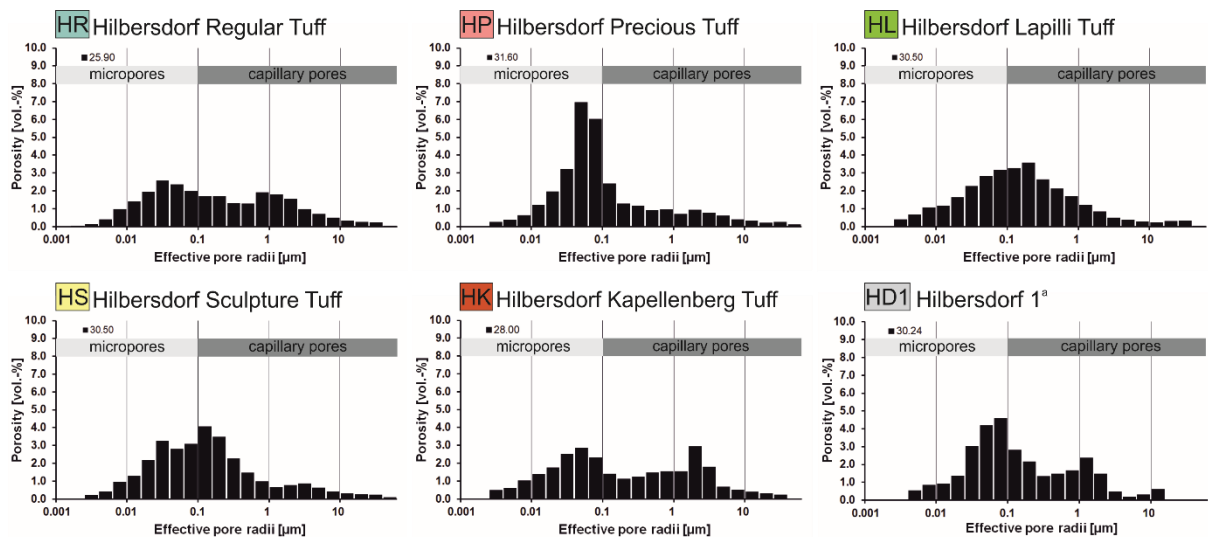


Figure 6.7: Pore radii distribution of the investigated tuffs measured by mercury intrusion porosimetry (MIP) <sup>a</sup>Wedekind et al. (2013)

## 6 Clay swelling mechanism in tuff stones – case study Hilbersdorf

### 6.4.3 Capillary water absorption and water vapor diffusion

The capillary water adsorption coefficient ( $w$ ) of the Hilbersdorf varieties ranges from 0.9 kg/m<sup>2</sup>Vh for HR up to 2.85 kg/m<sup>2</sup>Vh for HL. The average value of 1.75 kg/m<sup>2</sup>Vh from Siedel (1995) and the values of Wedekind et al. (2013) match with the value for HS measured in this study. Two groups can be distinguished. The first group consists of HR, HP and HK, which show lower values and distinct anisotropies of up to 24 % between the different directions. HS, HL and HD1 show higher values and more consistent behavior between the different directions (Table 6.2).

Regarding the water vapor diffusion resistance ( $\mu$ ), the tuffs usually show anisotropic behavior with up to 26 % for HD1, with the highest values in the Z direction. Exceptions are HS and HK with higher values in the X and Y direction, respectively. The minimum value is 8.51 for HL, and the maximum is displayed by HD1 with 17.

### 6.4.4 Hygroscopic water sorption and saturation degree

The sorption values are measured by weighing and are given in percentage of the bulk sample (wt.%). Three groups could be distinguished. HR, HL and HP show lower values of 1.8, 2.3 and 2.4 wt.%, respectively. HS shows a moderate value of 2.8 wt.% and HK represents the variety with the highest sorption value of 3.7 wt.%. The values of Siedel (1995) vary between 1.75 wt.% and slightly over 3 wt.% and therefore cover nearly the whole range of the varieties (Table 6.2).

The saturation coefficient ( $S$ ) describes the amount of the total pore space that is accessible to water adsorption and thus provides a value for the evaluation of the frost resistance (Siegesmund and Dürrast 2011). For HP, HR and HK, the values are at 0.55 and 0.64, respectively. HL and HS show values of 0.73 and 0.76. Therefore, after Hirschwald (1912) HR, HP, HK and HL are rated frost resistant and for HS the frost resistance is uncertain.

### 6.4.5 Tensile strength

The resistance against tensile stresses is an important parameter for all physical weathering processes. The existence and spatial orientation of any foliation or sedimentary layering can highly affect the tensile strength of the rock. Therefore, some rock types can show high anisotropic behavior regarding their tensile strength (TS) (Siegesmund and Dürrast 2011).

The Hilbersdorf varieties can be divided into two groups of lower (HS, HL) and higher TS values (HR, HP, HD1 and HK). Under dry conditions, the values vary between 2.3 MPa for HS and 4.62 MPa for HD1 (Table 6.3). Under water-saturated conditions, the TS values are reduced by up to 55 % and vary between 1.14 MPa for HS and HD1, and 3.1 MPa for HD1. All samples show an anisotropic behavior of up to 27 % (under dry conditions) with highest values in the Z direction. After water saturation, the values of the TS are lowered between 32 and 55 % for all samples, with a reduction of up to 69 % for HD1.

## 6 Clay swelling mechanism in tuff stones – case study Hilbersdorf

Table 6.3: Tensile strength (TS) under dry and water-saturated conditions, as well as the TS reduction in X, Y and Z direction.  
<sup>a</sup>Wedekind et al. (2013)

Sample	HR	HP	HL	HS	HK	HD 1 <sup>a</sup>
<b>Tensile strength dry</b>						
$\beta_{SZ}$ (MPa)						
X	3.63	3.78	2.88	2.30	4.13	3.70
Y	3.74	3.45	2.87	2.69	4.29	-
Z	4.04	4.07	2.93	3.17	3.32	4.62
Anisotropy [%]	10	15	2	27	23	20
<b>Tensile strength wet</b>						
$\beta_{SZ}$ (MPa)						
X	2.00	2.27	-	1.19	2.60	1.14
Y	2.32	2.23	1.35	1.14	-	-
Z	2.41	2.44	1.63	1.33	2.45	3.10
Anisotropy [%]	17	9	17	14	6	63
<b>TS Reduction [%]</b>						
X	45	40	-	48	37	69
Y	38	35	53	58	-	-
Z	40	40	44	58	26	33
∅	41	38	49	55	32	51

### 6.4.6 Moisture expansion

The hydric expansion of the samples varies significantly (Table 6.4). Due to the fact that especially the Hilbersdorf Regular Tuff (HR) displays a very heterogeneous material, hydric expansion was measured at a minimum of twenty samples per direction. Two groups of different anisotropic behavior can be distinguished. The first group shows

medium anisotropic behavior from 24 to 37 % and consists of HD1, HS and HL. The second group shows high anisotropy of 54–75 % and is represented by HK, HR and HP. In general, the tuffs show their highest values perpendicular to the bedding (Z direction). The lowest average values in the Z direction are shown by HP with an expansion of 1.01 mm/m. HR shows the highest average values in the Z direction with 2.24 mm/m. Several horizons of HR can show hydric expansion values of up to 7.47 mm/m (Fig. 6.8). The values of Siedel (1995) show the highest average expansion of 2.79 mm/m but cannot be attributed to a certain direction. The hydric expansion measured by Wedekind et al. (2013) is close to the HR samples of this study, since they mentioned higher expansion in the Z direction of up to 6 mm/m, but did not include the data in their study.

## 6 Clay swelling mechanism in tuff stones – case study Hilbersdorf

Table 6.4: Hydric and thermal expansion of the Hilbersdorf varieties in X, Y and Z direction, as well as the number of salt cycles until weight loss >30 wt.%. <sup>a</sup>Wedekind et al. (2013), <sup>b</sup>Siedel (1995)

Sample	HR	HP	HL	HS	HK	HD 1 <sup>a</sup>	HD 95 <sup>b</sup>
hydric expansion [mm/m]							
X	0.70	0.25	1.27	1.66	0.98	0.47	-
Y	0.57	0.47	1.17	2.04	1.03	0.58	-
Z	2.24	1.01	1.87	2.21	2.13	0.62	2.79
Anisotropie [%]	74	75	37	25	54	24	-
Max	7.47	1.97	2.02	3.75	2.29	-	-
thermal expansion [mm/m]							
X	0.48	0.35	0.35	0.35	-	-	-
Y	0.45	0.37	0.35	0.33	0.30	-	-
Z	0.39	0.35	0.35	0.36	0.43	-	-
Anisotropie [%]	20	6	2	10	32	-	-
Max	0.49	0.39	0.38	0.37	0.60	-	-
Salt cycles	11	21	16	12	15	-	-

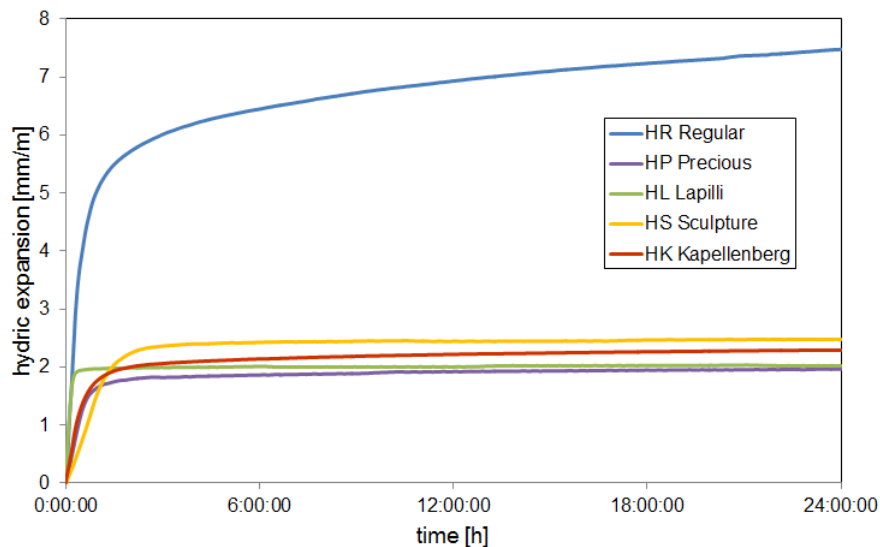


Figure 6.8: Maximum hydric expansion of the different Hilbersdorf varieties

### 6.4.7 Thermal expansion

The thermal expansion of the Hilbersdorf Tuff is around one-tenth of the hydric expansion. While HP, HL and HS show lower values around 0.35 mm/m, HR and HK can expand up to an average of 0.48 mm/m (Table 6.4). An interesting observation is the lack of anisotropic behavior in HP, HL and HS.

### 6.4.8 Salt weathering resistance

Three groups can be distinguished with regard to the salt weathering behavior. Group one consists of HR and HS, which were destroyed after 11 cycles and 12 cycles, respectively. Group two consists of HK and HL with 15 and 16 cycles until destruction. HP lost 30 % of its mass after 21 cycles, but was still intact until cycle 35 and a loss of about 60 % of its mass (Fig. 6.9).



## 6 Clay swelling mechanism in tuff stones – case study Hilbersdorf

The Hilbersdorf varieties also show variable reactions to salt stress in their weathering characteristic. All varieties show an increase in weight within the first cycles and a characteristic loss of clasts especially in the bright, clay rich areas. HR and HK additionally show an intensive loss of material due to break off of material in the marginal areas. HP and HL are characterized by a slow and steady flaking and rounding of the sample cube in which the clasts of HL show a higher resistance than the matrix. HS shows flaking in the marginal areas and the creation of a crack that split the sample in two after 12 cycles.

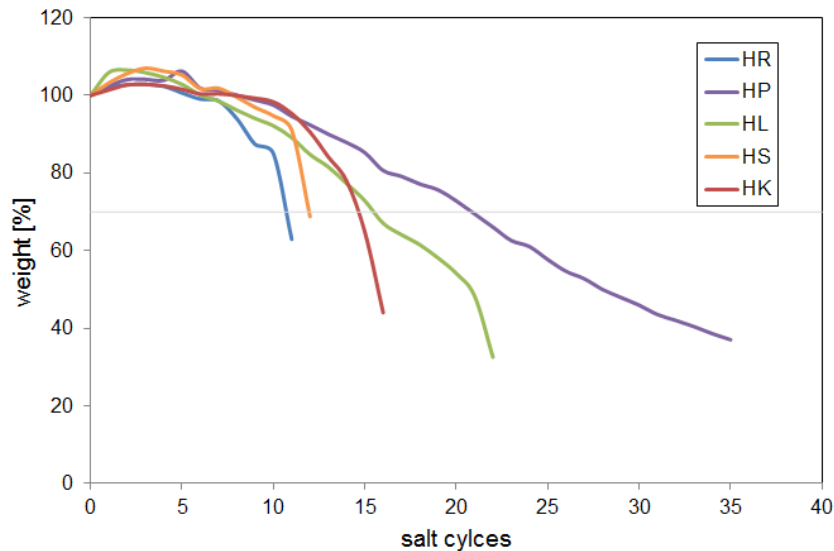


Figure 6.9: Mass weight of the samples as a function of the salt weathering cycles

### 6.5 Swelling experiments

In order to identify the mechanisms active during the hydric expansion, different swelling experiments were performed that proved to be useful for the identification of the primary swelling mode in clay-bearing sandstones (Wangler and Scherer 2008).

To test the mechanism of osmotic swelling, samples of HR and HS were placed in distilled water. When full saturation was reached, the water was syringed out and replaced by a concentrated salt solution of about 1 M. As soon as the salt diffuses into the pore space of the rock, the water of the interlayer space or interparticle space would flow into the pore space to balance the concentration. Thus, an osmotic effect would result in a contraction of the stone. Minor contraction of less than 5 % of the original swelling was observed in both varieties.

In a second experiment, the hydric expansion was measured after the pre-treatment of the samples with various cations. While potassium reduced the swelling of both varieties by up to 31 % (25 % for HR), magnesium and sodium increased the swelling by an average of 7 % and 18 %, respectively (Fig. 6.10).

## 6 Clay swelling mechanism in tuff stones – case study Hilbersdorf

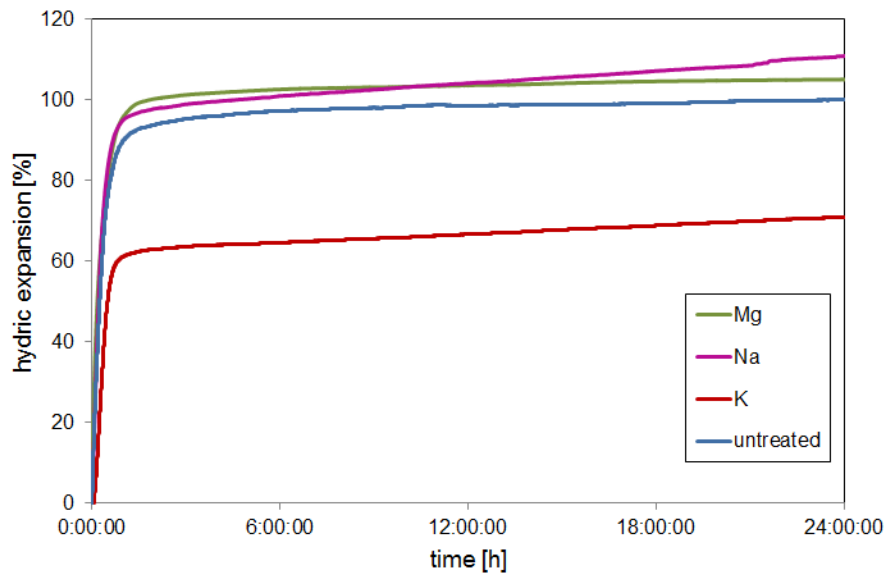


Figure 6.10: Percentual change of the hydric expansion of HS after cationic pre-treatment with Na, Mg and K in comparison to the untreated tuff

### 6.6 Type, location and structure of clay minerals

SEM micrographs show that the content of clay minerals, their location, as well as their structure can vary in the different varieties (Figs. 6.11, 6.12). Only the Hilbersdorf Regular (HR) and Hilbersdorf Precious (HP) contain minerals of the kaolin group (kaolinite and possibly dickite). The kaolin minerals have a pseudo-hexagonal shape and are structured like booklets (see Fig. 6.12a, b). They are mainly situated in the open pores, where single crystals can reach sizes of up to 100  $\mu\text{m}$ . All varieties are characterized by a large amount of muscovite-illite, partly as interstratified minerals with expandable (smectitic) layers (Tab. 6.1, Fig. 6.4). For simplification, these minerals are called illite in the following description. In the reddish areas of the rocks, illite often covers the matrix along with quartz and feldspar crystals and coats the open pores (Fig. 6.11a). In the bright, clay-rich areas of the rock, the coating can appear in different forms. HR and HS show vast amounts of illite coating in form of a cornflake-like microstructure (Fig. 6.11b) or honeycomb structure, where every large crystal is encircled by fine-grained clay material (Fig. 6.11c). The pore coating and filling are characterized by illite aggregates that show ribbon-like filaments on their edges (Fig. 6.11a, b). The structure of some illite aggregates can also be described as fibrous (Fig. 6.11e). HR additionally shows large areas covered by smooth and glossy illite (Fig. 6.11d). In these areas, flaking and detachment of the material in the microscale can often be observed. In an unpublished sample of the Wedekind et al. (2013) study, a well-shaped and pure illite aggregate of nearly 20  $\mu\text{m}$  thickness was observed (Fig. 6.11e). Note that HR and HL are more or less free of swellable clay minerals (Fig. 6.4).

## 6 Clay swelling mechanism in tuff stones – case study Hilbersdorf

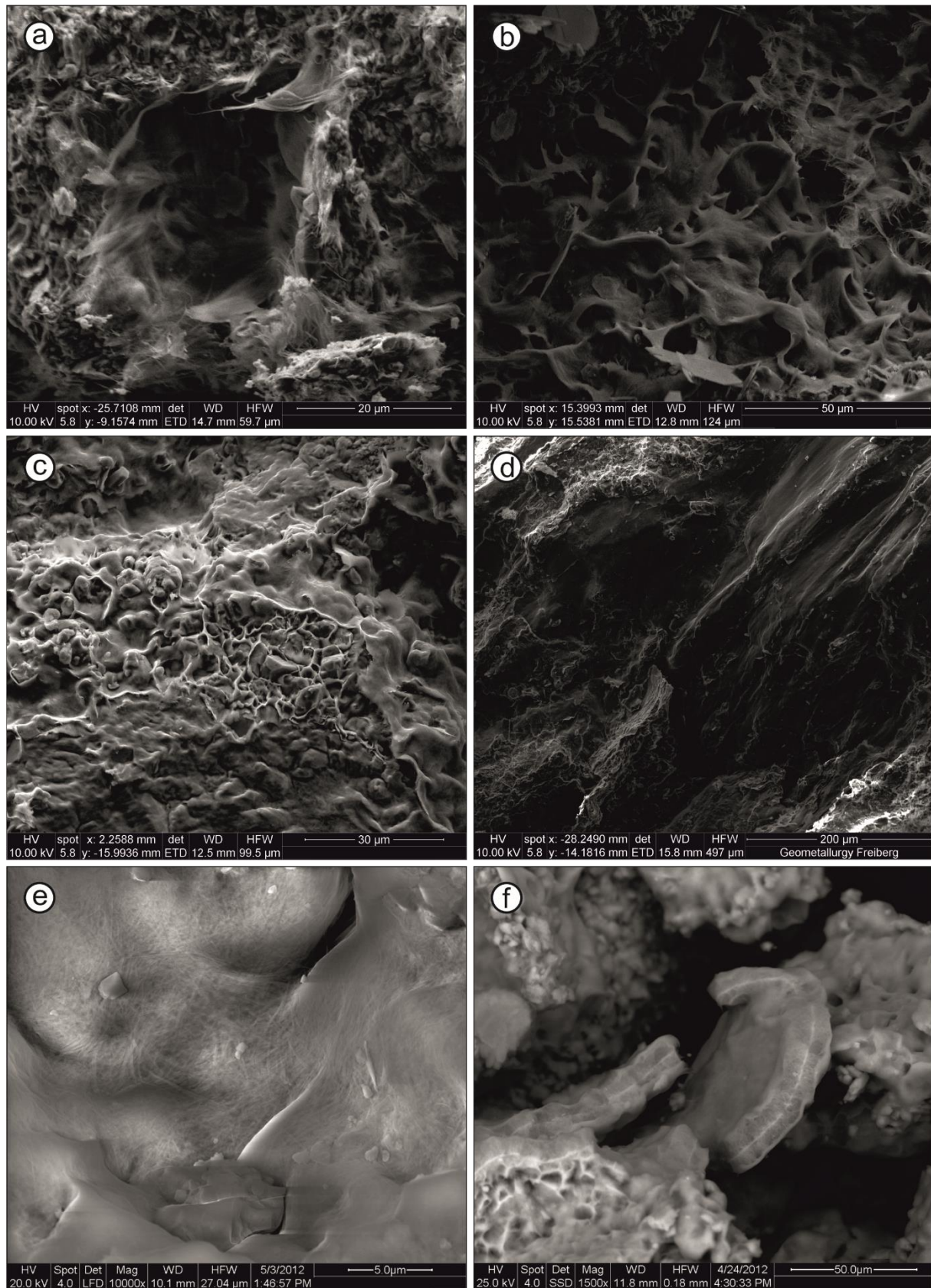


Figure 6.11: Different appearance and location of clay material in SEM photomicrographs. **a** Coating/filling of open pores with illite aggregates that show ribbon-like filaments on their edges (HR). **b** Cornflake microstructure of illites (HR). **c** Honeycomb structure that coats single quartz and feldspar crystals (HR). **d** Smooth and glossy coating of illites with indicated flaking and detachment (HR). **e** Fibrous structure of interwoven illite aggregates (HD1). **f** Well-shaped illite aggregate in the center of the photomicrograph (HD1)

## 6 Clay swelling mechanism in tuff stones – case study Hilbersdorf

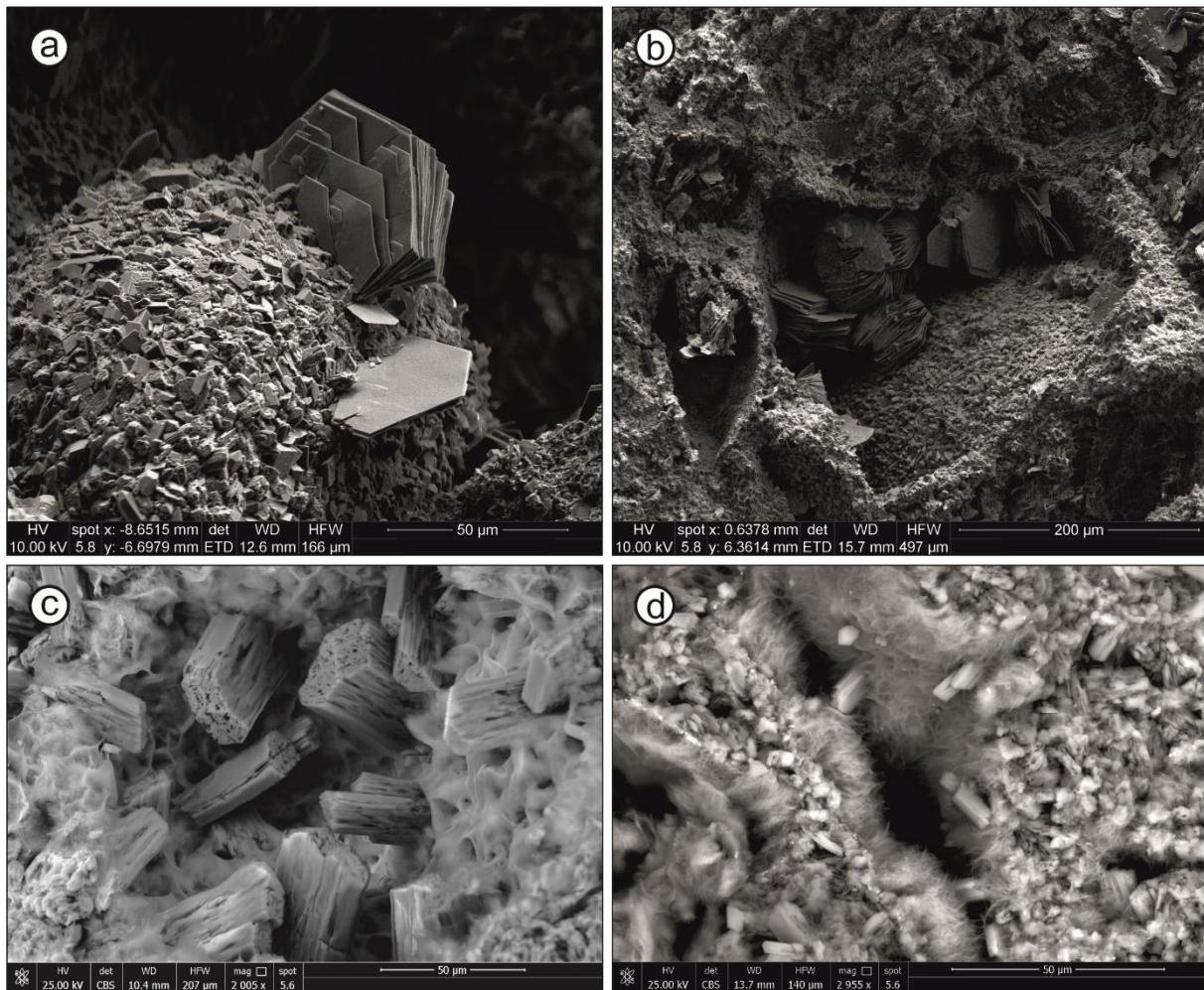


Figure 6.12: SEM photomicrographs of pore filling. **a** Pseudohexagonal kaolinite crystals embedded in a matrix cover of quartz and feldspar (HR). **b** Booklets of kaolinite in an open pore space (HR). **c** Large perforated feldspar crystals in the open pores of HS and HL. **d** Open pore coated with illite aggregates and perforated feldspar crystals extending into the pore space of HS and HL

### 6.7 Discussion

No clear correlation between the hydric expansion and the CEC values can be found for the tuffs of this study (Fig. 6.13). Hilbersdorf Regular (HR) with nearly no swellable clay minerals shows the highest expansion. Therefore, it is proposed that a non-swellable clay associated swelling mechanism has to be at play, potentially disjoining pressure. The tuffs with CEC > 2 meq/100 g show an increasing expansion with increasing CEC.

Comparing the petrographical and petrophysical properties of the Hilbersdorf varieties reveals certain similarities. Since HD95 represents a data compilation of different Hilbersdorf varieties (Siedel 1995), it cannot be directly attributed to a single variety of this study. The range of the determined values, however, pretty much displays the data range of all single investigated varieties of this study and other previous studies.

Hilbersdorf Sculpture (HS), Hilbersdorf Lapilli (HL) and HD1 show a similar geochemical composition as well as the similar type, structure and distribution of clay material in the rock (with exception of the absence of swellable clay minerals in HL and HD1). Pore space properties, mechanical properties and thermal expansion behavior of HS and HL are almost

## 6 Clay swelling mechanism in tuff stones – case study Hilbersdorf

identical (Tables 6.2, 6.3, 6.4). Minor differences can be observed in their capillary water transport property, where HL shows higher values, and in the slightly higher hydric expansion of HS. Although both HS and HL show the highest saturation degrees, their frost resistance has to be questioned due to their observed low weathering resistance.

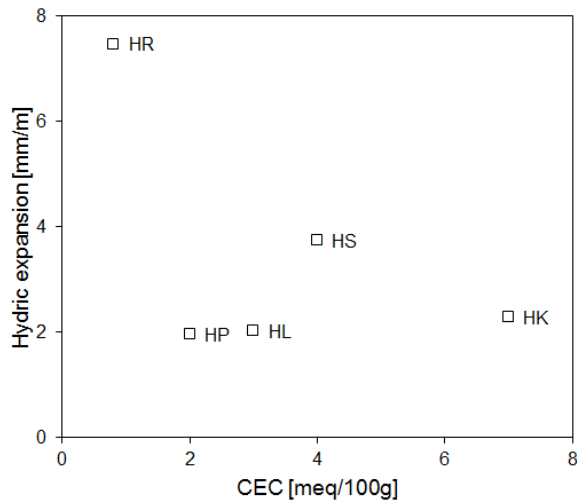


Figure 6.13: Hydric expansion as a function of the CEC value

Hilbersdorf Regular (HR), Hilbersdorf Precious (HP) and Hilbersdorf Kapellenberg (HK) show similar values in their water transport and retention properties, as well as their mechanical properties (Tables 6.2, 6.3). Even though similar trends in their hydric and thermal expansion can be observed, HR and HK show values partly two times higher than those of HP (Tab. 6.4). This cannot exclusively be caused by clay minerals, especially since the XRD on clay fractions revealed that swellable clay minerals are  $\pm$  absent in HR. Even though SEM micrographs of HP proved the presence of interstratified illite–smectite with minor amounts of intracrystalline swellable layers, that are additionally situated in the open pores rather than coating the whole matrix and grain contacts, like in HR (Fig. 6.11b–d), HR barely contains any swellable clay minerals. The question arises why HR with  $\pm$  no swellable clay minerals shows higher hydric expansion. For further understanding, it is worth to take a closer look at the pore space properties. Previous studies from Ruedrich et al. (2011) and Wedekind et al. (2013) indicated that not all moisture-related expansion has to be attributed to the presence and amount of swellable clay minerals. They discussed the possible influence of the disjoining pressure that originates due to interaction of surface forces, which are van der Waals attraction, electrostatic double layer and solvation repulsion, and is controlled by microporosity and moisture films. Contrary to these studies, HP with a higher porosity and a higher amount of micropores shows less hydric and thermal expansion, as well as higher resistance against water vapor diffusion and salt weathering (Tables 6.2, 6.3, 6.4). It has to be noted that the majority of micropores in HP are located around 0.1–0.04  $\mu\text{m}$ , while the peak of micropores in HR is located around 0.025  $\mu\text{m}$ . Additionally, HR is the only Hilbersdorf variety with at least traces of micropores smaller than 2 nm (Fig. 6.7), and therefore, conditions are present where disjoining pressure can play a more significant role in an expansion process (Schult and Shi 1997). Nevertheless, swelling experiments proved that swelling can be partly inhibited in HR with cation exchange. Due to the virtual absence of swellable clay minerals and consequently no possibility of intracrystalline swelling inhibition in HR, another process may have been

## 6 Clay swelling mechanism in tuff stones – case study Hilbersdorf

inhibited and HR has to be considered an exceptional case that cannot be explained with the applied model.

### 6.7.1 Location of clay material

Although swellable clay minerals were barely observed in HR, their location makes them play an important role in the moisture expansion of the rock. Thin sections showed that certain areas like lithoclasts are enriched with clay material in HR and HS, and SEM micrographs show that the clay minerals are situated in crucial parts of the rock fabric, like grain contacts (Fig. 6.11c). Since the clay-rich lithoclasts have the ability to transfer stresses within the rock fabric, the presence of even small amounts of swellable clay minerals can have a large impact on the swelling pressure (Ruedrich et al. 2011). The importance of the location of swellable clay minerals can also be observed in HP. Here, swellable clay minerals coat the pores but do not influence the grain boundaries (Fig. 6.3f). Thus, the transfer of stress within the rock fabric is smaller compared to HS resulting in a lower hydric expansion. This finding illustrates the important role of the location of clay minerals with regard to the weathering resistance of the Hilbersdorf Tuff varieties.

### 6.7.2 Primary mode of swelling

In order to identify the primary cause of the moisture expansion due to clay swelling, the swelling experiments delivered distinct results. Due to the lack of contraction on exposure to a concentrated salt solution, the elimination experiment proved that osmotic swelling has only a minor influence on the clay swelling in these tuffs. The effect of the cationic pre-treatment on the hydric expansion revealed that intracrystalline swelling plays a crucial role for the clay swelling. Wangler and Scherer (2008) discussed the important role of the counterbalancing cation to the swelling process. The fixation of potassium to clay minerals is known and has been well studied. Simulations showed that during hydration the potassium remains close to the negatively charged clay interlayer surface and thus inhibits crystalline swelling (Boek et al. 1995; Chang et al. 1998). Consequently, the reduction of the swelling pressure due to exchange of the counterbalancing cation for potassium is good evidence for the crystalline swelling inhibition.

However, not all moisture expansion can be attributed to swellable clays. Since XRD on separated clay fractions proved almost absence of swellable clay minerals in HR and HL (Tab. 6.1), a third mechanism has to be involved. Wedekind et al. (2013) already considered disjoining pressure to play a role in HD1. With exception of the effective porosity, HR shows similar pore space properties than HD1. The honeycomb and cornflake-like structures of the clay minerals in HR generate smaller pores and a higher microporosity. As mentioned above, HR shows pores smaller than 2 nm, so conditions are present where disjoining pressure can play a more significant role in an expansion process. So even non-swellable clay minerals can passively contribute to the swelling process by their microporosity.

### 6.7.3 Softening properties and weathering resistance as a function of moisture content

Hirschwald (1908) discussed the softening of natural building stones as a decrease in strength upon wetting. The degree of softening can vary for different lithotypes. Siedel (2010) observed a strength reduction of up to 50% in porous sandstones and tuffs. For sandstones, the strength

## 6 Clay swelling mechanism in tuff stones – case study Hilbersdorf

reduction can be correlated with the magnitude of moisture expansion (Morales Demarco et al. 2007; Ruedrich et al. 2011). With the exception of HR, the tuffs of this study show a slight correlation of the hydric expansion with the reduction in tensile strength upon wetting (Fig. 6.14). The outlier of HR may be potentially explained by the fabric of the non-swellable clay minerals in the rock. As mentioned above, SEM micrographs proved an extensive coating of the tuff with non-swellable illites. The illites often possess an interwoven fibrous structure (Fig. 6.11e) that may support its fabric, and therefore give stability to the rock's fabric. These characteristics are known from other fibrous materials that are used for stability purposes in industrial products like polymers and carbon fibers.

The tuffs show a clear correlation of the resistance of water vapor diffusion with the resistance against salt weathering (Fig. 6.14), indicating that tuffs with lower resistance against water transport tend to be less resistant against salt weathering. Since the main transport of salts in building stones happens due to water in any form, it is coherent that the moisture transport properties have a large influence on the weathering behavior due to salt crystallization in tuff stones. These observations match with recent studies regarding salt weathering behavior of tuff rocks (López-Doncel et al. 2016).

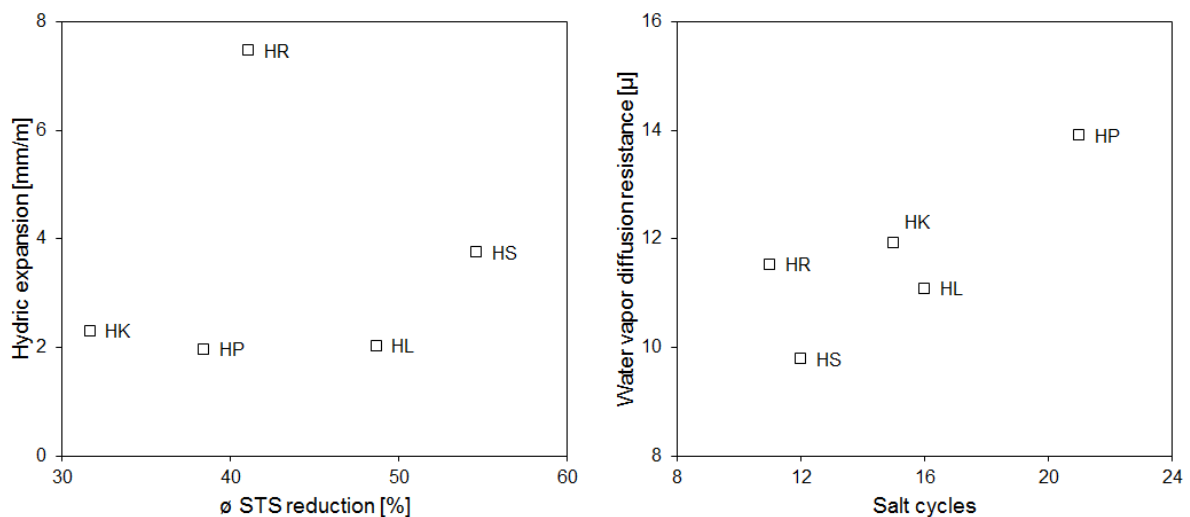


Figure 6.14: Hydric expansion as a function of the tensile Strength (STS) (left) and water vapor diffusion resistance  $\mu$  as a function of the salt weathering resistance (right)

### 6.8 Conclusions

The swelling experiments have shown that intracrystalline swelling is the predominant mechanism for clay swelling in the Hilbersdorf Tuff. The osmotic swelling on the other hand has only a minor influence on the clay swelling. Therefore, with a clay mineral analyses at hand, the swelling experiments proved to be a useful tool to differentiate between these two clay swelling mechanisms in tuff rocks. Another important finding of this study is the importance of the location of the clay minerals in the tuff rock. SEM photomicrographs showed that even small amounts of swellable clay minerals can cause significant expansion of the material if they are located in critical spots in the rock fabric. The disjoining pressure most likely plays a role, but to which extent is still uncertain. New analytical techniques have to be developed to quantify its role in moisture expansion of tuff rocks. As demonstrated on the

## 6 Clay swelling mechanism in tuff stones – case study Hilbersdorf

example of HR and HP, the amount of micropores can allow estimations of their possible impact on the intensity of moisture expansion, but only with a closer examination of the pore classes reliable information can be received regarding their contribution to the swelling process.



# 7 Consolidation of volcanic tuffs

## 7.1 Introduction

Weathering processes cause a progressive deterioration of stone material in our monumental heritage. The delay of this deterioration and the preservation of our cultural heritage for future generations is the primary aim of stone conservation.

Volcanic tuff is a widespread material used in countless heritage monuments worldwide (Fig. 7.1) and considered a problematic stone when it comes to conservation measures. Compared to other popular heritage building stones like marble, sandstone or granite, tuffs usually show higher sensitivity to weathering. The reasons are manifold and often traced back to their diverse depositional environments that cause a strong mineralogical and fabric heterogeneity (Auras and Steindlberger 2005; Steindlberger 2020). The heterogeneous character of the tuffs leads to a wide range of properties and weathering behavior. Increased porosity and capability for water absorption, together with an overall low strength and a frequent occurrence of swelling clays, leading to additional stress due to expansional processes, result in a reduced durability of the material and ultimately to pronounced forms of deterioration (Pötzl et al. 2018a). The deterioration leads to a reduction of strength, progressing from the surface into the core of the stone. Stone consolidation therefore aims to equalize this strength discrepancy and to restore a uniform strength profile, comparable to the sound, unweathered rock (Snethlage and Sterflinger 2011).

Satisfactory consolidation of volcanic tuffs has shown to be a challenging task. Due to their high porosities and unfavorable pore size distributions, as well as their partly high content of swelling clays, there are several criteria for a successful consolidation of volcanic tuffs. Standardized techniques applied on tuffs do often not lead to satisfying results. Instead, special procedures with formulations adjusted to the individual case have to be developed, which is a time consuming and costly endeavor (Steindlberger 2020; Wendler et al. 1996; Wendler 2005).

One reason for the reduced penetration ability of the consolidant can be the blocking of the pore entrance of small pores due to present pore water. Some tuffs have the ability to absorb considerable amounts of water from the air at low relative humidity levels (Yasar 2020). This water can be retained by micropores for a considerable amount of time. The ability to store water may be additionally increased by the presence of clay minerals and zeolites. If, for example a bottleneck passage is filled with water, this water will block the consolidant from migrating further into the pore network of the stone (Wendler 2005; Wendler 2016). If the migration of the consolidant comes to a halt in this location, a part of the water in the bottleneck will be used for the hydrolysis of the consolidant and the bottleneck will be sealed irreversibly. This effect not only has a negative influence on the attempted conservation measure, but also complicates any future treatment.

## 7 Consolidation of volcanic tuffs

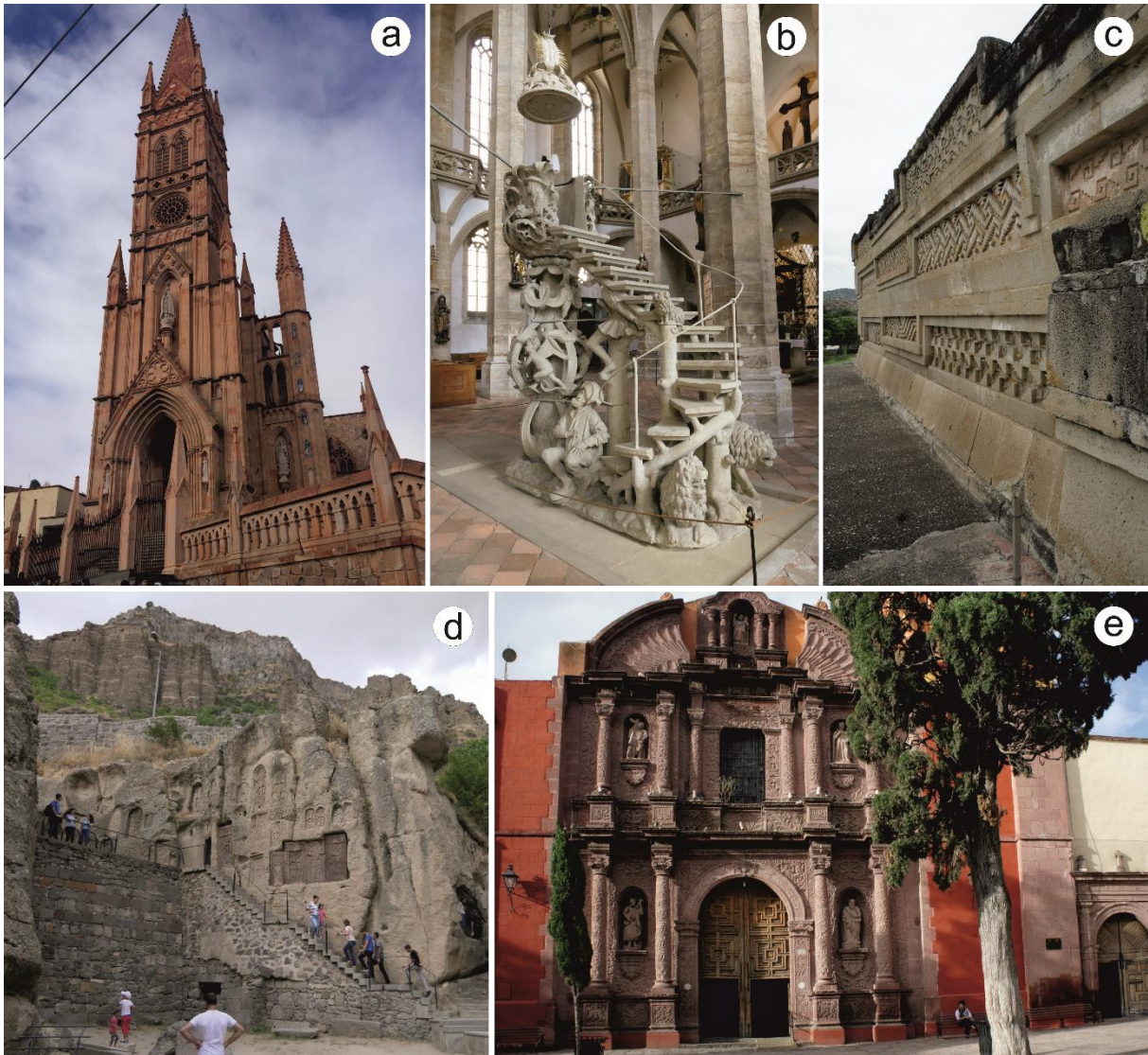


Figure 7.1: Application of different tuff varieties in architectural heritage around the globe. **a** 19<sup>th</sup> century Templo de Fatima in Zacatecas, Mexico; **b** 16<sup>th</sup> century Tulip Pulpit in the Freiberg Cathedral, Germany; **c** 2<sup>nd</sup> century Mitla Pyramids, Mexico; **d** Cross stones at the 4<sup>th</sup> century Geghard Monastery, Armenia; **e** Richly ornamented facade of the 18<sup>th</sup> century Templo de Nuestra Señora de la Salud in San Miguel de Allende, Mexico

Another limiting factor to overcome the problem of small pore entries is the molecular size of the consolidant itself. Many commercial consolidation products contain oligomeric molecule complexes that are too big to penetrate through pore entries that are in the nanometer scale. Highly sophisticated formulations of monomeric stone consolidants, like KSE 300 from Remmers company, contain monomeric molecules as small as 1 – 1.5 nm. This size tends to be sufficiently small to penetrate the pore network of the majority of stone materials. However, some tuffs can contain micropores even smaller than 1 nm (Pötzl et al. 2018b). Especially micropores caused by zeolites, which are abundant in many tuffs, are usually smaller than 2 nm and frequently show ultramicropores <0.7 nm (Korkuna et al. 2006). Even small amounts of these pores can lead to a sealing of bottlenecks and an inhibition of further migration of the consolidant (Wendler 2016).

A further reduction of the molecular size of the consolidants is possible, but only to a certain degree, as the ethoxy group is already the second simplest existing group out of the alcoxy

## 7 Consolidation of volcanic tuffs

groups. A downsizing may be reached by an exchange of the already simple ethoxy groups in the molecules of the silicic acid ester, by the simplest (and smaller) methoxy groups.

Bonding agents (primer) increase the chemical attraction for the consolidant and help the cross-linking of the silica gel with the substrate. The primer is inserted into the stone prior to the consolidation treatment and is meant to coat the pore walls. Because the mineral surface of calcite possesses few hydroxyl groups to which the consolidant can link, this kind of bonding assistance is frequently used for limestones and marble, to secure a better bonding between the consolidant and the substrate (Steinhäuser and Wendler 2004; Wheeler et al. 2000). Although siliceous stones possess more hydroxyl groups for the bonding of the consolidant, Wendler (2005) tested five potential primer components on tuffs, in order to investigate their effect on the efficiency of diluted consolidation products. Tartaric acid was identified to increase the efficiency of the consolidation most effectively, without showing any drawbacks due to the application. Based on these results, tartaric acid was chosen as a primer component for this study.

Finally, the inhibition of moisture expansion in tuffs is frequently a further demand, to minimize the future damage potential within the stones' fabric. The expansion that is mostly controlled by the swelling and shrinking of clay minerals can be reduced by an anti-swelling agent. The anti-swelling agent enters the interlayer of swelling clays and replaces the exchangeable cations, that previously allowed the accumulation of additional water molecules that lead to a swelling process (Wendler et al. 1991). A full inhibition of the expansion is not possible, but the amount of expansion may be significantly reduced.

### 7.2 Materials and methods

#### 7.2.1 Selected tuffs

Nine volcanic tuffs that are used as building stones in Armenia, Germany and Mexico were selected: three (comparably) low porous tuffs labelled as Blanca Pachuca (BP), Blue Sevan (BS) and Loseros (LOS), as well as six moderately to highly porous tuffs Noyemberyan (NB), Cantera Verde (CV), Cantera Rosa (CR), Hoktemberyan Red (HR), Weibern (WB) and San Miguel el Alto (SMA) (in ascending order). Sample specimens of all nine tuffs were prepared as follows and subjected to the same treatment:

- cubes of 65 mm edge length, for porosity, density and water absorption measurements
- cylindric samples of 40 mm height and diameter in X and Z direction (X = parallel, Z = perpendicular to the bedding), which were later cut into 10 mm discs to measure the water vapor diffusion resistance
- cylindric samples of 50 mm height and 15 mm diameter in X and Z direction, for ultrasonic velocity, hydric, thermal and thermo-hydric expansion measurements

The selection of tuffs was based on preliminary analyses of petrographical and petrophysical properties. The goal was to evaluate the different consolidation treatments for a wide range of tuffs with highly varying mineralogy and other properties. The fraction of micropores  $<0.1 \mu\text{m}$  and the hygroscopic water sorption behavior were especially decisive, in order to

## 7 Consolidation of volcanic tuffs

identify potential problems with differential water absorption capabilities of the tuffs. Another decisive reason was the abundance (or absence) of swelling clays that increase hydric expansion. Therefore, most of the selected tuffs show considerable amounts of swelling clays and/or an abundance of zeolites.

### 7.2.2 Conservation materials and application

Two silicic acid esters were selected for the consolidation. The selection of the consolidants based on their molecular size (<2 nm). As described above, micropores that show small pore entrance radii may limit the intake of the consolidant and therefore molecular sizes should be as small as possible.

The first consolidant KSE 300 from Remmers is based on ethyl silicate (tetraethoxysilane TEOS) and frequently used in stone conservation. The commercially available KSE 300 (for the rest of this study labeled as TEOS or KSE) is a single-component system with a gel deposition rate of approximately 30 % and characterized by mainly monomeric molecules of 1 – 1.5 nm size. However, the formulation of KSE 300 can contain up to octamers. Since 2010, the formulation of KSE 300 from Remmers does not longer contain organostannic compounds as catalysts. The currently applied catalyst is company secret (verbal communication from J. Engel (Remmers) 2020).

The second consolidant is a silicic acid ester based on methyl silicate (tetramethoxysilane TMOS) which was used as stone consolidant in the 60s and 70s, before it was withdrawn from the market for its toxicity (Snethlage and Sterflinger 2011). Scherer and Wheeler (2008) point out that of the methoxysilanes that may be used as consolidants, 99 % of the time methyltrimethoxysilane (MTMOS) was applied under the commercial name BRETHANE, rather than TMOS. Main health hazards are the release of methanol during hydrolysis reaction, affecting the eyes and respiratory tract during application (GESTIS Substance Database, URL1). The indoor critical value in the air is 250 ppm, which may be reached easily by an indoor conservation measure. However, outdoor application normally should not have severe consequences. Note that methanol is also called wood spirit, since it is evolved from heated wood, thus one is exposed to it even during sitting around a campfire. The fully cured silica gel, however, is not harmful. TMOS is characterized by monomeric molecules, low viscosity and high reactivity. The methoxy groups bound to the silicon atom in a TMOS molecule are smaller than the ethoxy groups in a TEOS molecule, so that TMOS provides a smaller overall molecular size (<1 nm). In this study TMOS was applied uncatalyzed as a neat monomer.

Following the approach of Wendler (2005), the samples were impregnated with either of the two consolidants on base of ethyl silicate (TEOS  $\triangleq$  KSE 300 from Remmers) or methyl silicate (TMOS from Acros Organics) as well as in combination with a primer component (tartaric acid C<sub>4</sub>H<sub>6</sub>O<sub>4</sub> from Merck) and/or an anti-swelling agent (Antihydro from Remmers). The tartaric acid (labelled as WS for the rest of the study) obtained from Merck was used as a primer component and is meant to line the walls of the pores and enhance the bonding with the consolidant (Wheeler et al. 2000). By increasing the attraction for the consolidant, the efficiency of the absorption, penetration depth and bonding to the substrate is expected to be increased. The anti-swelling agent (Antihydro) obtained from Remmers (aqueous solution of 1,4-Diaminobutane dihydrochloride) is meant to enter the interlayer of swelling clays and

## 7 Consolidation of volcanic tuffs

replace the exchangeable cations (Wendler et al. 1991). The cation exchange ensures a reduced swelling of the stone due to a reduced potential of water accumulation in the interlayer of the clay minerals. However, the Antihydro is an additional chemical that has an impact on the materials petrophysics and should only be applied after adequate laboratory testing (Snethlage and Pfanner 2020). Following this recommendation, the anti-swelling agent was additionally applied to tuffs that lack swelling clays or do not show considerable expansional behavior, in order to identify potential drawbacks. The Antihydro (A) was always applied prior to the consolidation and the primer.

In order to evaluate the impact of all the above mentioned components, nine different combinations of treatment were conducted (see Fig. 7.2):

1) Exclusive treatment with the anti-swelling agent. 2) Exclusive treatment with the consolidant TEOS (KSE) or 3) TMOS. 4) Anti-swelling agent (A) in combination with TEOS (A + KSE) or 5) with TMOS (A + TMOS). 6) Tartaric acid with TEOS (WS + KSE) or 7) TMOS (WS + TMOS). 8) Anti-swelling agent in combination with tartaric acid and TEOS (A + WS + KSE) or 9) with TMOS (A + WS + TMOS). For all combinations, the petrophysical properties and weathering behavior of the rocks were analyzed before and after the treatments, in accordance to the European standards parallel (X direction) and perpendicular (Z direction) to the bedding.

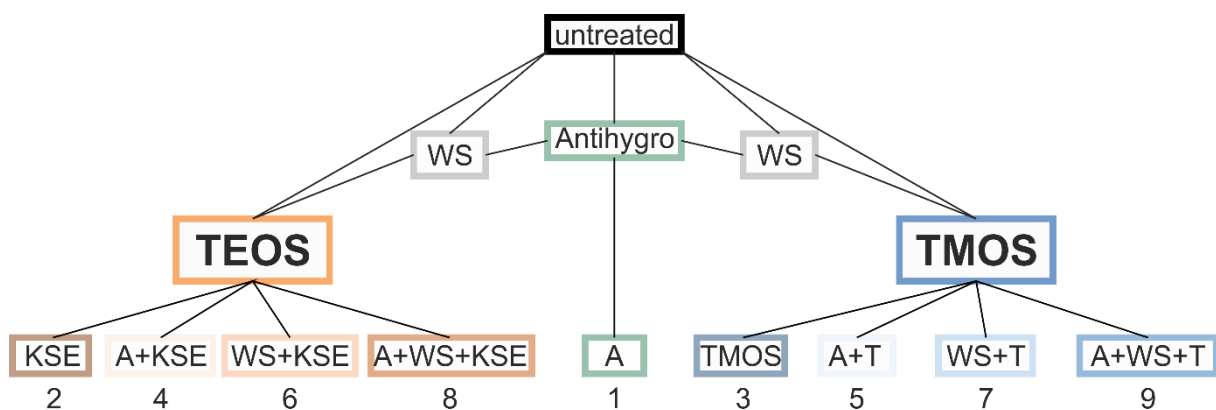


Figure 7.2: Flowchart of the 9 conducted combinational consolidation treatments (bottom row). A = Antihydro (anti-swelling agent); WS = tartaric acid; KSE = TEOS; T = TMOS

The Antihydro and tartaric acid (0.3 %) were applied to oven dried samples (40°C) after an equilibration time of 60 min to room temperature. The samples were placed in a plastic tub and absorbed the chemicals by capillary forces for around 30 min before they were fully immersed for 1 h. After the Antihydro treatment, the samples were dried for several days and subsequently treated with either tartaric acid or a consolidant (consolidation only after being preconditioned). The fully saturated samples treated with tartaric acid were left at room conditions (~23°C and 50 % relative humidity) for 24 hours (40 x 40 mm cylinders for 48 hours, 65 x 65 mm cubes for 72 hours) before they were treated with the consolidant. In this way the moisture content of the specimens should be approximated to the preconditioned samples from the climate chamber (23°C/70 % RH). Untreated specimens and specimens treated with Antihydro were preconditioned in a climate chamber at 23°C and 75 % relative humidity for at least one week, before being treated with the consolidant.

## 7 Consolidation of volcanic tuffs

For the consolidation treatment, the specimens were placed in a solvent resistant plastic tub and first capillary absorbed the solutions for about 20 min under continuous refill of the consolidant, until the samples were fully covered. The samples were left under full immersion for 4-6 hours to ensure full saturation. After the application of the consolidants, the samples were subsequently stored in a 23°C/60 % relative humidity climate for 6 weeks, until full curing of the consolidants. For TMOS consolidated samples, the storage conditions were adjusted to 85 % relative humidity, since it evaporated too quickly when taken out of the consolidation bath and stored at 60 % RH. After 6 weeks of curing, the samples were dried to mass constance (40°C) and subsequently analyzed.

It should be noted that this work has to be seen as a pure laboratory (efficacy) study. The goal was to determine if and how different combinations of conservation materials influence the petrophysical properties of different types of tuffs and to identify whether or not certain treatments may ensure an enhancement of the rock properties. To exclude that any extrinsic factors affect the results of the consolidation treatment, all samples were fully saturated. The consolidants were applied on fresh quarry material, so the conditions for every combination of treatments were roughly the same. However, the partly strong heterogeneity of the individual tuff specimens needs to be taken into account. Especially in the lapilli tuffs, large pumice clasts within the specimens for example may affect the water absorption and other petrophysical properties.

### 7.3 Results

#### 7.3.1 Petrography

Geochemically most of the investigated volcanic tuffs are acid rhyolites or trachytes. Only the Weibern tuff (WB) shows an intermediate trachytic to phonolitic composition. After the classification scheme of Schmid (1981) BP, CR, CV, BS and NB can be defined as crystal tuffs. SMA, and HR, can be classified as vitric tuffs and LOS and WB are lithic tuffs (Tab. 7.1). Regarding the size of pyroclastic fragments (Fisher 1966), the investigated tuffs are mainly defined as ash tuffs and lapilli tuffs. The crystal rich tuffs are mostly ash tuffs and lapilli tuffs with high ash content. Only the vitric tuffs show higher amounts of lapilli and bombs, which are often present in the form of pumice clasts. Most of the tuffs show considerable amounts of swelling clays and/or an abundance of zeolites. The petrographic and petrophysical properties of the tuffs are compiled in Tables 7.1 – 7.3. In the following, the individual tuffs will be presented in short profiles. Supplementary data (e.g. XRF, XRD, thin section and SEM photomicrographs) can be found in Chapter 3.

The Blanca Pachuca (BP) is a fine-grained ash tuff of rhyolitic composition, with a whitish groundmass and plenty of greyish-brownish, rarely reddish and black, phenocrysts that give a slightly speckled appearance (Fig. 7.3), but cannot be identified macroscopically. In thin section, quartz, potassium feldspar, plagioclase, biotite and clay minerals can be observed in a cryptocrystalline matrix. XRD identified swelling clays (smectite) and a range of zeolites (mordenite, heulandite, clinoptilolite). SEM photomicrographs show mordenite needles reaching into the pore space. Overall, the glassy matrix is mainly altered to zeolite and clay. BP has a notably high cation exchange capacity (CEC) of 12 meq/100 g and specific surface

## 7 Consolidation of volcanic tuffs

area (BET) of 17 m<sup>2</sup>/g (Tab. 7.2). The former glass rich BP is, due to alteration processes, now characterized as highly rich in clay and zeolite crystals. After the classification system of Schmid (1981) and Fisher (1966), BP categorizes as crystal-rich ash tuff (Tab. 7.1).

Table 7.1: Petrographic classification of the nine volcanic tuffs

Sample	ID	Origin	Age	Classification LeBas et al. (1986)	Classification Schmidt (1981)	Classification Fisher (1966)
Blanca Pachuca	BP	Mexico	Pliocene	Rhyolite	crystal	ash tuff
Cantera Rosa	CR	Mexico	Oligocene	Rhyolite	crystal	ash-lapilli tuff
Cantera Verde	CV	Mexico	Miocene	Rhyolite	crystal	ash tuff
Blue Sevan	BS	Armenia	Cretaceous	Rhyolite	crystal	ash tuff
Noyemberyan	NB	Armenia	Cretaceous	Rhyolite	crystal	ash tuff
San Miguel el Alto	SMA	Mexico	Paleogene	Rhyolite	vitric	lapilli tuff
Hoktemberyan Red	HR	Armenia	Pleistocene	Trachyte	vitric	lapilli tuff
Loseros	LOS	Mexico	Oligocene	Rhyolite	lithic	ash tuff
Weibern	WB	Germany	Pleistocene	Phonolite	lithic	lapilli tuff

Cantera Rosa (CR) is a massive, crystal rich, rhyolitic tuff of characteristic pinkish color. It macroscopically and microscopically shows a porphyritic texture, with large amounts of quartz and feldspar phenocrysts as well as pumice clasts of up to 20 mm in size, embedded in a fine cryptocrystalline groundmass (Fig. 7.3). In thin section, quartz and sanidine crystals are especially abundant. In SEM photomicrographs the groundmass shows to be altered and devitrified and now consists of a mix of clay, quartz and feldspar crystals. XRD identified the clay minerals as swellable smectite, as well as muscovite/illite and kaolinite. The CEC is accordingly increased (6 meq/100 g). CR is classified as crystal tuff according to Schmid (1981) and as lapilli rich ash tuff according to Fisher (1966).

The Loseros tuff (LOS) is characterized by a greenish laminated appearance (sometimes with a slightly purple or reddish tint), which is mainly caused by sand-sized crystals and rock fragments embedded in a fine, ash-rich matrix (Fig. 7.3). LOS is of rhyolitic composition and classifies as lithic ash tuff (Fisher 1966; Schmid 1981). In thin section, the main components are identified as lithic fragments, as well as quartz, feldspar and plagioclase phenocrysts, whereby the lithic components dominate. LOS contains around 10 % of opaques and shows chloritization phenomena. The individual grains are cemented with a calcareous and argillaceous matrix. XRD identified smectitic mixed-layer minerals and kaolinite. SEM analyses located the clay minerals preferably at grain contacts. LOS shows a moderately high CEC of 5 meq/100 g (Tab. 7.2).

The rhyolitic San Miguel el Alto tuff (SMA) consist of a fine and homogenous vitric groundmass of characteristic pinkish color, in which plenty of elongated pumice clasts are embedded (Fig. 7.3). The pumice clasts are typically in the millimeter to centimeter range and indicate direction. In thin section, SMA shows an abundance of small quartz and feldspar crystals, embedded in a glass rich matrix. XRD identified rare kaolinite-smectite mixed-layer minerals, which are abundant in SEM photomicrographs. Glass shards and biotite are rarely seen. With

## 7 Consolidation of volcanic tuffs

4 meq/100 g, the CEC is moderately high. According to Schmid (1981) and Fisher (1966), SMA can be classified as vitric lapilli tuff.

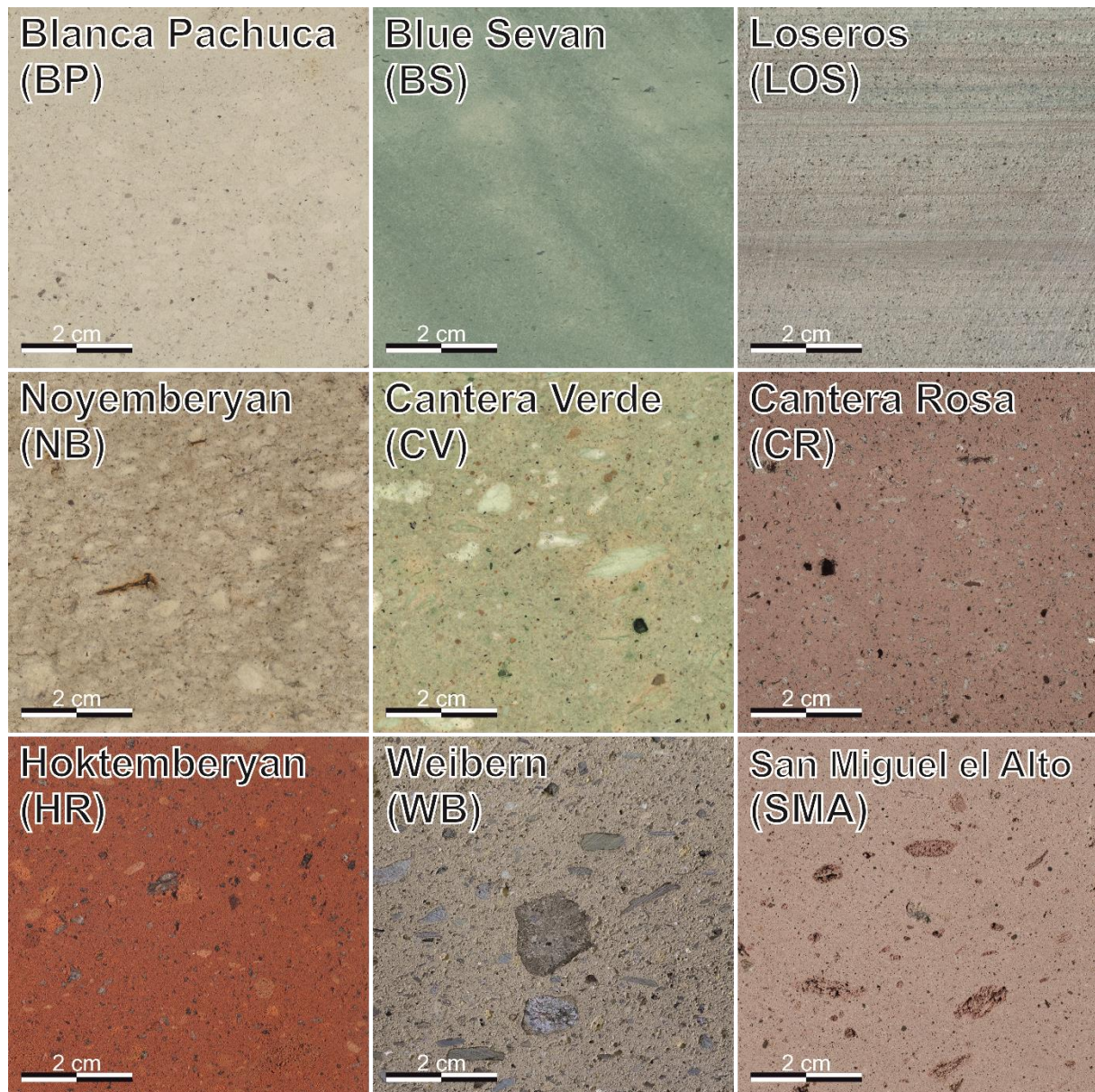


Figure 7.3: Macroscopic photographs of the nine volcanic tuffs from Armenia, Germany and Mexico

Cantera Verde (CV) is a relatively homogenous, light-pistaccio green, crystal-rich ash tuff (according to Fisher (1966) and Schmid (1981)) of rhyolitic composition. Macroscopically noticeable are white clay lenses (Fig. 7.3), which partly disintegrate when in contact with water. CV has a hypocrySTALLINE to cryptocrystalline matrix with vitrophyric texture. The vitreous matrix, however, is strongly altered to zeolite (clinoptilolite and mordenite) and clay minerals (smectite, illite, chlorite and potentially kaolinite). Phenocrysts are often strongly weathered.  $\text{SiO}_2$  is present in the form of cristobalite. Pablo-Galán (1986) describes the formation of zeolites in CV by alkaline diagenesis of rhyolitic glass. SEM photomicrographs reveal very fine-grained zeolites in CV, causing its high specific surface area. They are mainly euhedral mordenite needles and clinoptilolite laths.



## 7 Consolidation of volcanic tuffs

The Blue Sevan (BS) has a characteristic intense green color and is of rhyolitic composition. It is very fine-grained and bottle-green elongated fragments, in the micrometer to millimeter scale, indicate a lamination (Fig. 7.3). In thin section, this tuff shows about 80 % cryptocrystalline matrix, with few mono- and polycrystalline quartz crystals as well as feldspar phenocrysts embedded. The bottle-green fragments often show chloritization processes. In SEM photomicrographs, huge amounts of frayed edge clay minerals are oriented parallel to the bedding. They are located both at grain contacts and mixed into the fine-grained matrix consisting of quartz and feldspar. XRD of separated clay fractions identified them as intracrystalline swellable smectites (Tab. 7.2). Illite/muscovite, kaolinite and analcime, a mineral of the zeolite group, could also be identified. Huge apatites and feldspar relics as well as muscovites can occasionally be observed. The CEC is very high (9 meq/100 g). BS is classified as crystal-rich ash tuff according to Fisher (1966) and Schmid (1981).

Table 7.2: Mineralogical composition (XRD), cation exchange capacity (CEC) [meq/100 g] and specific surface area (SSA) by N<sub>2</sub> adsorption. The x's display the semiquantitative occurrence of the minerals. xxx: dominating mineral phase, xx: major component, x: minor component, ?: trace phase possibly present.

sample	CEC (meq/100 g)		clay minerals						zeolites				other										
	CEC (meq/100 g)	BET (m <sup>2</sup> /g)	smectite	smectitic mixed layer	corrensite	muscovite/illite	chlorite	kaolinite	mordenite	heulandite	clinoptilolite	analcime	glass/amorphous	quartz	tridymite	crystalite	K-feldspar	plagioclase	hematite	augite	hornblende	calcite	
BP	12	17	xx						x	xx	x		xx		x	x	x						
CR	6	5	xx		x		x						xx			x	x						
LOS	5	12		xxx				x					x			x	x					x	
SMA	4	7		xx									xx	x		x	xx						
CV	6	26	x			x	x	?	x	xx						xx	xx						
BS	9	8		xx		x		x				x					x						
HR	1	1				?							xx	x		xx		x					
NB	9	3		x		x			x				x			x				x			x
WB	5	14				x						xx	x			xx	x						x

The Hoktemberyan Red (HR) has a striking brick-red color and chemically classifies as trachyte. In its glass rich ground mass, huge amounts of elongated white feldspar phenocrysts and glass particles are embedded and give a slightly speckled appearance (Fig. 7.3). Black and red elongated pumice at the millimeter to centimeter scale, are embedded in the groundmass and indicate an orientation. In thin section, HR shows feldspar and amphibole phenocrysts embedded in a high amount of glassy matrix (~75 %), with high amounts of iron oxides. Volcanic lithoclasts and opaque minerals each make about 5 % of the sample. In SEM photomicrographs, the difference in porosity between matrix and clasts is striking. Huge parts of these consist of amorphous glass and especially in the matrix area, tiny pores are present. Rarely clay minerals with characteristic frayed edges in the pores of the glassy matrix are observed. HR shows a low CEC (1.2 meq/100 g). HR is classified as vitric lapilli tuff (Fisher 1966; Schmid 1981).

## 7 Consolidation of volcanic tuffs

The Noyemberyan tuff (NB) is a massive, white to slightly greenish tuff of rhyolitic composition, which shows a weak lamination in form of white and grey elongated lithic fragments (Fig. 7.3). Many of the grey lithic fragments are framed by slightly orange to reddish margins. Macroscopic, NB appears to be a fine-grained tuff. Only in exceptional cases the lithic fragments reach sizes up to one centimeter. Thin section images confirm the large amounts of fine matrix groundmass (70 %). The remaining 30 % of the rock consist of partly large angular and zoned plagioclase crystals as well as small, rounded quartz fragments. SEM photomicrographs identify huge amounts of fibrous mordenite clusters and frayed edge clay minerals. Calcites and muscovites can reach dimensions up to 300  $\mu\text{m}$ . Rarely apatite can be observed. Huge amounts of mordenite, a mineral of the zeolite group, and intracrystalline swellable smectitic layers in an illite–smectite mixed layer mineral were identified by XRD on separated clay fractions and confirm a moderate CEC of 3.1 meq/100 g. The classification system after Schmid (1981) and Fisher (1966) categorize NB as crystal-rich ash tuff.

The Weibern tuff (WB) is of trachytic to phonolitic composition. In the literature, the reported composition of WB is usually phonolitic (Egloffstein 1998; Poschlod 1990; Stück et al. 2008). It has a characteristic fine-grained, yellowish to brownish groundmass, in which plenty of partly elongated volcanic and sedimentary clasts are embedded (Fig. 7.3). Beside basalt, chert and sandstone clasts on the centimeter scale, yellowish pumice clasts of few millimeter size are abundant. Quartz, feldspar, leucite, calcite, hornblende and biotite could be identified in thin section. Some opaque minerals could not be identified. In thin section, also the high amount of lithics is striking (~40 %). Other authors report far less lithic components and higher amounts of vitric groundmass (Egloffstein 1998; Stück et al. 2008; Wedekind et al. 2013). These authors did also report significantly smaller sizes for the embedded rock fragments. SEM analyses were not conducted on WB. However, XRD analyses identified an abundance of zeolite material (analcime) and potential smectitic mixed-layer minerals, which points to the fact that the vitric groundmass of the tuff is already altered, like reported by van Hees et al. (2003). The CEC is moderately high (5meq/100 g). WB can be classified as lithic lapilli tuff according to Schmid (1981) and Fisher (1966). The boundary, however, is fluid, since the cryptocrystalline groundmass was not determined any further by SEM, it as well may not be altered to zeolite yet and therefore classify as vitric tuff.

### 7.3.2 Quantitative absorption of TEOS and TMOS

The quantitative absorption of the consolidants was indirectly determined by dry weight measurements of the cylindrical samples (50 mm length, 15 mm diameter) before and after the treatment. The weight measurements were conducted after 6 weeks of storage at 23°C/60 % RH (85 % RH for TMOS), for full curing of the consolidants. After 6 weeks the samples were dried in an oven at 40°C until constant mass was achieved and subsequently equilibrated at room temperature for one hour. Figure 7.4 displays the respective increase in weight percentage of each sample.

The consolidation with TMOS in any combination lead to a significant higher weight increase than TEOS, indicating a general stronger absorption and gel deposition rate of TMOS. Only in HR the application of TEOS with Antihygro pretreatment (A + KSE) lead to a higher absorption. The difference between both consolidants is especially striking for the comparatively low

## 7 Consolidation of volcanic tuffs

porous tuffs with a high fraction of micropores, like BP, LOS, CV and NB. The combination of TMOS with Antihydro (A + T) turned out to be most effective. The application of TEOS shows the strongest increase in combination with tartaric acid (WS + KSE/ A + WS + KSE) for most tuffs.

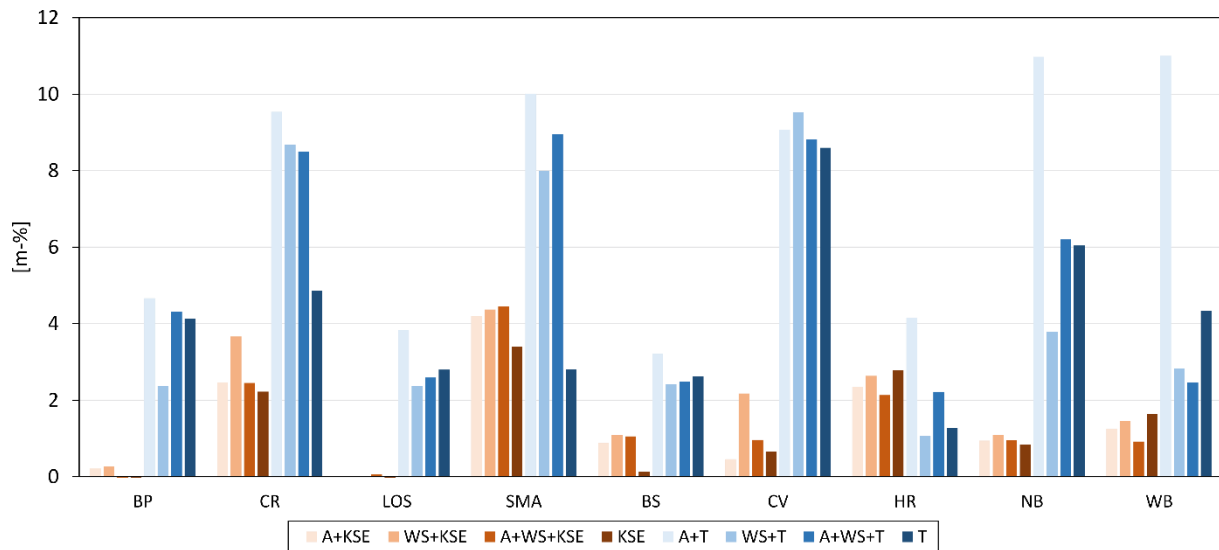


Figure 7.4: Quantitative absorption of the consolidants by dry weight change of the sample before and after the treatment

The extremely low absorption of TEOS by BP and LOS may represent an analytical artifact from their specific pore space characteristics, which regulate the water absorption of the stone. Both tuffs contain considerable amounts of swelling clays and/or zeolites, causing a distinct occurrence of nanopores (Tab. 7.2, Tab. 7.3) that lead to a high hygroscopic water sorption potential already at low humidities. A possible interpretation would be that BP and LOS already absorb considerable amounts of moisture from the ambient humidity during the one hour temperature equilibration outside the oven. In doing so, their subsequently determined dry weight before the treatment would be increased and an absorption of the consolidant in terms of weight difference before and after accordingly reduced.

### 7.3.3 Aesthetic changes

If possible, the visual appearance of the tuffs should not be changed through a consolidation treatment. A darkening of the stone is, however, a common side effect of many consolidation measures and may diminish over time (Nishiura 1987; Wheeler and Newman 1994). If that is not the case, the consolidation product may be considered inappropriate (Snethlage and Sterflinger 2011).

In this study both consolidants cause different aesthetic changes. The application of TEOS, especially in combination with Antihydro, leads to partial darkening of the highly porous tuffs. The effect is most striking in WB, SMA and CR (Fig. 7.5). TMOS causes a partial darkening of all tuffs. Compared to TEOS the effect is less intense on the highly porous tuffs. However, the combination of TMOS with anti-swelling agent and tartaric acid (A + T / A + WS + T) leads to a glossy appearance on the surface of BP, CV and CR (Fig. 7.6). The glossy appearance may indicate that the moisture content during the application was too high, so that the silica gel already precipitates at the surface of the specimen (Snethlage and Sterflinger 2011). The humidity conditions during the application of TMOS (75 % RH preconditioning; 85 % RH

## 7 Consolidation of volcanic tuffs

storage), in combination with the Antihygro, on the low porous tuffs BP, CV and CR consequently have to be evaluated as inappropriate.

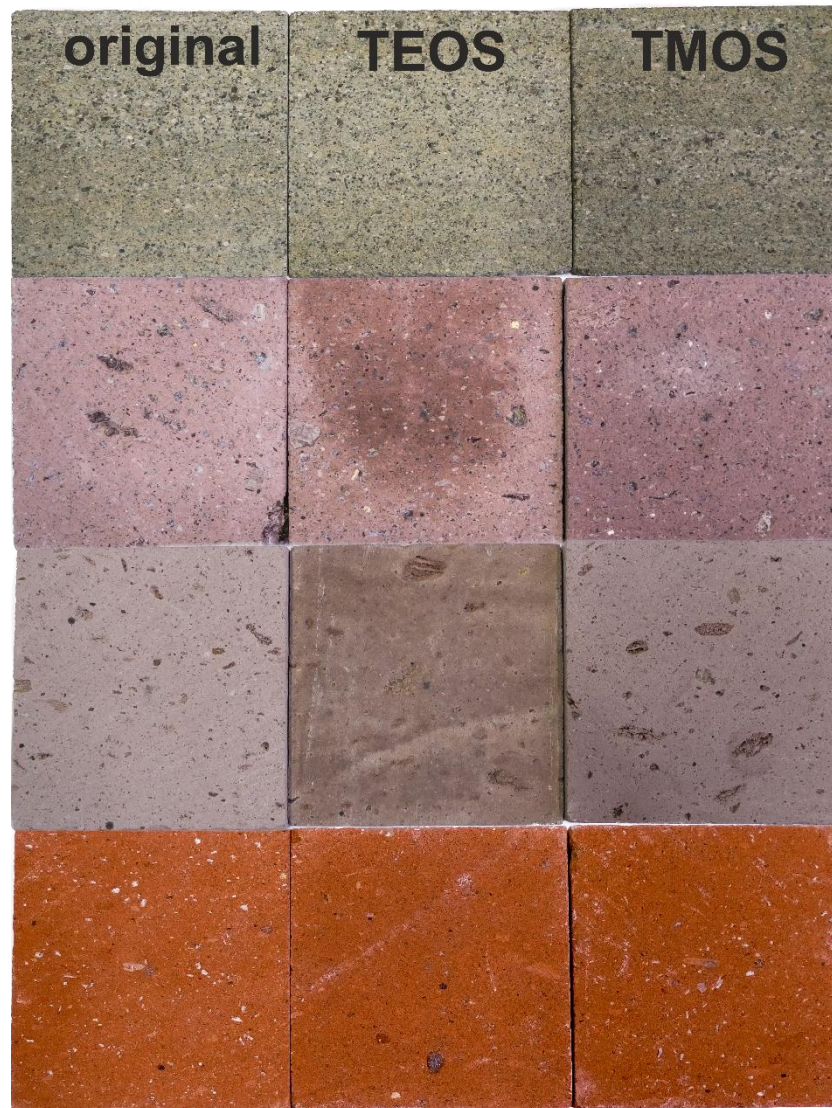


Figure 7.5: Comparison of visual appearance of untreated (left row) sample cubes (65 mm edge length) with cubes treated with TEOS (middle row) and TMOS (right row). Examples of LOS, CR, SMA and HR (from top to bottom)

Another unfavorable side effect is the occurrence of salt efflorescence on the highly porous SMA, HR and WB after treatment with Antihygro (Fig. 7.6). These salts do not only have an unpleasant aesthetic effect, but also influence the petrophysical properties of the tuffs, as will be seen in the following sections. Note, that the samples were not desalinated before the consolidation treatment. Since none of these three tuffs did show significant hydric expansion in an untreated condition, the treatment with Antihygro was not necessary in the first place. As the Antihygro could not interact with any clay minerals, it potentially led to an excessive supply of salt that migrated to the surface. This once more underlines the importance of constant benefit-risk assessment prior to an intervention.

## 7 Consolidation of volcanic tuffs

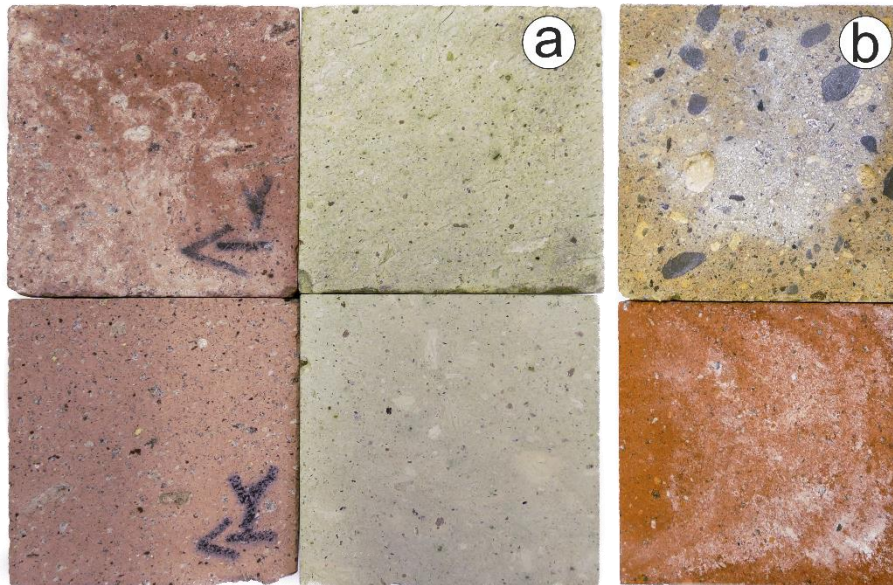


Figure 7.6: a Glossy appearance of CR and CV (top) compared to the untreated sample (bottom). b Salt efflorescence as a result of the treatment with Antihygro in WB (top) and HR (bottom). Sample cubes of 65 mm edge length

### 7.3.4 Modification of petrophysical properties

The consolidation treatments modified properties like pore space properties and water transport mechanisms and therefore the strength and durability to varying degrees (Tab. 7.3). A comparison of the petrophysical properties and expansional behavior before and after the treatment for each individual tuff can be found in Tab. A.2 – 10 in the appendix. For the simultaneous visualization of the data of all nine tuff samples with all nine combinations of treatments at once, scatter and line plots were used. The lines, however, do not imply a relation between the individual points. Histograms, displaying the percentual changes due to the consolidation treatments can be found in the appendix (Figs. A.4 – A.10).

#### 7.3.4.1 Modification of pore space properties

##### *Porosity*

The deposition of the consolidant in the pore space inevitably leads to a reduction of the effective porosity. The reduction takes place to varying degrees in the different types of tuff and appears especially extreme for the less porous tuffs. BP, BS and LOS are characterized by moderate porosities of 15 – 17 vol.%. The other tuffs show significantly higher porosities between 26 and 41 vol.%. With one exception (TEOS only on BS) all treatments successfully decreased the porosity of the stones (Fig. 7.7). For TEOS the treatment in combination with the tartaric acid (WS + KSE/ A + WS + KSE) was most efficient, while the treatment of TMOS showed the strongest effects in combination with the Antihygro or when applied solely (TMOS/ A + T). Substantial reduction of the porosity of NB was only achieved by consolidation with TMOS (especially A + T). In general, TEOS showed to be slightly more effective on highly porous tuffs, while TMOS showed more pronounced changes for tuffs with lower porosity. Some extreme porosity reductions between 60 – 80 % were achieved by TMOS treatment on BP, BS and LOS. However, these strong reductions may be owed to the sealing of the pore channels by the silica gel and the creation of an inaccessible porosity.

## 7 Consolidation of volcanic tuffs

Table 7.3: Summary of the technical parameter of the untreated volcanic tuffs. X = parallel to the bedding, Z = perpendicular to the bedding. SSA = specific surface area, CEC = cation exchange capacity,  $\alpha$  = coefficient of linear thermal expansion

Sample ID	BP	CR	LOS	SMA	BS	CV	HR	NB	WB
Porosity [vol%]	14.9	31.1	16.8	40.8	14.9	29.5	33.1	25.7	36.9
Bulk density [g/cm <sup>3</sup> ]	1.85	1.78	2.07	1.52	2.06	1.54	1.62	1.73	1.51
Matrix density [g/cm <sup>3</sup> ]	2.17	2.58	2.49	2.57	2.42	2.18	2.43	2.34	2.40
Water absorption vac. [wt%]	8	18	8	27	7	19	20	15	24
Water absorption atm. [wt%]	7	14	7	17	6	16	15	13	20
Saturation coefficient S	0.86	0.77	0.81	0.65	0.83	0.85	0.75	0.87	0.84
Micropores [%]	79	18	85	10	90	88	4	37	14
Capillary pores [%]	21	82	15	90	10	12	96	63	86
Mean pore radius [ $\mu$ m]	0.05	0.52	0.04	1.50	0.03	0.04	3.93	0.14	0.51
SSA via BET [m <sup>2</sup> /g]	17	5	12	7	8.0	26	1.2	3.1	
SSA via MIP [m <sup>2</sup> /g]	9.7	5.1	9.6	4.7	4.0	20.8	1.8	6.5	9.7
CEC [meq/100g]	12	6	5	4	8.9	6	1.0	9.2	
w-value [kg/m <sup>2</sup> v/h]									
X	0.8	9.4	0.8	7.3	0.8	2.8	45.1	3.9	14.9
Z	0.8	7.1	0.7	4.7	0.5	2.6	31.0	3.8	14.2
$\mu$ -value									
X	11.9	7.5	27.9	7.4	14.4	9.2	8.1	14.4	9.1
Z	11.1	8.4	13.4	8.1	14.2	10.1	9.7	14.5	9.1
Sorption 95% RH [wt%]	4.5	2.6	2.9	1.2	2.9	7.9	0.1	3.5	3.2
$\phi$ hydric exp. [mm/m]									
X	0.71	0.10	0.58	0.07	0.35	1.39	-0.07	0.67	0.56
Z	0.96	0.24	1.22	0.23	1.57	1.68	-0.13	0.76	0.65
MAX	1.14	0.29	1.78	0.34	2.52	2.01	-0.16	0.97	0.66
$\phi \alpha$ [ $10^{-6} K^{-1}$ ] <b>dry</b>									
X	13.4	8.5	9.8	8.8	8.3	10.9	6.3	8.4	5.9
Z	13.4	8.6	11.7	9.4	10.2	10.6	7.0	7.5	6.8
resid. strain $\epsilon$ X [mm/m]	0.16	-0.03	-0.03	0	0.05	-0.45	-0.01	0.05	0.05
resid. strain $\epsilon$ Z [mm/m]	0.17	-0.02	0.05	2E-05	0.08	-0.36	-0.005	0.07	0.07
$\phi \alpha$ [ $10^{-6} K^{-1}$ ] <b>wet</b>									
X	23.6	9.5	12.9	10.7	14.1	47.2	8.5	27.0	13.9
Z	24.2	9.7	32.1	12.0	27.1	50.7	7.2	26.7	18.7
resid. strain $\epsilon$ X [mm/m]	-0.08	0.04	-0.01	0.07	-0.16	-0.05	-0.08	0.13	0.06
resid. strain $\epsilon$ Z [mm/m]	-0.10	0.04	-0.74	-0.03	-0.51	-0.21	-0.005	0.07	0.07
P-wave velocity [km/s]									
X	3.3	2.8	3.7	2.7	3.9	2.7	2.9	3.1	2.5
Z	3.2	2.6	2.8	2.3	3.1	2.6	2.3	3.2	2.5
Youngs's Modulus [GPa]									
X	20	14	28	11	31	11	14	17	9
Z	19	12	16	8	20	10	9	18	9

## 7 Consolidation of volcanic tuffs

### Pore radius

Tuffs with a high share of micropores proved to be especially susceptible to weathering (Pötzl et al. 2018b, compare Chapter 4) and because micropores ( $<0.1 \mu\text{m}$ ) have a strong influence on the drying behavior of rocks, a reduction of micropores is highly desirable. The fraction of micropores in BP, LOS, BS and CV (79 – 90 %) is significantly higher than in the other tuffs ( $<37\%$ ) (Tab. A.2 – 10 in the appendix). The deposition of the consolidant in the pore space does visibly change the fraction of micropores and thus the pore size distribution of the tuffs to varying degrees, and depending on the applied consolidant, in opposite directions. While treatment with TEOS generally decreases the share of micropores and thus increases the mean pore radii (with the exception of HR), the application of TMOS in any form usually increases the fraction of micropores and decreases the mean pore radii. For an overview the general trends are displayed in Figure 7.7, but the effect of the different treatments on the pore size distributions become more apparent, when looking at the pore size histograms of the individual tuffs (Figs. A.1 – 3 in the appendix).

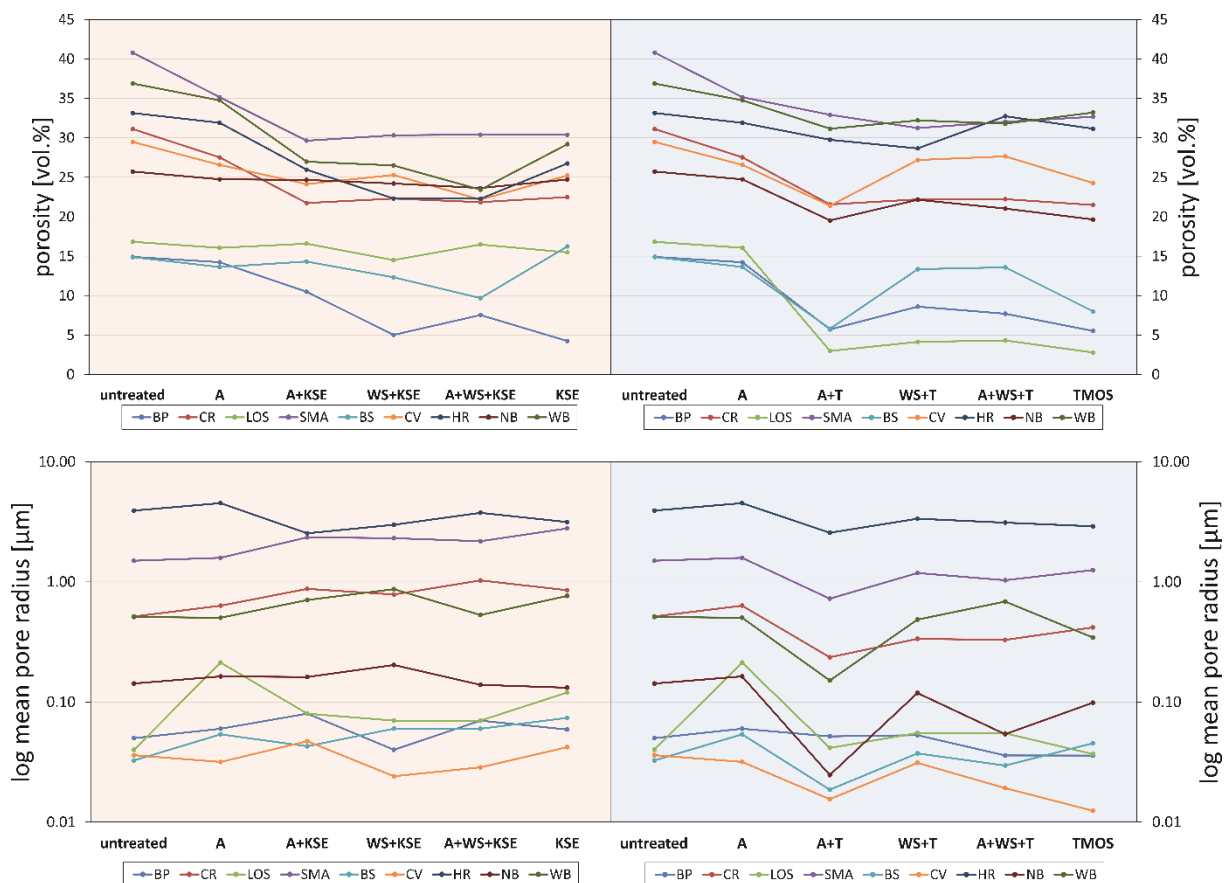


Figure 7.7: Modification of the effective porosity and mean pore radii due to the consolidation treatments. Left) TEOS, right) TMOS. Due to the wide range of values, the mean pore radii are displayed on a logarithmic scale

The most striking observation in nearly all consolidation treatments is the shift of the most occurring pore class in opposite directions, depending on the applied consolidant. These shifts are especially striking in low to moderately porous tuffs, like BP, BS, LOS, CV and NB, and most intense when consolidated with TMOS. With the exception of CV pretreated with tartaric acid, the consolidation with TEOS results in a peak shift of one or two pore classes towards larger pores (Fig. 7.8; please find the figures for the other tuffs in the appendix). The intensity of the

## 7 Consolidation of volcanic tuffs

shift, however, does not seem to strongly differ by a combinational treatment with tartaric acid or anti-swelling agent. Treatments with TEOS do not result in a significant redistribution of pore classes.

In contrast, tuffs consolidated with TMOS in any combinational treatment experience a strong shift towards smaller pores and in doing so, a partly strong redistribution of the occupied pore classes. The shift is not only happening on the scale of one or two classes, like observed in samples treated with TEOS, but rather up to six or seven pore classes (e.g. CV). A common outcome is a highly increased fraction of micropores on the single-digit nanometer scale, which in turn correlates with an increased specific surface area (SSA) that is subsequently available for additional adsorption processes and chemical interaction (see Tab. A.2 – 10 in the appendix). Figure 7.9 shows clear trends of decreasing SSA due to TEOS treatment and partly strong increase of SSA due to the consolidation with TMOS. Especially the combination of TMOS with Antihydro (A + T/ A + WS + T) leads to some extreme doubling, tripling or even quadrupling of the SSA.

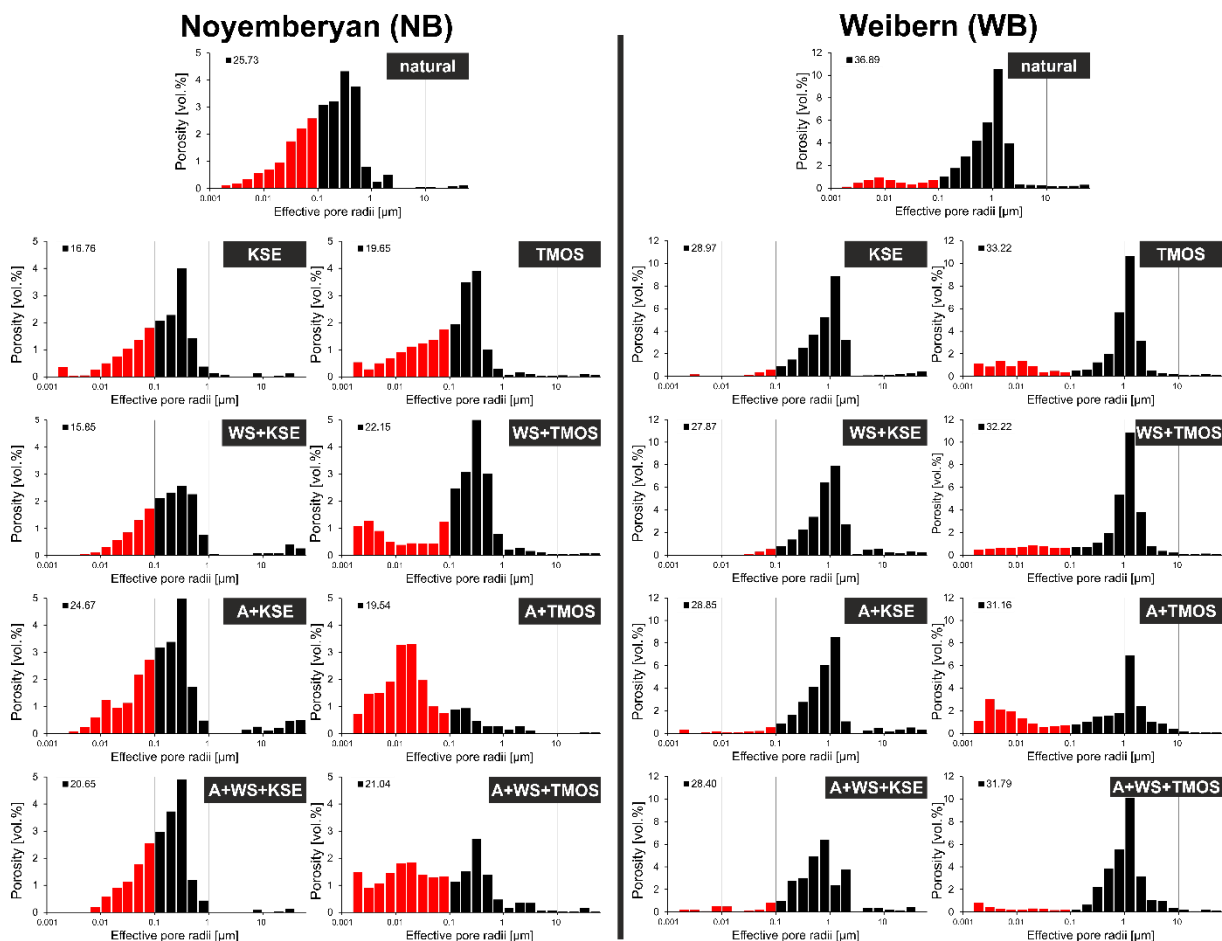


Figure 7.8: Modification of the pore radii characteristics of NB and WB due to the consolidation treatments. Left row) TEOS, right row) TMOS; red = micropores, black = capillary pores

In some cases, the redistribution of the pore size changes the whole pore character of the tuff. According to the pore radii distribution type model of Ruedrich and Siegesmund (2006), SMA and HR are characterized as unimodal equal pore radii type (Type A), BP and NB are characterized as unimodal unequal pore radii type (Type B) and the rest is characterized as bimodal pore radii type (Type C). In Figure 7.8 (and Fig. A.1 – 3 in the appendix) it can be



## 7 Consolidation of volcanic tuffs

observed that the strong shift of occupied pore classes in BP, NB, SMA and HR changes the distribution type from unimodal to bimodal (and partly trimodal). In bimodal pore radii types the distribution usually shows a flattening effect, due to a relative decrease of the higher peak and a simultaneous increase of the lower peak. A good example for this effect is WB (Fig. 7.8). The flattening effect may also be increased in some tuffs by a divergent shift of pore classes. While the main share of pores moves in direction of smaller pore radii, a small fraction shifts towards larger capillary pores (e.g., in CV; see Fig. A.2 in the appendix). This way the tuffs maintain the ability of capillary water transport inside the stone, while increasing their ability for water retention in pores  $<0.1 \mu\text{m}$ . The shift towards capillary pores is most likely the result of the narrowing of larger pores that were previously outside the analysis spectrum. Bimodal pore size distributions in tuffs have been evaluated critically in the literature (López-Doncel et al. 2016; Pötzl et al. 2018a; Pötzl et al. 2018b; Wedekind et al. 2013), amongst others because of their increased risk of susceptibility towards salt weathering and hydric expansion.



Figure 7.9: Modification of the specific surface area (SSA) due to the consolidation treatments, derived from the mercury intrusion porosimetry (MIP). Left) TEOS, right) TMOS

### 7.3.4.2 Modification of the water transport and retention properties

A strongly water absorbing stone should ideally also show a high water vapor permeability, so that after a fast/intense water absorption (e.g., due to a rain event) the stone has the ability to dry equally fast (Snethlage and Pfanner 2020). However, due to their partly high fractions of micropores, tuffs tend to retain the water in their pore space for a considerable amount of time.

#### *Capillary water absorption and water vapor diffusion resistance*

The low porous tuffs BP, BS and LOS show comparatively low capillary water absorption ( $w$  value  $< 1 \text{ kg/m}^2\text{v/h}$ ) and high water vapor diffusion resistance ( $\mu$  value). Water transport in both directions is accordingly low for these tuffs. NB and CV show moderate  $w$  values of up to  $4 \text{ kg/m}^2\text{v/h}$  and moderate to high water vapor diffusion resistance. Considering their pronounced capillary water absorption, these tuffs may retain the water for too long and inhibit an effective drying. CR, SMA and WB show high capillary water absorption, with  $w$  values between 5 and  $15 \text{ kg/m}^2\text{v/h}$ . They also show appropriately reduced  $\mu$  values that may balance an intense water uptake. It is, however, striking that SMA with the highest porosity (41 vol.%) and a fraction of 90 % capillary pores, does show lower capillary water uptake than

## 7 Consolidation of volcanic tuffs

WB and CR. Especially perpendicular to the bedding (in Z direction) the water uptake is significantly reduced, which points to a rather poorly connected pore network. With up to 43 kg/m<sup>2</sup>h, HR shows by far the highest capability of capillary water uptake (Tab. 7.3). Its  $\mu$  value is comparably low and should allow for a considerably fast drying.

Depending on the type of tuff and the applied consolidation measure, the water transport and retention properties of the tuffs change in parts dramatically and confirm the findings regarding the pore space properties made in the previous section. Low porous tuffs consolidated with TMOS tend to show a stronger reduction of their total water absorption under atmospheric conditions and capillary water absorption, while for highly porous tuffs these values could be reduced more effectively with TEOS (Fig. 7.10). When applying TEOS, the combination with the tartaric acid proved to be most effective, while the consolidation with TMOS proved to be most effective in combination with the anti-swelling agent. However, with the exception of BS and CV, the water transport properties of the tuffs were more strongly influenced by the treatment with TEOS. This may be due to the hydrophobic effect of some ethyl groups that did not react during the gelation. A temporary hydrophobic effect of TEOS is somewhat expected and may diminish over time (Doehne and Price 2010). A residual hydrophobicity of TEOS can be removed in the short term by 2-4 treatments with 1:1 v/v solutions of ethanol:water, which, however, was not done in this study.

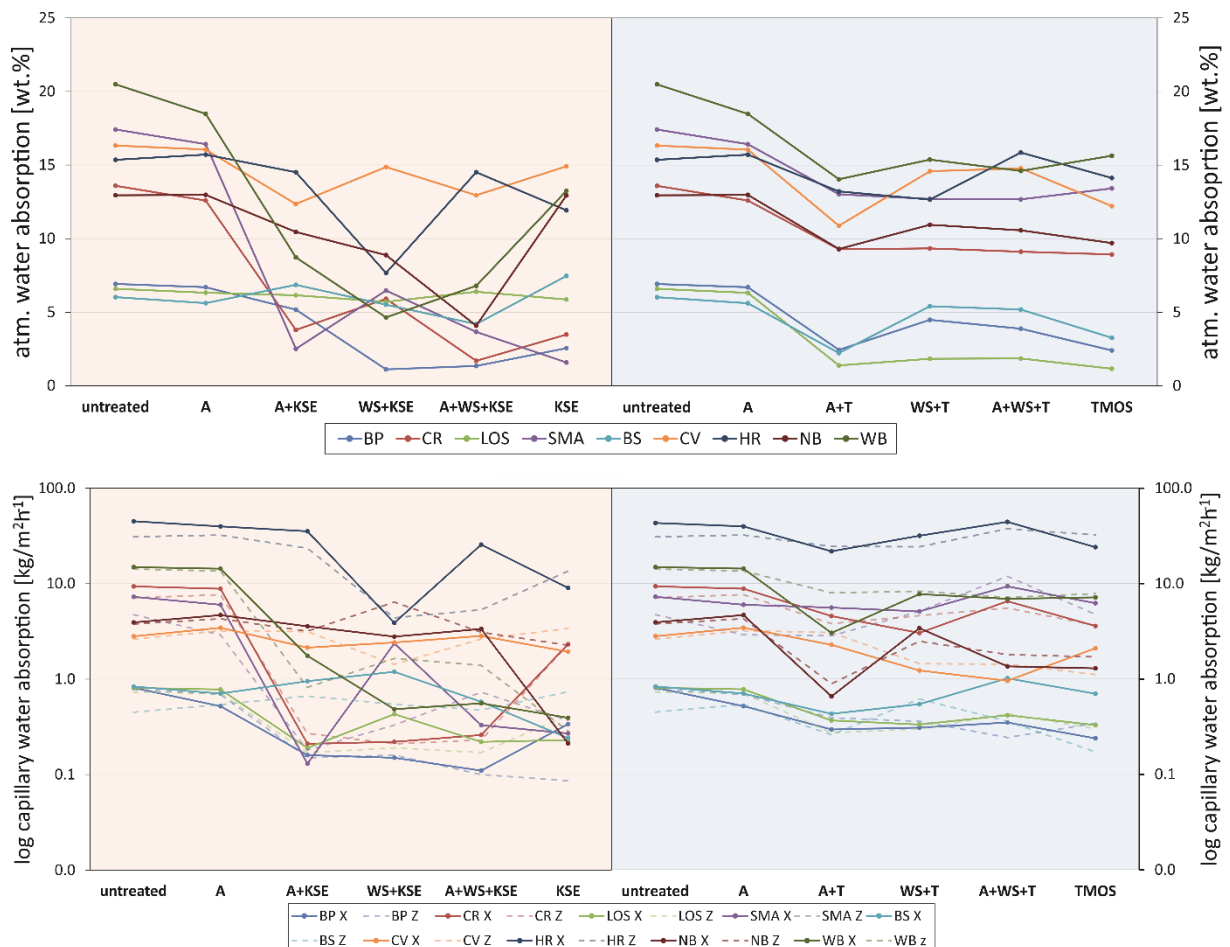


Figure 7.10: Modification of the total water absorption under atmospheric conditions and the capillary water absorption due to the consolidation treatments. Left) TEOS, right) TMOS

## 7 Consolidation of volcanic tuffs

Samples that were treated with tartaric acid prior to the TMOS/TEOS application, exhibit better water transport properties, which is likely the result of the residues of the acid that cause preferential hydrolysis of the ethoxy groups and therefore reduces or eliminates the hydrophobicity. If a hydrophobic effect does not apply, the strong reduction of the capillary water absorption as well as extreme increase of water vapor diffusion resistance may point to a significant narrowing of pathways and reduced accessibility of liquids to the pore network. While the decreasing capillary water absorption fits the catalog of requirements after Snethlage and Pfanner (2020), the strongly increasing water vapor diffusion resistance in most consolidated tuffs often surpasses the maximum recommended increase of the  $\mu$  value ( $\leq 20\%$ ) (Fig. 7.11). Since the creation of a diffusion barrier is to be avoided by all means, most treatments have to be evaluated critically in this regard. The fact that CV and CR still show the ability of water transport, suggests that the previously mentioned glossy coating after the TMOS treatment in combination with Antihydro does at least not seal the pore entries and pathways. In fact, Antihydro exhibits a basic pH of 8.5 and higher pHs promote rapid condensation and gelation, which might be responsible for the gloss in the TMOS samples as TMOS can react much more quickly than TEOS. General remark: Please note, that Snethlage and Pfanner (2020) highlight that the critical values of their catalog of requirements should not be considered as unconditional, rigid rules, but rather as recommendations based on scientific findings and experience on stone consolidation of the last decades.

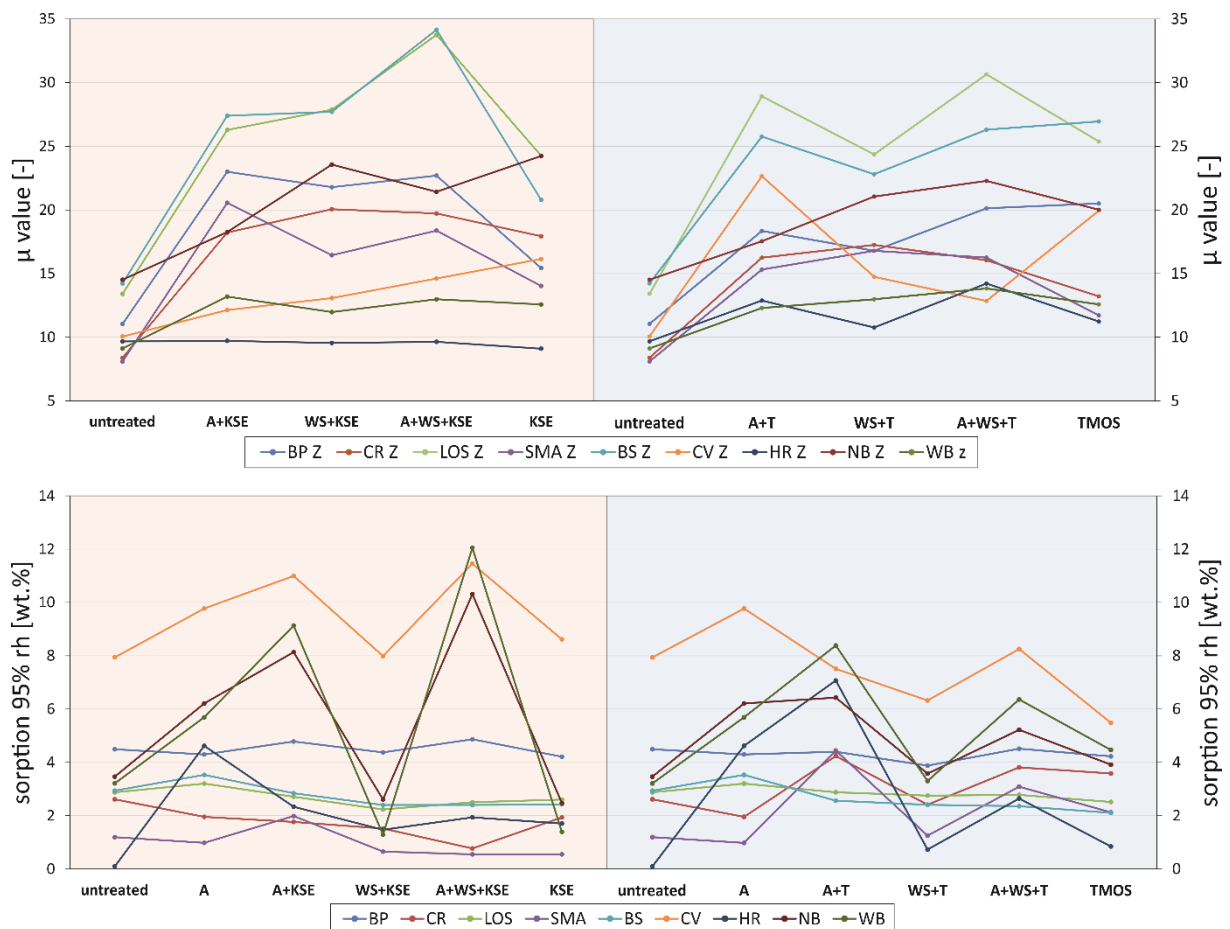


Figure 7.11: Modification of the water vapor diffusion resistance coefficient  $\mu$  and the maximum hygroscopic water sorption value at 95 % relative humidity due to the consolidation treatments. Left) TEOS, right) TMOS

## 7 Consolidation of volcanic tuffs

A pronounced anisotropic behavior of the tuffs, with usually higher capillary water absorption and lower water vapor diffusion resistance parallel to the bedding plane (X direction) indicates a better connection of the pore network in this direction. The pathways perpendicular to the bedding plane (Z direction) seem to be more poorly developed, by showing half the capillary water uptake and double the water vapor diffusion resistance in some samples (see Tab. A.2 – 10 in the appendix).

### *Hygroscopic water sorption*

The nine investigated tuffs show diverse potential for moisture absorption from the air (Figs. 7.11 – 7.13). Considering their high total water absorption potential under full imbibition, untreated HR and SMA show very low hygroscopic water sorption of 0.1 and 1.2 wt.%, respectively. High hygroscopic water absorption of 7.9 wt.% is shown by CV, while the rest of the tuffs show moderate values between 2.6 and 4.5 wt.%. The highest values are thereby shown by tuffs that are rich in zeolites and swelling clay minerals (compare Tab. 7.2). The adsorption isotherms of the untreated tuffs in Figures 7.12 and 7.13 generally show a significant increase of hygroscopic water sorption between 75 and 95 % relative humidity (RH). BP and LOS show already a considerably increased adsorption at low relative humidities.

Except for the low porous tuffs BP, LOS and BS, the consolidation measures changed the absorption behavior drastically and these drastic changes correlate very well with the modification of the pore size distribution (Fig. 7.8; Fig. A.1 – 3 in the appendix). A representative example is CR, whose fraction of micropores was decreased by TEOS treatments, so that TEOS treated CR shows decreased hygroscopic water sorption potential (Fig. 7.12). Another reason for a decreasing hygroscopic water sorption may be a narrowing or sealing of the pathways, which potentially inhibits further absorption. On the other hand, the increasing fraction of micropores due to TMOS treatments subsequently leads to an increasing hygroscopic water sorption of CR. It is striking that the strongest increase of hygroscopic water sorption is often connected to a pretreatment with the anti-swelling agent. The ion exchange with the anti-swelling agent may have led to the formation of hygroscopic salts. Particularly HR, SMA and WB, which showed minor salt efflorescence after the application of the anti-swelling agent, demonstrate this very clearly. Hygroscopic salts are known to efficiently adsorb moisture from the air and may therefore be responsible for the increased hygroscopic water sorption behavior of the addressed samples. The hygroscopic nature of salts is further discussed in Steiger et al. (2011).

## 7 Consolidation of volcanic tuffs

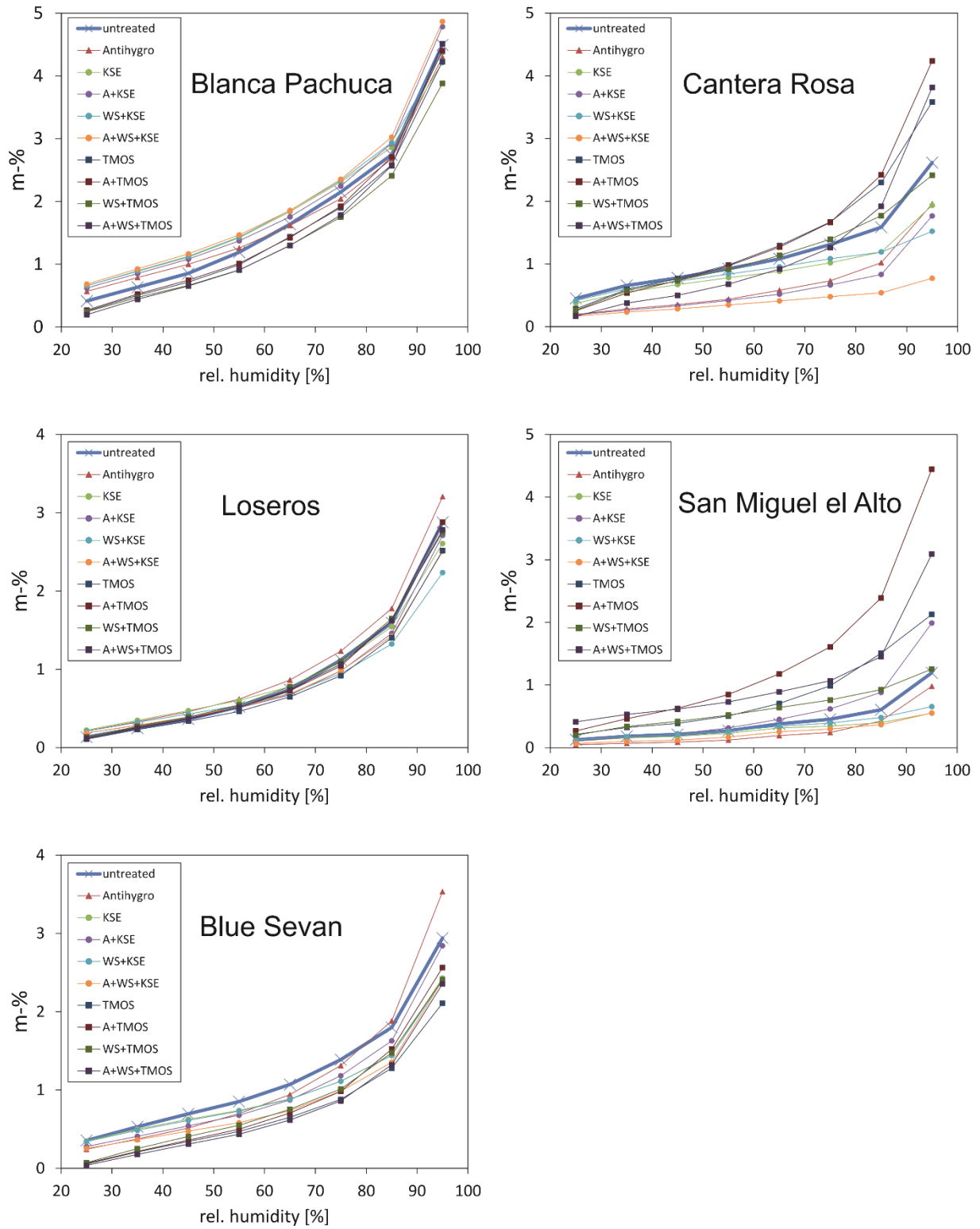


Figure 7.12: Modification of the adsorption isotherm of BP, CR, LOS, SMA and BS due to the consolidation treatments

## 7 Consolidation of volcanic tuffs

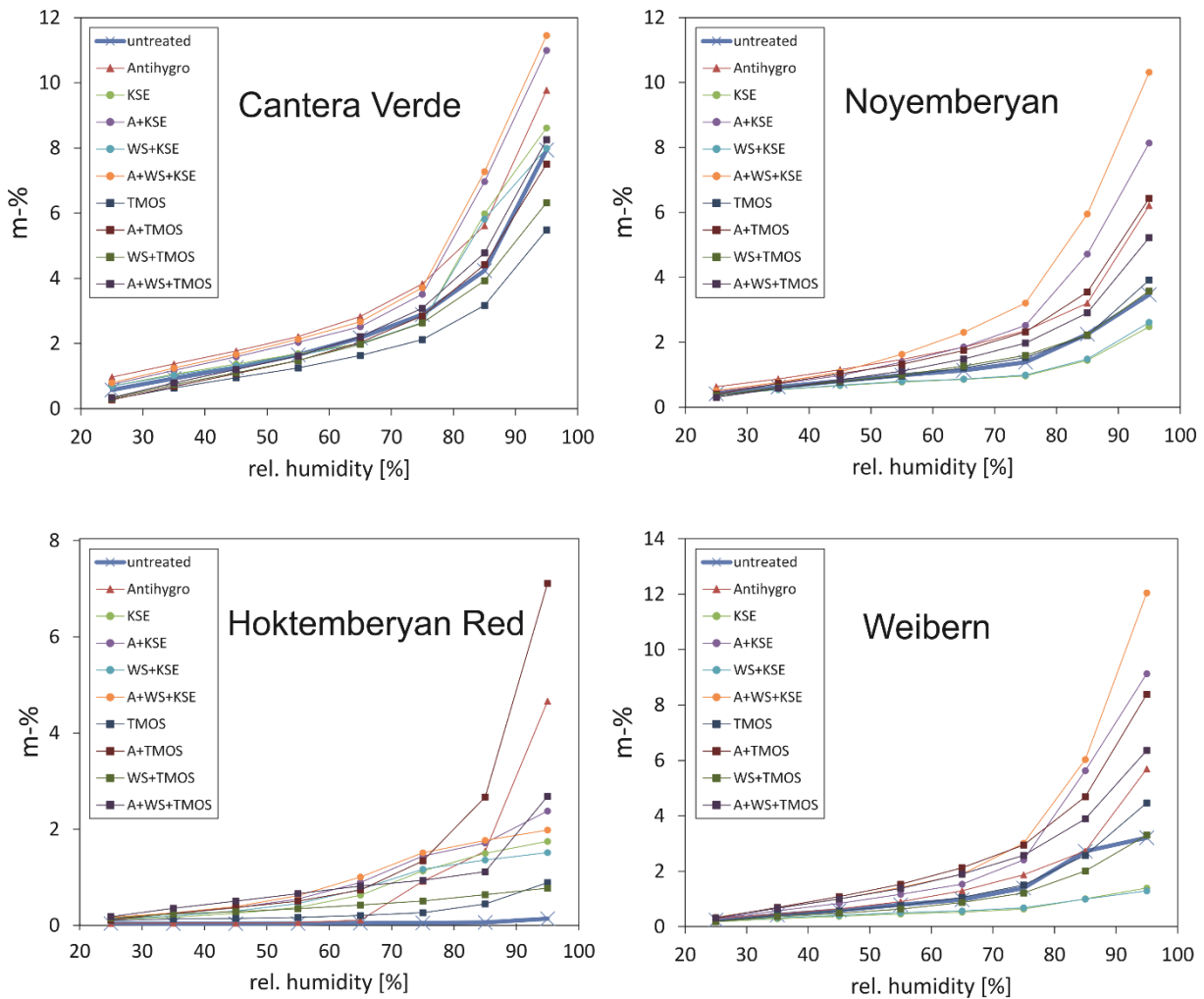


Figure 7.13: Modification of the adsorption isotherm of CV, NB, HR and WB due to the consolidation treatments

### 7.3.4.3 Modification of the expansional behavior

#### *Hydric expansion*

Apart from HR and WB, swelling clays were identified in all investigated tuff stones, so that moisture expansion most likely plays a role in their deterioration. A general observation is an ubiquitous anisotropic expansional behavior of all tuffs with distinct higher expansion in the Z direction (perpendicular to the bedding) (Tab. 7.3). Extreme examples are BS and LOS, showing anisotropies of up to 78 %. In the following, the expansional behavior in Z direction will be representatively discussed (Fig. 7.14).

CR and SMA show considerably low hydric expansion of around 0.2 mm/m when compared to WB (0.7 mm/m) and NB (0.8 mm/m), which expand moderately. High expansion >1.0 mm/m is shown by BP, LOS, BS and CV, with maximum values of up to 2.5 mm/m (BS). HR is a special case, that shows slight contraction of -0.1 mm/m. This phenomenon was also observed on one SMA sample. Already Sneathlage and Wendler (1997) observed a contractional behavior upon moisture absorption and an extension upon drying on a clay-rich sandstone, that was pretreated with a salt solution (NaCl). Steiger et al. (2011) explain this behavior with the influence of salt crystallization-dissolution on the process of hydric expansion. They argue that if salt crystallizes from saturated solutions in the pore space during drying periods, it creates

## 7 Consolidation of volcanic tuffs

a crystallization pressure, inducing an expansion in the stone fabric. The dissolution of these salt crystals will consequently lead to a relaxation and contraction. Thus, in dry conditions, a salt enriched sample will already be expanded and may show a contractional behavior upon wetting, because the salt crystals will dissolve. The excess of salts in the pore space of both HR and SMA after the treatment with Antihygro (see surface efflorescence in Fig. 7.6) may cause this exact phenomenon. The salts were, however, not further analyzed in this study.

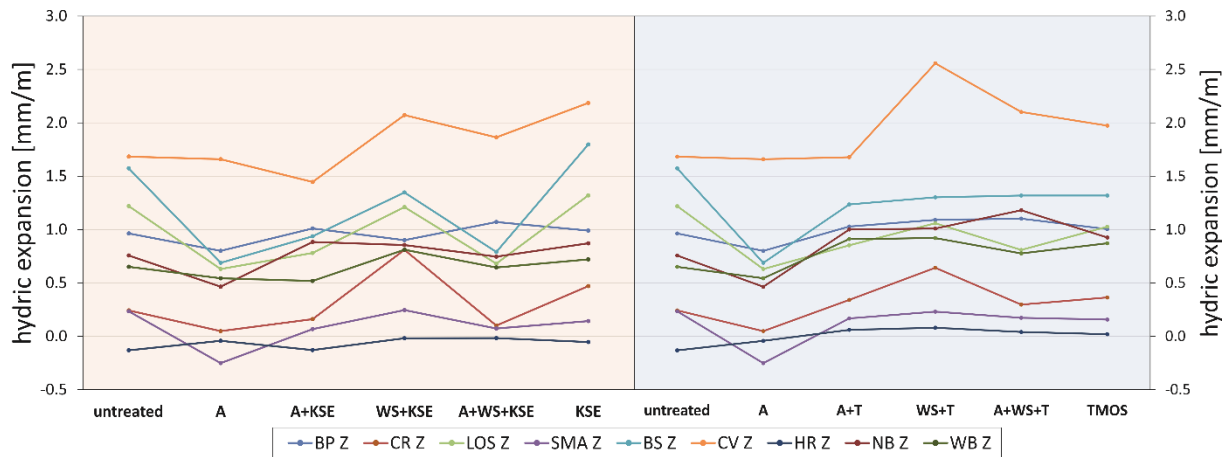


Figure 7.14: Modification of the hydric expansion in Z direction due to the consolidation treatments. Left) TEOS, right) TMOS

According to Snethlage and Pfanner (2020) an increase of the expansional behavior due to the conservational treatment should be avoided under any circumstances. The application of TEOS only, however, lead to a higher hydric expansion of the tuffs. This effect was even increased with a primer component (WS) pretreatment (Fig. 7.14). The hydric expansion of CR, for example, was more than tripled, up to 0.8 mm/m. The application of an anti-swelling agent (A), on the other hand, reduced the hydric expansion in nearly every case. Even in combination with TEOS (or primer component and TEOS) the hydric expansion of the tuffs could be reduced or did not increase. In BP and NB, as well as CV in combination A + WS + KSE, the anti-swelling agent could not compensate the increased swelling due to the consolidation. Another observation after the treatments is an often reduced anisotropic behavior in hydric expansion of the investigated rocks.

The consolidation with TMOS produced quite similar trends for the different combinational treatments. However, the increase of hydric expansion is often markedly lower. Exceptions are NB and WB, which show a slightly stronger increase of expansion compared to consolidation with TEOS.

### *Thermal and thermo-hydric expansion*

The enormous mineralogical variety and broad range of textural and fabric variability has a great impact on the expansional behavior of tuffs, since the thermal expansion coefficient  $\alpha$  is a result of the expansion of the individual minerals present in the rock. This makes the prediction of the thermal expansional behavior of tuffs very difficult. López-Doncel et al. (2018) give an overview of these problematics and observed some trends like increased thermal expansion of acid, crystal-rich and more homogeneous tuffs. In general,  $\alpha$  is only considered with regard to the thermal expansion under dry conditions. In this section it will,

## 7 Consolidation of volcanic tuffs

however, also be used as an expression of the expansional behavior under thermo-hydric (wet) conditions.

Regarding the thermal (dry) and thermo-hydric (wet) expansion, the tuffs of this study show coefficients of linear thermal expansion ( $\alpha$ ) between  $6.8 - 13.4 \times 10^{-6} \text{K}^{-1}$  under dry conditions, that increase significantly under wet conditions ( $7.2 - 50.7 \times 10^{-6} \text{K}^{-1}$ ) (Tab. 7.3). In doing so, the highest values often coincide with the tuffs that contain formidable amounts of swelling clays and/or zeolites and simultaneously showing the highest hydric expansion values (compare Tab. 7.2 and Tab. 7.3). Under wet conditions the strong influence of hydric expansion has to be considered, since most minerals would not be able to produce such high  $\alpha$ -values on their own (compare  $\alpha$  for different minerals in Steiger et al. (2011)).

The change of expansional behavior due to thermal stress (dry) for most consolidated tuffs is within the framework of  $\pm 20\%$  with regard to their untreated state. CV is an exception, showing an extreme increase of its'  $\alpha$  value after any combinational treatment with both TEOS and TMOS, when tested under dry conditions (Fig. 7.15). Under wet conditions, the thermo-hydric expansion of CV is reduced strongly after both TEOS and TMOS treatment, especially when consolidated in combination with the anti-swelling agent. The sole application of TEOS tends to slightly increase the thermal and thermo-hydric expansion of the tuffs. On the contrary, the sole consolidation with TMOS, and most combinational treatments with TMOS, lead to a decreasing thermal and thermo-hydric expansion. Modifications are typically stronger for low porous tuffs. The expansional behavior of SMA and HR was barely affected by any treatment, neither under dry nor wet conditions.

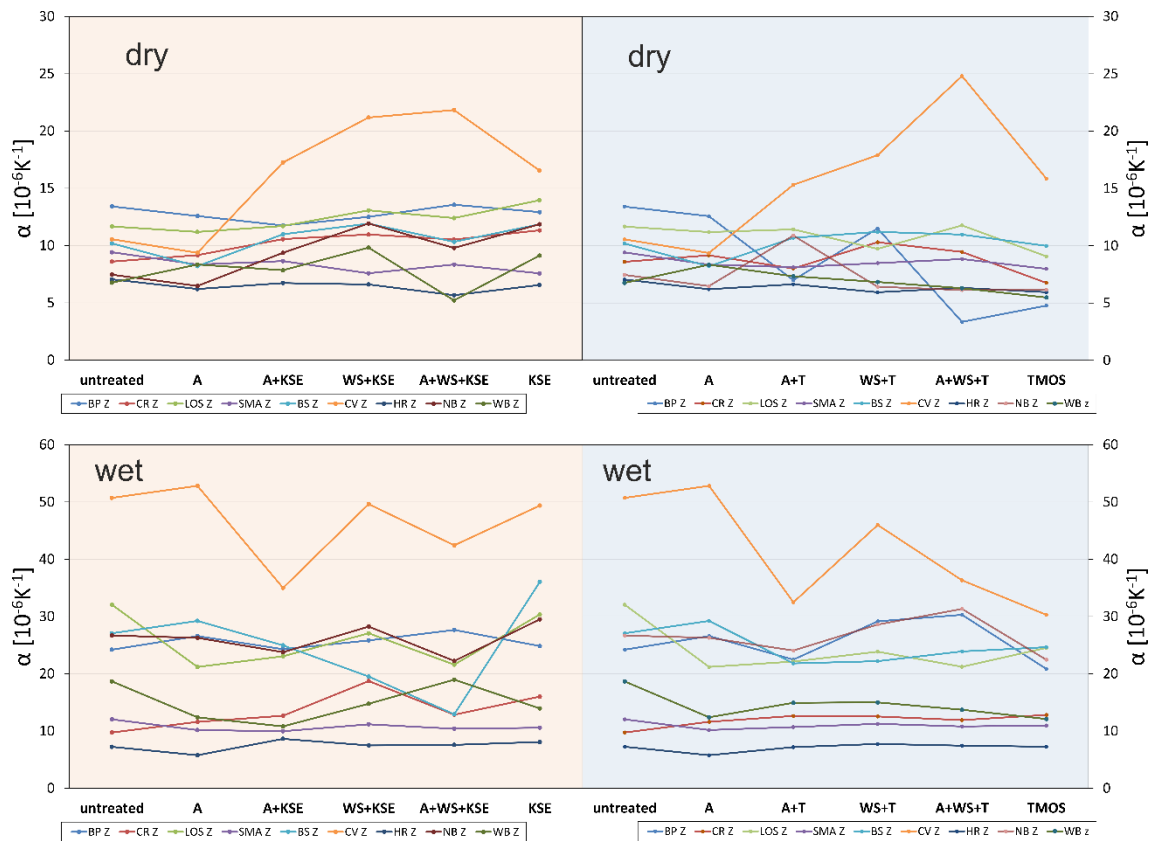


Figure 7.15: Modification of the thermal expansion coefficient  $\alpha$  under dry and wet conditions in Z direction due to the consolidation treatments. Left) TEOS, right) TMOS



## 7 Consolidation of volcanic tuffs

Despite their partly high  $\alpha$ -values, only BP and CV show considerable residual strain ( $\epsilon$ ) after thermal treatment under dry conditions (Fig. 7.16). In doing so, BP shows positive residual strain around 0.17 mm/m while CV shows a strong negative residual strain of up to 0.54 mm/m. Under wet conditions both samples show reduced negative residual strain of up to 0.10 mm/m (BP) and 0.25 mm/m (CV), respectively. LOS and BS develop highly negative residual strains in Z direction (perpendicular to the bedding) under wet conditions of 0.74 mm/m and 0.51 mm/m, respectively.

While SMA, HR and for the most part CR do not experience considerable changes in their residual strain after thermal and thermo-hydric stress, WB, NB and BP consolidated with TEOS show significant higher residual strains after thermo-hydric stress. Furthermore, after thermal stress under dry conditions, NB, LOS and BS consolidated with TEOS in any combinational treatment show moderate increase of the residual strain. The strongest increase is usually caused by the application of TEOS (KSE) only or in combination with tartaric acid (WS + KSE).

Most of the tuffs consolidated with TMOS do not show an increase of their residual strain. On the contrary, the highly negative residual strains of LOS, BS and CV under wet conditions were drastically reduced (Fig. 7.16). On BP, however, the combination of TMOS with an anti-swelling agent or tartaric acid lead to highly negative residual strain (up to 0.45 mm/m) under dry conditions (A + T / A + WS + T) and highly positive residual strain (up to 0.50 mm/m) under wet conditions (WS + T / A + WS + T / TMOS).

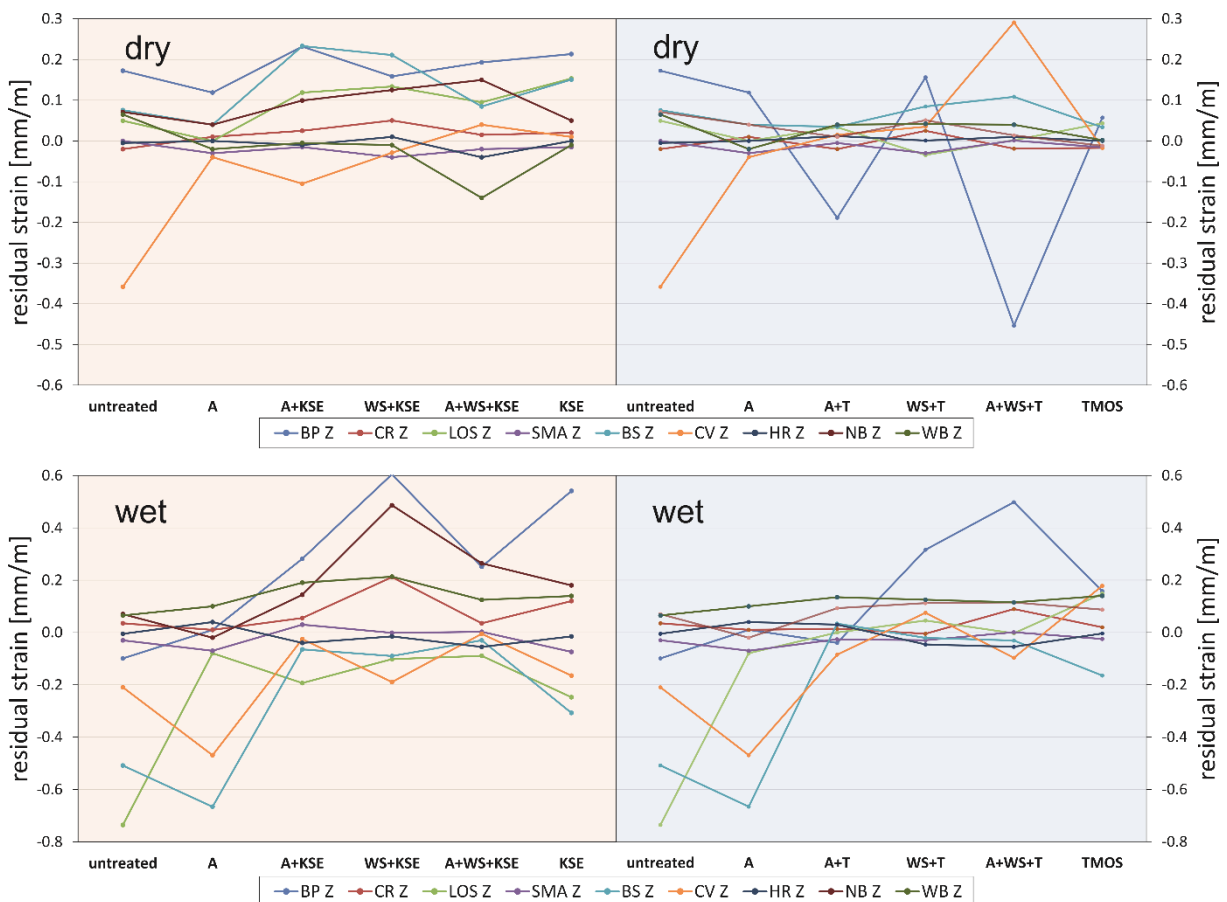


Figure 7.16: Modification of the residual strain  $\epsilon$  after thermal (dry) and thermo-hydric (wet) expansion in Z-direction due to the consolidation treatments. Left) TEOS, right) TMOS

## 7 Consolidation of volcanic tuffs

### 7.3.4.4 Modification of the ultrasonic velocity and dynamic modulus of elasticity

In general, only a direct assessment of the strength parameters via compressive, tensile or flexural strength test can verify the true strength gain or loss after a consolidation treatment. The strength of rock material is, however, proportional to the dynamic modulus of elasticity (Young's Modulus), which can be determined from ultrasonic measurements (Siegesmund and Dürrast 2011). Chapter 5 revealed a strong correlation of the ultrasonic velocity with both compressive and tensile strength on over 200 tuffs (Fig. 5.8). As the correlations are rock-dependent they should be specified for the rocks under consideration in further research. The results for the ultrasonic velocities and dynamic Young's Moduli parallel to the bedding (X direction) are displayed in Figure 7.17. The ultrasonic velocities of the untreated tuffs range between 2.5 and 3.9 km/s, whereby the highest velocities are shown by the low porous tuffs BP, LOS and BS and typically parallel to the bedding.

All tuffs experience an increase of the ultrasonic velocity after consolidation treatment. Except for SMA and BS, the increase is higher after the application of TMOS, especially in combination with the Antihydro (A + T/A + WS + T). Combinational treatment of TEOS with the Antihydro (A + KSE / A + WS + KSE) produced the strongest increase for BP, LOS, HR, NB and WB, while the combination with the tartaric acid (WS + KSE) led to the strongest increase of ultrasonic velocity for BS, CR, CV and SMA (Fig. 7.17).

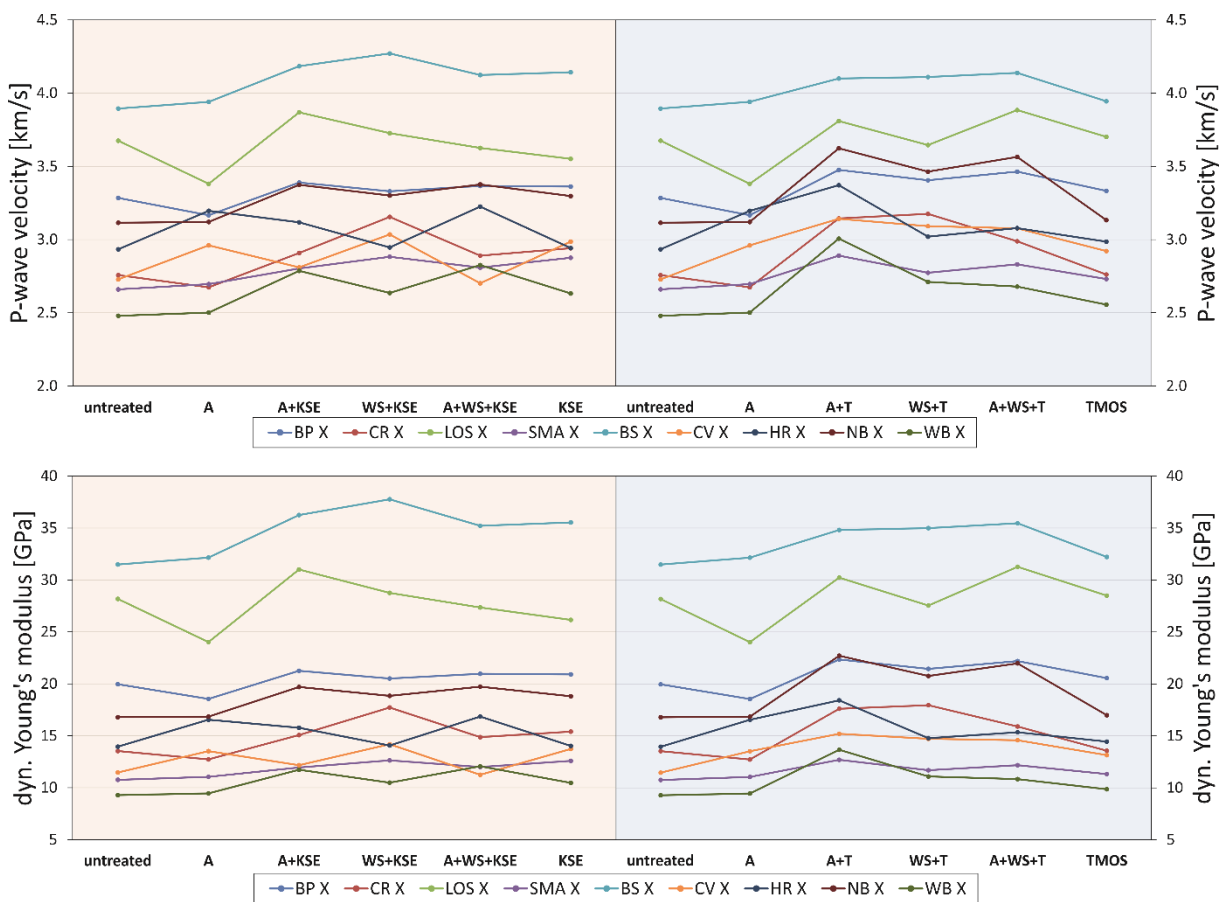


Figure 7.17: Modification of the ultrasonic velocity and dynamic modulus of elasticity (Young's Modulus) due to the consolidation treatments. Left) TEOS, right) TMOS

## 7 Consolidation of volcanic tuffs

Except for WB, all tuffs show a more or less pronounced directional dependence on their ultrasonic velocities, with higher velocities in X direction (Tab. 7.3). After the consolidation the anisotropic behavior remains unchanged for most tuffs. In WB and CV the application of both TEOS and TMOS lead to increased directional dependence, while in LOS the treatment with TMOS and in HR the treatment with TEOS slightly decreased the anisotropic effects.

The dynamic Young's Moduli naturally show trends similar to the ones that can be observed for the ultrasonic velocities, pointing to a general increase of strength by all consolidation treatments (Fig. 7.17). The increase in strength is more pronounced in the highly porous tuffs and the highest increase in strength for most samples can be observed after treatment with Antihydro and TMOS (A + T). Other than that, when TEOS is applied, the strongest increase is observed in combination with the tartaric acid (WS + KSE / A + WS + KSE). In their catalog of requirements Sneath and Pfanner (2020) consider an increase of the dynamic Young's Moduli of more than 1.5 times the value of the unweathered stone as critical. An overstrengthening of the consolidated zone should be prevented by all means, since it may induce considerable stress at the interface of treated and untreated material. This limit is exceeded only once for HR, by the treatment TMOS in combination with Antihydro (A + T).

A reduction of strength is shown by CV when treated with TEOS in combination with Antihydro (A + KSE). With additional tartaric acid (A + WS + KSE) the strength reduction is intensified up to -20 %. Apart from that, a strength reduction of up to -15 % can be observed for BP, CR and LOS due to the treatment only with Antihydro.

### 7.4 Discussion

The treatment of nine different tuffs with a commercially available stone consolidant (TEOS) and the utilization of a neat product with smaller molecule size (TMOS), in different combinations of applications with a primer component and a swelling reducer, generated clear but ambivalent results:

#### *TEOS*

The consolidation with TEOS led to a significant reduction of the porosity, fraction of micropores, total and capillary water absorption. These modifications of the stone properties are expected to lead to a higher weathering resistance. Increasing water vapor diffusion resistance, however, can possibly lead to drying problems of the stone and in extreme cases to the creation of a diffusion barrier that can trap water inside the stone, which is subsequently involved in e.g. crystallization-dissolving processes. In this regard, especially the low to moderate porous tuffs show an alarming development.

Regarding the moisture expansion, slight increases up to a partial tripling of the hydric expansion could be observed. This is obviously an undesired side effect and reduces the weathering resistance of the tuffs. However, this negative side effect could be counteracted by pretreating the sample with an anti-swelling agent. Therefore, given a pretreatment with an anti-swelling agent, an application of TEOS on the investigated tuffs is expected to increase their weathering resistance. The same applies with regard to the thermal expansion. The consolidation shows limited effects on the thermal expansion behavior of most tuffs. The clay-rich, low to moderate porous tuffs BS, NB and LOS show moderately increased residual strain.

## 7 Consolidation of volcanic tuffs

Under wet conditions, the alarming increase of residual strain in the zeolite-rich samples BP, NB and WB has to be evaluated negatively. The clay and zeolite-rich CV experienced significantly stronger expansion, its' residual strain, however, could be reduced by the TEOS treatment.

The application of tartaric acid as a primer component strikingly enhances the effect of the consolidation with TEOS. Especially the modifications on water transport and retention are strongly increased in comparison to an application of consolidant only. As mentioned above, this is likely because residual tartaric acid would promote hydrolysis and reduce hydrophobicity which is usually caused by the consolidant. It should be noted, however, that a pretreatment with the primer component always enhances both positive and negative effects of the consolidant, e.g. further reduction of the porosity or increase of hydric expansion, respectively. A very positive effect observed during the consolidation treatment itself, was a strongly accelerated absorption of the consolidant after the pretreatment with the primer component (see also Fig. 7.4).

The lack of significant strength increase can be evaluated as a positive outcome, because it reveals that the consolidation did not result in an over-strengthening of the material, since in this study unweathered material was treated. Thus, no major stress disparities between treated and untreated areas of the tuffs are expected. In addition, it allows for a repeated treatment to increase the consolidation effects. As mentioned in the previous section, in the future direct measurements of the compressive, tensile or flexural strength have to verify the findings on rock strength modifications, that were derived by ultrasonic measurements in this study.

Figure 7.18 displays precipitated TEOS and TMOS in the pore space of a low porous (BP) and a highly porous (SMA) tuff. We can observe a significant coating of the pore space and the silica gel shows typical dry cracks that explain the development of smaller micropores registered in the pore radii distribution of the tuffs (Tab. A.2 – A.10 in the appendix). The initial bonding to the substrate appears to be good.

### *TMOS*

The consolidation with TMOS generated similar results regarding the reduction of the porosity, total and capillary water absorption, as well as an increase of the water vapor diffusion and hydric expansion. However, compared to the treatments with TEOS, the changes are usually less pronounced, especially in high porous tuffs, but more intense in low porous tuffs with an abundance in zeolites and swelling clays.

In contrast to TEOS, TMOS significantly increased the fraction of micropores and therefore the specific surface area, especially in the low porous tuffs. The changes towards a bimodal pore character with a high share of micropores are alarming, since bimodal pore size distributions have shown to increase the weathering susceptibility of tuffs (López-Doncel et al. 2016; Pötzl et al. 2018a; Pötzl et al. 2018b; Wedekind et al. 2013). However, the tuffs do not show a resulting increase in hydric, thermal or thermo-hydric expansion. In fact, the expansional behavior of tuffs treated with TMOS is less negatively influenced than with TEOS. Thermal expansion is even decreased (with exception of CV). The clay and zeolite-rich, low porous BP develops residual strain after thermal stress, which has to be evaluated critically.. Consolidation with TMOS led to a slightly stronger strength increase than TEOS, but is still

## 7 Consolidation of volcanic tuffs

within the acceptable range of deviation after (Snethlage and Pfanner 2020). That the modified pore character of the tuffs might negatively influence their durability should be further explored using salt bursting tests. An increased fraction of micropores, for example, may potentially retain aqueous (salt saturated) solutions for a longer period of time that lead to a delayed drying behavior of the tuff and an extended supply of salt solution for the crystallization of halides in adjacent pores.

Unlike for TEOS, the pretreatment with tartaric acid did not significantly increase the effect of TMOS. On the contrary, in many cases the application of sole TMOS led to more intense modifications. The most significant enhancement of the consolidation effects of TMOS were reached by the pretreatment with the anti-swelling agent. The Antihydro itself is basic (pH = 8.5) and may have a catalytic impact on the consolidation process, since we know that the hydrolysis reaction can be enhanced by either acidic or alkaline catalysis (Snethlage and Sterflinger 2011).

The SEM photomicrographs in Figure 7.18 reveal that the silica gel formed by TMOS is generally thicker than the gel formed by TEOS and shows a smoother surface. Dry cracks are more abundant and create a secondary porosity in the submicrometer range, likely in the nanometer range. In general, TMOS treated samples show a significant higher amount of silica gel in their pore space than samples treated with TEOS.

### *General remarks*

The petrophysical properties of the tuffs were partly modified to a point, such that they did not meet the requirements of the quality catalog of Snethlage and Pfanner (2020) anymore. Especially the water vapor diffusion resistance was often increased by more than 50 %, which bears the risk of the creation of a diffusion barrier and potentially trapped water may induce freeze-thaw attack upon temperature changes or interact with salts and clay minerals. The reduction in strength through water absorption was successfully identified in the literature (Çelik and Ergül 2015; Hashiba and Fukui 2015; Hirschwald 1908; Morales Demarco et al. 2007; Pötzl et al. 2018a; Siedel 2010; Török et al. 2004; Vásárhelyi 2002) and even small amounts of moisture may induce significant strength reduction (Yasar 2020).

A darkening of the stone is an undesired side effect, that was primarily observed on high porous tuffs by the application of TEOS and on low porous tuffs by the application of TMOS (Fig. 7.5). In addition, the application of TMOS on zeolite rich tuffs pretreated with Antihydro showed a glossy appearance. A glossy appearance is to be avoided by any means and usually indicates that the moisture content during the application was too high, so that the silica gel already precipitates at the surface of the specimen (Snethlage and Sterflinger 2011). In this case, however, the accelerated precipitation at the surface of the tuff was likely caused by the pH of the Antihydro (pH=8.5) as higher pHs promote rapid condensation and gelation.

## 7 Consolidation of volcanic tuffs

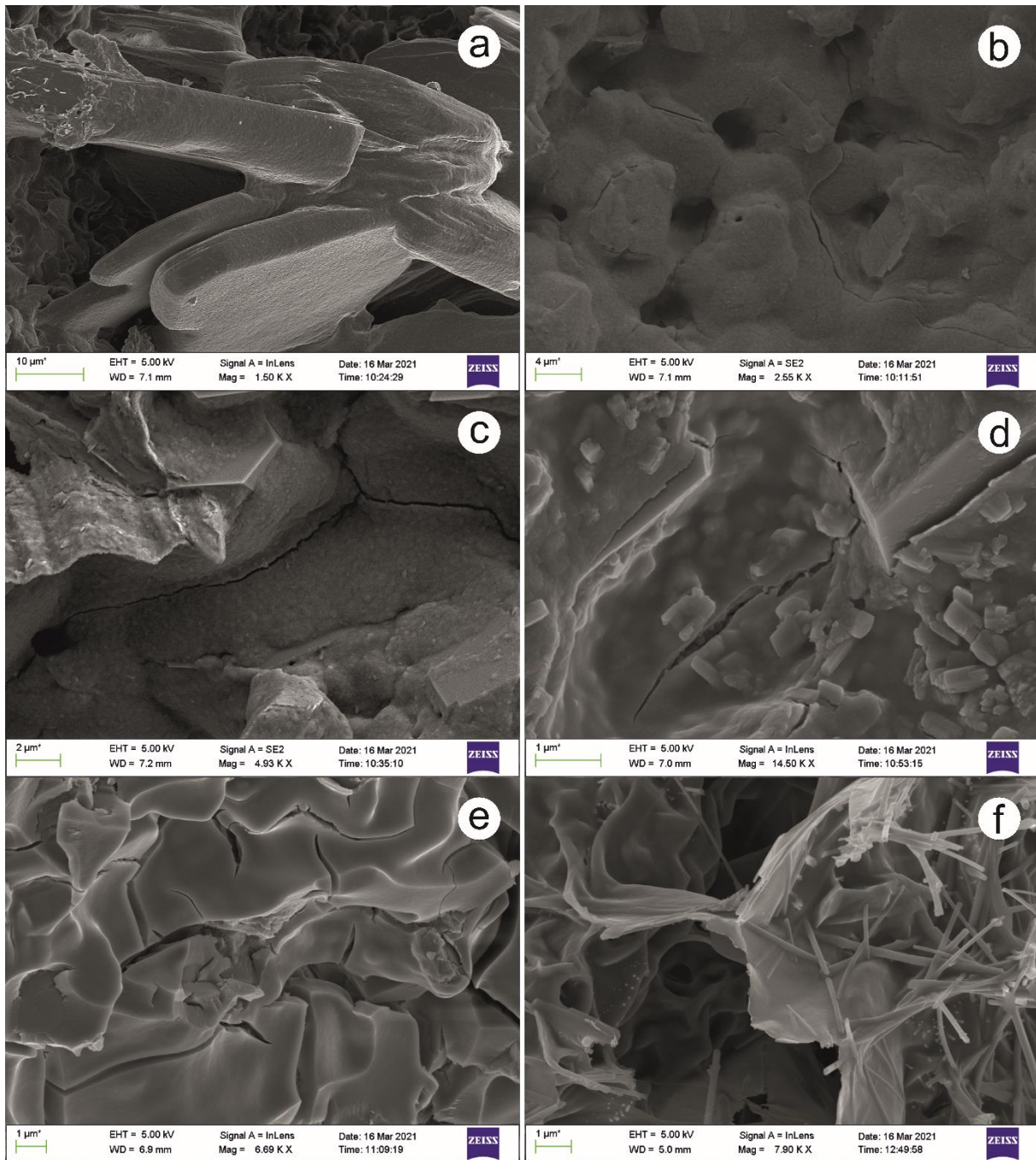


Figure 7.18: SEM photomicrographs of the fully silica gel produced by either TEOS or TMOS treatment. **a** Individual crystals covered with silica gel from TEOS treatment in the tuff SMA. **b** The silica gel, with typical dry cracks, covers the matrix and leads to a reduction of pore space and narrowing of pathways in SMA treated with TEOS. **c** Feldspar crystals barely stand out of the cover of silica gel in SMA. The silica gel formed by TEOS treatment has a rather rough surface. **d+e** The silica gel formed by TMOS treatment of the same tuff (SMA) is thicker, has a smoother surface and more pronounced dry cracks. **f** In the rather low porous tuff BP, the silica gel formed by TMOS treatment works like a glue and sticks together the individual mordenite needles

## 7 Consolidation of volcanic tuffs

### 7.5 Conclusions

The consolidation of volcanic tuffs is a challenging topic. Many products that proved to produce satisfying results for other types of porous stones fail in the application on tuff. Essential problems are the water retention of some tuffs and small nanopores that aggravate the absorption of the consolidant. The main goals of this study were:

- (1) to investigate the general suitability and influence of TEOS and TMOS on the petrophysical properties and material behavior of different types of tuffs
- (2) to determine the effects of a primer component (tartaric acid) and anti-swelling agent (Antihygro) on consolidation treatments of different volcanic tuffs
- (3) to investigate if TMOS, due to the smaller molecule size of its monomers, is being absorbed more effectively than common TEOS products

The evaluation of the petrophysical properties before and after the consolidation with TEOS and TMOS identified varying efficiency and suitability for different types of tuff. Some findings of this laboratory investigation may also prove useful for the practical in-situ application:

- The effect of the consolidation with both TEOS and TMOS is generally higher on clay and zeolite-rich, low porous tuffs. Comparing the effectiveness of both consolidants, TEOS appears to induce modifications of the petrophysical properties more effectively on highly porous rock, while TMOS showed to be more effective on low porous tuffs.
- The pretreatment with tartaric acid significantly enhanced the effects of TEOS, both beneficial and unfavorable. In this regard a benefit-risk assessment is crucial before the practical application. For example, does an increased strengthening effect outweigh a potential increase in expansional behavior? An enhancing effect of the primer to the degree observed for TEOS cannot be noted for TMOS.
- In combination with TEOS and TMOS, the anti-swelling agent significantly counteracted the increasing hydric expansion, originating from the consolidants.
- The anti-swelling agent showed almost exclusively positive modifications of the stone properties and may be applied in most cases without expecting negative side effects if the tuffs are rich in swelling clays. The highly porous tuffs containing no (HR, WB) or barely (SMA) swelling clay minerals, did show salt efflorescence after the application of the anti-swelling agent which itself is a salt (1,4-Diaminobutane dihydrochloride). It can be assumed that the Antihygro is causing the excess of salt in these tuffs, since the specimens of the same lithology that were not treated with Antihygro did not show any efflorescence. The two molecules of dihydrochloride in diaminobutane dihydrochloride dissociate in aqueous solution and produce two  $\text{Cl}^-$  that may react with cations of alkaline or alkaline earth metals, namely Na, K, Mg and Ca, and form corresponding halides. The most natural halide to crystallize under ambient conditions (20 °C, RH < 70 %) is sodium chloride or halite. SMA and HR experienced an increasing contractional behavior upon wetting after the treatment with Antihygro. Steiger et al. (2011) state that such contractional behavior upon wetting, points to the fact that salt crystals, build in the pore space from the excess salt during dry periods, induce constant

## 7 Consolidation of volcanic tuffs

crystallization pressure to the stone fabric. The stone fabric that is therefore under expansion during dry conditions, will contract upon wetting and subsequent dissolution of the salt crystals. In the case of recurring wet-dry cycles, the salt will induce progressive damage to the stones, which underlines the importance of a desalination prior to the consolidation. Considering the relatively low hydric expansion values of untreated HR, SMA and WB, the application of an anti-swelling agent does not seem to benefit its petrophysical modification enough to outweigh a slight decrease of hydric expansion. In conclusion, it seems only recommendable to apply Antihygro on tuffs when an inhibition of the hydric expansion is truly needed and never as a prophylactic measure, as there is a risk of excessive salt efflorescence. In any case, if salt efflorescence is visible, the stone should be desalinated prior to the consolidation treatment.

- Low porous tuffs absorbed TMOS significantly stronger than TEOS (Fig. 7.4), with drawbacks only in exceptional cases. The partly extreme change of the pore size character due to the shift of pore classes towards single digit nanopores suggest that the TMOS either entered and precipitated inside the smaller micropores (clogging of pore throats). Or the silica gel itself caused an extreme amount of secondary micropores, for example due to dry cracks as a result of the polycondensation. SEM photomicrographs of TMOS treated tuff revealed, that both is the case (Fig. 7.18).

In summary, this study provides a variety of data that indicates, that TMOS may be a suitable candidate to overcome the bottlenecks in the pore space of tuffs, which limit the consolidation success of current products. Note that the study was conducted under controlled laboratory conditions on fresh quarry material. The samples were first preconditioned and then fully saturated during the consolidation, to guarantee the same conditions for every stone and identify general suitability. On-site application would neither allow such controlled preconditioning of the stone (building elements), nor a full saturation with the consolidant. The results of the treatment of unweathered material are moreover not transferable one-to-one to weathered material, which may show entirely altered pore space, for example due to the creation of cracks. The next step should be the investigation of the depth profile of suitable candidates and the characterization of their capillary absorption of the consolidants. Regarding the strength increase due to a consolidation measure, Doehne and Price (2010) refer to the results of Félix (1996) and Scherer and Jiménez-González (2008), who observed a loss of the initially increased strength in consolidated clay-bearing stones, after only three to ten dry/wet cycles. Subsequent steps should be the durability testing of the consolidation in long term experiments and a potential application on on-site test fields. Our investigation demonstrates that supplementary treatments of both TEOS and TMOS could be also conceivable. Once more it has to be highlighted that prior to every practical on-site application, extensive preliminary investigations have to be undertaken, to maximize the desired consolidation effect and minimize the risk of causing irreversible damage.



## 8 General conclusions

### Chapter 4 – Deterioration of volcanic tuff rocks from Armenia

The net result of the case study was the identification of the significant influence of pore space properties and the clay mineral content on the salt crystallization resistance as well as the moisture expansion behavior.

- Tuff rocks showing a bimodal pore radii distribution with considerable amounts of micropores ( $< 0.1 \mu\text{m}$ ) and especially unimodal pore radii distributions with almost exclusively micropores have shown to be particularly susceptible to salt crystallization. Therefore, the important influence of the micropores on salt weathering in tuff rocks could be clearly demonstrated.
- Zeolites showed to significantly contribute to the sorption rate and potentially to the hydric expansion (see 4.4) of tuffs by creating extreme small micropores  $< 0.7 \text{ nm}$  and therefore enable conditions for disjoining pressure to take place
- The Armenian glass-rich tuffs, undergoing the exact same salt bursting test procedure than crystal rich tuffs from Mexico (López-Doncel et al. 2016) and Germany (Chapter 6) showed to be significantly more resistant and indicate a differential durability of crystal and glass tuffs
- A remark on the procedure of the salt bursting test is that the swelling behavior during the full immersion in the salt solution, as well as the thermal stress during the drying process of the test procedure ( $60^\circ\text{C}$ ) can be potentially additional factors, contributing to the decay of the tuff rocks.

### Chapter 5 – Key parameters of volcanic tuffs

The goal of this chapter was to identify key parameters that may be useful in the estimation of the strength and durability of tuffs by analyzing a dataset of more than 500 samples from the literature. Fifteen selected tuffs were investigated in more detail, in order to extrapolate to the very comprehensive, but less detailed dataset from the literature and achieve larger representability.

Tuffs demonstrate to bear great mineralogical and fabric heterogeneity, and along with this heterogeneity they show a wide range of technical parameters and responses to weathering. Especially the porosity, water absorption and hydric expansion can exceed values multiple times higher than other rock types (compare Siegesmund and Dürrast 2011). Although the analyses in this study are accompanied by a partly wide scattering of data, some strong correlations can be observed:

- Both porosity and bulk density are strongly related to the uniaxial compressive strength (UCS) and tensile strength (TS) and are therefore reliable estimators to predict the strength and durability of tuffs (UCS reduction).

## 8 General conclusions

- Both porosity and bulk density have a strong relation to the ultrasonic velocity, which in turn shows to be a good estimator for the strength of tuffs. This observation is not trivial, since tuffs can incorporate huge amounts of pumice clasts and lithics, that may considerably influence the propagation of the P-wave, e.g. due to increasing the pore space. Therefore, an ultrasonic testing device can help for a fast and non-destructive assessment of the materials quality parameters, like it is reliably done for more homogenous natural stones and concrete (Sharma and Singh 2008).
- The hydric expansion is connected to both strength reduction and salt weathering. The higher the hydric expansion, the lower the tuffs durability. Similar to the observations of Wedekind et al. (2013) and contrary to other studies on clay bearing tuffs (Pötzl et al. 2018b, compare Chapter 4) or sandstones (Ruedrich et al. 2011), the tuffs of this study do not show a clear correlation between the cation exchange capacity (CEC) and the intensity of their moisture expansion. This is possibly because the samples partly contain zeolites that may not increase the CEC, but contribute to the moisture expansion.
- The pore size distribution, categorized in one of the three pore radii types suggested by Ruedrich and Siegesmund (2006) (type I = unimodal equal, type II = unimodal unequal, type III = bimodal), showed to be helpful in estimating general trends of material behavior. In doing so, unimodal unequal pore radii types are associated with crystal tuffs and unimodal equal pore radii types are associated with vitric tuffs. Tuffs with bimodal pore radii distribution turned out to be the most unpredictable in terms of their durability and their pore radii distribution alone may not give meaningful prognosis.
- Crystal and vitric tuffs show strongly differential characteristics in their technical parameters and durability and are potentially useful for their estimation. Some key observations regarding crystal and vitric tuffs are (listed in Tab 5.4): (1) Vitric tuffs are described by high porosity, with usually large mean pore radii and high water absorption. Their water vapor diffusion resistance, hygroscopic water sorption and hydric expansion is generally low. The influence of water on their strength properties is considerably low and they show typically high resistance to salt weathering. (2) Crystal tuffs show typically lower porosity, with small mean pore radii and low to moderate water absorption. They often contain high amounts of swelling clays and zeolites that are connected to an increasing hydric expansion and hygroscopic water sorption, as well as a high resistance to water vapor diffusion. Crystal tuffs show the highest strength values, but also the strongest decrease in strength due to water saturation. Their resistance to salt weathering is typically lower. In the practical applicability the initial categorization of crystal and vitric tuffs after the classification system of Schmid (1981) may therefore help to give a broad picture of the expected material parameters (see Tab. 5.4). These observations need validation in future studies, as the literature does not provide sufficient constraints.

The basic relationships between the individual rock parameters found in this study confirm the results of previous studies on other rock types (Siegesmund and Dürrast 2011). They also confirm many findings of case studies on tuffs with relatively small datasets mentioned in the introduction (Chapter 5.1; also compare Chapter 4). The comprehensive dataset of this study,

## 8 General conclusions

however, does finally allow for more general statements, as this study provides the highest representability of tuffs so far.

### Chapter 6 - Clay swelling mechanism in tuff stones

- The swelling experiments in Chapter 6 have shown that intracrystalline swelling is the predominant mechanism for clay swelling in the Hilbersdorf Tuff. The osmotic swelling on the other hand has only a minor influence on the clay swelling. Therefore, with a clay mineral analyses at hand, the swelling experiments proved to be a useful tool to differentiate between these two clay swelling mechanisms in tuff rocks. Swelling reducer on the market, like the Antihygro used in Chapter 7, provide for the inhibition of intracrystalline swelling by cation exchange. Until further studies elucidate, if the observations of this study can be transferred to other clay bearing tuff rocks, it is to be expected, that no other mechanism may inhibit the clay swelling in tuff rocks more effectively than these swelling reducer currently do.
- Another important finding of Chapter 6 is the importance of the location of the clay minerals in the tuff rock. SEM photomicrographs showed that even small amounts of swellable clay minerals can cause significant expansion of the material if they are located in critical spots in the rock fabric. The role of the disjoining pressure is still unclear. New analytical techniques have to be developed to quantify its role in moisture expansion of tuff rocks.
- This seems of particular interest, because the study showed, that not all moisture expansion can be attributed to swellable clays and another mechanism has to be involved in the expansion of HR (XRD on separated clay fractions proved almost absence of swellable clay minerals). The non-swellable clay minerals in HR can passively contribute to the swelling process by their microporosity, if disjoining pressure is at play.
- As demonstrated on the example of the Hilbersdorf tuff, the amount of micropores can allow estimations of their possible impact on the intensity of moisture expansion, but only with a closer examination of the pore classes reliable information can be received regarding their contribution to the swelling process. Once more the importance of the characterization of the pore space properties is highlighted.

### Chapter 7 – Consolidation of volcanic tuffs

The consolidation of volcanic tuffs is a challenging topic. Many products that proved to produce satisfying results for other types of porous stones fail in the application on tuff. Essential problems are the water retention of some tuffs and small nanopores that aggravate the absorption of the consolidant. The main goals of this study were:

- (1) to investigate the general suitability and influence of TEOS and TMOS on the petrophysical properties and material behavior of different types of tuffs
- (2) to determine the effects of a primer component (tartaric acid) and anti-swelling agent (Antihydro) on consolidation treatments of different volcanic tuffs
- (3) to investigate if TMOS, due to the smaller molecule size of its monomers, is being absorbed more effectively than common TEOS products

The evaluation of the petrophysical properties before and after the consolidation with TEOS and TMOS identified varying efficiency and suitability for different types of tuff. Some findings of this laboratory investigation may also prove useful for the practical in-situ application:

- The effect of the consolidation with both TEOS and TMOS is generally higher on clay and zeolite-rich, low porous tuffs. Comparing the effectiveness of both consolidants, TEOS appears to induce modifications of the petrophysical properties more effectively on highly porous rock, while TMOS showed to be more effective on low porous tuffs.
- The pretreatment with tartaric acid significantly enhanced the effects of TEOS, both beneficial and unfavorable. In this regard a benefit-risk assessment is crucial before the practical application. For example, does an increased strengthening effect outweigh a potential increase in expansional behavior? An enhancing effect of the primer to the degree observed for TEOS cannot be noted for TMOS.
- In combination with TEOS and TMOS, the anti-swelling agent significantly counteracted the increasing hydric expansion, originating from the consolidants.
- The anti-swelling agent showed almost exclusively positive modifications of the stone properties and may be applied in most cases without expecting negative side effects if the tuffs are rich in swelling clays. The highly porous tuffs containing no (HR, WB) or barely (SMA) swelling clay minerals, did show salt efflorescence after the application of the anti-swelling agent which itself is a salt (1,4-Diaminobutane dihydrochloride). It can be assumed that the Antihydro is causing the excess of salt in these tuffs, since the specimens of the same lithology that were not treated with Antihydro did not show any efflorescence. The two molecules of dihydrochloride in diaminobutane dihydrochloride dissociate in aqueous solution and produce two  $\text{Cl}^-$  that may react with cations of alkaline or alkaline earth metals, namely Na, K, Mg and Ca, and form corresponding halides. The most natural halide to crystallize under ambient conditions (20 °C, RH < 70 %) is sodium chloride or halite. SMA and HR experienced an increasing contractional behavior upon wetting after the treatment with Antihydro. Steiger et al. (2011) state that such contractional behavior upon wetting, points to the fact that salt crystals, build in the pore space from the excess salt during dry periods, induce constant crystallization pressure to the stone fabric. The stone fabric that is therefore under expansion

## 8 General conclusions

during dry conditions, will contract upon wetting and subsequent dissolution of the salt crystals. In the case of recurring wet-dry cycles, the salt will induce progressive damage to the stones, which underlines the importance of a desalination prior to the consolidation. Considering the relatively low hydric expansion values of untreated HR, SMA and WB, the application of an anti-swelling agent does not seem to benefit its petrophysical modification enough to outweigh a slight decrease of hydric expansion. In conclusion, it seems only recommendable to apply Antihygro on tuffs when an inhibition of the hydric expansion is truly needed and never as a prophylactic measure, as there is a risk of excessive salt efflorescence. In any case, if salt efflorescence is visible, the stone should be desalinated prior to the consolidation treatment.

- Low porous tuffs absorbed TMOS significantly stronger than TEOS (Fig. 7.4), with drawbacks only in exceptional cases. The partly extreme change of the pore size character due to the shift of pore classes towards single digit nanopores suggest that the TMOS either entered and precipitated inside the smaller micropores (clogging of pore throats). Or the silica gel itself caused an extreme amount of secondary micropores, for example due to dry cracks as a result of the polycondensation. SEM photomicrographs of TMOS treated tuff revealed, that both is the case (Fig. 7.18).

In summary, this study provides a variety of data that indicates, that TMOS may be a suitable candidate to overcome the bottlenecks in the pore space of tuffs, which limit the consolidation success of current products. Note that the study was conducted under controlled laboratory conditions on fresh quarry material. The samples were first preconditioned and then fully saturated during the consolidation, to guarantee the same conditions for every stone and identify general suitability. On-site application would neither allow such controlled preconditioning of the stone (building elements), nor a full saturation with the consolidant. The results of the treatment of unweathered material are moreover not transferable one-to-one to weathered material, which may show entirely altered pore space, for example due to the creation of cracks. The next step should be the investigation of the depth profile of suitable candidates and the characterization of their capillary absorption of the consolidants. Regarding the strength increase due to a consolidation measure, Doehne and Price (2010) refer to the results of Félix (1996) and Scherer and Jiménez-González (2008), who observed a loss of the initially increased strength in consolidated clay-bearing stones, after only three to ten dry/wet cycles. Subsequent steps should be the durability testing of the consolidation in long term experiments and a potential application on on-site test fields. Our investigation demonstrates that supplementary treatments of both TEOS and TMOS could be also conceivable. Once more it has to be highlighted that prior to every practical on-site application, extensive preliminary investigations have to be undertaken, to maximize the desired consolidation effect and minimize the risk of causing irreversible damage.

## 9 References

- Adamia S, Zakariadze G, Chkhotua T, Sadradze N, Tsereteli N, Chabukiani A, Gventsadze A (2011) Geology of the Caucasus: A review. *Turkish Journal of Earth Sciences* 20:489–544
- Akın M, Özvan A, Dinçer İ, Topal T (2017) Evaluation of the physico-mechanical parameters affecting the deterioration rate of Ahlat ignimbrites (Bitlis, Turkey). *Environmental earth sciences* 76:827
- Allen MB, Armstrong HA (2008) Arabia–Eurasia collision and the forcing of mid-Cenozoic global cooling. *Palaeogeography, Palaeoclimatology, Palaeoecology* 265:52–58
- Allen MB, Kheirkhah M, Neill I, Emami MH, McLeod CL (2013) Generation of arc and within-plate chemical signatures in collision zone magmatism: Quaternary lavas from Kurdistan Province, Iran. *Journal of petrology* 54:887–911
- Auras M, Egloffstein P, Steindlberger E (2000) Vulkanische Tuffsteine—Entstehung, Verwitterung, Konservierung. *IFS-Bericht, Mainz* 10:35–52
- Auras M, Steindlberger E (2005) Verwitterung und Festigung vulkanischer Tuffe. *Zeitschrift der Deutschen Gesellschaft für Geowissenschaften*:167–175
- Aydan Ö, Ulusay R (2003) Geotechnical and geoenvironmental characteristics of man-made underground structures in Cappadocia, Turkey. *Engineering Geology* 69:245–272
- Azizi H, Moinevaziri H (2009) Review of the tectonic setting of Cretaceous to Quaternary volcanism in northwestern Iran. *Journal of Geodynamics* 47:167–179
- Barahim AA, Al-Akhaly IA, Is' haq RS (2017) Engineering Properties of Volcanic Tuff from the Western Part of Yemen. *Sultan Qaboos University Journal for Science [SQUJS]* 22:81–88
- Barbero-Barrera MM, Flores-Medina N, Moreno-Fernández E (2019) Thermal, physical and mechanical characterization of volcanic tuff masonries for the restoration of historic buildings. *Materiales de Construcción* 69. <https://doi.org/10.3989/MC.2019.12917>
- Benavente D, Cueto N, Martínez-Martínez J, Del Cura MG, Cañaveras JC (2007) The influence of petrophysical properties on the salt weathering of porous building rocks. *Environmental geology* 52:215–224
- Benavente D (2011) Why pore size is important in the deterioration of porous stones used in the built heritage. 1885-7264
- Benavente D, del Cura MG, Fort R, Ordóñez S (2004) Durability estimation of porous building stones from pore structure and strength. *Engineering Geology* 74:113–127
- Beyhan S, Sensogut C, Özgür A, Yuvka S (2018) The Effect of Freeze-Thaw Cycles on Physical-Mechanical Properties of Tuff. In: Çınar Ö (ed) *ICENS Proceedings 2018*
- Bianchetti PL, Lombardi G, Marini S, Meucci C (1990) The volcanic rocks of the monuments of the Forum and Palatine (Rome): characterization, alterations, and results of chemical

## 8 General conclusions

- treatments. In: Charola AE (ed) *Lavas and volcanic tuffs: Proceedings of the international meeting, Easter Island, Chile, 25 - 31 October, 1990*. ICCROM, Rome, pp 83–105
- Binal A (2009) Prediction of mechanical properties of non-welded and moderately welded ignimbrite using physical properties, ultrasonic pulse velocity, and point load index tests. *Quarterly journal of engineering geology and hydrogeology* 42:107–122
- Bodnár N, Kovács J, Török Á (2011) Multivariate analysis of Miocene sediments: Rákóczi Square, new metro station area, Budapest, Hungary. *Central European Geology* 54:391–405
- Boek ES, Coveney PV, Skipper NT (1995) Monte Carlo molecular modeling studies of hydrated Li-, Na-, and K-smectites: Understanding the role of potassium as a clay swelling inhibitor. *Journal of the American Chemical Society* 117:12608–12617
- Bozdağ A, Ince I (2018) Predicting strength parameters of igneous rocks from slake durability index. *Afyon Kocatepe Üniversitesi Fen Ve Mühendislik Bilimleri Dergisi* 18:1102–1109
- Bozdağ A, Bayram AF, İnce İ, Asan K (2016) The relationship between weathering and welding degree of pyroclastic rocks in the Kilistra ancient city, Konya (Central Anatolia, Turkey). *Journal of African Earth Sciences* 123:1–9
- Bullmann B (2001) *Vergleichende Untersuchungen unteschiedlicher Steinfestiger auf Kieselsäureesterbasis*. Diplomarbeit, FH Wiesbaden
- Büttgenbach T (1990) *Statistische Untersuchungen der Geschwindigkeits-Dichte Relation in kristallinen Gesteinen auf der Basis einer Datenbank*. na
- Calcaterra D, Cappelletti P, Langella A, Morra V, Colella A, Gennaro R de (2000) The building stones of the ancient centre of Naples (Italy): Piperno from Campi Flegrei: A contribution to the knowledge of a long-time-used stone. *Journal of Cultural Heritage* 1:415–427
- Calcaterra D, Cappelletti P, Langella A, Colella A, Gennaro M de (2004) The ornamental stones of Caserta province: the Campanian Ignimbrite in the medieval architecture of Casertavecchia. *Journal of Cultural Heritage* 5:137–148
- Calcaterra D, Langella A, Gennaro R de, de'Gennaro M, Cappelletti P (2005) Piperno from Campi Flegrei: a relevant stone in the historical and monumental heritage of Naples (Italy). *Environmental geology* 47:341–352
- Çelik SB, Çobanoğlu İ (2019) Comparative investigation of Shore, Schmidt, and Leeb hardness tests in the characterization of rock materials. *Environmental earth sciences* 78:554
- Çelik MY, Aygün A (2019) The effect of salt crystallization on degradation of volcanic building stones by sodium sulfates and sodium chlorides. *Bulletin of Engineering Geology and the Environment* 78:3509–3529
- Çelik MY, Ergül A (2015) The influence of the water saturation on the strength of volcanic tuffs used as building stones. *Environmental earth sciences* 74:3223–3239

## 8 General conclusions

- Çelik MY, Ergül A (2018) Pore characterization of volcanic tuffs used as building stone in Afyonkarahisar (Turkey). *Politeknik Dergisi* 21:101–112
- Çelik MY, Kaçmaz AU (2016) The investigation of static and dynamic capillary by water absorption in porous building stones under normal and salty water conditions. *Environmental earth sciences* 75:307
- Çelik MY, Sert M (2020) The role of different salt solutions and their concentration ratios in salt crystallization test on the durability of the Döğür tuff (Afyonkarahisar, Turkey) used as building stones of cultural heritages. *Bulletin of Engineering Geology and the Environment*:1–16. <https://doi.org/10.1007/s10064-020-01896-7>
- Çelik MY, Akbulut H, Ergül A (2014) Water absorption process effect on strength of Ayazini tuff, such as the uniaxial compressive strength (UCS), flexural strength and freeze and thaw effect. *Environmental earth sciences* 71:4247–4259
- Chang F-RC, Skipper NT, Sposito G (1998) Monte Carlo and molecular dynamics simulations of electrical double-layer structure in potassium–montmorillonite hydrates. *Langmuir* 14:1201–1207
- Chen TC, Yeung, Mori N (2004) Effect of water saturation on deterioration of welded tuff due to freeze-thaw action. *Cold Regions Science and Technology* 38:127–136
- Christidis GE (2013) Assessment of industrial clays. In: *Developments in Clay Science*, vol 5. Elsevier, pp 425–449
- Colella A, Calcaterra D, Cappelletti P, Langella A, Papa L, Gennaro M de (2009) I tuffi zeolitizzati nell'architettura della Campania. *La diagnostica per il restauro del patrimonio culturale*:327–341
- Colella A, Di Benedetto C, Calcaterra D, Cappelletti P, D'Amore M, Di Martire D, Graziano SF, Papa L, Gennaro M de, Langella A (2017) The Neapolitan Yellow Tuff: an outstanding example of heterogeneity. *Construction and Building Materials* 136:361–373
- Columbu S, Gioncada A, Lezzerini M, Marchi M (2014) Hydric dilatation of ignimbritic stones used in the church of Santa Maria di Otti (Oschiri, northern Sardinia, Italy). *Italian Journal of Geosciences* 133:149–160
- Correns CW, Steinborn W (1939) Experimente zur Messung und Erklärung der sogenannten Kristallisationskraft. *Zeitschrift für Kristallographie-Crystalline Materials* 101:117–133
- Cueto Mendoza N, Vieira De Sousa, José F, Fernandes C, Benavente D, Urbani F, Meza R, Santos Pernetá JP, García del Cura M (2018) Water transport in lapilli tuff from Madeira Iland, Portugal: implications on degradation mechanisms and durability. In: *Atas do 16º Congresso Nacional de Geotecnia*
- Davarpanah SM, Ván P, Vásárhelyi B (2020) Investigation of the relationship between dynamic and static deformation moduli of rocks. *Geomechanics and Geophysics for Geo-Energy and Geo-Resources* 6:1–14



## 8 General conclusions

- De la Calle C, Suquet H (1988) Vermiculite. *Reviews in Mineralogy and Geochemistry* 19:455–496
- Derjaguin BV, Obukov EV (1936) Anomalien dünner Flüssigkeitsschichten III *Acta Physicochim. URSS* 5:1–22
- Dhilawala S (1997) *Armenia. Cultures of the world*. Marshall Cavendish, New York
- Di Benedetto C (2012) Evaluation of petrophysical parameters of the Neapolitan Yellow Tuff and the Vicenza Stone: Experimental investigation on conservation of macroporous building stones. *Plinius* 38
- Dinçer I, Acar A, Çobanoğlu I, Uras Y (2004) Correlation between Schmidt hardness, uniaxial compressive strength and Young's modulus for andesites, basalts and tuffs. *Bulletin of Engineering Geology and the Environment* 63:141–148
- Dinçer İ, Bostancı M (2019) Capillary water absorption characteristics of some Cappadocian ignimbrites and the role of capillarity on their deterioration. *Environmental earth sciences* 78:7
- Dixon JB, Weed SB (1989) *Minerals in soil environments*. Soil Science Society of America Inc.(SSSA)
- Doehne E (2002) Salt weathering: a selective review. Geological society, London, special publications 205:51–64
- Doehne E, Price CA (2010) Stone conservation: an overview of current research. An overview of Current Research. Getty Conservation Institute (ed). Canada
- Dohrmann R, Kaufhold S (2009) Three new, quick CEC methods for determining the amounts of exchangeable calcium cations in calcareous clays. *Clays and Clay Minerals* 57:338–352
- Dohrmann R, Kaufhold S (2010) Determination of exchangeable calcium of calcareous and gypsiferous bentonites. *Clays and Clay Minerals* 58:79–88
- Doveton JH (1987) Log analysis of petrofacies and lithofacies. GFZ Logging Course. Geoforschungszentrum Potsdam, Potsdam
- Egloffstein P (1998) *Vulkanische Tuffsteine als Werksteine an historischen Bauwerken in Ungarn und Deutschland–Verwitterungsverhalten und Konservierungskonzepte* (1998)
- Emir E, Konuk A, Daloğlu G (2011) Strength enhancement of Eskisehir tuff ashlar in Turkey. *Construction and Building Materials* 25:3014–3019
- Engidasew TA (2014) Engineering geological characterization of volcanic rocks of Ethiopian and Sardinian highlands to be used as construction materials. Dissertation, Università di Cagliari
- Ergenç D, Saltık ENC, Topal T (2016) Antique stone quarries in Turkey: a case study on tuffs in the Temple of Apollon Smintheus. Geological society, London, special publications 416:133–144

## 8 General conclusions

- Erguler ZA, Ulusay R (2009) Water-induced variations in mechanical properties of clay-bearing rocks. *International Journal of Rock Mechanics and Mining Sciences* 46:355–370
- Eulenberger S, Tunger B, Fischer F (1995) Neue Erkenntnisse zur Geologie des Zeisigwaldes bei Chemnitz. *Veröffentlichungen Museum für Naturkunde Chemnitz* 18:25–34
- Félix C (1996) Peut-on consolider les grès tendres du Plateau suisse avec le silicate d'éthyle? In: *Preservation and restoration of cultural heritage: proceedings of the 1995 LCP Congress, Montreux, 24-29 September 1995= Conservation et restauration des biens culturels: actes du congrès LCP 1995, Montreux, 24-29 septembre 1995*, pp 267–274
- Fischer F (1990) Lithologie und Genese des Zeisigwald-Tuffs (Rotliegendes, Vorerzgebirgs-Senke). *Veröffentlichungen des Museums für Naturkunde Chemnitz* 14:61–74
- Fisher RV (1961) Proposed classification of volcanoclastic sediments and rocks. *Geological Society of America Bulletin* 72:1409–1414
- Fisher RV (1966) Rocks composed of volcanic fragments and their classification. *Earth-Science Reviews* 1:287–298
- Fisher RV, Schmincke H-U (2012) *Pyroclastic rocks*. Springer Science & Business Media
- Fitzner B, Basten D (1994) Gesteinsporosität--Klassifizierung, meßtechnische Erfassung und Bewertung ihrer Verwitterungsrelevanz. In: *Jahresberichte aus dem Forschungsprogramm Steinzerfall, Steinkonservierung*. Band 4, 1992, pp 19–32
- Fitzner B, Sneath R (1982) Einfluss der Porenradialverteilung auf das Verwitterungsverhalten ausgewählter Sandsteine. *Bautenschutz+ Bausanierung* 1982:97–103
- Flatt RJ (2002) Salt damage in porous materials: how high supersaturations are generated. *Journal of Crystal Growth* 242:435–454
- Fratini C, Manganelli del Fa C, Pecchioni E, Scala A (1990) The sculptures in Bomarzo Park, Viterbo, Italy. In: Charola AE (ed) *Lavas and volcanic tuffs: Proceedings of the international meeting, Easter Island, Chile, 25 - 31 October, 1990*. ICCROM, Rome, pp 129–141
- Gasparyan MA, Safaryan YA (2014) The Problem of Preservation of National Traditions in Modern Armenian Architecture. *Advanced Materials Research*
- Germinario L, Török Á (2019) Variability of technical properties and durability in volcanic tuffs from the same quarry region—examples from Northern Hungary. *Engineering Geology* 262:105319
- Germinario L, Siegesmund S, Maritan L, Mazzoli C (2017) Petrophysical and mechanical properties of Euganean trachyte and implications for dimension stone decay and durability performance. *Environmental earth sciences* 76:739
- Ghobadi MH, Beydokhti AT, Nikudel, Asiabanha A, Karakus M (2016) The effect of freeze–thaw process on the physical and mechanical properties of tuff. *Environmental earth sciences* 75:846

## 8 General conclusions

- Gioncada A, Gonzalez-Ferran O, Lezzerini M, Mazzuoli R, Bisson M, Rapu SA (2010) The volcanic rocks of Easter Island (Chile) and their use for the Moai sculptures. *European Journal of Mineralogy* 22:855–867
- Gioncada A, Leoni L, Lezzerini M, Miriello D (2011) Relationships between mineralogical and textural factors in respect to hydric dilatation of some sandstones and meta-sandstones from the Northern Apennine. *Italian Journal of Geosciences* 130:394–403
- Gonzalez IJ, Scherer GW (2004) Effect of swelling inhibitors on the swelling and stress relaxation of clay bearing stones. *Environmental geology* 46:364–377
- González J, Saldaña M, Arzúa J (2019) Analytical Model for Predicting the UCS from P-Wave Velocity, Density, and Porosity on Saturated Limestone. *Applied Sciences* 9:5265
- Graf v. Reichenbach H, Beyer J (1995) Dehydration and rehydration of vermiculites. II: Phlogopitic CA-vermiculite. *Clay minerals* 30:273–286
- Gregg SJ, Sing KSW, Gregg SJ, Sing KS (1982) Adsorption, surface area and porosity, 2nd edn. Academic Press, London
- Hashemi M, Basmenj AK, Banikheir M (2018) Engineering geological and geoenvironmental evaluation of UNESCO World Heritage Site of Meymand rock-hewn village, Iran. *Environmental earth sciences* 77:3
- Hashiba K, Fukui K (2015) Effect of water on the deformation and failure of rock in uniaxial tension. *Rock Mechanics and Rock Engineering* 48:1751–1761
- Heap MJ, Baud P, Meredith PG, Vinciguerra S, Reuschlé T (2014) The permeability and elastic moduli of tuff from Campi Flegrei, Italy: implications for ground deformation modelling. *Solid Earth* 5:25–44
- Heap MJ, Farquharson JI, Kushnir ARL, Lavallée Y, Baud P, Gilg HA, Reuschlé T (2018) The influence of water on the strength of Neapolitan Yellow Tuff, the most widely used building stone in Naples (Italy). *Bulletin of Volcanology* 80:51.  
<https://doi.org/10.1007/s00445-018-1225-1>
- Hernández Gutiérrez LE (2014) Caracterización geomecánica de las rocas volcánicas de las Islas Canarias. Dissertation, Universidad de La Laguna
- Hirschwald J (1908) Die Prüfung der natürlichen Bausteine auf ihre Wetterbeständigkeit. W. Ernst & Sohn
- Hirschwald J (1912) Die Prüfung der natürlichen Bausteine auf ihre Wetterbeständigkeit. W. Ernst & Sohn, Berlin
- Hosono T, Uchida E, Suda C, Ueno A, Nakagawa T (2006) Salt weathering of sandstone at the Angkor monuments, Cambodia: Identification of the origins of salts using sulfur and strontium isotopes. *Journal of Archaeological Science* 33:1541–1551

## 8 General conclusions

- İnce İ, Fener M (2016) A prediction model for uniaxial compressive strength of deteriorated pyroclastic rocks due to freeze–thaw cycle. *Journal of African Earth Sciences* 120:134–140
- İnce İ, Bozdağ A, Fener M, Kahraman S (2019) Estimation of uniaxial compressive strength of pyroclastic rocks (Cappadocia, Turkey) by gene expression programming. *Arabian Journal of Geosciences* 12:756
- Jackson MD, Marra F, Hay RL, Cawood C, Winkler EM (2005) The judicious selection and preservation of tuff and travertine building stone in ancient Rome. *Archaeometry* 47:485–510
- Jamshidi A, Nikudel MR, Khamechiyan M (2013) Estimating the durability of building stones against Salt crystallization: considering the physical properties and strength characteristics. *Geopersia* 3:35–48
- Jamshidi A, Zamanian H, Sahamieh RZ (2018) The effect of density and porosity on the correlation between uniaxial compressive strength and P-wave velocity. *Rock Mechanics and Rock Engineering* 51:1279–1286
- Jentsch F (2012) Steine in der Stadt Chemnitz. In: Chemnitzer Roland, vol 56. Chemnitzer Journalistische Vereinigung, pp 19–23
- Kaljahi EA, Birami FA (2015) Engineering geological properties of the pyroclastic cone-shaped rocky houses of Kandovan, Iran. *Bulletin of Engineering Geology and the Environment* 74:959–969. <https://doi.org/10.1007/s10064-014-0679-4>
- Karapetian SG, Jrbashian RT, Mnatsakanian AK (2001) Late collision rhyolitic volcanism in the north-eastern part of the Armenian Highland. *Journal of Volcanology and Geothermal Research* 112:189–220
- Kaufhold S, Dohrmann R, Klinkenberg M, Siegesmund S, Ufer K (2010) N<sub>2</sub>-BET specific surface area of bentonites. *Journal of colloid and interface science* 349:275–282
- Keskin M (2007) Eastern Anatolia: A hotspot in a collision zone without a mantle plume. *SPECIAL PAPERS-GEOLOGICAL SOCIETY OF AMERICA* 430:693
- Kılıç A, Teymen A (2008) Determination of mechanical properties of rocks using simple methods. *Bulletin of Engineering Geology and the Environment* 67:237
- Kılıç A, Teymen A, Özdemir O, Atış CD (2019) Estimation of Compressive Strength of Concrete Using Physico-Mechanical Properties of Aggregate Rock. *Iranian Journal of Science and Technology, Transactions of Civil Engineering* 43:171–178
- Kleb B, Vászrhelyi B (2003) Test results and empirical formulas of rock mechanical parameters of rhyolitic tuff samples from Eger's cellars. *Acta Geologica Hungarica* 46:301–312
- Klopfer H (1985) Feuchte. In: Klopfer H (ed) *Lehrbuch der Bauphysik*

## 8 General conclusions

- Kocher M (2005) Quelldruckmessungen und thermische Druckmessungen an ausgewählten Sandsteinen. Dissertation
- Koizumi M (1953) The differential thermal analysis curves and the dehydration curves of zeolites. *Mineralogical Journal* 1:36–47
- Koralay T, Çelik SB (2019) Minero-petrographical, physical, and mechanical properties of moderately welded ignimbrite as a traditional building stone from Uşak Region (SW Turkey). *Arabian Journal of Geosciences* 12:732
- Koralay T, Özkul M, Kumsar H, Celik SB, Pektaş K (2011) The effect of welding degree on geotechnical properties of an ignimbrite flow unit: the Bitlis castle case (eastern Turkey). *Environmental earth sciences* 64:869–881
- Korat L, Mirtič B, Mladenovič A, Pranjić AM, Kramar S (2015) Formulation and microstructural evaluation of tuff repair mortar. *Journal of Cultural Heritage* 16:705–711
- Korkanç M, Solak B (2016) Estimation of engineering properties of selected tuffs by using grain/matrix ratio. *Journal of African Earth Sciences* 120:160–172
- Korkanç M, Tuğrul A, Savran A, Özgür FZ (2015) Structural–geological problems in Gümüşler archeological site and monastery. *Environmental earth sciences* 73:4525–4540
- Korkuna O, Lebeda R, Skubiszewska-Zie J, Vrublevs'ka T, Gun'ko VM, Ryczkowski J (2006) Structural and physicochemical properties of natural zeolites: clinoptilolite and mordenite. *Microporous and Mesoporous Materials* 87:243–254
- Kral A (2014) Tuffsteine in Querétaro-City (México): Schadensanalyse, Verwitterungsverhalten und gesteintechnische Untersuchungen. Bachelorarbeit, Georg-August-Universität
- Kück A (2019) Weathering behaviour and petrophysical properties of volcanic tuff as historical building stone in Oaxaca, Mexico. Masterarbeit, Georg-August-Universität
- Kück A, Pöttl C, López-Doncel RA, Dohrmann R, Siegesmund S (2020a) Effects of zeolites and swellable clay minerals on water related properties and thermal dilatation in volcanic tuff rocks. In: Siegesmund S, Middendorf B (eds) *Monument Future: Decay and Conservation of Stone*, 1st edn. Mitteldeutscher Verlag, Halle
- Kück A, Pöttl C, López-Doncel RA, Dohrmann R, Siegesmund S (2020b) Weathering behavior and petrophysical properties of the natural building stones used in the archeological site of Mitla and colonial buildings in Oaxaca, Mexico. In: Siegesmund S, Middendorf B (eds) *Monument Future: Decay and Conservation of Stone*, 1st edn. Mitteldeutscher Verlag, Halle
- La Russa MF, Ruffolo SA, Buergo MÁ de, Ricca M, Belfiore CM, Pezzino A, Crisci GM (2017) The behaviour of consolidated Neapolitan yellow Tuff against salt weathering. *Bulletin of Engineering Geology and the Environment* 76:115–124
- Lange P, Steiner W (1974) Der Rochlitzer Porphyrtuff und seine Anwendung im Bauwesen der DDR. *Zeitschrift für angewandte Geologie* 20:520–525

## 8 General conclusions

- Langella A, Bish D, Calcaterra D, Cappelletti P, Cerri G, Colella A, de'Gennaro R, Papa L, Graziano S, Perrotta A, Scarpati C, de'Gennaro M (2013) L'ignimbrite Campana (IC). In: Gennaro M de, Calcaterra D, Langella A (eds) *Le Pietre Storiche della Campania-dall'oblio alla riscoperta*. Luciano Editore
- Laurenzi Tabasso M, Am Mecchi, Santamaria U (1990) Interaction between volcanic tuffs and products used for consolidation and waterproofing treatment. In: Charola AE (ed) *Lavas and volcanic tuffs: Proceedings of the international meeting, Easter Island, Chile, 25 - 31 October, 1990*. ICCROM, Rome, pp 245–267
- Le Bas MJ, Le Maitre RW, Streckeisen A, Zanettin B (1986) A chemical classification of volcanic rocks based on the total alkali-silica diagram. *Journal of petrology* 27:745–750
- Le Maitre RW, Bateman P, Dudek A, Keller J, Lameyre J, Le BAS MJ, Sabine PA, Schmid R, Sorensen H, Streckeisen A (1989) A classification of igneous rocks and glossary of terms. Recommendations of the IUGS Subcommission on the Systematics of Igneous rocks. London: Blackwell Scientific Publications
- Le Maitre RW, Streckeisen A, Zanettin B, Le BAS MJ, Bonin B, Bateman P (2002) *Igneous Rocks: A Classification and Glossary of Terms: Recommendations of the International Union of Geological Sciences Subcommission on the Systematics of Igneous Rocks*, 2nd edn. Cambridge University Press, Cambridge
- Leiser T (2013) *Verwitterungscharakteristik von Tuff-Werksteinen in San Miguel de Allende (Mexiko): Schadensanalyse und gesteintechnische Eigenschaften*. Masterarbeit, Georg-August-Universität
- Li L, Tan Y, Huang B, Deng X (2020) Pore property as an indicator of macro-deterioration in slightly weathered tuffs. *Engineering Geology* 267:105492
- Lindner K (1994) *Die Naturwerksteine des Landkreises Altenburg*. Diplomarbeit, Bauhaus-Universität Weimar
- Liu J-b, Zhang Z-j, Li B (2019) Microscopic & macroscopic characterizations of Beijing marble as a building material for UNESCO heritage sites: New insights into physico-mechanical property estimation and weathering resistance. *Construction and Building Materials* 225:510–525
- Llanes-Monter MM, Olguín MT, Solache-Ríos MJ (2007) Lead sorption by a Mexican, clinoptilolite-rich tuff. *Environmental Science and Pollution Research-International* 14:397–403
- López-Arce P, Fort R, Gómez-Heras M, Pérez-Monserrat E, Varas-Muriel MJ (2011) Preservation strategies for avoidance of salt crystallisation in El Paular Monastery cloister, Madrid, Spain. *Environmental earth sciences* 63:1487–1509
- López-Doncel R, Wedekind W, Dohrmann R, Siegesmund S (2013) Moisture expansion associated to secondary porosity: An example of the Loseros Tuff of Guanajuato, Mexico. *Environmental earth sciences* 69:1189–1201

## 8 General conclusions

- López-Doncel R, Wedekind W, Leiser T, Molina-Maldonado S, Velasco-Sánchez A, Dohrmann R, Kral A, Wittenborn A, Aguillón-Robles A, Siegesmund S (2016) Salt bursting tests on volcanic tuff rocks from Mexico. *Environmental earth sciences* 75:212
- López-Doncel R, Wedekind W, Aguillón-Robles A, Dohrmann R, Molina-Maldonado S, Leiser T, Wittenborn A, Siegesmund S (2018) Thermal expansion on volcanic tuff rocks used as building stones: examples from Mexico. *Environmental earth sciences* 77:338
- Lubelli B, van Hees RPJ, Nijland TG (eds) (2014) Salt crystallization damage: how realistic are existing ageing tests?
- Lubelli B, Nijland TG, Tolboom H-J (2018a) Moisture induced weathering of volcanic tuffstone. *Construction and Building Materials* 187:1134–1146
- Lubelli B, Cnudde V, Diaz-Goncalves T, Franzoni E, van Hees RPJ, Ioannou I, Menendez B, Nunes C, Siedel H, Stefanidou M (2018b) Towards a more effective and reliable salt crystallization test for porous building materials: State of the art. *Materials and Structures* 51:55
- Lukaszewicz JW (1990) The application of silicone products in the conservation of volcanic tuffs. In: Charola AE (ed) *Lavas and volcanic tuffs: Proceedings of the international meeting, Easter Island, Chile, 25 - 31 October, 1990*. ICCROM, Rome, pp 191–202
- Marmoni GM, Martino S, Heap MJ, Reuschlé T (2017a) Gravitational slope-deformation of a resurgent caldera: New insights from the mechanical behaviour of Mt. Nuovo tuffs (Ischia Island, Italy). *Journal of Volcanology and Geothermal Research* 345:1–20
- Marmoni GM, Martino S, Heap MJ, Reuschlé T (2017b) Multiphysics laboratory tests for modelling gravity-driven instabilities at slope scale. *Procedia Engineering* 191:142–149
- Masuda K (2001) Effects of water on rock strength in a brittle regime. *Journal of Structural Geology* 23:1653–1657
- Meier L, Kahr G (1999) Determination of the cation exchange capacity (CEC) of clay minerals using the complexes of copper (II) ion with triethylenetetramine and tetraethylenepentamine. *Clays Clay Miner* 47:386–388
- Meliksetian K, Savov I, Connor C, Halama R, Jrbashyan R, Navasardyan G, Ghukasyan Y, Gevorgyan H, Manucharyan D, Ishizuka O (eds) (2014) *Aragats stratovolcano in Armenia-volcano-stratigraphy and petrology*, vol 16
- Mirwald P (1997) *Physikalische Eigenschaften der Gesteine*. Ebner Verlag, Ulm
- Molina-Maldonado S (2016) *Estudios geológicos, petrográficos, geoquímicos y geotécnicos en las rocas de construcción del centro histórico de Santiago de Querétaro y su comportamiento al intemperismo*. Masterarbeit, Universidad Autonoma de San Luis Potosi
- Möllenkamp E (1996) *Möglichkeiten der Tuffsteinkonservierung: Die Portalfiguren des Kölner Rathauses. Kölner Beiträge zur Restaurierung und Konservierung von Kunst- und Kulturgut*, vol 4. Anton Siegl GmbH Fachbuchhandlung, München

## 8 General conclusions

- Moon VG (1993) Geotechnical characteristics of ignimbrite: A soft pyroclastic rock type. *Engineering Geology* 35:33–48
- Moore DM, Reynolds RC (1989) X-ray Diffraction and the Identification and Analysis of Clay Minerals, vol 378. Oxford university press, Oxford
- Morales Demarco M, Jahns E, Rüdric J, Oyhantcabal P, Siegesmund S (2007) The impact of partial water saturation on rock strength: an experimental study on sandstone. *Zeitschrift der Deutschen Gesellschaft für Geowissenschaften* 158:869–882
- Mosch S, Siegesmund S (2007) Statistisches Verhalten petrophysikalischer und technischer Eigenschaften von Naturwerksteinen [Petrophysical and technical properties of dimensional stones: a statistical approach]. *Zeitschrift der Deutschen Gesellschaft für Geowissenschaften* 158:821–868
- Mumpton FA (1973) First reported occurrence of zeolites in sedimentary rocks of Mexico. *American Mineralogist: Journal of Earth and Planetary Materials* 58:287–290
- Neill I, Meliksetian K, Allen MB, Navarsardyan G, Karapetyan S (2013) Pliocene–Quaternary volcanic rocks of NW Armenia: Magmatism and lithospheric dynamics within an active orogenic plateau. *Lithos* 180:200–215
- Nijland TG, van Hees RPJ, Bolondi L (2010) Evaluation of three Italian tuffs (Neapolitan Yellow Tuff, Tufo Romano and Tufo Etrusco) as compatible replacement stone for Römer tuff in Dutch built cultural heritage. Geological society, London, special publications 333:119–127
- Nishiura T (1987) Laboratory test on the color change of stone by impregnation with silane. In: ICOM committee for conservation: 8th triennial meeting, Sydney, Australia, 6-11 September, 1987. Preprints, pp 509–512
- Oguchi CT, Yuasa H (2010) Simultaneous wetting/drying, freeze/thaw and salt crystallization experiments of three types of Oya tuff. Geological society, London, special publications 333:59–72
- Okubo S, Nishimatsu Y, He C, CHU SY (1992) Loading rate dependency of uniaxial compressive strength of rock under water-saturated condition. *Zairyo* 41:403–409
- Öner F, Türkmen S, Özbek A, Karakaya T (2006) Engineering properties of Hınıs ignimbrites and their usability as a building stone (Erzurum, Turkey). *Environmental geology* 50:275–284
- Özbek A (2014) Investigation of the effects of wetting–drying and freezing–thawing cycles on some physical and mechanical properties of selected ignimbrites. *Bulletin of Engineering Geology and the Environment* 73:595–609
- Özşen H, Bozdağ A, İnce İ (2017) Effect of salt crystallization on weathering of pyroclastic rocks from Cappadocia, Turkey. *Arabian Journal of Geosciences* 10:258



## 8 General conclusions

- Özvan A, Dinçer İ, Akin M, Oyan V, Tapan M (2015) Experimental studies on ignimbrite and the effect of lichens and capillarity on the deterioration of Seljuk Gravestones. *Engineering Geology* 185:81–95
- Pablo-Galán L de (1986) Geochemical trends in the alteration of Miocene vitric tuffs to economic zeolite deposits, Oaxaca, Mexico. *Applied geochemistry* 1:273–285
- Padilla-Ceniceros R, Pacheco-Martínez J, López-Doncel RA, Orenday-Tapia EE (2017) Rock deterioration in the masonry walls of the Cathedral Basilica of Aguascalientes, Mexico. *Revista Mexicana de Ciencias Geológicas* 34:138–139
- Papa L (2011) I Tufi vulcanici nel costruito storico: vulnerabilità e possibili trattamenti per la conservazione e il restauro. Dissertation, Università degli Studi di Sassari
- Pappalardo G, Punturo R, Mineo S, Contrafatto L (2017) The role of porosity on the engineering geological properties of 1669 lavas from Mount Etna. *Engineering Geology* 221:16–28
- Peschel A (1983) *Natursteine*. VEB Deutscher Verlag für Grundstoffindustrie, Leipzig
- Pola A, Crosta G, Fusi N, Barberini V, Norini G (2012) Influence of alteration on physical properties of volcanic rocks. *Tectonophysics* 566:67–86
- Pola A, Crosta GB, Fusi N, Castellanza R (2014) General characterization of the mechanical behaviour of different volcanic rocks with respect to alteration. *Engineering Geology* 169:1–13
- Poschlod K (1990) *Das Wasser im Porenraum kristalliner Naturwerksteine und sein Einfluss auf die Verwitterung*. Münchener Geowiss Abh B 7
- Pötzl C (2015) *Las Casas Tapadas de Plazuelas - Bauschäden, Verwitterungscharakteristik und gesteintechnische Eigenschaften von Tuffsteinen in Guanajuato, Mexiko*. Masterarbeit, Georg-August-Universität
- Pötzl C, Dohrmann R, Siegesmund S (2018a) Clay swelling mechanism in tuff stones: an example of the Hilbersdorf Tuff from Chemnitz, Germany. *Environmental earth sciences* 77:188
- Pötzl C, Siegesmund S, Dohrmann R, Koning JM, Wedekind W (2018b) Deterioration of volcanic tuff rocks from Armenia: Constraints on salt crystallization and hydric expansion. *Environmental earth sciences* 77:660
- Rodriguez-Navarro C, Doehne E (1999) Time-lapse video and ESEM: integrated tools for understanding processes in situ. *American laboratory* 31:28–35
- Rolland Y, Billo S, Corsini M, Sosson M, Galoyan G (2009) Blueschists of the Amassia-Stepanavan suture zone (Armenia): Linking Tethys subduction history from E-Turkey to W-Iran. *International Journal of Earth Sciences* 98:533–550
- Rolland Y (2017) *Caucasus collisional history: Review of data from East Anatolia to West Iran*. *Gondwana Research* 49:130–146

## 8 General conclusions

- Rossi-Manaresi R, Tuccillo A (1990) Texture and mechanical dis-aggregation of tuffs from Italy and Ecuador. In: Charola AE (ed) *Lavas and volcanic tuffs: Proceedings of the international meeting, Easter Island, Chile, 25 - 31 October, 1990*. ICCROM, Rome, p 73
- Rößler R, Kretzschmar R, Annacker V, Mehlhorn S, Merbitz M, Schneider JW, Luthardt L (2009) Auf Schatzsuche in Chemnitz—Wissenschaftliche Grabungen'09. *Veröffentlichungen des Museums für Naturkunde Chemnitz* 32:25–46
- Rotare HM, Prenzlau CF (1967) Surface areas from mercury porosimetry measurements. *J. Phys. Chem* 71:2733–2736
- Rößler R, Annacker V, Kretzschmar R, Eulenberger S, Tunger B (2008) Auf Schatzsuche in Chemnitz—Wissenschaftliche Grabungen'08. *Veröffentlichungen Museum Naturkunde* 31:5–44
- Rucker S, Pötzl C, Wendler E, Dohrmann R, López-Doncel RA, Siegesmund S (2020) Improved consolidation of volcanic tuff rocks with TEOS. In: Siegesmund S, Middendorf B (eds) *Monument Future: Decay and Conservation of Stone*, 1st edn. Mitteldeutscher Verlag, Halle
- Ruedrich J, Siegesmund S (2006) Fabric dependence of length change behaviour induced by ice crystallisation in the pore space of natural building stones. In: *Heritage, Weathering & Conservation: Proceedings of the International Conference on Heritage, Weathering and Conservation*. Taylor & Francis, p 497
- Ruedrich J, Siegesmund S (2007) Salt and ice crystallisation in porous sandstones. *Environmental geology* 52:225–249
- Ruedrich J, Kirchner D, Seidel M, Siegesmund S (2005) Beanspruchungen von Naturwerksteinen durch Salz- und Eiskristallisation im Porenraum sowie hygroskopische Dehnungsvorgänge. *Zeitschrift der Deutschen Gesellschaft für Geowissenschaften* 156:59–73
- Ruedrich J, Bartelsen T, Dohrmann R, Siegesmund S (2011) Moisture expansion as a deterioration factor for sandstone used in buildings. *Environmental earth sciences* 63:1545–1564
- Sato M, Hattajiri T (2018) A laboratory experiment on salt weathering by humidity change: salt damage induced by deliquescence and hydration. *Progress in Earth and Planetary Science* 5:1–10
- Scherer G, Jiménez-González I (2008) Swelling clays and salt crystallization: The damage mechanisms and the role of consolidants. In: *Stone Consolidation in Cultural Heritage: Research and Practice; Proceedings of the International Symposium, Lisbon, 6–7 May 2008*, pp 29–40
- Scherer GW (1999) Crystallization in pores. *Cement and Concrete research* 29:1347–1358
- Scherer GW, Wheeler GS (2008) Silicate Consolidants for Stone. *KEM* 391:1–25. <https://doi.org/10.4028/www.scientific.net/KEM.391.1>

## 8 General conclusions

- Schmid R (1981) Descriptive nomenclature and classification of pyroclastic deposits and fragments: recommendations of the IUGS Subcommittee on the Systematics of Igneous Rocks. *Geology* 9:41–43
- Schneider JW, Rößler R, Fischer F (2012) Rotliegend des Chemnitz-Beckens (syn. Erzgebirge-Becken). *Stratigraphie von Deutschland X. Rotliegend. Teil I: Innervariscische Becken: Schriftenreihe der Deutschen Gesellschaft für Geowissenschaften* 61:530–588
- Schön JH (2015) *Physical properties of rocks: Fundamentals and principles of petrophysics*. Elsevier
- Schuh H (1987) *Physikalische Eigenschaften von Sandsteinen und ihren verwitterten Oberflächen. Münchner geowissenschaftliche Abhandlungen. Reihe B, Allgemeine und angewandte Geologie, vol 6*. F. Pfeil, München
- Schult A, Shi G (1997) Hydration swelling of crystalline rocks. *Geophysical Journal International* 131:179–186
- Sengun N, Demirdag S, Akbay D, Ugur I, Altindag R, Akbulut A (2014) Investigation of the relationships between capillary water absorption coefficients and other rock properties of some natural stones, V. In: *Global stone congress*, pp 22–25
- Sert M, Özkahraman H (2016) The Importance of Welded Tuff Stones in Construction Industry According to Their Physico-Mechanical Properties. *Harran University Journal of Engineering* 1:8–18
- Sharma PK, Singh TN (2008) A correlation between P-wave velocity, impact strength index, slake durability index and uniaxial compressive strength. *Bulletin of Engineering Geology and the Environment* 67:17–22
- Sheth H, Meliksetian K, Gevorgyan H, Israyelyan A, Navasardyan G (2015) Intracanyon basalt lavas of the Debed River (northern Armenia), part of a Pliocene–Pleistocene continental flood basalt province in the South Caucasus. *Journal of Volcanology and Geothermal Research* 295:1–15
- Shirinyan CG (1962) Volcanic tuffs and tuff lavas of Armenia. *Bulletin Volcanologique* 24:171–175
- Siedel H (1995) *Materialien der Kanzel und des Fundaments*. Arndt Kiesewetter, Heiner Siedel und Michael Stühr (Hg.): *Die Tulpenkanzel im Dom zu Freiberg, Bd 2*:68–74
- Siedel H (2006) Sächsische "Porphyrtuffe" aus dem Rotliegend als Baugesteine: Vorkommen und Abbau, Anwendung, Eigenschaften und Verwitterung. *IFS-Bericht* 22:47–57
- Siedel H (2010) Historic building stones and flooding: changes of physical properties due to water saturation. *Journal of performance of constructed facilities* 24:452–461
- Siedel H (2017) Verwendung, Eigenschaften und Verwitterung von Chemnitzer Zeisigwald-Tuff („Hilbersdorfer Porphyrtuff“) als Bau- und Bildhauergestein. *Veröffentlichungen des Museums für Naturkunde Chemnitz* 40:69–92

## 8 General conclusions

- Siegesmund S, Dürrast H (2011) Physical and mechanical properties of rocks. In: Siegesmund S, Snethlage R (eds) *Stone in architecture*. Springer, pp 97–225
- Siegesmund S, Ullemeyer K, Weiss T, Tschegg EK (2000) Physical weathering of marbles caused by anisotropic thermal expansion. *International Journal of Earth Sciences* 89:170–182
- Siegesmund S, Sousa L, Knell C (2018) Thermal expansion of granitoids. *Environmental earth sciences* 77:41
- Snethlage R (1984) *Steinkonservierung*. Arbeitsheft Bayer. Landesamt f. Denkmalpflege
- Snethlage R, Wendler E, Klemm DD (1995) Tenside im Gesteinsschutz-bisherige Resultate mit einem neuen Konzept zur Erhaltung von Denkmälern aus Naturstein. *Denkmalpflege und Naturwissenschaft-Natursteinkonservierung I*. Verlag Ernst & Sohn, Berlin:127–146
- Snethlage R, Pfanner M (2020) *Leitfaden Steinkonservierung: Planung von Untersuchungen und Maßnahmen zur Erhaltung von Denkmälern aus Naturstein*, 5th edn.
- Snethlage R, Sterflinger K (2011) Stone conservation. In: Siegesmund S, Snethlage R (eds) *Stone in architecture*. Springer, pp 411–544
- Snethlage R, Wendler E (1997) Moisture cycles and sandstone degradation. *Environmental Sciences Research Report ES 20:7–24*
- Sousa L, Siegesmund S, Wedekind W (2018) Salt weathering in granitoids: An overview on the controlling factors. *Environmental earth sciences* 77:502
- Sousa LMO (2014) Petrophysical properties and durability of granites employed as building stone: a comprehensive evaluation. *Bulletin of Engineering Geology and the Environment* 73:569–588
- Spizzichino D, Boldini D, Frodella W, Elashvili M, Margottini C (2017) Landslide risk analysis and mitigation for the ancient rock-cut city of Vardzia (Georgia). In: *Proceedings of the 2017 IPL Symposium UNESCO, Paris, France*, pp 1–8
- Sramek J, Nishiura T (1990) Assessment, by radioactive labelling, of the efficiency of conservation treatments applied to volcanic tuffs. In: Charola AE (ed) *Lavas and volcanic tuffs: Proceedings of the international meeting, Easter Island, Chile, 25 - 31 October, 1990*. ICCROM, Rome, pp 205–216
- Steiger M (2005a) Crystal growth in porous materials—I: The crystallization pressure of large crystals. *Journal of crystal growth* 282:455–469
- Steiger M (2005b) Crystal growth in porous materials—II: Influence of crystal size on the crystallization pressure. *Journal of crystal growth* 282:470–481
- Steiger M, Charola AE, Sterflinger K (2011) Weathering and deterioration. In: Siegesmund S, Snethlage R (eds) *Stone in architecture*. Springer, pp 227–316

## 8 General conclusions

- Steindlberger E (2002) Untersuchungen zum physiko-chemischen Verwitterungsverhalten hessischer Tuffsteine. Geologisch-Paläontologisches Inst. der Johann-Wolfgang-Goethe-Univ
- Steindlberger E (2003) Vulkanische Gesteine aus Hessen und ihre Eigenschaften als Naturwerksteine. Teilw. zugl.: Frankfurt am Main, Univ., Diss., 2002 u.d.T.: Steindlberger, E.: Untersuchungen zum physiko-chemischen Verwitterungsverhalten hessischer Tuffsteine. Geologische Abhandlungen Hessen, vol 110. HLUG, Wiesbaden
- Steindlberger E (2004) Volcanic tuffs from Hesse (Germany) and their weathering behaviour. *Environmental geology* 46:378–390
- Steindlberger E (2007) Schalstein als Werkstein: Eigenschaften und Verwitterungsproblematik. In: IFS-Bericht, Institut für Steinkonservierung e.V. (ed) Die Konservierung des Heidenportals am Wetzlarer Dom. Neuartige Ansätze zur Erhaltung eines Problemgesteins, vol 27. IFS, Mainz, pp 9–22
- Steindlberger E (2020) Konservierung hessischer Tuffe und Schalsteine unter Langzeitbeobachtung. In: Institut für Steinkonservierung e.V. (ed) Konservierungsstrategien für Rhyolithtuffmauerwerk, vol 60, Mainz, pp 51–70
- Steinhäuser U, Wendler E (2004) Conservation of limestone by surfactants and modified ethylsilicate. In: Proceedings of the 10th International congress on Deterioration and Conservation of Stone; Vol. 1, p-439
- Streckeisen A (1978) IUGS Subcommittee on the Systematics of Igneous Rocks. Classification and Nomenclature of Volcanic Rocks, Lamprophyres, Carbonatites and Melilitic Rocks. Recommendations and Suggestions. *Neues Jahrbuch für Mineralogie. Stuttgart. Abhandlungen* 143:1–14
- Stück H (2006) Materialeigenschaften und Verwitterungsprozesse bruchfrischer und konsolidierter Vulkanite. Diplomarbeit, Georg-August-Universität
- Stück H, Forgó LZ, Rüdric J, Siegesmund S, Török A (2008) The behaviour of consolidated volcanic tuffs: weathering mechanisms under simulated laboratory conditions. *Environmental geology* 56:699–713
- Stück H, Koch R, Siegesmund S (2013) Petrographical and petrophysical properties of sandstones: statistical analysis as an approach to predict material behaviour and construction suitability. *Environmental earth sciences* 69:1299–1332
- Teipel M (2020) Schadenskartierung und Charakterisierung armenischer Tuffsteine mit dem Ziel der Entwicklung kompatibler Steinerfüllmassen für die Instandsetzung. Masterarbeit, Georg-August-Universität
- Teymen A (2018) Prediction of Basic Mechanical Properties of Tuffs Using Physical and Index Tests. *Journal of Mining Science* 54:721–733
- Thomachot C, Matsuoka N (2007) Dilation of building materials submitted to frost action. *Geological society, London, special publications* 271:167–177

## 8 General conclusions

- Topal T, Doyuran V (1997) Engineering geological properties and durability assessment of the Cappadocian tuff. *Engineering Geology* 47:175–187
- Topal T, Sözmen B (2001) Characteristics of the weathering zones developed within the tuffs of the Midas monument. *Turkish Journal of Earth Sciences* 10:83–91
- Toprak MU, Arslanbaba MA (2016) Possibility of using Kütahya Volcanic Tuff as building stone: Microstructural evaluation and strength enhancement through heat treatment. *Construction and Building Materials* 110:128–134
- Török A, Gálos M, Kocsányi-Kopecskó K (2004) Experimental weathering of rhyolite tuff building stones and the effect of an organic polymer conserving agent. *Stone Decay: Its Causes and Controls*:109–127
- Török Á, Forgó LZ, Vogt T, Löbens S, Siegesmund S, Weiss T (2007) The influence of lithology and pore-size distribution on the durability of acid volcanic tuffs, Hungary. *Geological society, London, special publications* 271:251–260
- Török Á, Bögöly G, Czinder B, Görög P, Kleb B, Vásárhelyi B, Lovas T, Barsi Á, Molnár B, Koppányi Z (eds) (2016) Terrestrial laser scanner aided survey and stability analyses of rhyolite tuff cliff faces with potential rock-fall hazards, an example from Hungary. *International Society for Rock Mechanics and Rock Engineering*
- Tukey JW (1977) *Exploratory data analysis*, vol 2. Reading, MA
- Türkdönmez O, Bozcu M (2012) The Geological, petrographical and engineering properties of rhyolitic tuffs (Çan Stone) in Çan-Etili Area (Çanakkale), NW Turkey: their Usage as building and covering stones. *Open Journal of Geology* 2:25–33
- Ufer K, Kleeberg R, Bergmann J, Dohrmann R (2012a) Rietveld refinement of disordered illite-smectite mixed-layer structures by a recursive algorithm. I: One-dimensional patterns. *Clays and Clay Minerals* 60:507–534
- Ufer K, Kleeberg R, Bergmann J, Dohrmann R (2012b) Rietveld refinement of disordered illite-smectite mixed-layer structures by a recursive algorithm. II: powder-pattern refinement and quantitative phase analysis. *Clays and Clay Minerals* 60:535–552
- Uğur İ, Toklu HÖ (2020) Effect of multi-cycle freeze-thaw tests on the physico-mechanical and thermal properties of some highly porous natural stones. *Bulletin of Engineering Geology and the Environment* 79:255–267
- Ünal M (2011) The effect of salt crystallization on tuff used as building material. *Engineering Sciences* 6:41–49
- Useche LA (1990) Studies for the consolidation of the facade of the church of Santo Domingo, Popayan, Colombia. In: Charola AE (ed) *Lavas and volcanic tuffs: Proceedings of the international meeting, Easter Island, Chile, 25 - 31 October, 1990*. ICCROM, Rome, pp 165–172
- Utudjian E (1968) *Armenian Architecture: 4th to 17th Century*. Editions A. Morancé

## 8 General conclusions

- van Hees RPJ, Brendle S, Nijland TG, Haas G de, Tolboom HJ (2003) Decay of Rhenish tuffs in Dutch monuments. Part 2: Laboratory experiments as a basis for the choice of restoration stone. *Heron*, Vol. 48 (2003) No. 3, pp. 167-177
- Vásárhelyi B (ed) (2002) Influence of the water saturation on the strength of volcanic tuffs. *International Society for Rock Mechanics and Rock Engineering*
- Velasco Sánchez A (2013) Estudio petrográfico, petrofísico y geoquímico de las rocas de construcción del Templo de la Compañía de Jesús, Guanajuato, México. Licenciatura, Universidad Autónoma de San Luis Potosí
- Vernik L, Bruno M, Bovberg C (1993) Empirical relations between compressive strength and porosity of siliciclastic rocks. In: *International journal of rock mechanics and mining sciences & geomechanics abstracts*. Elsevier, pp 677–680
- Wangler T, Scherer GW (2008) Clay swelling mechanism in clay-bearing sandstones. *Environmental geology* 56:529–534
- Wedekind W (2016) Weathering and conservation of monuments constructed from tuff and sandstone in different environmental conditions. *Georg-August-Universität Göttingen*
- Wedekind W, Ruedrich J, Siegesmund S (2011) Natural building stones of Mexico—Tenochtitlán: their use, weathering and rock properties at the Templo Mayor, Palace Heras Soto and the Metropolitan Cathedral. *Environmental earth sciences* 63:1787–1798
- Wedekind W, López-Doncel R, Dohrmann R, Kocher M, Siegesmund S (2013) Weathering of volcanic tuff rocks caused by moisture expansion. *Environmental earth sciences* 69:1203–1224
- Weimann MB (2001) Hygrische Eigenschaften von Polymerbeton im Vergleich mit porösen mineralischen Werkstoffen des Bauwesens. Dissertation, ETH Zurich
- Weiss G (1992) Die Eis- und Salzkristallisation im Porenraum von Sandsteinen und ihre Auswirkungen auf das Gefüge unter besonderer Berücksichtigung gesteinspezifischer Parameter. *Münchener geowissenschaftliche Abhandlungen. Reihe B, Allgemeine und angewandte Geologie*, vol 9. F. Pfeil, München
- Weiss T, Siegesmund S, Kirchner Dt, Sippel J (2004) Insolation weathering and hygric dilatation: two competitive factors in stone degradation. *Environmental geology* 46:402–413
- Wellman HW, Wilson AT (1965) Salt weathering, a neglected geological erosive agent in coastal and arid environments. *Nature* 205:1097–1098
- Wendler E (2005) Probleme, Lösungsansätze und Erfolge bei der Konservierung von verwittertem Lapillituff. In: *Evangelische Kirche von Kurhessen-Waldeck (ed) Konservierungskonzepte zum Erhalt von nordhessischem Tuffstein an historischen Bauwerken: Tagungsband ; Abschlußbericht des DBU-Projektes "Innovative Konzepte zur Konservierung und zum Schutz umweltgeschädigter historischer Tuffsteinflächen am Beispiel von drei nordhessischen Kirchen ; Projekt Nr.: 18981-45, Kassel*

## 8 General conclusions

- Wendler E (2007) Entwicklung von materialspezifischen Konservierungsstrategien zur Konsolidierung und Prophylaxe. In: IFS-Bericht, Institut für Steinkonservierung e.V. (ed) Die Konservierung des Heidenportals am Wetzlarer Dom. Neuartige Ansätze zur Erhaltung eines Problemgesteins, vol 27. IFS, Mainz, pp 69–76
- Wendler E, Klemm DD, Snethlage R (1991) Consolidation and Hydrophobic treatment of Natural Stone. In: Baker JM, Nixon PJ, Majumdar AJ, Davies H (eds) Durability of building materials and components: Proceedings of the fifth international conference held in Brighton, UK, 7 - 9 November 1990, 1st edn. Spon, London, pp 203–212
- Wendler E (2016) Engpässe im Porenraum: Kriterien für die gezielte Auswahl und Rezeptierung von Steinfestigern. In: IFS-Bericht, Institut für Steinkonservierung e.V. (ed) Unsere Denkmäler sind steinreich, vol 51. IFS, Mainz, pp 21–26
- Wendler E, Charola AE, Fitzner B (1996) Easter Island tuff: Laboratory studies for its consolidation. In: Proceedings of the 8th International Conference on the Deterioration and Conservation of Stone, Riederer, J.(ed.), Berlin, pp 1159–1170
- Wheeler G, Mendez-Vivar J, Goins ES, Fleming SA, Brinker CJ (2000) Evaluation of alkoxy silane coupling agents in the consolidation of limestone. Proc. of the 9th Int. Cong. on “Deterioration and Conservation of Stone “, Edited by Vasco Fassina, Elsevier Science:541–545
- Wheeler GS, Newman R (1994) Analysis and treatment of a stone urn from the Imperial Hotel, Tokyo. In: Lavas and volcanic tuffs: proceedings of the international meeting, Easter Island, Chile, 25-31 October, 1990, pp 157–163
- Wittenborn A (2015) Tuffverwitterung am Franziskaner Konvent in Zacatecas, Mexiko: Schadenskartierung und gesteintechnische Charakterisierung der Verwitterungsphänomene. Bachelorarbeit, Georg-August-Universität
- Xue Y, Kong F, Li S, Zhang L, Zhou B, Li G, Gong H (2020) Using Indirect Testing Methods to Quickly Acquire the Rock Strength and Rock Mass Classification in Tunnel Engineering. International Journal of Geomechanics 20:5020001
- Yasar E, Tolgay A, Teymen A (2009) Industrial usage of Nevsehir-Kayseri (Turkey) tuff stone. World Applied Sciences Journal 7:271–284
- Yasar S (2020) Long term wetting characteristics and saturation induced strength reduction of some igneous rocks. Environmental earth sciences 79:1–12
- Yavuz AB, Akal C, Türk N, Çolak M, Tanyu BF (2015) Investigation of discrepancy between tuff used as building stones in historical and modern buildings in western Turkey. Construction and Building Materials 93:439–448
- Yu S, Oguchi CT (2010) Role of pore size distribution in salt uptake, damage, and predicting salt susceptibility of eight types of Japanese building stones. Engineering Geology 3:226–236



## 8 General conclusions

Yüksek S (2019) Mechanical properties of some building stones from volcanic deposits of mount Erciyes (Turkey). *Materiales de Construcción* 69:187

Yüksek S, Demirci A (eds) (2010) Geotechnical properties of volcanic materials of the Mount Erciyes. International Society for Rock Mechanics and Rock Engineering

URL1 <https://gestis.dguv.de/data?name=106781&lang=en> (20.03.2021)

### Acknowledgments

Grundlage für die Realisierung der vorliegenden Arbeit war ein Promotionsstipendium der Deutschen Bundesstiftung Umwelt (DBU), bei der ich mich für die Unterstützung bedanken möchte. Ebenso danke ich dem DAAD und GAUSS für die finanzielle Unterstützung der Forschungsaufenthalte in Mexiko und Armenien.

Viele tolle Menschen haben zum Gelingen dieser Arbeit beigetragen. Dafür bedanke ich mich ausdrücklich und entschuldige mich, wenn ich jemanden übersehen sollte:

Bei Prof. Dr. Siegfried Siegesmund möchte ich mich ganz herzlich für die Initiierung und Betreuung der Arbeit bedanken. Vielen Dank für die stete Unterstützung, die zahlreichen Diskussionen und geteilten Lebensweisheiten. Für die Übernahme des Korreferats und die damit verbundenen Mühen möchte ich mich bei Prof. Dr. Rolf Snethlage bedanken.

Dr. Rubén López Doncel danke ich von ganzen Herzen für die vielen Jahre der Betreuung und Zusammenarbeit bei allen Aufenthalten in Mexico und Deutschland. Dr. Reiner Dohrmann danke ich vielmals für unzählige Messungen und Lektionen zu Tonmineralen. Prof. Dr. Tobias Licha und Dr. Eberhard Wendler danke ich für die Unterweisungen zu den Tränkungsmittelein und allen chemischen Fragen. Dr. Klaus Wemmer sei herzlich für die Bereitstellung der Laboratorien am GZG gedankt. Dr. Maria Sitnikova, Sabine Haser und Dr. Kirsten Techmer danke ich für die Messungen am REM. Vagharshak Safaryan sei für die Unterstützung beim Versenden der Proben aus Armenien gedankt.

Ganz besonders möchte ich mich bei all den wunderbaren Menschen aus dem TekLab für die gemeinsame Zeit und Unterstützung, sowie reichlich Kaffee bedanken: Maxim Bogdanowitsch, Alena Broge, Christian Gross, Marie-France Hesse, Dr. Mathias Hueck, Calvin Klein, Christian Knell, Tobias Koch, Jordy Koning, Alexandra Kück, Falko Malis, Dr. Johanna Menningen, Malte Teipel, Sofia Pascual, Amanda Ricardo, Stine Rucker, Hernan Silva, Dr. Luis Sosa, Dr. Wanja Wedekind.

Dr. Johanna Menningen, Dr. Mathias Hueck, Dr. Rubén López Doncel und Anthea Pötzl danke ich vielmals für das akribische Korrekturlesen. Einen ganz besonderen Dank möchte ich Johanna Menningen aussprechen, für ihre stete Diskussions- und Hilfsbereitschaft.

Zu guter Letzt möchte ich meiner Familie für jegliche Unterstützung, lieben Worte und Gesten danken. Vor allem danke ich Sandra, die in den letzten Jahren unendliche Geduld bewiesen hat und mir täglich Kraft spendet. Te amo mucho morenita.

## Lebenslauf

Christopher Pötzl, geb. 07.08.1988 in Duderstadt

### *Akademische Ausbildung*

- |                   |  |
|-------------------|--|
| 2016 – 2020       | <b>Promotion Geowissenschaften, Georg-August-Universität Göttingen</b><br>-gefördert durch ein Langzeitstipendium der DBU (07/2017-06/2020)<br>- Thema: Volcanic tuffs as natural building stones: Mineralogy, technical properties, deterioration and conservation strategies |
| 02/2016 – 11/2016 | <b>Forschungsaufenthalt, Autonome Universität San Luis Potosi, Mexiko</b><br>-gefördert durch ein Forschungsstipendium des DAAD  |
| 10/2012 – 12/2015 | <b>M.Sc. Geowissenschaften, Georg-August-Universität Göttingen</b><br>- Thema der Thesis: Bauschäden, Verwitterungscharakteristik und gesteintechnische Eigenschaften von Tuffsteinen in Guanajuato, Mexiko  |
| 10/2009 – 09/2012 | <b>B.Sc. Geowissenschaften, Georg-August-Universität Göttingen</b><br>- Thema der Thesis: Geotechnische Untersuchung und Bewertung der geplanten Umgehungsstraße bei Waake (Göttingen)   |

### *Berufserfahrungen*

- |                   |  |
|-------------------|--|
| Seit 07/2020      | <b>Wissenschaftlicher Mitarbeiter, Georg-August-Universität Göttingen</b><br>Tuffe als Werksteine der historischen Kulturgüter Mexikos: Geologische, mineralogische und petrophysikalische Parameter als Basis für das Verständnis der Verwitterung, Konservierung und Erhaltung |
| 05/2020 – 06/2020 | <b>Wissenschaftliche Hilfskraft, Georg-August-Universität Göttingen</b><br>- Lektoratsarbeiten in Review- und Proofreading-Prozessen Stone2020   |
| 02/2019 – 09/2019 | <b>Wissenschaftliche Hilfskraft, Georg-August-Universität Göttingen</b><br>- Ultraschalltomographie Messungen im Projekt Marmorbild<br>- Bestimmung gesteintechnischer Eigenschaften   |

### *Forschungsstipendien*

- |                   |  |
|-------------------|--|
| 07/2017 – 07/2020 | Promotionsstipendium der Deutschen Bundesstiftung Umwelt (DBU) |
| 04/2019 – 05/2019 | Forschungsreisestipendium für Doktoranden (GAUSS) - Armenien   |
| 05/2016 – 10/2016 | Forschungsreisestipendium für Doktoranden (DAAD) - Mexiko      |
| 01/2016 – 03/2016 | Kurzstipendium für Feldarbeiten (CONACYT) - Mexiko             |
| 08/2014 – 09/2014 | Kurzstipendium für Feldarbeiten (CONACYT) - Mexiko             |

## Appendix

### Appendix I – Tables

Table A.1: Literature used for the compilation of the tuff database

---

#### References

---

Akin et al. 2017; Auras et al. 2000; Aydan and Ulusay 2003; Barahim et al. 2017; Barbero-Barrera et al. 2019; Beyhan et al. 2018; Bianchetti et al. 1990; Binal 2009; Bozdağ et al. 2016; Bozdağ and Ince 2018; Bullmann 2001; Calcaterra et al. 2000; Calcaterra et al. 2004; Calcaterra et al. 2005; Çelik et al. 2014; Çelik and Aygün 2019; Çelik and Çobanoğlu 2019; Çelik and Ergül 2015, 2018; Çelik and Kaçmaz 2016; Çelik and Sert 2020; Chen et al. 2004; Colella et al. 2009; Colella et al. 2017; Columbu et al. 2014; Cueto Mendoza et al. 2018; Di Benedetto 2012; Dinçer et al. 2004; Dinçer and Bostancı 2019; Egloffstein 1998; Emir et al. 2011; Engidasew 2014; Ergenç et al. 2016; Fitzner 1985; Fratini et al. 1990; Germinario and Török 2019; Ghobadi et al. 2016; Gioncada et al. 2010; Hashemi et al. 2018; Heap et al. 2014; Hernández Gutiérrez 2014; Ince et al. 2019; Ince and Fener 2016; Jackson et al. 2005; Jamshidi et al. 2013; Kaljahi and Birami 2015; Katschmann et al. 2006; Kılıç et al. 2019; Kılıç and Teymen 2008; Koralay et al. 2011; Koralay and Çelik 2019; Korat et al. 2015; Korkanç et al. 2015; Korkanç and Solak 2016; Kral 2014; Kück 2019; Kück et al. 2020a, 2020b; La Russa et al. 2017; Lange and Steiner 1974; Langella et al. 2013; Laurenzi Tabasso et al. 1990; Leiser 2013; Li et al. 2020; Lindner 1994; López-Doncel et al. 2013; López-Doncel et al. 2016; López-Doncel et al. 2018; Lukaszewicz 1990; Marmoni et al. 2017a, 2017b; Molina-Maldonado 2016; Möllenkamp 1996; Moon 1993; Nijland et al. 2010; Oguchi and Yuasa 2010; Öner et al. 2006; Özbek 2014; Özşen et al. 2017; Özvan et al. 2015; Papa 2011; Pola et al. 2012; Pola et al. 2014; Poschlod 1990; Pötzl 2015; Pötzl et al. 2018a; Pötzl et al. 2018b; Rossi-Manaresi and Tucci 1990; Rucker et al. 2020; Sato and Hattanji 2018; Sert and Özkahraman 2016; Siedel 1995; Spizzichino et al. 2017; Sramek and Nishiura 1990; Steindlberger 2002, 2003, 2020; Stück 2006; Stück et al. 2008; Teipel 2020; Teymen 2018; Thomachot and Matsuoka 2007; Topal and Doyuran 1997; Topal and Sözmen 2001; Toprak and Arslanbaba 2016; Török et al. 2004; Török et al. 2007; Török et al. 2016; Türkdönmez and Bozcu 2012; Uğur and Toklu 2020; Ünal 2011; Useche 1990; van Hees et al. 2003; Velasco Sánchez 2013; Wedekind et al. 2011; Wedekind et al. 2013; Wendler et al. 1996; Wittenborn 2015; Yasar et al. 2009; Yavuz et al. 2015; Yüksek 2019; Yüksek and Demirci 2010

---

## Appendix

Table A.2: Modified petrophysical properties and expansional behavior of Blanca Pachuca (BP) after the consolidation treatments. SSA = specific surface area; CEC = cation exchange capacity;  $\alpha$  = coefficient of thermal expansion

<b>Blanca Pachuca (BP)</b>	<b>Untrea- ted</b>	<b>A</b>	<b>A+KSE</b>	<b>WS+ KSE</b>	<b>A+WS+ KSE</b>	<b>KSE</b>	<b>A+T</b>	<b>WS+T</b>	<b>A+WS+ T</b>	<b>TMOS</b>
Porosity [vol%]	14.9	14.2	10.5	5.0	7.5	4.2	5.7	8.6	7.7	5.5
Bulk density [g/cm <sup>3</sup> ]	1.85	1.84	1.82	1.81	1.81	1.85	1.87	1.82	1.86	1.86
Matrix density [g/cm <sup>3</sup> ]	2.17	2.15	2.03	1.91	1.96	1.93	1.98	1.99	2.01	1.97
Water absorp. vac. [wt%]	8	8	6	3	4	3	3	5	4	3
Water absorp. atm. [wt%]	7	7	5	1	1	3	2	4	4	2
Saturation coefficient S	0.86	0.87	0.90	0.40	0.32	0.76	0.80	0.95	0.94	0.81
Micropores [%]	79	79	73	86	71	76	75	74	86	79
Capillary pores [%]	21	21	27	14	29	24	25	26	14	21
Mean pore radius [ $\mu$ m]	0.05	0.06	0.08	0.04	0.07	0.06	0.05	0.05	0.04	0.04
SSA via BET [m <sup>2</sup> /g]	17	-	-	-	-	-	-	-	-	-
SSA via MIP [m <sup>2</sup> /g]	9.7	8.2	8.1	10.9	8.3	9.2	13.9	16.7	14.4	18.9
CEC [meq/100g]	12	-	-	-	-	-	-	-	-	-
w-value [kg/m <sup>2</sup> v(h)]										
X	0.8	0.5	0.2	0.2	0.1	0.3	0.3	0.3	0.4	0.2
Z	0.8	0.7	0.2	0.2	0.1	0.1	0.4	0.4	0.2	0.3
$\mu$ -value										
X	11.9	-	18.8	13.4	19.3	16.0	18.1	15.2	18.6	15.3
Z	11.1	-	23.0	21.8	22.7	15.4	18.4	16.8	20.1	20.5
Sorption 95% rh [wt-%]	4.5	4.3	4.8	4.4	4.9	4.2	4.4	3.9	4.5	4.2
$\phi$ hydric exp. [mm/m]										
X	0.71	0.80	0.87	0.83	0.99	0.92	0.87	0.96	0.97	0.92
Z	0.96	0.80	1.01	0.90	1.07	0.99	1.03	1.09	1.10	1.00
MAX	1.14	0.86	1.01	0.92	1.08	1.00	1.06	1.15	1.13	1.06
$\phi$ $\alpha$ [10 <sup>-6</sup> K <sup>-1</sup> ] <b>dry</b>										
X	13.4	14.6	11.6	11.3	12.0	13.2	7.3	12.3	3.6	10.0
Z	13.4	12.6	11.7	12.5	13.6	12.9	7.0	11.5	3.4	4.8
resid. strain $\epsilon$ X [mm/m]	0.16	0.14	0.16	0.11	0.16	0.09	-0.15	0.11	-0.38	0.03
resid. strain $\epsilon$ Z [mm/m]	0.17	0.12	0.23	0.16	0.19	0.21	-0.19	0.16	-0.45	0.06
$\phi$ $\alpha$ [10 <sup>-6</sup> K <sup>-1</sup> ] <b>wet</b>										
X	23.6	25.9	23.6	25.0	26.9	24.0	21.8	17.8	28.6	22.0
Z	24.2	26.6	24.3	25.8	27.6	24.8	22.5	29.2	30.3	20.8
resid. strain $\epsilon$ X [mm/m]	-0.08	-0.03	0.19	0.44	0.33	0.56	0.03	-0.08	0.40	0.09
resid. strain $\epsilon$ Z [mm/m]	-0.10	0.01	0.28	0.60	0.25	0.54	-0.04	0.32	0.50	0.16
P-wave velocity [km/s]										
X	3.3	3.2	3.4	3.3	3.4	3.4	3.5	3.4	3.5	3.3
Z	3.2	3.1	3.3	3.3	3.3	3.2	3.4	3.2	3.4	3.3
Youngs's Modulus [GPa]										
X	20	19	21	21	21	21	22	21	22	21
Z	19	18	20	20	20	19	21	19	21	20

## Appendix

Table A.3: Modified petrophysical properties and expansional behavior of Cantera Rosa (CR) after the consolidation treatments. SSA = specific surface area; CEC = cation exchange capacity;  $\alpha$  = coefficient of thermal expansion

<b>Cantera Rosa (CR)</b>	<b>Untrea- ted</b>	<b>A</b>	<b>A+KSE</b>	<b>WS+ KSE</b>	<b>A+WS+ KSE</b>	<b>KSE</b>	<b>A+T</b>	<b>WS+T</b>	<b>A+WS+ T</b>	<b>TMOS</b>
Porosity [vol%]	31.1	27.5	21.7	22.3	21.9	22.5	21.6	22.2	22.2	21.5
Bulk density [g/cm <sup>3</sup> ]	1.78	1.79	1.85	1.86	1.85	1.83	1.90	1.89	1.89	1.90
Matrix density [g/cm <sup>3</sup> ]	2.58	2.47	2.37	2.39	2.37	2.36	2.43	2.43	2.43	2.42
Water absorp. vac. [wt%]	18	15	12	12	12	12	11	12	12	11
Water absorp. atm. [wt%]	14	13	4	6	2	3	9	9	9	9
Saturation coefficient S	0.77	0.82	0.32	0.49	0.14	0.28	0.82	0.79	0.77	0.79
Micropores [%]	18	16	6	8	2	8	26	22	21	21
Capillary pores [%]	82	84	94	92	98	92	74	78	79	79
Mean pore radius [ $\mu$ m]	0.52	0.63	0.88	0.79	1.03	0.85	0.24	0.34	0.33	0.42
SSA via BET [m <sup>2</sup> /g]	5	-	-	-	-	-	-	-	-	-
SSA via MIP [m <sup>2</sup> /g]	5.1	2.8	1.1	1.3	0.7	1.1	10.5	9.0	13.5	6.5
CEC [meq/100g]	6	-	-	-	-	-	-	-	-	-
w-value [kg/m <sup>2</sup> v(h)]										
X	9.4	8.9	0.2	0.2	0.3	2.3	4.6	3.0	6.5	3.6
Z	7.1	7.7	0.3	0.2	0.2	2.3	3.8	4.6	5.6	3.7
$\mu$ -value										
X	7.5	-	17.7	17.0	16.1	14.7	15.2	15.2	15.0	12.4
Z	8.4	-	18.2	20.1	19.7	17.9	16.2	17.3	16.0	13.2
Sorption 95% rh [wt-%]	2.6	2.0	1.8	1.5	0.8	1.9	4.2	2.4	3.8	3.6
$\phi$ hydric exp. [mm/m]										
X	0.10	0.04	0.13	0.63	0.12	0.38	0.22	0.51	0.22	0.29
Z	0.24	0.05	0.16	0.81	0.10	0.47	0.34	0.64	0.30	0.36
MAX	0.29	0.07	0.17	0.82	0.14	0.48	0.34	0.68	0.35	0.40
$\phi$ $\alpha$ [10 <sup>-6</sup> K <sup>-1</sup> ] <b>dry</b>										
X	8.5	9.5	10.0	10.7	9.1	10.1	8.7	10.1	9.5	7.9
Z	8.6	9.2	10.6	11.0	10.5	11.3	8.0	10.3	9.5	6.8
resid. strain $\epsilon$ X [mm/m]	-0.03	0.02	0.01	0.05	0.02	-0.01	-0.02	-0.02	0.01	-
resid. strain $\epsilon$ Z [mm/m]	-0.02	0.01	0.03	0.05	0.02	0.02	-0.02	0.02	-0.02	-0.02
$\phi$ $\alpha$ [10 <sup>-6</sup> K <sup>-1</sup> ] <b>wet</b>										
X	9.5	11.7	11.7	16.7	11.6	14.9	12.7	11.6	11.8	13.2
Z	9.7	11.6	12.7	18.7	12.8	16.0	12.6	12.5	11.9	12.8
resid. strain $\epsilon$ X [mm/m]	0.04	-0.07	0.02	0.15	0.01	0.07	-0.07	0.01	0.07	-0.04
resid. strain $\epsilon$ Z [mm/m]	0.04	0.01	0.06	0.21	0.04	0.12	0.01	-0.005	0.09	0.02
P-wave velocity [km/s]										
X	2.8	2.7	2.9	3.2	2.9	2.9	3.1	3.2	3.0	2.8
Z	2.6	2.5	2.8	2.9	2.8	2.7	3.1	3.1	2.9	2.5
Youngs's Modulus [GPa]										
X	14	13	15	18	15	15	18	18	16	14
Z	12	11	14	15	14	13	17	17	15	12

## Appendix

Table A.4: Modified petrophysical properties and expansional behavior of Loseros (LOS) after the consolidation treatments. SSA = specific surface area; CEC = cation exchange capacity;  $\alpha$  = coefficient of thermal expansion

<b>Loseros (LOS)</b>	<b>Untrea- ted</b>	<b>A</b>	<b>A+KSE</b>	<b>WS+ KSE</b>	<b>A+WS+ KSE</b>	<b>KSE</b>	<b>A+T</b>	<b>WS+T</b>	<b>A+WS+ T</b>	<b>TMOS</b>
Porosity [vol%]	16.8	16.1	16.6	14.5	16.5	15.5	3.0	4.1	4.3	2.8
Bulk density [g/cm <sup>3</sup> ]	2.07	2.08	2.10	2.09	2.10	2.10	2.12	2.10	2.12	2.14
Matrix density [g/cm <sup>3</sup> ]	2.49	2.47	2.52	2.44	2.51	2.48	2.18	2.19	2.21	2.20
Water absorp. vac. [wt%]	8	8	7	7	8	7	1	2	2	1
Water absorp. atm. [wt%]	7	6	6	6	6	6	1	2	2	1
Saturation coefficient S	0.81	0.80	0.88	0.77	0.81	0.79	0.98	0.93	0.91	0.89
Micropores [%]	85	41	64	59	64	55	66	63	57	77
Capillary pores [%]	15	59	36	41	36	45	34	37	43	23
Mean pore radius [ $\mu$ m]	0.04	0.21	0.08	0.07	0.07	0.12	0.04	0.06	0.05	0.04
SSA via BET [m <sup>2</sup> /g]	12	-	-	-	-	-	-	-	-	-
SSA via MIP [m <sup>2</sup> /g]	9.6	5.5	4.5	4.2	4.4	4.0	14.1	11.5	12.0	13.6
CEC [meq/100g]	5	-	-	-	-	-	-	-	-	-
w-value [kg/m <sup>2</sup> v(h)]										
X	0.8	0.8	0.2	0.4	0.2	0.2	0.4	0.3	0.4	0.3
Z	0.7	0.7	0.2	0.2	0.2	0.4	0.3	0.3	0.4	0.3
$\mu$ -value										
X	27.9	-	65.7	61.3	51.4	51.7	43.1	28.9	34.1	40.1
Z	13.4	-	26.3	27.9	33.8	24.3	28.9	24.4	30.7	25.4
Sorption 95% rh [wt-%]	2.9	3.2	2.7	2.2	2.5	2.6	2.9	2.8	2.8	2.5
$\phi$ hydric exp. [mm/m]										
X	0.58	0.35	0.35	0.45	0.35	0.62	0.32	0.48	0.23	0.43
Z	1.22	0.63	0.78	1.21	0.68	1.32	0.85	1.06	0.81	1.03
MAX	1.78	0.67	0.78	1.28	0.68	1.33	0.91	1.08	0.84	1.04
$\phi \alpha$ [ $10^{-6} K^{-1}$ ] <b>dry</b>										
X	9.8	9.6	10.7	11.2	11.0	10.9	10.2	9.7	10.4	9.5
Z	11.7	11.2	11.7	13.1	12.4	14.0	11.4	9.7	11.8	9.1
resid. strain $\epsilon$ X [mm/m]	-0.03	0.03	0.06	0.07	0.05	0.05	0.03	-0.04	0.01	0.01
resid. strain $\epsilon$ Z [mm/m]	0.05	0	0.12	0.13	0.10	0.15	0.03	-0.03	0.002	0.04
$\phi \alpha$ [ $10^{-6} K^{-1}$ ] <b>wet</b>										
X	12.9	13.8	14.8	15.4	15.1	18.4	14.5	17.1	13.4	16.4
Z	32.1	21.2	23.0	27.1	21.6	30.4	22.1	23.8	21.2	24.5
resid. strain $\epsilon$ X [mm/m]	-0.01	-0.04	-0.005	3E-17	0.005	-0.07	0.01	-0.02	0.05	0.04
resid. strain $\epsilon$ Z [mm/m]	-0.74	-0.08	-0.19	-0.10	-0.09	-0.25	0	0.05	-0.003	0.15
P-wave velocity [km/s]										
X	3.7	3.4	3.9	3.7	3.6	3.6	3.8	3.6	3.9	3.7
Z	2.8	2.8	3.0	3.0	2.9	2.9	3.1	3.1	3.1	3.0
Youngs's Modulus [GPa]										
X	28	24	31	29	27	26	30	28	31	28
Z	16	16	18	18	18	18	20	20	19	19

## Appendix

Table A.5: Modified petrophysical properties and expansional behavior of San Miguel el Alto (SMA) after the consolidation treatments. SSA = specific surface area; CEC = cation exchange capacity;  $\alpha$  = coefficient of thermal expansion

<b>San Miguel el Alto (SMA)</b>	<b>Untreated</b>	<b>A</b>	<b>A+KSE</b>	<b>WS+KSE</b>	<b>A+WS+KSE</b>	<b>KSE</b>	<b>A+T</b>	<b>WS+T</b>	<b>A+WS+T</b>	<b>TMOS</b>
Porosity [vol%]	40.8	35.2	29.6	30.3	30.4	30.4	32.9	31.2	32.0	32.7
Bulk density [g/cm <sup>3</sup> ]	1.52	1.52	1.59	1.59	1.58	1.57	1.59	1.62	1.61	1.59
Matrix density [g/cm <sup>3</sup> ]	2.57	2.35	2.25	2.28	2.26	2.26	2.37	2.36	2.37	2.36
Water absorp. vac. [wt%]	27	23	19	19	19	19	21	19	20	21
Water absorp. atm. [wt%]	17	16	3	6	4	2	13	13	13	13
Saturation coefficient S	0.65	0.71	0.13	0.34	0.19	0.08	0.63	0.66	0.64	0.65
Micropores [%]	10	8	1	1	0.1	0.2	16	8	8	10
Capillary pores [%]	90	92	99	99	99.9	99.8	84	92	92	90
Mean pore radius [ $\mu$ m]	1.50	1.59	2.35	2.31	2.18	2.79	0.73	1.19	1.03	1.26
SSA via BET [m <sup>2</sup> /g]	7	-	-	-	-	-	-	-	-	-
SSA via MIP [m <sup>2</sup> /g]	4.7	2.1	0.7	0.4	0.3	0.3	13.0	8.8	6.1	11.2
CEC [meq/100g]	4	-	-	-	-	-	-	-	-	-
w-value [kg/m <sup>2</sup> v(h)]										
X	7.3	6.0	0.1	2.4	0.3	0.3	5.6	5.1	9.4	6.2
Z	4.7	2.9	0.2	0.3	0.7	0.4	2.8	5.1	11.9	4.8
$\mu$ -value										
X	7.4	-	12.6	13.1	14.9	11.9	12.8	14.2	14.4	10.5
Z	8.1	-	20.6	16.4	18.4	14.0	15.3	16.8	16.3	11.7
Sorption 95% rh [wt-%]	1.2	1.0	2.0	0.7	0.6	0.6	4.4	1.3	3.1	2.1
$\phi$ hydric exp. [mm/m]										
X	0.07	-0.06	0.08	0.18	0.06	0.14	0.15	0.14	0.13	0.13
Z	0.23	-0.25	0.07	0.24	0.07	0.14	0.17	0.23	0.17	0.16
MAX	0.34	-0.32	0.08	0.32	0.08	0.18	0.18	0.25	0.19	0.16
$\phi \alpha$ [ $10^{-6} K^{-1}$ ] <b>dry</b>										
X	8.8	8.7	8.7	7.3	8.5	7.7	7.4	8.5	8.1	8.2
Z	9.4	8.3	8.6	7.6	8.3	7.6	8.1	8.5	8.8	8.0
resid. strain $\epsilon$ X [mm/m]	0	-0.01	0	-0.06	-0.02	-0.02	-0.01	-0.03	0.03	-0.004
resid. strain $\epsilon$ Z [mm/m]	2E-05	-0.03	-0.02	-0.04	-0.02	-0.02	-0.01	-0.03	0.001	-0.02
$\phi \alpha$ [ $10^{-6} K^{-1}$ ] <b>wet</b>										
X	10.7	9.6	10.5	11.6	10.6	10.1	10.6	10.4	11.3	11.1
Z	12.0	10.2	10.0	11.2	10.4	10.6	10.7	11.2	10.8	11.0
resid. strain $\epsilon$ X [mm/m]	0.07	-0.05	-0.05	-0.004	-0.05	-0.04	0.09	-0.01	-0.11	-0.04
resid. strain $\epsilon$ Z [mm/m]	-0.03	-0.07	0.03	-0.001	0.003	-0.07	-0.03	-0.03	0.001	-0.02
P-wave velocity [km/s]										
X	2.7	2.7	2.8	2.9	2.8	2.9	2.9	2.8	2.8	2.7
Z	2.3	2.4	2.5	2.6	2.5	2.6	2.5	2.5	2.5	2.4
Youngs's Modulus [GPa]										
X	11	11	12	13	12	13	13	12	12	11
Z	8	9	9	10	9	10	10	9	10	9



## Appendix

Table A.6: Modified petrophysical properties and expansional behavior of Blue Sevan (BS) after the consolidation treatments. SSA = specific surface area; CEC = cation exchange capacity;  $\alpha$  = coefficient of thermal expansion

<b>Blue Sevan (BS)</b>	<b>Untrea- ted</b>	<b>A</b>	<b>A+KSE</b>	<b>WS+ KSE</b>	<b>A+WS+ KSE</b>	<b>KSE</b>	<b>A+T</b>	<b>WS+T</b>	<b>A+WS+ T</b>	<b>TMOS</b>
Porosity [vol%]	14.9	13.6	14.3	12.3	9.7	16.2	5.8	13.3	13.6	8.0
Bulk density [g/cm <sup>3</sup> ]	2.06	2.07	2.02	2.06	2.15	2.03	2.17	2.04	2.06	2.11
Matrix density [g/cm <sup>3</sup> ]	2.42	2.40	2.36	2.35	2.38	2.43	2.31	2.35	2.38	2.29
Water absorp. vac. [wt%]	7	7	7	6	5	8	3	7	7	4
Water absorp. atm. [wt%]	6	6	7	6	4	7	2	5	5	3
Saturation coefficient S	0.83	0.85	0.97	0.92	0.93	0.93	0.83	0.82	0.79	0.86
Micropores [%]	90	85	91	83	81	75	92	84	87	80
Capillary pores [%]	10	15	9	17	19	25	8	16	13	20
Mean pore radius [ $\mu$ m]	0.03	0.05	0.04	0.06	0.06	0.07	0.02	0.04	0.03	0.05
SSA via BET [m <sup>2</sup> /g]	8.0	-	-	-	-	-	-	-	-	-
SSA via MIP [m <sup>2</sup> /g]	4.0	5.7	5.2	5.0	4.4	5.4	9.6	7.8	7.2	9.2
CEC [meq/100g]	8.9	-	-	-	-	-	-	-	-	-
w-value [kg/m <sup>2</sup> v(h)]										
X	0.8	0.7	1.0	1.2	0.6	0.2	0.4	0.5	1.0	0.7
Z	0.5	0.5	0.7	0.5	0.5	0.7	0.3	0.6	0.4	0.2
$\mu$ -value										
X	14.4	-	14.8	15.9	19.8	18.1	24.1	18.9	25.5	20.7
Z	14.2	-	27.4	27.7	34.2	20.8	25.8	22.8	26.3	27.0
Sorption 95% rh [wt-%]	2.9	3.5	2.8	2.4	2.4	2.4	2.6	2.4	2.4	2.1
$\phi$ hydric exp. [mm/m]										
X	0.35	0.25	0.35	0.51	0.39	0.54	0.45	0.53	0.40	0.50
Z	1.57	0.69	0.94	1.35	0.79	1.80	1.24	1.30	1.32	1.32
MAX	2.52	0.71	1.18	1.46	0.89	2.10	1.25	1.42	1.40	1.35
$\phi$ $\alpha$ [10 <sup>-6</sup> K <sup>-1</sup> ] <b>dry</b>										
X	8.3	6.9	8.3	8.5	8.5	8.0	4.9	6.5	7.6	7.5
Z	10.2	8.2	11.0	11.9	10.3	11.9	10.7	11.2	11.0	10.0
resid. strain $\epsilon$ X [mm/m]	0.05	0.01	0.11	0.02	0.11	0.05	-0.05	-0.11	0.04	-0.02
resid. strain $\epsilon$ Z [mm/m]	0.08	0.04	0.23	0.21	0.08	0.15	0.03	0.08	0.11	0.03
$\phi$ $\alpha$ [10 <sup>-6</sup> K <sup>-1</sup> ] <b>wet</b>										
X	14.1	11.3	15.7	9.7	15.1	15.8	13.0	13.3	11.8	11.9
Z	27.1	29.2	24.9	19.5	12.9	36.0	21.8	22.2	23.9	24.6
resid. strain $\epsilon$ X [mm/m]	-0.16	-0.11	-0.09	-0.10	-0.04	-0.08	-0.15	-0.005	-0.04	0.03
resid. strain $\epsilon$ Z [mm/m]	-0.51	-0.67	-0.06	-0.09	-0.03	-0.31	0.03	-0.02	-0.03	-0.16
P-wave velocity [km/s]										
X	3.9	3.9	4.2	4.3	4.1	4.1	4.1	4.1	4.1	3.9
Z	3.1	3.3	3.6	3.4	3.7	3.1	3.5	3.6	3.3	3.1
Youngs's Modulus [GPa]										
X	31	32	36	38	35	36	35	35	35	32
Z	20	23	27	24	29	20	26	27	23	20

## Appendix

Table A.7: Modified petrophysical properties and expansional behavior of Cantera Verde (CV) after the consolidation treatments. SSA = specific surface area; CEC = cation exchange capacity;  $\alpha$  = coefficient of thermal expansion

<b>Cantera Verde (CV)</b>	<b>Untreated</b>	<b>A</b>	<b>A+KSE</b>	<b>WS+KSE</b>	<b>A+WS+KSE</b>	<b>KSE</b>	<b>A+T</b>	<b>WS+T</b>	<b>A+WS+T</b>	<b>TMOS</b>
Porosity [vol%]	29.5	26.6	24.1	25.3	22.2	25.2	21.4	27.2	27.7	24.3
Bulk density [g/cm <sup>3</sup> ]	1.54	1.57	1.66	1.60	1.65	1.66	1.71	1.60	1.60	1.65
Matrix density [g/cm <sup>3</sup> ]	2.18	2.14	2.19	2.14	2.13	2.23	2.18	2.20	2.21	2.18
Water absorp. vac. [wt%]	19	17	15	16	13	15	12	17	17	15
Water absorp. atm. [wt%]	16	16	12	15	13	15	11	15	15	12
Saturation coefficient S	0.85	0.95	0.85	0.94	0.97	0.98	0.87	0.86	0.85	0.83
Micropores [%]	88	90	86	88	89	86	89	83	85	87
Capillary pores [%]	12	10	14	12	11	14	11	17	15	13
Mean pore radius [ $\mu$ m]	0.04	0.03	0.05	0.02	0.03	0.04	0.02	0.03	0.02	0.01
SSA via BET [m <sup>2</sup> /g]	26	-	-	-	-	-	-	-	-	-
SSA via MIP [m <sup>2</sup> /g]	20.8	24.6	19.6	22.2	20.7	18.2	26.1	20.9	33.6	32.1
CEC [meq/100g]	6	-	-	-	-	-	-	-	-	-
w-value [kg/m <sup>2</sup> v(h)]										
X	2.8	3.5	2.1	2.4	2.8	1.9	2.3	1.2	1.0	2.1
Z	2.6	3.2	3.1	1.4	2.6	3.4	3.1	1.4	1.4	1.1
$\mu$ -value										
X	9.2	-	10.7	13.5	13.7	13.3	13.2	12.6	11.9	13.1
Z	10.1	-	12.1	13.1	14.6	16.1	22.7	14.7	12.9	19.9
Sorption 95% rh [wt-%]	7.9	9.8	11.0	8.0	11.5	8.6	7.5	6.3	8.3	5.5
$\phi$ hydric exp. [mm/m]										
X	1.39	1.57	1.65	1.68	1.48	1.78	1.42	2.25	2.04	1.81
Z	1.68	1.66	1.45	2.07	1.86	2.19	1.68	2.56	2.10	1.97
MAX	2.01	1.89	1.66	2.09	1.93	2.31	1.70	2.59	2.13	2.05
$\phi \alpha$ [ $10^{-6} K^{-1}$ ] <b>dry</b>										
X	10.9	10.8	15.7	19.4	18.2	17.3	18.1	28.1	26.7	17.0
Z	10.6	9.4	17.3	21.2	21.8	16.6	15.3	17.9	24.8	15.9
resid. strain $\epsilon$ X [mm/m]	-0.45	-0.04	0.14	0.02	-0.07	0.03	-0.02	0.10	0.14	0.03
resid. strain $\epsilon$ Z [mm/m]	-0.36	-0.04	-0.11	-0.03	0.04	0.01	0.02	0.03	0.29	-0.02
$\phi \alpha$ [ $10^{-6} K^{-1}$ ] <b>wet</b>										
X	47.2	47.5	34.3	41.7	34.6	45.2	34.1	38.0	37.5	27.5
Z	50.7	52.8	35.0	49.6	42.4	49.4	32.5	46.0	36.3	30.3
resid. strain $\epsilon$ X [mm/m]	-0.05	-0.34	-0.20	-0.21	-0.01	-0.10	0.09	0.05	0.08	-0.03
resid. strain $\epsilon$ Z [mm/m]	-0.21	-0.47	-0.03	-0.19	-0.01	-0.16	-0.09	0.08	-0.10	0.18
P-wave velocity [km/s]										
X	2.7	3.0	2.8	3.0	2.7	3.0	3.1	3.1	3.1	2.9
Z	2.6	2.6	2.5	2.8	2.3	2.8	2.8	3.0	2.9	2.6
Youngs's Modulus [GPa]										
X	11	14	12	14	11	14	15	15	15	13
Z	10	10	10	12	8	12	12	14	13	11

## Appendix

Table A.8: Modified petrophysical properties and expansional behavior of Hoktemberyan Red (HR) after the consolidation treatments. SSA = specific surface area; CEC = cation exchange capacity;  $\alpha$  = coefficient of thermal expansion

<b>Hoktemberyan (HR)</b>	<b>Untreated</b>	<b>A</b>	<b>A+KSE</b>	<b>WS+KSE</b>	<b>A+WS+KSE</b>	<b>KSE</b>	<b>A+T</b>	<b>WS+T</b>	<b>A+WS+T</b>	<b>TMOS</b>
Porosity [vol%]	33.1	31.9	26.0	22.3	22.3	26.7	29.8	28.7	32.7	31.2
Bulk density [g/cm <sup>3</sup> ]	1.62	1.60	1.61	1.71	1.61	1.68	1.67	1.69	1.61	1.65
Matrix density [g/cm <sup>3</sup> ]	2.43	2.35	2.18	2.20	2.08	2.29	2.38	2.37	2.39	2.40
Water absorp. vac. [wt%]	20	20	16	13	14	16	18	17	20	19
Water absorp. atm. [wt%]	15	16	15	8	14	12	13	13	16	14
Saturation coefficient S	0.75	0.79	0.90	0.59	0.99	0.75	0.74	0.75	0.78	0.75
Micropores [%]	4	3	10	8	5	7	11	7	6	9
Capillary pores [%]	96	97	90	92	95	93	89	93	94	91
Mean pore radius [ $\mu$ m]	3.93	4.53	2.54	2.99	3.76	3.15	2.57	3.36	3.11	2.90
SSA via BET [m <sup>2</sup> /g]	1.2	-	-	-	-	-	-	-	-	-
SSA via MIP [m <sup>2</sup> /g]	1.8	1.8	6.3	4.2	4.3	5.7	7.9	6.0	4.9	9.1
CEC [meq/100g]	1.0	-	-	-	-	-	-	-	-	-
w-value [kg/m <sup>2</sup> v(h)]										
X	45.1	39.8	35.3	3.9	25.7	9.0	21.8	31.8	44.4	24.1
Z	31.0	32.3	23.5	4.4	5.3	13.5	24.6	24.3	37.6	32.4
$\mu$ -value										
X	8.1	-	7.9	8.2	7.7	7.8	11.1	9.6	11.9	10.4
Z	9.7	-	9.7	9.6	9.6	9.1	12.9	10.8	14.2	11.2
Sorption 95% rh [wt-%]	0.1	4.6	2.3	1.5	1.9	1.7	7.1	0.7	2.6	0.8
$\phi$ hydric exp. [mm/m]										
X	-0.07	-0.67	-0.24	-0.01	-0.01	-0.11	0.02	0.03	-0.08	-0.07
Z	-0.13	-0.04	-0.13	-0.02	-0.02	-0.05	0.06	0.08	0.04	0.02
MAX	-0.16	-0.89	-0.33	-0.03	-0.03	-0.22	0.07	0.08	0.05	0.04
$\phi \alpha$ [ $10^{-6} K^{-1}$ ] <b>dry</b>										
X	6.3	5.7	6.8	6.6	7.1	6.9	5.6	6.4	5.8	6.1
Z	7.0	6.2	6.7	6.6	5.7	6.6	6.6	5.9	6.3	5.9
resid. strain $\epsilon$ X [mm/m]	-0.01	-0.01	-0.01	0.01	0	0	0.005	-0.01	0.01	0.01
resid. strain $\epsilon$ Z [mm/m]	-0.005	0.00	-0.01	0.01	-0.04	0	0.01	0.001	0.01	-1E-05
$\phi \alpha$ [ $10^{-6} K^{-1}$ ] <b>wet</b>										
X	8.5	7.3	7.2	7.8	7.5	7.7	7.8	6.7	7.8	6.4
Z	7.2	5.8	8.6	7.5	7.6	8.1	7.2	7.7	7.4	7.3
resid. strain $\epsilon$ X [mm/m]	-0.08	-0.08	0.02	-0.03	0.02	-0.005	-0.03	0.03	-0.08	-0.01
resid. strain $\epsilon$ Z [mm/m]	-0.005	0.04	-0.04	-0.02	-0.06	-0.02	0.03	-0.05	-0.05	-0.004
P-wave velocity [km/s]										
X	2.9	3.2	3.1	2.9	3.2	2.9	3.4	3.0	3.1	3.0
Z	2.3	2.8	2.7	2.6	2.6	2.6	3.0	2.5	2.5	2.4
Youngs's Modulus [GPa]										
X	14	17	16	14	17	14	18	15	15	14
Z	9	12	12	11	11	11	14	10	10	10

## Appendix

Table A.9: Modified petrophysical properties and expansional behavior of Noyemberyan (NB) after the consolidation treatments. SSA = specific surface area; CEC = cation exchange capacity;  $\alpha$  = coefficient of thermal expansion

<b>Noyemberyan (NB)</b>	<b>Untreated</b>	<b>A</b>	<b>A+KSE</b>	<b>WS+KSE</b>	<b>A+WS+KSE</b>	<b>KSE</b>	<b>A+T</b>	<b>WS+T</b>	<b>A+WS+T</b>	<b>TMOS</b>
Porosity [vol%]	25.7	24.7	24.7	24.2	23.6	24.7	19.5	22.2	21.0	19.6
Bulk density [g/cm <sup>3</sup> ]	1.73	1.73	1.76	1.76	1.76	1.76	1.84	1.80	1.82	1.85
Matrix density [g/cm <sup>3</sup> ]	2.34	2.30	2.34	2.32	2.31	2.33	2.29	2.31	2.31	2.30
Water absorp. vac. [wt%]	15	14	14	14	13	14	11	12	12	11
Water absorp. atm. [wt%]	13	13	10	9	4	13	9	11	11	10
Saturation coefficient S	0.87	0.91	0.75	0.65	0.30	0.92	0.88	0.89	0.92	0.91
Micropores [%]	37	36	37	31	35	37	82	30	60	42
Capillary pores [%]	63	64	63	69	65	63	18	70	40	58
Mean pore radius [ $\mu$ m]	0.14	0.16	0.16	0.20	0.14	0.13	0.02	0.12	0.05	0.10
SSA via BET [m <sup>2</sup> /g]	3.1	-	-	-	-	-	-	-	-	-
SSA via MIP [m <sup>2</sup> /g]	6.5	4.3	5.5	3.2	3.0	7.5	18.1	13.1	14.7	8.9
CEC [meq/100g]	9.2	-	-	-	-	-	-	-	-	-
w-value [kg/m <sup>2</sup> v(h)]										
X	3.9	4.7	3.6	2.8	3.4	0.2	0.7	3.4	1.4	1.3
Z	3.8	4.3	3.2	6.4	3.1	2.3	0.9	2.5	1.8	1.7
$\mu$ -value										
X	14.4	-	17.6	22.5	22.4	20.9	17.9	21.1	22.0	24.1
Z	14.5	-	18.3	23.6	21.4	24.2	17.5	21.1	22.3	20.0
Sorption 95% rh [wt-%]	3.5	6.2	8.1	2.6	10.3	2.5	6.4	3.6	5.2	3.9
$\phi$ hydric exp. [mm/m]										
X	0.67	0.43	0.86	0.67	0.76	0.84	0.87	0.88	1.04	0.91
Z	0.76	0.46	0.88	0.85	0.75	0.87	1.00	1.01	1.18	0.93
MAX	0.97	0.49	0.99	0.87	0.80	0.92	1.03	1.04	1.21	0.96
$\phi \alpha$ [ $10^{-6} K^{-1}$ ] <b>dry</b>										
X	8.4	6.5	9.6	11.7	9.4	9.7	10.9	6.8	9.9	6.5
Z	7.5	6.5	9.4	11.9	9.8	11.9	10.9	6.4	6.1	6.1
resid. strain $\epsilon$ X [mm/m]	0.05	0.04	0.12	0.05	0.11	0.09	0.12	0.01	0.11	-0.004
resid. strain $\epsilon$ Z [mm/m]	0.07	0.04	0.10	0.13	0.15	0.05	0.01	0.05	0.01	-0.01
$\phi \alpha$ [ $10^{-6} K^{-1}$ ] <b>wet</b>										
X	27.0	26.6	26.8	27.2	21.6	22.1	18.5	28.3	19.1	22.4
Z	26.7	26.3	23.8	28.2	22.2	29.5	24.1	28.6	31.3	22.4
resid. strain $\epsilon$ X [mm/m]	0.13	0	0.45	0.54	0.31	0.40	0.03	0.07	0.02	0.04
resid. strain $\epsilon$ Z [mm/m]	0.07	-0.02	0.14	0.49	0.26	0.18	0.09	0.11	0.11	0.09
P-wave velocity [km/s]										
X	3.1	3.1	3.4	3.3	3.4	3.3	3.6	3.5	3.6	3.1
Z	3.2	3.3	3.5	3.5	3.4	3.4	3.7	3.5	3.6	3.2
Youngs's Modulus [GPa]										
X	17	17	20	19	20	19	23	21	22	17
Z	18	18	21	21	21	20	23	22	22	18

## Appendix

Table A.10: Modified petrophysical properties and expansional behavior of Weibern (WB) after the consolidation treatments. SSA = specific surface area; CEC = cation exchange capacity;  $\alpha$  = coefficient of thermal expansion

<b>Weibern (WB)</b>	<b>Untrea- ted</b>	<b>A</b>	<b>A+KSE</b>	<b>WS+ KSE</b>	<b>A+WS+ KSE</b>	<b>KSE</b>	<b>A+T</b>	<b>WS+T</b>	<b>A+WS+ T</b>	<b>TMOS</b>
Porosity [vol%]	36.9	34.8	27.0	26.5	23.4	29.2	31.2	32.2	31.8	33.2
Bulk density [g/cm <sup>3</sup> ]	1.51	1.52	1.58	1.61	1.62	1.57	1.63	1.62	1.61	1.59
Matrix density [g/cm <sup>3</sup> ]	2.40	2.33	2.16	2.19	2.12	2.22	2.36	2.39	2.36	2.38
Water absorp. vac. [wt%]	24	23	17	16	14	19	19	20	20	21
Water absorp. atm. [wt%]	20	18	9	5	7	13	14	15	15	16
Saturation coefficient S	0.84	0.81	0.51	0.28	0.47	0.71	0.73	0.77	0.74	0.75
Micropores [%]	14	13	6	9	9	5	40	19	9	24
Capillary pores [%]	86	87	94	97	91	95	60	81	91	76
Mean pore radius [ $\mu$ m]	0.51	0.50	0.71	0.87	0.53	0.76	0.15	0.48	0.69	0.34
SSA via BET [m <sup>2</sup> /g]	-	-	-	-	-	-	-	-	-	-
SSA via MIP [m <sup>2</sup> /g]	9.7	8.1	4.4	1.2	3.0	2.8	30.1	10.0	10.3	18.0
CEC [meq/100g]	-	-	-	-	-	-	-	-	-	-
w-value [kg/m <sup>2</sup> v(h)]										
X	14.9	14.4	1.8	0.5	0.6	0.4	3.0	7.8	6.9	7.2
Z	14.2	13.6	0.8	1.6	1.4	0.3	8.0	8.3	7.2	7.8
$\mu$ -value										
X	9.1	-	12.6	11.6	12.7	11.4	11.8	13.7	14.0	13.5
Z	9.1	-	13.2	12.0	13.0	12.6	12.3	13.0	13.8	12.6
Sorption 95% rh [wt-%]	3.2	5.7	9.1	1.3	12.0	1.4	8.4	3.3	6.4	4.5
$\phi$ hydric exp. [mm/m]										
X	0.56	0.44	0.45	0.60	0.58	0.63	0.61	0.80	0.66	0.72
Z	0.65	0.54	0.52	0.81	0.64	0.72	0.91	0.92	0.78	0.87
MAX	0.66	0.55	0.54	0.84	0.69	0.73	0.95	0.96	0.81	0.88
$\phi$ $\alpha$ [10 <sup>-6</sup> K <sup>-1</sup> ] <b>dry</b>										
X	5.9	7.9	8.1	9.6	7.7	8.5	7.4	6.5	4.7	5.5
Z	6.8	8.3	7.8	9.8	5.2	9.1	7.3	6.8	6.3	5.5
resid. strain $\epsilon$ X [mm/m]	0.05	0	0.005	-0.04	0.01	-0.02	0.06	0.03	0	0.02
resid. strain $\epsilon$ Z [mm/m]	0.07	-0.02	-0.01	-0.01	-0.14	-0.01	0.04	0.04	0.04	0.002
$\phi$ $\alpha$ [10 <sup>-6</sup> K <sup>-1</sup> ] <b>wet</b>										
X	13.9	11.7	11.3	13.4	11.7	15.7	11.8	13.6	10.2	13.1
Z	18.7	12.4	10.8	14.8	19.0	13.9	14.9	15.0	13.7	12.1
resid. strain $\epsilon$ X [mm/m]	0.06	0.15	0.19	0.24	0.15	0.16	0.07	0.09	0.06	0.09
resid. strain $\epsilon$ Z [mm/m]	0.07	0.10	0.19	0.21	0.12	0.14	0.13	0.12	0.11	0.14
P-wave velocity [km/s]										
X	2.5	2.5	2.8	2.6	2.8	2.6	3.0	2.7	2.7	2.6
Z	2.5	2.4	2.6	2.6	2.5	2.6	2.8	2.5	2.5	2.5
Youngs's Modulus [GPa]										
X	9	9	12	10	12	10	14	11	11	10
Z	9	9	10	10	9	11	12	10	10	9

## Blue Sevan (BS)

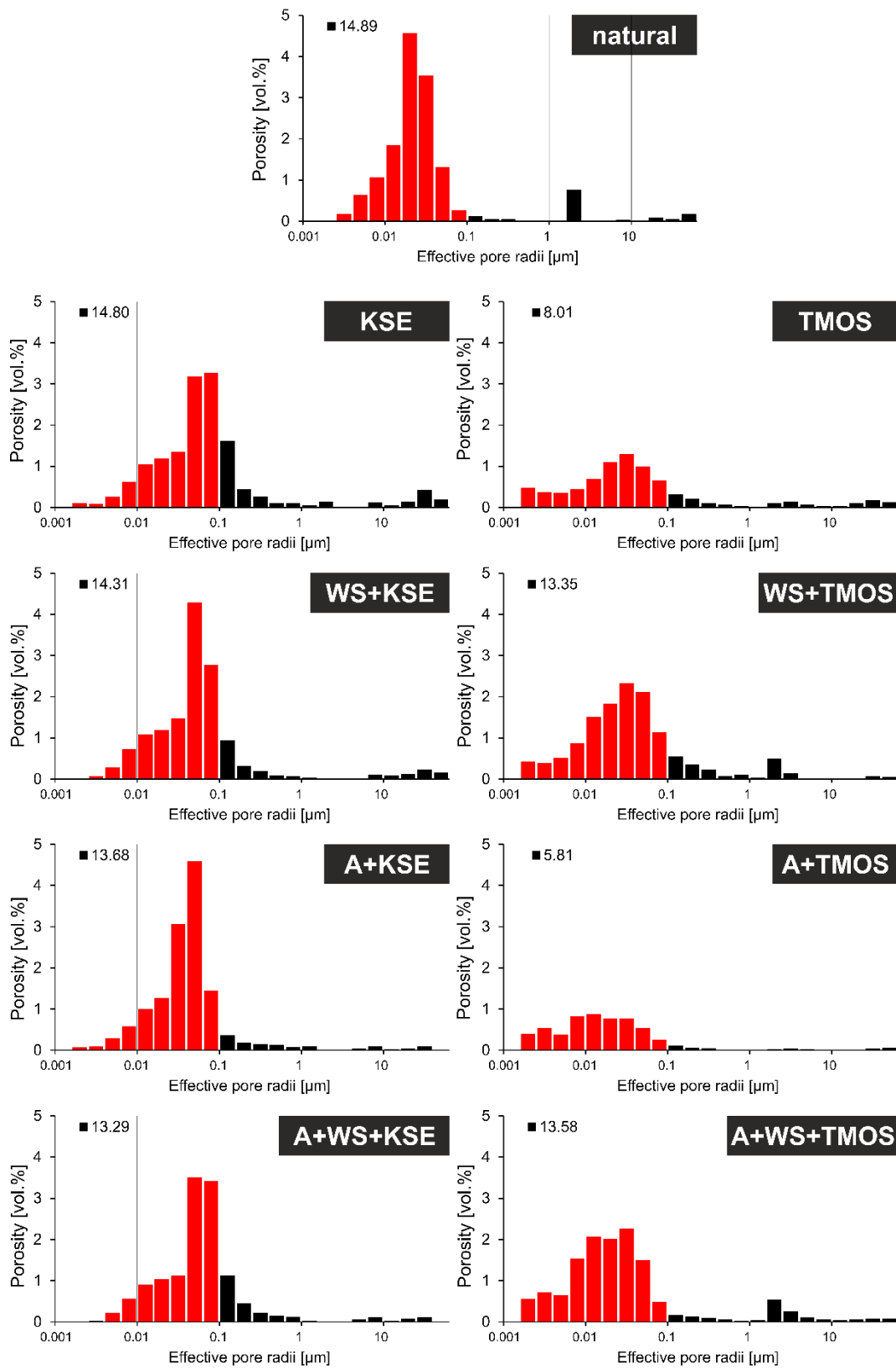


Figure A.1: Modification of the pore radii characteristics of BS due to the consolidation treatments. Left row) TEOS, right row) TMOS; red = micropores, black = capillary pores

# Appendix

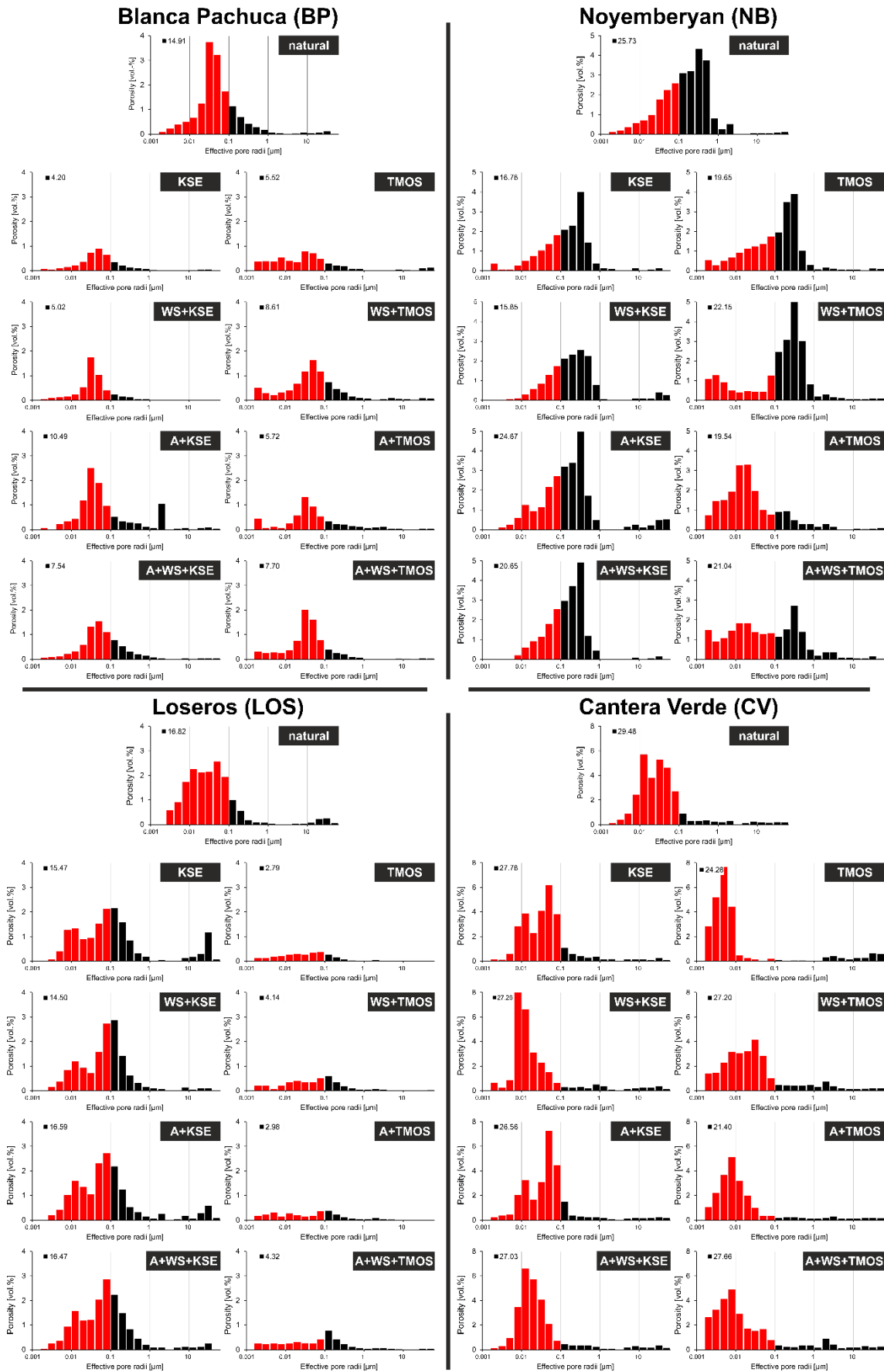


Figure A.2: Modification of the pore radii characteristics of BP, NB, LOS and CV due to the consolidation treatments. Left row) TEOS, right row) TMOS; red = micropores, black = capillary pores

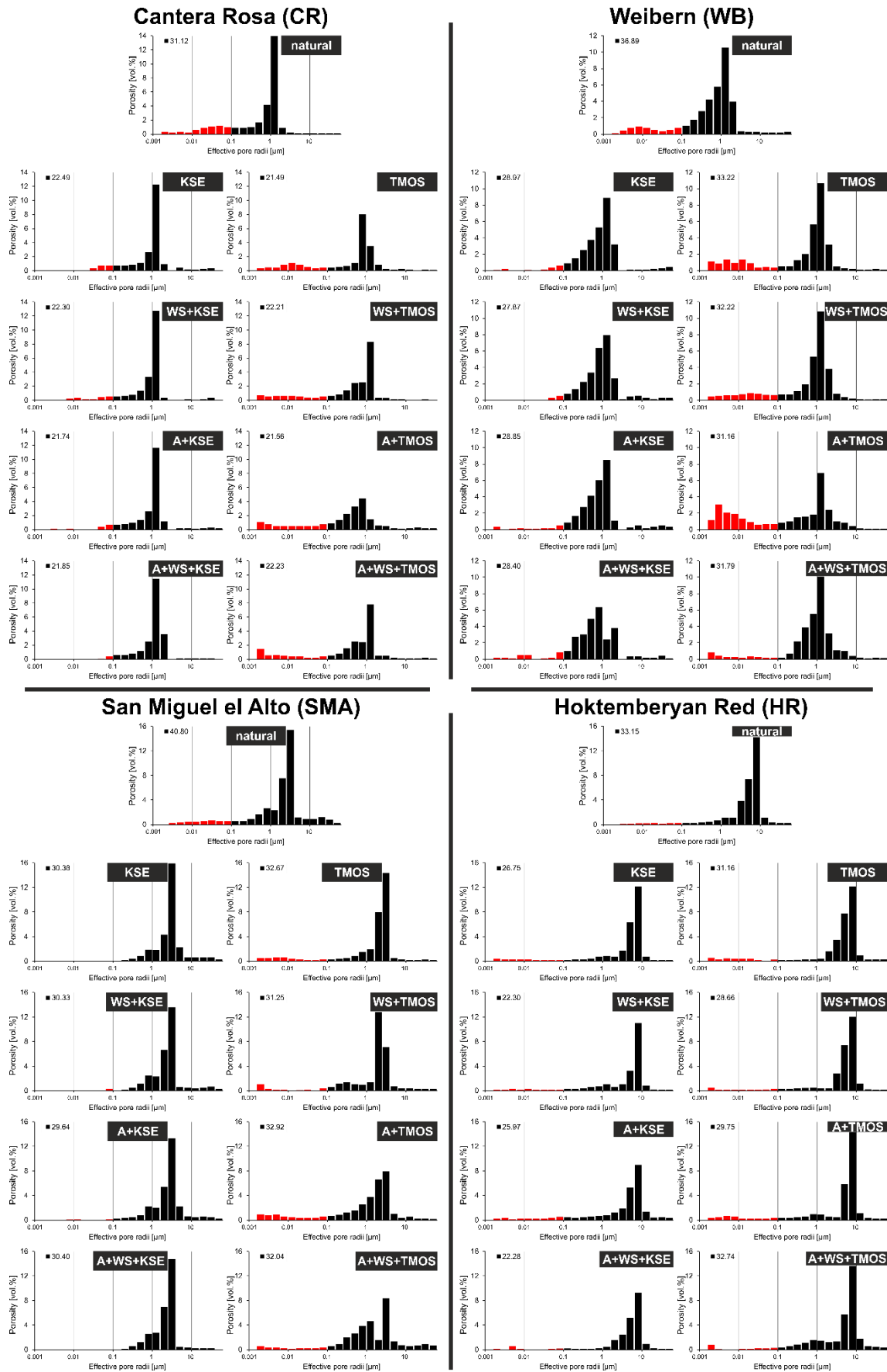


Figure A.3: Modification of the pore radii characteristics of CR, WB, SMA and HR due to the consolidation treatments. Left row) TEOS, right row) TMOS; red = micropores, black = capillary pores



Appendix

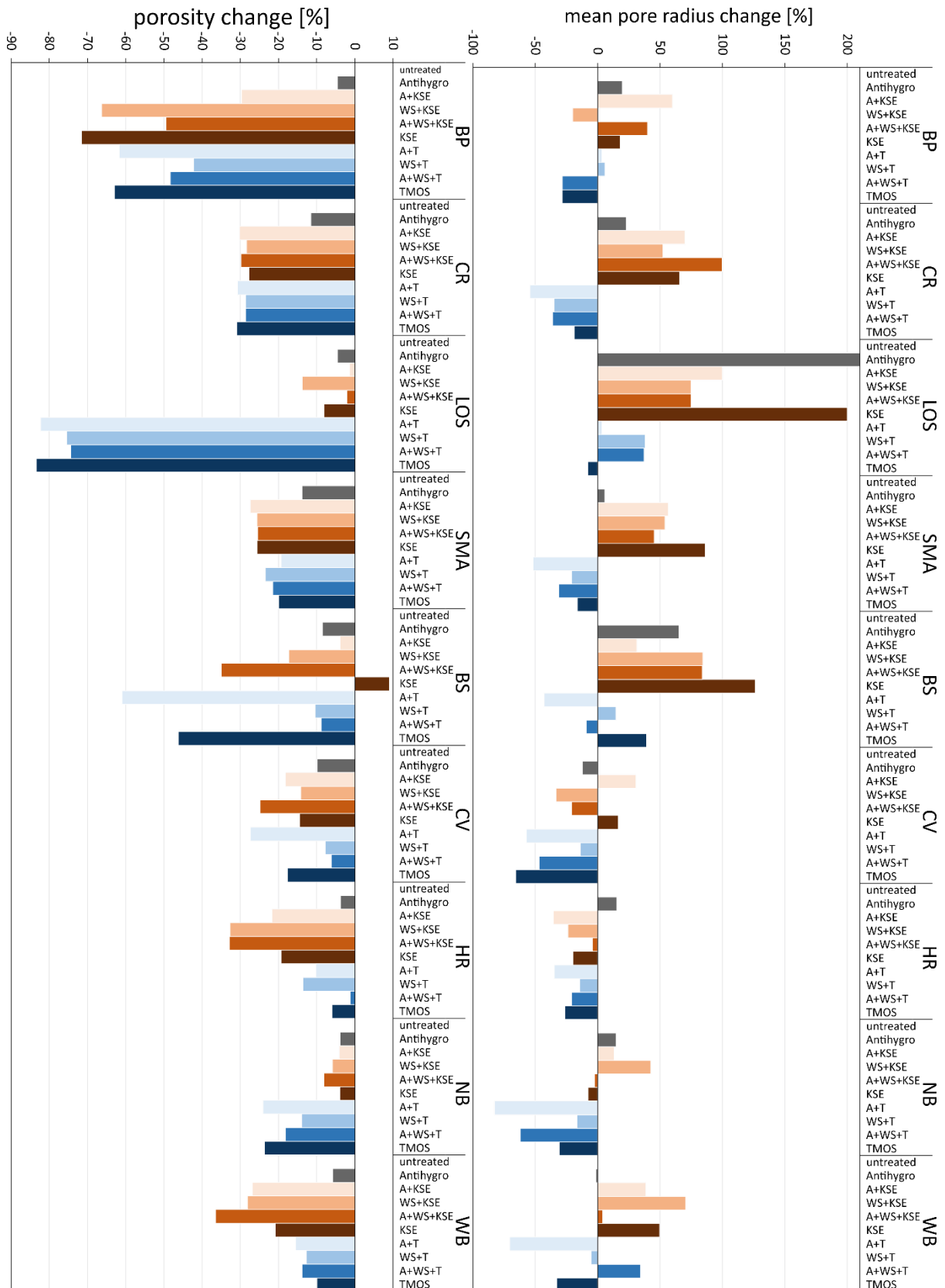


Figure A.4: Percentage increase or decrease of the effective porosity (left) and mean pore radius (right). Brown colors for TEOS, blue colors for TMOS

# Appendix



Figure A.5: Percentage increase or decrease of the micropores (left) and specific surface area (SSA) determined by MIP (right). Brown colors for TEOS, blue colors for TMOS

# Appendix



Figure A.6: Percentage increase or decrease of the total water absorption under vacuum (left) and atmospheric conditions (right). Brown colors for TEOS, blue colors for TMOS

# Appendix

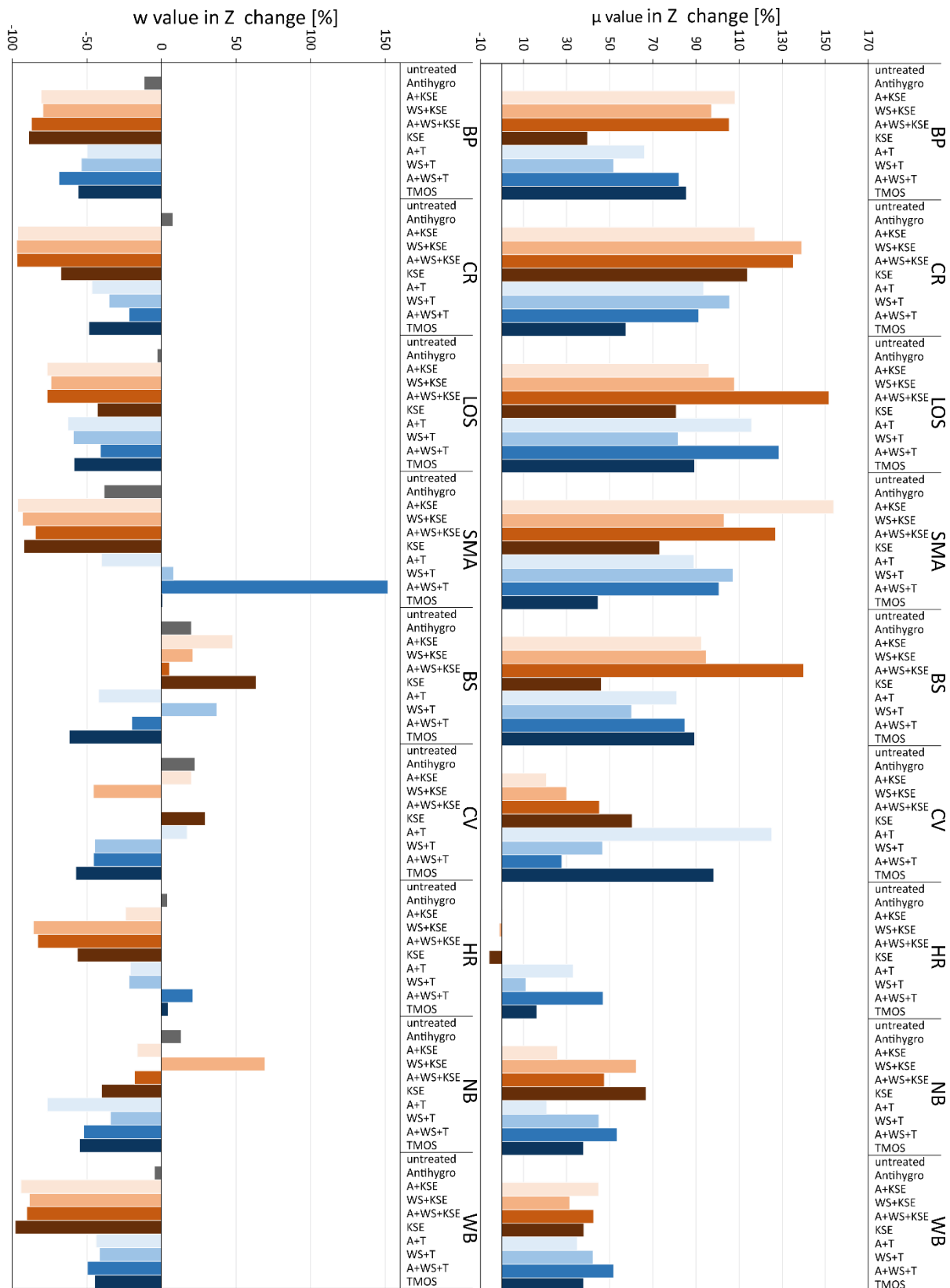


Figure A.7: Percentage increase or decrease of the coefficient of capillary water absorption ( $w$  value) (left) and the water vapor diffusion resistance coefficient ( $\mu$  value) (right). Brown colors for TEOS, blue colors for TMOS

# Appendix



Figure A.8: Percentage increase or decrease of the hygroscopic water sorption at 95 % relative humidity (left) and hydric expansion in Z direction (right). Brown colors for TEOS, blue colors for TMOS

Appendix

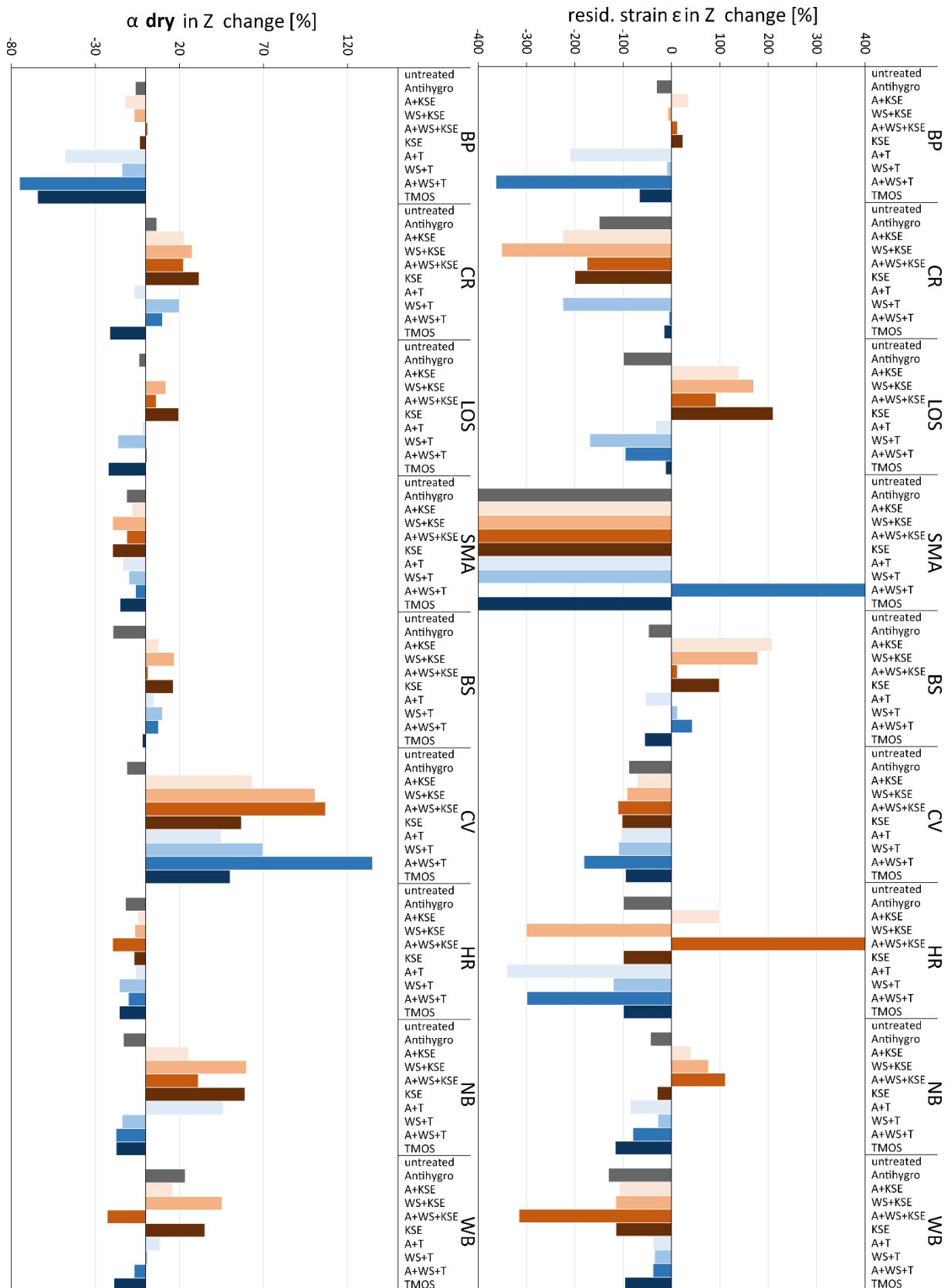


Figure A.9: Percentage increase or decrease of the thermal expansion coefficient  $\alpha$  in Z direction (left) and residual strain in Z direction after 1 cycle of thermal stress (right). Brown colors for TEOS, blue colors for TMOS

# Appendix

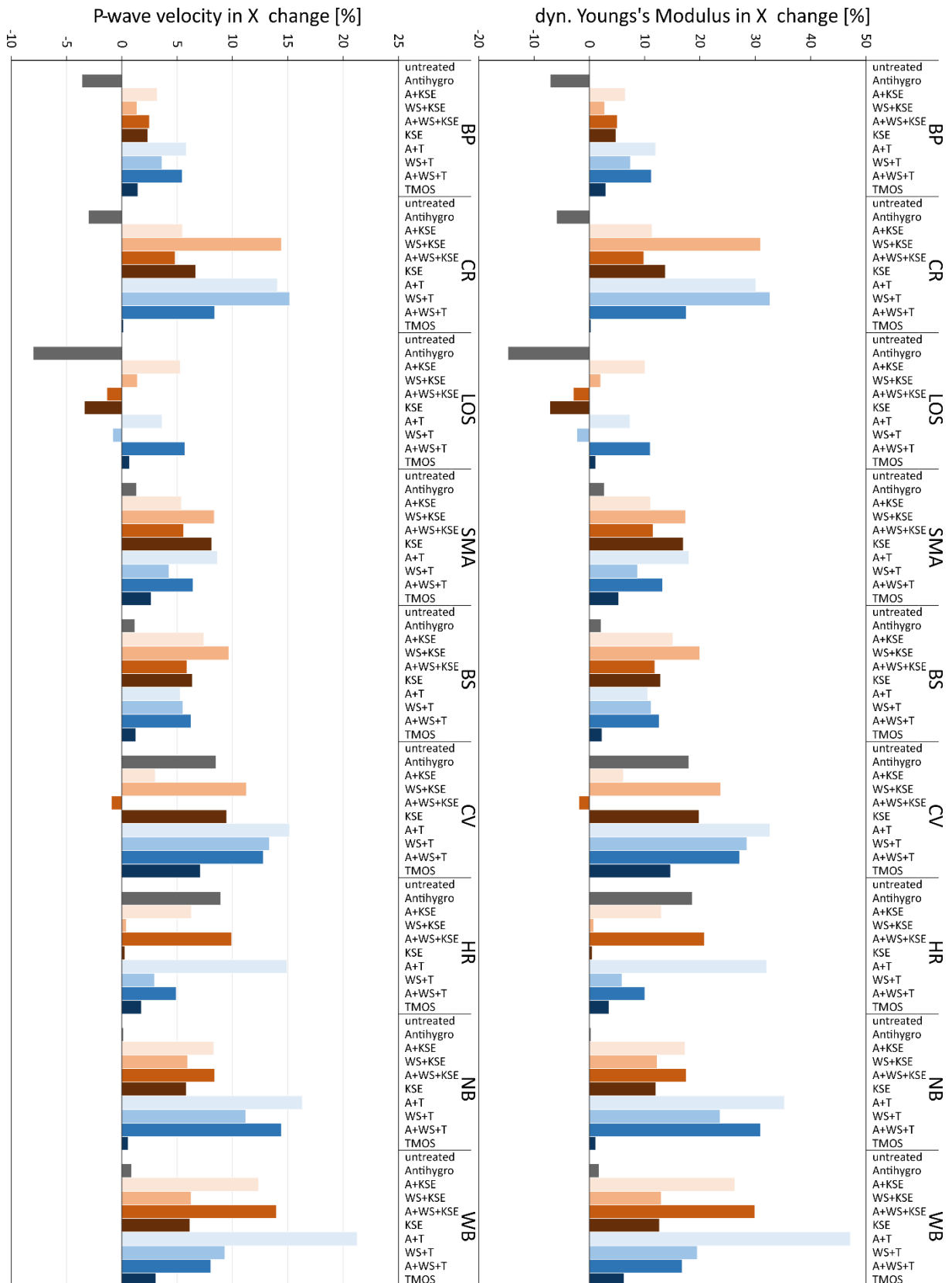


Figure A.10: Percentage increase or decrease of the P-wave velocity in X direction (left) and dynamic Young's modulus in X direction (right). Brown colors for TEOS, blue colors for TMOS